# Effects of point mutations on the block of SK3 small-conductance calcium-activated potassium channels expressed in mammalian cell lines

Yousaf Shah

submitted in partial fulfilment of the requirements for the degree of

Doctor of Philosophy

Pharmacology department

University College London, WC1E 6BT, UK

February, 2005





ProQuest LLC
789 East Eisenhower Parkway
P.O. Box 1346
Ann Arbor, MI 48106-1346

## Abstract

Small conductance calcium-activated $K^+$ channels (SK channels) form a subfamily of $K^+$-selective, voltage-insensitive channels that have been recently cloned. This thesis is concerned primarily with an investigation of the pharmacology of these channels. Understanding their pharmacology is of potential clinical importance since SK channels participate in diverse physiological roles, for example, generating neuronal afterhyperpolarizations (that set tonic firing frequencies) and regulating smooth muscle contraction. This thesis consists of two parts. The first is concerned with expressing and establishing recording conditions for rSK3 in mammalian cell lines. This was made difficult because of channel run up and run down. However, some progress was made towards stabilizing channels through MgATP regulation and this allowed progress towards the second part (the major part) of this thesis: a functional characterization of site-directed point mutants that were created to better understand the pharmacology of these channels. First, two mutations were made to examine similarities between the pore structures of the KcsA and Shaker channels and the SK channels. The first of these mutants would be predicted to increase Tetraethylammonium (TEA) affinity to the sub-millimolar range, and the second to provide increased sensitivity to charybdotoxin (CTX) block. Both these predictions were fulfilled suggesting that the KcsA/Shaker pore structure can provide a reasonable model for the SK channel pore. However, an important difference was identified in the TEA sensitive mutant, indicating that although the channels are similar, they are not identical. Three UCL compounds were then studied; UCL 1848, UCL 1684, and UCL 1530 with six channel mutants. The effects of these mutations on blocker affinity provided the basis of a "map" of the channel residues interacting with UCL compounds and establishes that these blockers bind in the channel pore region. Further, experiments co-expressing wildtype (WT) and mutant subunits demonstrate

that UCL compounds do not require all four "sensitive" subunits for block, suggesting an asymmetric interaction with the channel outer pore. Finally, some work has also been done to define the possible assembly patterns of SK subunits in forming heteromeric channels. Evidence is presented that SK1 and SK3 can co-assemble. Overall, this thesis provides a starting point for understanding the pharmacology of small molecule SK channel blockers at the molecular level.

*This thesis is dedicated to my parents, Dr J & Dr R Shah, and Omar Shah for all the support they have given me.*

# Contents

# List of Figures

# List of Tables

# Abbreviations

**4-AP** 4-aminopyridine.

**AGXN** Agitoxin.

**AHP** Afterhyperpolarization.

**Arg** Arginine.

**ATP** Adenosine 5'-triphosphate.

**$Ba^{2+}$** Barium.

**BK** Big calcium-activated $K^+$ (channel).

**BNFC** Benign neonatal familial convulsion.

**bp** Base pairs.

**CaM** Calmodulin.

**CaMBD** Calmodulin binding domain.

**cAMP** Adenosine 3', 5'-cyclic monophosphate.

**CHO** Chinese hamster ovary.

**CIAP** Calf intestinal alkaline phosphatase.

**CMV** Cytomegaovirus promoter.

**CNS** Central nervous system.

**CTX** Charybdotoxin.

**Cys** Cysteine.

**DAB** 2,4-Diaminobutyric acid.

**DMEM** Dulbecco's modified eagles medium.

**DNA** Deoxyribonucleic acid.

**EAG** ether-a-go-go (channel).

**EBIO** 1-ethyl-2-benzimidazolinone.

**$EC_{50}$** Effective concentration 50%.

**EDTA** Ethylenediaminetetraacetate.

**GFP** Green fluorescence protein.

**Glu** Glutamic acid.

**HEDTA** Hydroxyethylethylene-diaminetriacetic acid.

**HEK** Human embryonic kidney.

**hERG** human-ether-a-go-go-related (potassium channel).

**I-V** Current-voltage.

**$I_{AHP}$** medium afterhyperpolarization current.

**$IC_{50}$** Inhibitory concentration 50%.

**IK** Intermediate conductance calcium-activated $K^+$ (channel).

**KAT** $K^+$ transporter of *Arabidopsis thaliana*.

**$K_{ATP}$** ATP-sensitive potassium (channel).

**$K_{ATP}^{Ca}$** Effective dissociation equilibrium constant of ATP for calcium.

**$K_{ATP}^{Mg}$** Effective dissociation equilibrium constant of ATP for magnesium.

**KChAP** $K^+$ channel associated protein.

**$K_d$** dissociation equilibrium constant.

**$K_{HEDTA}^{Ca}$** Effective dissociation equilibrium constant of HEDTA for calcium.

**$K_{HEDTA}^{Mg}$** Effective dissociation equilibrium constant of HEDTA for magnesium.

**$K_{ir}$** Inward rectifier potassium (channel).

**LB** Lurea-Bertani.

**Lei-$DAB_7$** Leuirotoxin I-2,4-Diaminobutyric acid.

**ln$IC_{50}$** Natural logarithm of the $IC_{50}$ value.

**Lys** Lysine.

**mAHP** Medium afterhyperpolarization.

**minK** Minimum potassium (channel).

**MTSEA** Methanethiosulfonate ethylammonium.

**NCBI** National Center for Biotechnology Information.

**NMR** Nuclear magnetic resonance.

**PCR** Polymerase chain reaction.

**PNS** Peripheral nervous system.

**RCK** Regulator of $K^+$ conductance domain.

**RNA** Ribonucleic acid.

**$R_{series}$** Series resistance.

**sAHP** Slow afterhyperpolarization.

**SCAM** Substituted cysteine accessibility method.

**SCG** Superior cervical ganglion.

**SCN** Suprachiasmatic nucleus.

**SD** Standard deviation.

**SEM** Standard error of the Mean.

**$sI_{AHP}$** slow afterhyperpolarization current.

**SK** Small conductance calcium-activated potassium (channel).

**slo** Slowpoke.

**STN** Subthalamic nucleus.

**SUR** Sulphonylurea.

**TALK** TWIK-related alkaline pH activated potassium (channel).

**TASK** TWIK-related acid-sensitive potassium (channel).

**TEA** Tetraethylammonium.

**THIK** Tandem pore domain halothane-inhibited potassium (channel).

**Thr** Threonine.

**TM** Transmembrane.

**TREK** TWIK-related potassium (channel).

**TRESK** TWIK-related spinal cord potassium (channel).

**TWIK** Tandem of P domains in a weak inwardly rectifying potassium (channel).

**WT** Wildtype.

# Chapter 1

# Introduction

Ion channels form pores in cell membranes that allow ions to flow rapidly down electrochemical gradients. The currents produced from the movement of these ions can induce rapid changes in membrane potential. Potassium ($K^+$) channels form a varied group of such integral membrane proteins that are ubiquitously expressed in prokaryotic and eukaryotic organisms (MacKinnon, 2003). Their diversity enables them to fulfil a broad range of cellular functions in both excitable and non-excitable cells. For example, $K^+$ channels in the nervous system help to encode the frequency characteristic of firing neurones and understanding how this characteristic is regulated is of great physiological importance. Ninety-three human $K^+$ channel $\alpha$-subunit genes have so far been identified (data obtained from the National Center for Biotechnology Information's (NCBI) Clone Registry database), with predicted amino acid sequences showing great molecular diversity. This variation is further enhanced through processes such as alternative splicing, and post-transcriptional RNA editing (Coetzee et al., 1999). Once the channel protein subunits have been made, they can form tetrameric (or dimeric) assemblies depending on the number of subunits that must aggregate to make a fully functional channel (Doyle et al., 1998; Tu & Deutsch, 1999). The subunits forming a channel can be identical, i.e. all products of the same gene, or subunits can assemble from different channel genes

forming a different and novel channel type. In addition the properties of potassium channels can be further modified through associations with auxiliary proteins (some of which are termed $\beta$-subunits). Such auxiliary subunits can confer different types of cell-specific mechanisms of regulation. The work in this thesis is centred on obtaining information about the regulation, assembly, and pharmacology of small conductance calcium-activated potassium channels (SK channels). The well known structure of the KcsA channel (Doyle et al., 1998) has been used as a structural basis for this work.

## 1.1 The crystal structure of the bacterial KcsA channel

KcsA is a potassium channel from the bacterium *Streptomyces lividans*. It shows a high level of sequence identity to other potassium channels in the pore region (Doyle et al., 1998) so much information from this channel is probably relevant to others. The channel's structure resolved to 3.2 Å has been determined in the closed state using X-ray crystallography. Because the crystal structure has been solved, it has been extensively used as a homology model for the pore in other $K^+$ channels (A. Williams et al., 2001; Wrisch & Grissmer, 2000). It is tetrameric with four-fold symmetry about the central pore axis. The channel comprises two transmembrane $\alpha$-helical regions (the outer and inner helices) connected by a "turret loop", a short pore helix and a segment forming the channel's selectivity filter (Figure 1.1 on page 28). Each of the inner helices contribute to the pore lining and are tilted 25° from the perpendicular to the membrane surface. Each outer helix faces the lipid bilayer and the pore helices are slotted in between. The geometry of these helices give rise to a converging intracellular aspect that makes the upright channel look like an "inverted teepee". The overall pore length is 45 Å and acidic (negative) amino acids are concentrated at the extracellular and intracellular openings which

would attract cations electrostatically. Two rings of aromatic amino acids on the membrane-facing surface of the channel also are present at either end.

**The selectivity filter** In KcsA, the selectivity filter which is formed by the sequence TVGYG, contains four separate ion binding sites, located 3.4 Å, 3.9 Å, and 3.3 Å apart (distances between the first and second, second and third, third and fourth sites respectively). Repulsion between ions at such close distances inside the selectivity filter will contribute to a throughput rate of more than a million $K^+$ ions per second (Doyle et al., 1998). All $K^+$ channels have the same pore selectivity signature sequence of G(Y/F)G suggesting that these ion binding sites in KcsA are likely to be conserved (Heginbotham et al., 1994).

Selectivity is achieved through a process of initial dehydration of the conducting ion, and subsequent stabilization provided by the carbonyl oxygens of the protein backbone that substitute for the lost water molecules (Doyle et al., 1998). The Pauling radius of a $K^+$ ion (~1.4 Å) enables it to fit perfectly between the carbonyl oxygens whereas that of $Na^+$ is smaller (~0.9 Å) and consequently cannot be effectively coordinated in the filter (Allen et al., 2000).

**The internal cavity and inner pore** The potassium channel's selectivity filter only extends for 12 Å of the pore region (Doyle et al., 1998). Below it (towards the intracellular side) there is a "cavity" in the pore. Electron density maps show a region of diffuse density in the central cavity of the KcsA channel. It is thought that this represents a $K^+$ ion "flooded" by water molecules rather than a $K^+$ binding site *per se* (Doyle et al., 1998). The flooded $K^+$ ion is stabilized through this shielding which compensates for the augmented ion destabilization (as a result of reduced water polarizability) which occurs at the lipid membrane centre (Roux & MacKinnon, 1999). The pore narrows towards the intracellular end and is lined with hydrophobic residues so that the $K^+$ ion has an inert path through to the end of

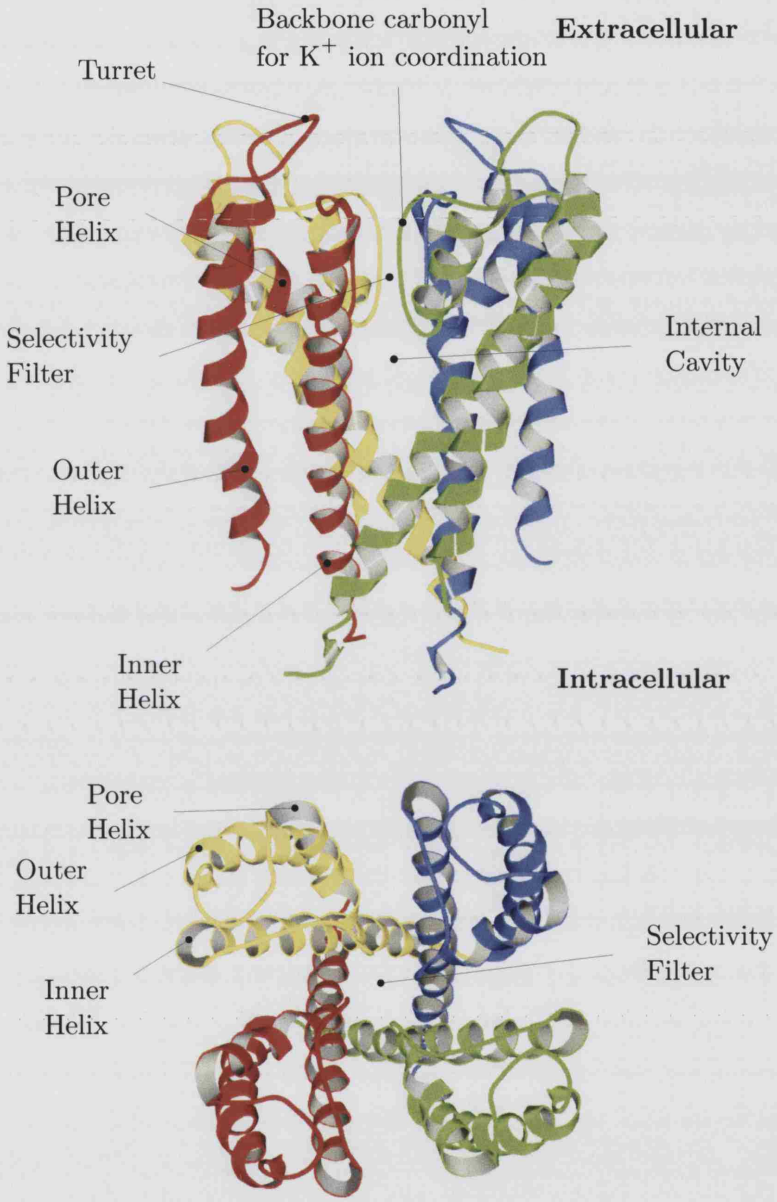


**Figure 1.1:** Ribbon diagram of the KcsA channel structure (Doyle et al., 1998). The main features of the pore are shown in a side view (upper diagram) and top view (lower diagram). The extracellular and intracellular sides of the channel in the upper diagram are labelled. Each subunit is shown in a different colour. Pictures were generated with Swisspdb viewer and Povray.

the channel.

**The pore helix** The pore-helix dipole moment contributes to ion conduction by providing an "energy well" along the axis of the central cavity that allows an ion to slide along the axis but not to deviate by more than 2 Å (Roux & MacKinnon, 1999). This focusing of the ion on the central pore axis stabilizes the ion and permits it to cross the dielectric barrier without impeding the ion flux (Roux & MacKinnon, 1999). The distance between the ends of the pore helices and the cavity centre (5 Å) together with the abundance of water molecules will tend to reduce the effect of the dipole, though it is thought to be sufficient to generate a high throughput of $K^+$ ions (Roux & MacKinnon, 1999).

## 1.2 Classification of $K^+$ channels

Potassium channels can be classified according to the number of putative TM elements contained per subunit. The main categories are 7TM, 6TM, 4TM, and 2TM classes of channels. These categories are briefly outlined below. Figure 1.2 on the next page summarizes the general architecture for each class of potassium channel.

### 1.2.1 Two transmembrane $K^+$ Channels

#### The inward rectifiers

The family of 2TM potassium channels are sometimes called inward rectifier or $K_{ir}$. This is because the first channels in this family (originally called anomalous rectifiers), produced a larger inward current than outward at equivalent driving forces (of opposite polarity) (Katz, 1949). Rectification of $K_{ir}$ was found to depend on block by magnesium ions or polyamines present on the inside of the cell and blocking from the intracellular face of the channel (Vandenberg, 1987; Nichols & Lopatin, 1997). Subsequent studies have shown that the $K_{ir}$ family is very large and

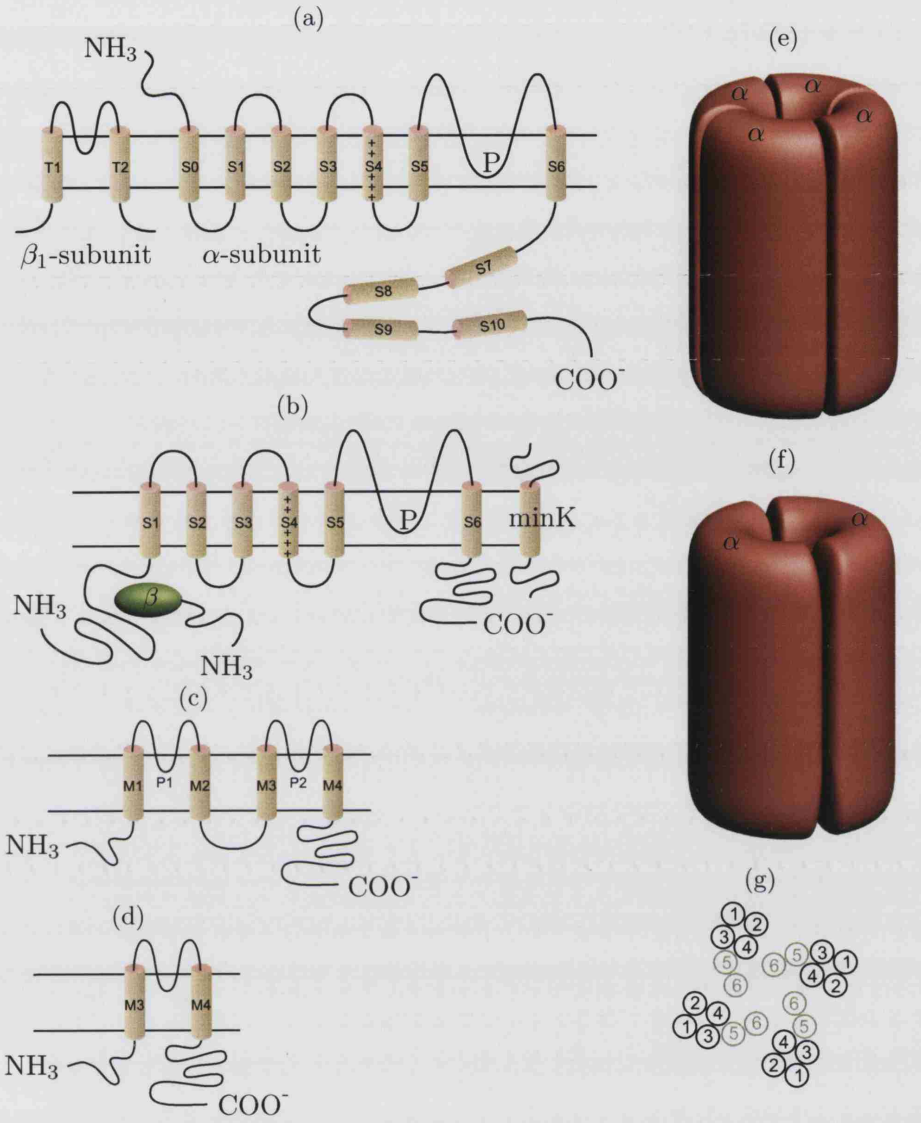


**Figure 1.2:** A structural overview of the classes of $K^+$ channel $\alpha$-subunits. (a)-(d) Saggital sections through membranes showing the TM topology of each class of $\alpha$-subunit. Membrane-spanning $\alpha$-helices (S0-S6, M1-M4), and intracellular $\alpha$-helices (S7-S10) are represented by cylinders. The pore region is formed by the P-loops (P/P1/P2) and their surrounding TM elements. (a) 7TM class. A 2TM $\beta_1$-subunit is shown, which can interact with 7 TM BK channel $\alpha$-subunits (McManus et al., 1995). A voltage sensor (positively charged amino acids) is located in the S4 TM domain of 7TM BK channels, as shown (b) 6TM class. Some members of this class can associate with 1TM $\beta$-subunits and an internal $\beta$-subunit (Sanguinetti et al., 1996; Xu & Li, 1998; Nakahira et al., 1996). As in BK channels, 6TM $K_v$ channels contain a voltage sensor in their S4 TM domain. (c) 4TM class ("two-pore" channels). (d) 2TM class (e.g. $K_{ir}$ family). (e) Tetrameric association of $\alpha$-subunits (e.g. BK (7TM) and $K_v$ (6TM) channels). (f) Tandem-pore $K^+$ channels are thought to associate as dimers. (g) Putative topographical arrangements of 6 TM helices in a tetrameric channel according to Li-Smerin et al. (2000).

some members don't rectify strongly but have other specialized roles. For example $K_{ATP}$ channels are octameric channels consisting of two subunits; an weak inwardly-rectifying subunit ($K_{ir}6.2$) and a sulphonylurea (SUR) receptor (Sakura et al., 1995). Assembly proceeds with a 4:4 stoichiometry where expression of $K_{ir}6.2$ alone does not result in functional channels (Aguilar-Bryan et al., 1995). The SUR subunits provide at least some of the nucleotide sensitivity of the channel (Nichols et al., 1996).

Other members of the $K_{ir}$ family include $K_{ir}4.1$, which is a weak inward rectifier, and so called "silent subunits" such as $K_{ir}5.1$ that do not produce functional channels when expressed alone (Bond et al., 1994). However, co-expression of these subunits in either congruent (4-4-5-5), or alternate (4-5-4-5) combinations produces functional channels and assemblies with different properties, illustrating the importance of subunit position in heteromeric channel profiles (Pessia et al., 1996).

### Channelopathies associated with $K_{ir}$ channels

The loss of functional $K_{ATP}$ channels ($K_{ir}6.2$/SUR receptor) underlies the pathogenesis of the childhood disorder known as persistent hyperinsulinemic hypoglycemia of infancy (PHHI). Hypersecretion of insulin from the pancreas results in reduced blood glucose levels in this disease. Mutations of $K_{ir}6.2$ that have been implicated in the pathogenesis of the disease include a proline for leucine point mutation in the second transmembrane region (Thomas et al., 1996) and a truncation of the channel (Nestorowicz et al., 1997). A single phenylalanine deletion in SUR1 causes PHHI though the inability of the mutant channel (formed by $K_{ir}6.2$ and the mutated SUR1 subunits) to traffic to the cell membrane (Cartier et al., 2001). Other mutations of the SUR1 gene which are associated with PHHI have also been found (Thomas et al., 1995; Nestrowicz et al., 1998; Nestorowicz et al., 1996; Kane et al., 1996; Dunne et al., 1997).

Bartter's syndrome is a channelopathy that has been associated with ROMK1

($K_{ir}1.1$) channels (Simon et al., 1996; Derst et al., 1997; Schwalbe et al., 1998). A symptom of this disease includes dehydration which is brought on by salt wasting and hypokalemia (Karolyi et al., 1998; Simon & Lifton, 1998). Point mutations, truncations and frameshift mutations in ROMK channels from the thick ascending limb of the Loop of Henle, which normally regulate luminal $K^+$ levels in the kidney nephron, have all been found to be associated with this disease (Simon et al., 1996).

Andersen's syndrome, a channelopathy that causes pleiotropic symptoms including arrhythmias and periodic paralysis (Tawil, 1994), is produced through dysfunctional $K_{ir}2.1$ channels. Two missense mutations of $K_{ir}2.1$ result in dominant negative channels and have been found in patients with Andersen's syndrome (Plaster et al., 2002). Heteromerization between $K_{ir}2.1$ channels and $K_{ir}2.2$ or $K_{ir}2.3$ channels have been found to give rise to the pleiotropy found in this channelopathy (Preisig-Muller et al., 2002).

### 1.2.2 Four Transmembrane $K^+$ Channels (Two-pore-domain or "leak" potassium channels)

These channels contain two pore domains and are thought to function as background channels involved in the modulation of the resting membrane potential (a negative resting membrane potential is critical for action potential generation in excitable cells). Fifteen two-pore-domain channels have so far been identified which can be classified into six subfamilies, TWIK, THIK, TREK, TASK, TALK and the recently discovered subfamily, TRESK. TWIK-1 and TWIK-2 channels from the TWIK subfamily and THEK-1 channels of the THIK subfamily are inward rectifiers (Lesage et al., 1996; Rajan et al., 2000), whereas all the other channels show little or no voltage-dependence. Leak potassium channels can be inhibited by a variety of neurotransmitters (Patel et al., 2000; Rajan et al., 2000; Rekling et al., 2000), but selective blockers of these channels remain to be described and hence mainly

indirect evidence for their functional roles has been cited, which will now briefly be described.

Members of the TASK subfamily (TASK-1, TASK-3, and TASK-5) are thought to play important sensory roles in regulating cellular oxygen tension (Buckler, 1997) and pH (Ballantyne & Schneid, 2000; Nattie, 2001; Sirois et al., 2000; Washburn et al., 2002) homeostasis through breathing regulation. TASK-1 and TASK-3 mRNAs have been found at high levels in motoneurones (Talley et al., 2001), including those of the hypoglossus nerve (Talley et al., 2000), which innervates respiratory musculature. Widespread distribution amongst chemoreceptors (Buckler, 1997; Yamamoto et al., 2002) and these motoneurones reveal a concerted monitoring of pH by central and peripheral leak potassium channels. Furthermore, TASK-1 and TASK-3 channels are thought to mediate the effects of volatile anaesthetics, together with TRESK, TREK-1 and TASK-2 (C. Liu et al., 2004; Patel et al., 1999; Meadows & Randall, 2001; Gray et al., 2000). The latter is a member of the TALK subfamily which is described next.

TALK-1 channels are expressed in the pancreas and may help to regulate hormone secretion from this organ via two distinct mechanisms. TALK-1 channels may serve as plasma pH sensors which regulate hormone secretion through changes in the membrane potential. Alternatively, activation of TALK-1 channels upon depolarization may induce negative feedback regulation of hormone secretion through the reduction of calcium influx into pancreatic cells (Han et al., 2003).

Channels forming the TREK subfamily, TREK-1, TREK-2 and TRAAK, probably play a role in thermoregulation (Maingret et al., 2000). For example, TREK-1 has been shown to be expressed in appropriate neurones of the dorsal root ganglia, where a voltage-insensitive potassium conductance is involved in the cold transduction response of thermosensing neurones (Reid & Flonta, 2001; Viana et al., 2002). The TREK subfamily are activated by membrane stretch (Patel et al., 1998; Bang et al., 2000; Maingret et al., 2000), which potentially make them ideally suited to

detect cell swelling (Kim, 2003). Furthermore, nitric oxide-induced phosphorylation of TREK-1 channels are thought to relax gastrointestinal smooth muscle (Koh et al., 2001).

Members of the TWIK subfamily are expressed in the taste buds of mice and may play a role in the mechanism of sour taste transduction (Richter et al., 2004). TWIK-2 channels have been found to be expressed in the inner ear region where they are thought to contribute to $K^+$ ion reabsorption into the endolymph (Mhatre et al., 2004).

### 1.2.3 Seven transmembrane $K^+$ Channels

#### Large conductance calcium-activated potassium channels (BK channels)

To date there is only a single mammalian gene in this category and it forms calcium and voltage-activated conductances, of magnitude typically greater than 100 pS in symmetrical $K^+$ (Sah & Davies, 2000). As a result, they have $EC_{50}$ values for calcium activation that vary with voltage, ranging from several micromolar near the resting membrane potential, to several nanomolar upon depolarization (in symmetrical $K^+$) (Latorre et al., 1989). They also appear to have several calcium-binding regions within the channel sequence (Braun & Sy, 2001) and gating occurs through direct calcium binding (in contrast to SK channels as discussed later). BK channels are blocked by low concentrations of TEA (0.5–1 mM) and iberiotoxin (≈250 pM) (Marty, 1989; Galvez et al., 1990; Haylett & Jenkinson, 1990) as well as charybdotoxin (CTX) (100 nM in neocortical neurones) (Kang et al., 1996). The only gene product that encodes BK channels, known as *Slo*, is thought to co-assemble both with auxiliary $\beta$-subunits (such as the $\beta_1$-subunit which induces hypertension in knockout mice (Brenner et al., 2000)) and with the product of another widely-expressed $K^+$ channel gene, *Slack* (Joiner et al., 1998). The resultant channel is an intermediate conductance calcium-activated potassium channel distinct from the

Gardos/IK channels (discussed later).

Recently, the crystal structure of a 2TM BK-like channel, known as MthK from *Methanobacterium thermoautotrophicum*(PDB code 1CNQ), was determined in the open state (Jiang et al., 2002). This channel's C-terminus contains a single endogenous "regulator of potassium conductance" (RCK) domain. In mammalian *slo* channels, the extended C-terminal region is comprised in part of two such RCK domains in tandem (Jiang et al., 2002). These RCK domains form the "gating ring" of the MthK channel which "hangs" from the intracellular aspect of the pore, rather like a gondola. Four are contributed from the channel and another four RCK domains of intracellular origin associate alternately with the four gene-derived RCKs to form an 8 RCK domain gating ring. Binding of calcium induces a structural change in the flexible interface between gene-derived and intracellularly-derived RCK domains from the same subunit. This is thought to eventually splay the intracellular end of the channel open by pulling the inner helices outward via the S6–RCK linker regions. Each inner helix pivots at a very conserved glycine residue known as the "gating hinge", which opens up the internal cavity to the cytoplasmic contents of the cell.

### 1.2.4 Six transmembrane $K^+$ Channels

This is the largest class of $K^+$ channels, including voltage-gated $K^+$ channels such as the $K_v$ and hERG subfamilies, and those not gated by voltage, such as the small conductance calcium-activated $K^+$ channels (SK channels) (Figure 1.3 on page 37).

This class of $K^+$ channel plays many important physiological roles in neurones and other excitable tissues. The first cloned $K^+$ channel, the so-called Shaker channel, was cloned from a shaking mutant of *Drosophila melanogaster* (the fruit fly) through genetic techniques (Jan et al., 1983). Shaker channels produce A-type currents that generate rapidly activating and inactivating currents (Timpe et al., 1988). There are several mammalian variants of this channel (Figure 1.3 on page 37), com-

monly expressed in brain, heart, retina, and pancreatic islets amongst other places (Manabe et al., 1998).

All voltage-gated $K^+$ channels have a positively charged amphipathic region consisting of a regular array of predominantly arginine amino acids every third residue in the fourth TM segment that acts as a "voltage sensor" (Noda et al., 1984; Jan & Jan, 1989). Transitions of this region, in response to changes in the electric field, gives rise to gating currents (Armstrong & Bezanilla, 1973). A tetrameric T1 domain of approximately 120 amino acids between the N-terminal inactivation ball ("plugs" the pore during N-type inactivation) and S1 may contribute to channel gating in Shaker and other voltage-gated $K^+$ channels (Cushman et al., 2000; Minor et al., 2000).

Many potassium channels in the 6TM family are known to associate with accessory subunits that dramatically alter their properties. For example, the $I_{SK}$ protein (or minK) associates with $K_v$LQT channels to induce the slow gating kinetics of the $I_{minK}$ channel (Busch & Suessbrich, 1999). The minK protein has a single transmembrane element with no similarity to other $K^+$ channels (Takumi et al., 1988). There are many other examples of accessory subunits such as the $K^+$ channel associated protein (KChAP) that increases the potassium current when co-expressed with $K_v2.1$ (Wible et al., 1998). Later, some data suggesting that SK channels also associate with auxiliary subunits will be discussed.

### Channelopathies associated with 6TM channels

The 6TM family of channels includes many that are associated with genetic disorders. Mutations in $K_v$LQT1 are associated with Long QT Syndrome in which an individual is prone to ventricular tachyarrhythmia (Wang et al., 1996). Missense mutations in the auxillary subunit of this channel, minK, are also associated with long QT syndrome (Splawski et al., 1997), as are intragenic deletions and missense mutations of the hERG channel (Curran et al., 1995; Satler et al., 1998). A deletion-

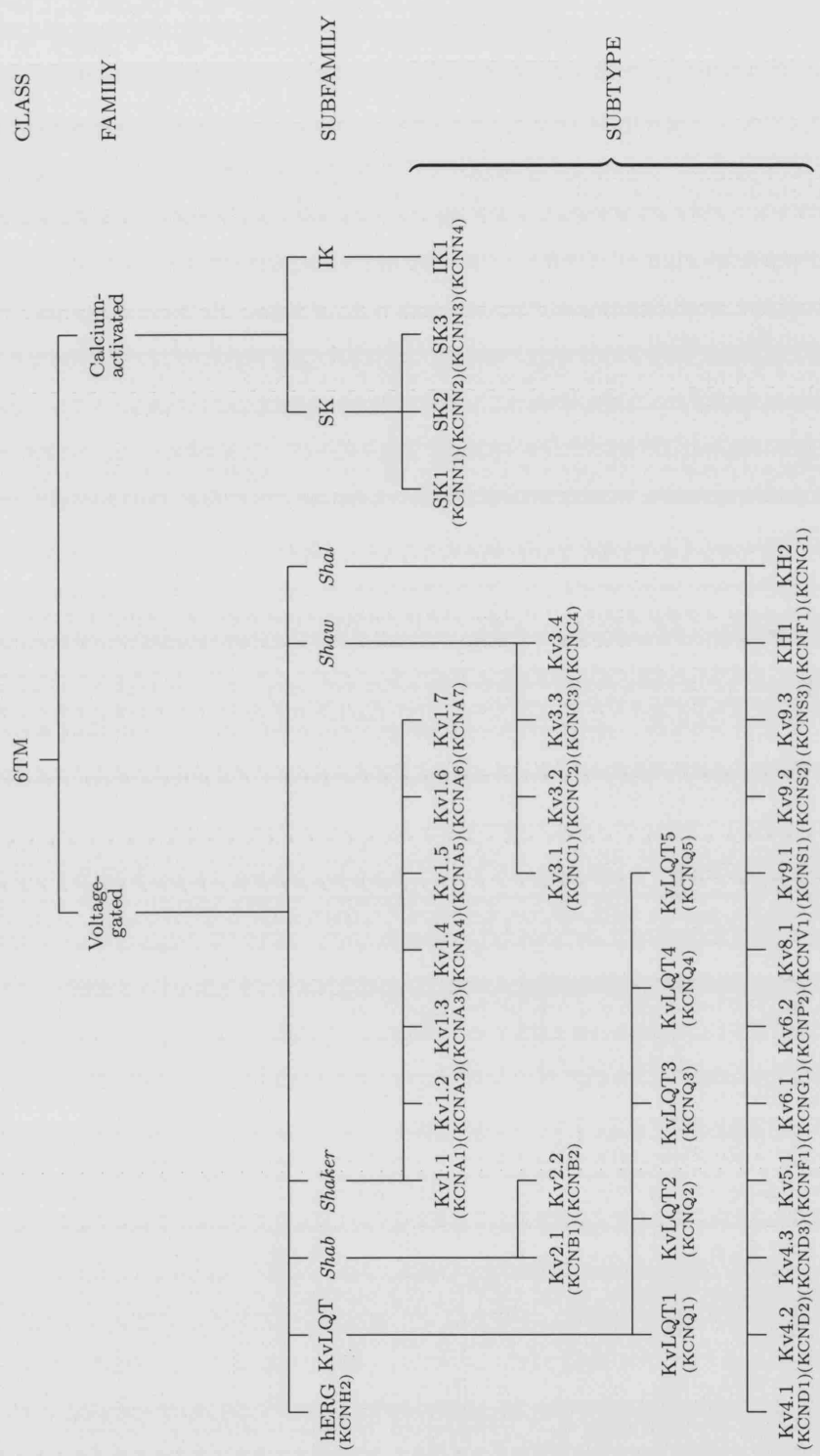


**Figure 1.3:** Tree diagram showing the $K^+$ channels belonging to the 6TM class. The family of calcium-activated 6TM $K^+$ channels is much smaller than the voltage-activated family. The genes from which each channel is transcribed are shown in parentheses.

insertion mutation in $K_v$LQT1 is found to give rise to Jervell and Lange-Nielsen syndrome, which is characterized by syncope and ventricular arrhythmias (Neyroud et al., 1997). Missense mutations of $K_v$LQT2 and $K_v$LQT3 (when expressed together form the M-channel) have been identified in benign neonatal familial convulsion (BNFC) pedigrees (Schroeder et al., 1998). Other disorders resulting from defective 6TM channels include episodic ataxia ($K_v$1.1) (Maylie et al., 2002) with myokymia ($K_v$1.1) (Browne et al., 1994), mental epilepsy ($K_v$LQT2) (Biervert et al., 1998) and deafness ($K_v$LQT4) (Coucke et al., 1999; Kubisch et al., 1999).

## 1.3 SK channels

In their simplest form, SK channels are thought to be a tetrameric complex consisting of four $\alpha$-subunits or monomers (Bond et al., 1999). The classical blocker of SK channels is a neurotoxin from the venom of the honeybee, *Apis mellifera*, known as apamin. Three subtypes, SK1, SK2, and SK3 have been discovered so far together with an intermediate conductance calcium-activated $K^+$ channel (IK) which is sometimes classed as an SK channel (SK4). In addition to the 6 transmembrane spanning (TM) elements found in each monomer, the SK1-3 proteins have unique intracellular N- and C-terminals that show considerable sequence diversity amongst subtypes and include potential sites for protein phosphorylation. Single channel conductances for native and cloned SK channels lie in the range of 5–20 pS (Castle, 1999). Cloned SK1-3 channel subtypes are maximally activated by 1 µM intracellular calcium (Xia et al., 1998). These three genes are widely expressed in both non-excitable and excitable tissues. Examples of channels recorded from the central nervous system (CNS) and the peripheral nervous system (PNS) are given in Caretta (1994); Hotson and Prince (1980); Lancaster and Adams (1986); Sah and Isaacson (1995); Storm (1989), while other reports of SK channels in the PNS come from intestinal smooth muscle (Banks et al., 1979), adrenal chromaffin cells (Neely & Lingle, 1992), skeletal

muscle cells (Blatz & Magleby, 1986), hepatocytes (Ogden et al., 1990), and epithelial cells (Pacha et al., 1992; Wiener et al., 1990). The closely related SK4 channel is found in T-lymphocytes (Grissmer et al., 1992), and its expression is limited to peripheral tissues (Kohler et al., 1996; Joiner et al., 1997). For a recent review of SK channel literature, see Stocker (2004).

### 1.3.1 Structure and gating

The 6TM elements of SK channels are extremely conserved within the cloned SK1-3 subtypes; approximately 80–90% identity (Castle, 1999) (Figure 1.4 on the following page). SK4 shares a lesser degree of identity with the other $K^+$ family members but is clearly related (Jensen et al., 1998). These cloned channels share much lower levels of identity to the other 6TM $K^+$ channels, except in the pore region. Surprisingly, the fourth TM of SK1-3 does contain several positively charged residues resembling the "voltage sensor" found at this position in voltage-gated potassium ion channels (Figure 1.2 on page 30) even though the channel gating itself does not appear to be voltage-dependent (Kohler et al., 1996).

SK3, the SK subtype used most frequently in this study has been found to have an extended N-terminus containing polyglutamine repeats (Figure 1.4 on the following page), which are not found in SK1 or in SK2 (Chandy et al., 1998). Such polyglutamine repeats are clinically important as they constitute a region of "unstable DNA" which has the potential to expand and give rise to congenital genetic disorders. The evidence for a role of SK channels in such disorders will be described in more detail later.

The entire carboxy-end region of SK channels is intracellular. Gating of SK channels is thought to be mediated by calmodulin (CaM) (Xia et al., 1998), which is constitutively bound to a portion of the carboxy-terminal region, known as the calmodulin binding domain (CaMBD). In other words, the CaMBD has both $Ca^{2+}$-dependent and $Ca^{2+}$-independent interactions with CaM. Charge reversals and mu-

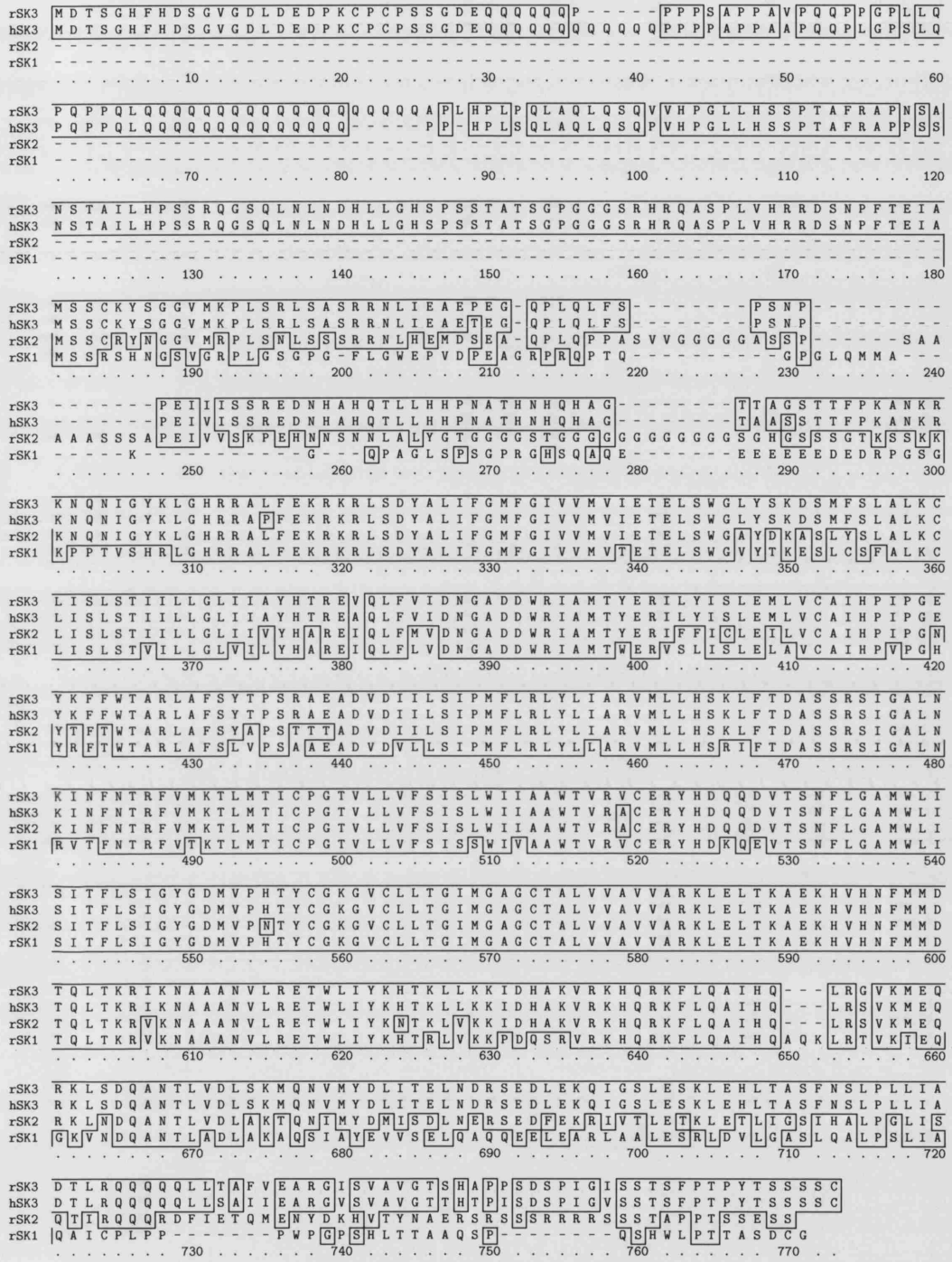


**Figure 1.4:** An alignment of the predicted protein sequences from rat SK1 (rSK1, accession number AF000973), rat SK2 (rSK2, accession number U69882), rat SK3 (rSK3, accession number U69884) and human SK3 (hSK3, accession number NM_002249) channels. Boxed amino acids are conserved between rSK3 and the other SK channels. Alignment was made using the BLOSUM weight matrix with a gap open penalty of 8 and a gap extension penalty of 2. This alignment standardizes the numbering of all the SK channel subtypes cloned to date. The SK numbering system used above is applied throughout this thesis. This figure is modified from Hosseini et al. (2001).

tations of hydrophobic residues in the CaMBD suggest that salt bridges and hydrophobic interactions are involved in producing this constitutive association (Lee et al., 2003; Wissmann et al., 2002). Although it has recently been established that constitutive binding of CaM to the CaMBD is not necessary for channel gating (Lee et al., 2003), the association between the CaMBD and CaM forms the basis of the channel's gating response to calcium and will be described in the next section in more detail.

### Molecular structure of the CaMBD and CaM complex in SK channels

CaM contains an N-lobe and a C-lobe joined by a linker region. Each lobe may bind up to two calcium ions, although when CaM is bound to the CaMBD, the induction of conformational changes that lead to channel activation are thought to only require the N-lobe calcium-binding site (Schumacher et al., 2001), despite earlier reports to the contrary (Xia et al., 1998). In fact, when CaM is bound to the CaMBD, the crystal structure shows that the third and fourth EF hands of the C-lobe cannot chelate calcium anymore (Schumacher et al., 2001).

The CaMBD in rSK2 is formed by amino acids 583→677 (Wissmann et al., 2002). X-ray crystallography has shown that in the presence of $Ca^{2+}$, the CaMBD consists of two $\alpha$ helices, $\alpha 1$ (601→628), and $\alpha 2$ (634→677) joined by a non-helical segment (629→633) (Schumacher et al., 2001). (Figure 1.5 on the next page). More recently the structure of the CaMBD in the absence of $Ca^{2+}$ has been modelled. In contrast to the more ordered, $\alpha$-helical arrangement seen in a $Ca^{2+}$ environment, the CaMBD is thought to only retain an ordered "core" region consisting of three helical turns (Wissmann et al., 2002). This core region, formed by residues 611 to 625 of rSK2, is thought to bind to both calcium-free CaM and calcium-bound CaM.

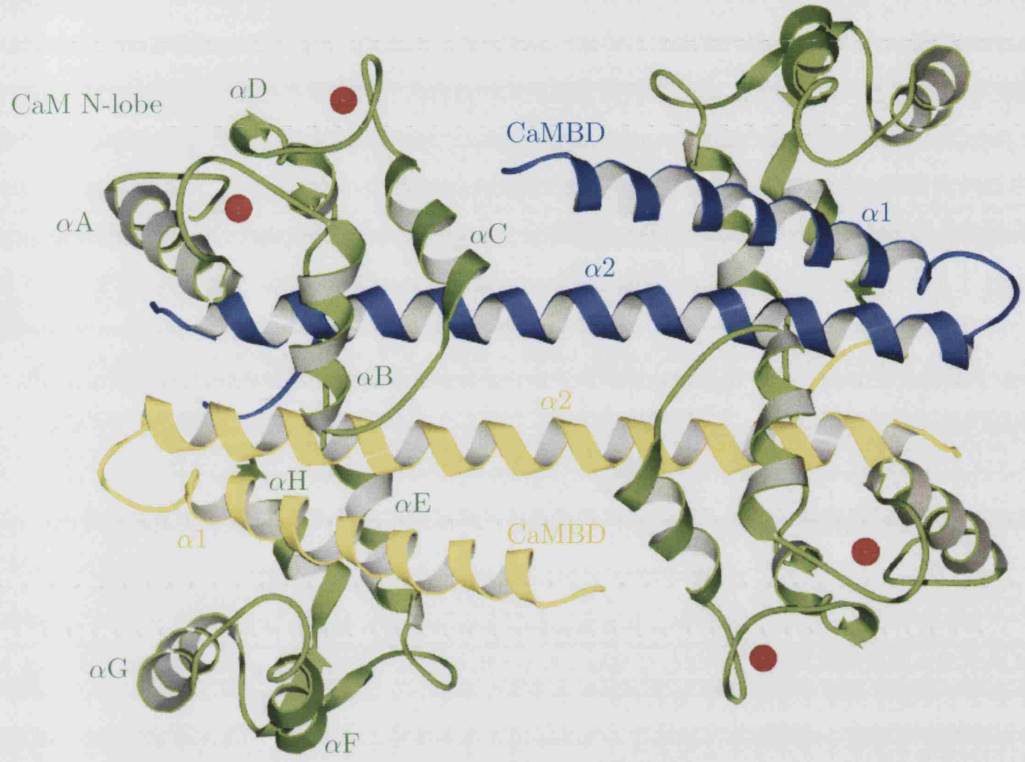


**Figure 1.5:** Ribbon diagram showing the crystal structure of the CaMBD of two SK channel subunits, complexed with $Ca^{2+}$-bound CaM (modified from Schumacher et al. (2001)). This is thought to be the "gating machinery" and is located on the intracellular aspect of the membrane. The S1-S6 TM domains of each subunit together with the membrane would be in the foreground. Each CaMBD (blue and yellow) is formed by residues 583→677 of the SK channel and consists of two helical portions (labelled as $\alpha 1/\alpha 2$) joined by a linker. CaM is shown in green and consists of an N-lobe and a C-lobe joined by a linker. Following binding of $Ca^{2+}$, each C-lobe CaM binds to the CaMBDs of different subunits to form the dimeric complex which is shown in the figure. Red spheres represent calcium ions, while $\alpha$A–$\alpha$H are CaM helices. Picture was generated using Swisspdb viewer and Povray. Monomeric structures were obtained from the Brookhaven protein databank.

### Gating mechanisms

**The SCAM-based chemo-mechanical gating model of SK channels** A putative model of calcium gating based on the pH-dependent gating of KcsA has been proposed (Schumacher et al., 2001). The model (Figure 1.6 on the following page) can be refined to take into account recent evidence, based on the substituted cysteine accessibility method (SCAM), suggesting that the "gate" *per se* might be located at, or extracellular to the selectivity filter of SK channels (Bruening-Wright et al., 2002). Figure 1.6 on the next page has calcium binding exposing a hydrophobic patch on CaM which then binds to the CaMBD of the opposite subunit sufficiently tightly so that the mechanical energy, generated in this process, is used to pull these opposing subunits apart, and open the selectivity filter. This is, in principle, similar to the mechanism proposed for gating of the MthK channel (Jiang et al., 2002). In the MthK channel, binding of calcium to the flexible interfaces causes structural rearrangements in these clefts, which induce a tilt in the adjacent RCK domains that are located either side of the fixed interfaces. In both cases, a chemical stimulus is proposed to generate structural rearrangements in a rigid unit. A linker region then pulls the gate open using the mechanical energy generated by these structural rearrangements. In MthK, the rigid units are the RCK domains either side of the fixed interfaces, whereas in the SCAM-based chemo-mechanical model of SK channel gating, they are the CaM/CaMBD dimers.

### Association of SK channels with accessory subunit

SK channels may associate with accessory subunits. Outlined below is some of the evidence which supports this view.

**Biochemical evidence** Using specific photolabile derivatives of $^{125}$I-apamin, Seagar et al. (1985) identified 86 kDa, 59 kDa, 44 kDa, ~30 kDa, 22 kDa, and 16 kDa receptors for this peptide in primary cultured neurones, rat synaptic plasma mem-

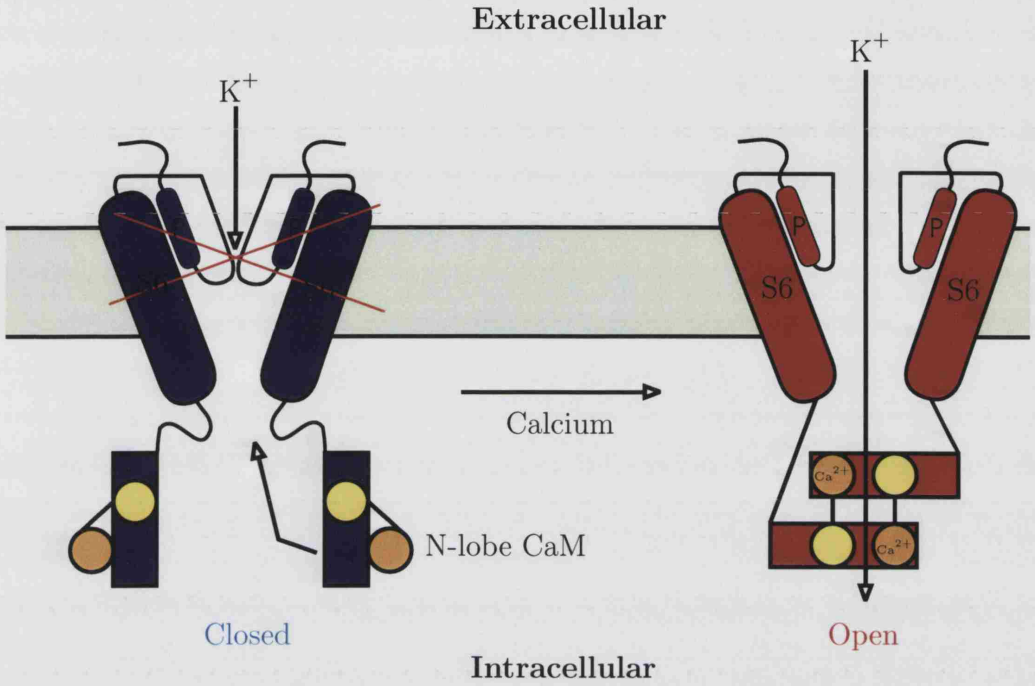


**Figure 1.6:** Illustration of the SCAM-based chemo-mechanical model of SK channel gating (modified from Schumacher et al., 2001). Shown in the diagram are two partial subunits (the pore helix (P), selectivity filter, external vestibule floor, S6 and CaMBD regions from each subunit) of the tetrameric channel (the remaining two subunits would be in the foreground). This model is based firstly on dynamic light scattering studies on the CaMBD/CaM complex, showing that it is monomeric in the absence of intracellular calcium but associates to form a dimeric complex of twice the molecular weight in the presence of internal calcium (Schumacher et al., 2001), and secondly on SCAM using the state-dependent availability of luminal residues to methanethiosulfonate ethylammonium (MTSEA) as an indicator for the approximate location of the channel "gate" (Bruening-Wright et al., 2002). When the N-lobe of CaM has no bound calcium, the pore is closed (left). Following calcium binding to the N-lobe, hydrophobic pockets form which allow each CaM to grab the $\alpha 1/\alpha 2$ helices of the opposite CaMBD. This "grabbing" motion generates a rotational motion of the CaMBDs which is used to open the pore (right), allowing $K^+$ ions to pass through the channel. Arrows indicate the direction of motion of the $K^+$ ions. A similar motion opens the two selectivity filter subunits in the foreground resulting in the open tetrameric channel.

branes, and astrocytes from rat brain. Assignment of the 86 kDa, 59 kDa, 44 kDa, and ~30 kDa components to putative SK channel subunits has been shown through affinity labelling experiments in which the $^{125}$I-apamin receptor is saturated with either SK channel blockers or by blockers of other $K^+$ channels. An excess of well known SK channel blockers, such as tubocurarine, gallamine, dequalinium and scyllatoxin, eliminated affinity labelling of these components, but saturation with CTX (which does not block SK1-3 (Dale et al., 2002; Grissmer et al., 1992; Carignani et al., 2002; Castle, 1999)) did not (Wadsworth et al., 1997). Taken together, this is good evidence that these molecular components are putative SK $\alpha$ or $\beta$-subunits. The 16 kDa and 22 kDa fragments were proposed to be proteolytic degradation products of the ~30 kDa component (Schmid-Antomarchi et al., 1984; Seagar et al., 1986, 1987). Similarly, the 59 kDa, and 44 kDa were believed to be proteolytic fragments of the 89 kDa component (Leveque et al., 1990). The size of this latter protein is consistent with the molecular weight for SK channels (Seagar et al., 1985, 1986). The distribution of the ~30 kDa protein in guinea-pig, rabbit, bovine and rat livers revealed an absence from the latter only (Wadsworth et al., 1994). This was significant because rat hepatocytes generally lack apamin-sensitive calcium-activated $K^+$ conductances in contrast to the other species (Burgess et al., 1981; Takanashi et al., 1992). Furthermore, the specificity of $^{125}$I-apamin for a 30 kDa protein that is associated with SK channels, was demonstrated by the fact that saturation of the $^{125}$I-apamin receptor with either apamin or scyllatoxin eliminated affinity-labelling of the ~30 kDa component (Wadsworth et al., 1994). Both these results provide serious evidence that the ~30 kDa protein (possibly a $\beta$-subunit) is closely associated structurally with SK channels. Syntaxin 1A (a 35 kDa protein) has recently been proposed to be associated with rSK1 at the carboxy-terminus (Fletcher et al., 2003), although a degree of caution was attached to this result. This protein has been found to have several functions in other channels, including trafficking (Bennett et al., 1993), anchoring of calcium channels near to the exocytotic machinery

(Leveque et al., 1994; Rettig et al., 1996), as well as the inactivation of calcium channels and their modulation through G-proteins (Degtiar et al., 2000; Jarvis et al., 2000). More recently, syntaxin 1A has been found to modulate the gating of the $K_v1.1$ voltage-gated potassium channel (Fili et al., 2001).

**Electrophysiological evidence** There is some evidence to suggest that apamin block of human SK1 channels (hSK1) varies with the expression system of choice and, further, that there are multiple components to the concentration-inhibition curve within a given expression system. The $IC_{50}$ for block of hSK1 by apamin in *Xenopus* oocytes has been reported to be >100 nM (Ishii et al., 1997), and 704 pM and 196 nM (Grunnet, Jensen, et al., 2001) (2 site binding fit). In mammalian expression systems, values of 3.3 nM in HEK 293 cells (Strobaek et al., 2000), 8 nM in HEK 293 cells (Shah & Haylett, 2000) and 12 nM in COS cells (Shah & Haylett, 2000), have all been obtained. In addition, some cells produced an unblocked component. It is interesting to note however, in contrast to the findings for hSK1, that rSK2 and rSK3 remain as sensitive to apamin in mammalian and *Xenopus* systems. rSK2 channels expressed in *Xenopus* have been reported to be blocked by apamin with an $IC_{50}$ of 60 pM (Kohler et al., 1996), and 27 pM (Grunnet, Jensen, et al., 2001). A roughly similar value of 83 pM has been obtained in HEK 293 cells (Strobaek et al., 2000). rSK3 has been reported to be blocked by apamin with $IC_{50}$s of 1 nM (Kohler et al., 1996) and 4 nM (Grunnet, Jensen, et al., 2001) in *Xenopus* oocytes, and 2 nM in HEK 293 (Hosseini et al., 2001). A change in the apamin-receptor pharmacology of one subtype in two different cell lines should lead to a change in the pharmacology of the other subtypes unless there are some drastic structural differences amongst them. This is doubtful bearing in mind the primary sequence homology between the SK channel subtypes. One possible explanation is that different $\beta$-subunits bind to different SK subtypes so that the $\beta$-subunit expressed with SK1 differs from SK2 and SK3. Hypothetically, if oocytes express the SK1 $\beta$-subunit but the mammalian

cell lines do not, then this could explain the cell line specific apamin affinities for this subtype. However, if both the oocytes and mammalian cell lines express the $\beta$-subunits of SK2 and SK3, which may be different from that of SK1, then this could give rise to similar apamin affinities for these subtypes in both cell lines.

In *Xenopus* oocytes and T84 cells, which endogenously express hSK4 channels, modulation via cAMP-dependent protein kinases has been demonstrated (Gerlach et al., 2001; Devor & Frizzell, 1998). However, when hSK4 was expressed in HEK 293 cells, this effect was not observed (Gerlach et al., 2000). CHO cells also have been found to show differences in regulatory properties associated with putative $\beta$-subunit expression. For example, hSK4 activity may be modulated in T-lymphocytes using calmodulin-dependent kinases whereas the same channel expressed in CHO cells is insensitive to the same kinase (Khanna et al., 1999).

Vagal motoneurones (Sah, 1995), myenteric neurones (North & Tokimasa, 1983; Hirst et al., 1985) and cultured hippocampal neurones (Lancaster et al., 1991), display apamin-insensitive SK-like currents associated with a slow post action potential afterhyperpolarization (sAHP), that are not inhibited with up to 200 nM apamin. Furthermore, other SK-like currents in pituitary gonadotrophs (L. Vergara et al., 1997), the lateral septum (Caretta, 1994), and the pancreatic islet $\beta$-cells (Ammala et al., 1993), are all insensitive to 1 $\mu$M apamin suggesting that these are not one of the known SK channels. Of course, heteromeric associations between SK1, SK2, and SK3, could produce new channels with different properties, although $\beta$-subunits may be conferring different properties on the channel in native tissue.

### 1.3.2 Assembly

CaM association with the rSK2 subunit protein is thought to take place in a calcium-free environment (Wissmann et al., 2002). Since the cytoplasm of the endoplasmic reticulum is calcium-free it has been proposed that, upon integration of the channel protein into the organelle's membrane during post-translational processing, the

exposure of the CaMBD to the calcium-free cytoplasmic milieu provides the appropriate conditions for assembly with CaM.

Peripheral and several central tissues indicate an overlapping distribution of SK subtype mRNA expression (Kohler et al., 1996; Stocker et al., 1999; Stocker & Pedarzani, 2000), that is particularly striking for SK1 and SK2. In these tissues it is possible for co-assembly to occur between the different SK channel subunits that might be expressed. For example, Ishii et al. (1997) found that 1:1 co-expression of SK1 and SK2 (by co-injecting equal amounts of each mRNA) in oocytes, resulted in a loss of apamin-insensitive currents and concluded that SK1 and SK2 can heteromerize, an idea further supported by work with tandem constructs. M. Miller et al. (2001) have shown that SK3 dominant negatives can combine with endogenous SK2 channels in human Jurkat cells. The Jurkat cell line expresses SK2 endogenously and transfection of SK4 into this cell line shows that these two subunits do not co-assemble (Fanger et al., 2001). The remainder of possible subunit permutations have not been investigated although the homology found amongst the various SK subunits suggests that heteromeric subunit assemblies are likely.

### 1.3.3 Physiological roles of SK channels

#### Generation of the afterhyperpolarization (AHP) in excitable cells

Action potentials are followed by a slow post-spike afterhyperpolarization (AHP) in many neurones. Excitable cells are able to progressively reduce their firing frequencies through the expression of an AHP in response to action potentials. This is known as spike frequency adaptation. The AHP can be divided into three temporally distinct phases of which two are produced predominantly by calcium-activated $K^+$ channels. The first is the apamin-sensitive medium AHP (mAHP) which is predominantly an SK current termed $I_{AHP}$ (Pennefather et al., 1985; Schwindt et al., 1988; Sah, 1996; Stocker et al., 1999). SK2 channels are thought to mediate $I_{AHP}$ in

rat hippocampal neurones (Savic et al., 2001) whereas it is likely that SK3 channels contribute substantially to $I_{AHP}$ in rat superior cervical sympathetic (SCG), rat dorsal vagal neurones and mouse midbrain dopaminergic neurones (Hosseini et al., 2001; Pedarzani et al., 2000; Wolfart et al., 2001). *In situ* hybridization experiments that have demonstrated the distribution of SK mRNA subtypes in central regions corroborate this pharmacological evidence (Stocker & Pedarzani, 2000). The other phase of the AHP, the slow AHP (sAHP), which is produced by a calcium-activated $K^+$ current, termed $sI_{AHP}$, is not apamin-sensitive, but is much longer lasting (ten-fold longer) than $I_{AHP}$. The underlying channels which produce $sI_{AHP}$ have not been identified. In cells exhibiting both $I_{AHP}$ and $sI_{AHP}$, the relatively fast activation of $I_{AHP}$ means that it contributes to "early adaptation" whereas the slower activation of $sI_{AHP}$ produces "late adaptation". Physiologically, both types of AHP play an important role in neuronal signalling through modulation of the information (in the form of a frequency code) being conveyed. The remainder of this section looks at specific examples of the physiological roles of the apamin-sensitive AHP in excitable cells, as well as the roles of SK channels in some non-excitable cells.

### Learning and Memory

The apamin-sensitive AHP in CA1 pyramidal neurones of the hippocampus is generated by SK channels, and can affect the sensitivity of the neurones (Lancaster et al., 1991). Changes in neuronal excitability that occur in the hippocampus, for example through long-term potentiation (LTP), provide a mechanism for learning and memory. LTP refers to the augmentation of the sensitivity of central synapses whereby a constant presynaptic stimulus is converted into a larger postsynaptic response. Blockade of SK channels intensifies the LTP in CA1 pyramidal neurones (Behnisch & Reymann, 1998), and elevated levels of SK3 have been shown to reduce the ability of aged mice to learn new tasks (Blank et al., 2003), consistent with a role for SK channels in learning and memory via the negative modulation of LTP.

### Modulation of circadian rhythms

Recently, apamin-sensitive SK channels have been shown to contribute to the electrical activity of suprachiasmatic nucleus (SCN) neurones (Teshima et al., 2003). These channels are likely to be of the SK3 subtype, since in situ hybridization studies have demonstrated that SK3 mRNA (but not SK1 or SK2 mRNA) is present in the SCN of rats (Stocker & Pedarzani, 2000; Tacconi et al., 2001). Cells from this hypothalamic nucleus (thought to be the rhythm generator) elicit spontaneous action potential firing, with each spike followed by an $I_{AHP}$ that is produced by SK channels (Teshima et al., 2003). It has been found that blockade of this $I_{AHP}$ by SK channel blockers, produces irregular spontaneous action potential firing in the rat SCN (Teshima et al., 2003). This modulation may be observed *in vitro* by apamin blockade of exogenously-induced phase changes to the circadian "clock" (Prosser et al., 1994), and at the behavioural level by apamin-induced insomnia and suppression of deep and paradoxical sleep cycles (Benington et al., 1995; Gandolfo et al., 1996).

### Activity of midbrain subthalamic neurones

SK channels generate the $I_{AHP}$ that follows action potentials during spontaneous discharge of subthalamic neurones. The physiological role of this AHP is threefold. Firstly, it is necessary to produce a regular discharge of spontaneous action potentials known as autonomous activity, since SK channel blockade results in irregular firing in these neurones (Hallworth et al., 2003). Secondly, the AHP limits the firing frequency of subthalamic neurones such that high level excitatory stimuli are filtered (Hallworth et al., 2003). This is achieved since SK channels fire tonically in these neurones at low discharge frequencies, preventing further discharge at higher frequencies. Thirdly, the $I_{AHP}$ also reduces the degree of rebound activity in subthalamic neurones. Rebound activity refers to the high frequency action potential discharge which occurs following the summation of inhibitory potentials. Calcium

entry during rebound activity activates SK channels which then reduce the duration and intensity of rebound activity (Hallworth et al., 2003).

### Smooth muscle relaxation but not normally innervated mature skeletal muscle function

SK channels generate an apamin-sensitive AHP in urinary bladder smooth muscle. This AHP reduces the duration of spontaneous action potential "bursts" and also regulates the amount of calcium entering myocytes since this is determined by action potential frequency (Herrera & Nelson, 2002). Action potential bursts are believed to correspond to single contractions of the smooth muscle tissue (Heppner et al., 1997), whereas calcium entry determines the amplitude of a contraction (Brading, 1992). SK channels therefore limit the basal level of urinary bladder smooth muscle contractions via these two mechanisms (Herrera & Nelson, 2002). Some smooth muscle cells from the canine proximal duodenum produce an apamin-sensitive inhibitory potential when electrically stimulated, that induces muscle relaxation (Bayguinov et al., 1992; Ward et al., 1992). These SK channels could be necessary for normal gastric emptying, since the relaxation which they ultimately produce would allow the stomach contents to easily enter the duodenum. SK channels are also likely to mediate smooth muscle relaxation in other regions of the alimentary canal, such as the gastric fundus (Kitamura et al., 1993), and the proximal colon (Watson et al., 1996; Klemm & Rang, 2002).

In skeletal muscle, SK channels are expressed in immature fibers (myotubes), but are downregulated following neural innervation of the muscle (Schmid-Antomarchi et al., 1985). They produce an AHP that allows repetitive action potential discharge and promotes hyperexcitability in myotubes (Neelands et al., 2001). Low level expression of SK channels is characteristic of normally innervated mature skeletal muscle (Roncarati et al., 2001).

### Other physiological roles of SK channels

**CNS roles** An apamin-sensitive $I_{AHP}$ is present in lateral nucleus neurones of the amygdaloid complex (Faber & Sah, 2002), although the physiological role of this $I_{AHP}$ is still not known. Within the amygdaloid complex, a structure which is thought to place emotional significance to sensory input (LeDoux, 2003), SK channels are not active at physiological calcium concentrations in lateral nucleus neurones as shown by the lack of effect of apamin on the activity of electrically stimulated neurones, but the induction of early spike frequency adaptation following the application of 1-ethyl-2-benzimidazolinone (EBIO) (Faber & Sah, 2002) (which augments the calcium sensitivity of SK channels (Pedarzani et al., 2001)). Elsewhere in the central nervous system, SK2 channels in immature rat Purkinje neurones form the majority of the current that comprises the apamin-sensitive AHP (Zeniou et al., 2002; Cingolani et al., 2002). This AHP may regulate the spontaneous calcium oscillations in Purkinje cells that are generated by its endogenous electrical activity (Cingolani et al., 2002). The $I_{AHP}$ in dorsal vagal neurones is generated by SK3 channels and modulates the spontaneous activity of these cells (Pedarzani et al., 2000), which in turn regulates parasympathetic cardiac and visceral functions.

**PNS roles** Apamin-sensitive potassium channels (hSK2) in hepatocytes are believed to sense changes in cell volume (Roman et al., 2002). However, since hepatocytes are non-excitable cells, SK channels do not contribute to an $I_{AHP}$ (as in central neurones). Adrenal medulla chromaffin cells are known to contain SK channels (Artalejo et al., 1993), and these channels are thought to inhibit catecholamine release in order to control cellular responses to nicotinic and muscarinic stimulation (Nagayama et al., 1997). T-cells are known to express SK2 and SK4 channels (Grissmer et al., 1992, 1993; Schlichter et al., 1993; Hanselmann & Grissmer, 1996), and are thought to play major roles in the regulation of cell volume, calcium signalling, cell membrane potential (Lewis & Cahalan, 1995), the mitogen activation

cascade leading to the antigenic activation of T-cells (Grissmer et al., 1992) and T-cell proliferation (Jensen et al., 2001) .

### 1.3.4 Pathophysiology and channelopathies of SK channels

#### Schizophrenia and Parkinson's disease

*In situ* hybridization experiments have shown that SK3 mRNA is particularly concentrated in midbrain dopaminergic nuclei (Stocker & Pedarzani, 2000; Kohler et al., 1996). Altered dopaminergic activity in midbrain neurones, which can occur through selective activation of SK channels via T-type calcium channels (Wolfart & Roeper, 2002), has been associated with schizophrenia (Svensson, 2000).

One of the neurological symptoms of Parkinson's disease is burst activity in neurones from the subthalamic nucleus (STN) (Bergman et al., 1994; Levy et al., 2000, 2001). SK channels are believed to oppose the transition from rhythmic to burst firing in neurones of the STN (Hallworth et al., 2003) and so SK channels may play some role in preventing this disease.

#### Denervated skeletal muscle and myotonic dystrophy

Following skeletal muscle denervation, SK3 mRNA gene expression increases significantly (Pribnow et al., 1999). The upregulation of SK channels in denervated muscle leads to the production of a post-spike AHP. Although the AHP hyperpolarizes the membrane, the net result is hyperexcitability (C. Vergara et al., 1993). This may be due to the recruitment of sodium channels out of the inactivated state as a result of the AHP-induced membrane hyperpolarization (Ramirez et al., 1996), or it may be due to the accumulation of $K^+$ in the narrow T-tubule structures, both of which have the effect of depolarizing the cell and bringing it closer to its threshold for firing (Neelands et al., 2001).

SK3 mRNA expression in muscle is also increased in adult patients with myotonic

dystrophy, in which affected persons cannot relax muscles normally due to muscle cell hyperexcitability (myotonia) (Kimura et al., 2003). Apamin injection into the muscles of patients with myotonic dystrophy virtually ablated myotonic discharge (Behrens et al., 1994). A mechanism has been proposed to account for myotonia based on the generation of hyperexcitability as seen in denervated muscle (Kimura et al., 2003).

### Hypertension

SCG neurones from spontaneously hypertensive rats show repetitive firing in response to a depolarizing pulse, whereas SCG neurones from wildtype (WT) rats show only one or two action potentials in response to the same pulse (Jubelin & Kannan, 1990). The lack of spike adaptation in the former had been shown to result from the lack of activation of apamin-sensitive SK channels. This may also form the basis of hypertension in some genetically hypertensive individuals.

### Sickle cell anaemia

An increased calcium permeability in erythrocytes is characteristic of the genetic disease, sickle cell anaemia. This calcium influx activates hSK4 channels in human erythrocytes. Under normal conditions, erythrocytes actively maintain high intracellular $K^+$ and low intracellular $Na^+$ levels through the $Na^+/K^+$ pump. This generates a strong diffusional gradient resulting in the efflux of $K^+$ and water through activated hSK4 channels in diseased erythrocytes (Hoffman et al., 2003). The loss of water in turn results in cell shrinkage or "sickling", which is characteristic of the disease.

### SK channelopathies

Following cloning of the human SK3 cDNA, Chandy et al. (1998) found two arrays of trinucleotide (CAG) repeats. The downstream repeat sequence was highly poly-

morphic in size, varying between 12 and 28 repeats. These extended polyglutamine repeats in the SK3 channel gene have been linked to certain hereditary neurodegenerative diseases (Reddy & Housman, 1997; Zhuchenko et al., 1997). A significant association was found between these extended SK3 alleles and schizophrenia (Chandy et al., 1998). However, other reports have not shown a significant association (Navon et al., 1998; Austin et al., 1999; Frebourg et al., 1998). Tomita et al. (2003) have proposed that the quantitative expression of SK3 and a dominant negative variant of SK3 which lacks an N-terminus and first transmembrane segment, SK3-1B, may be involved in the pathogenesis of schizophrenia. SK3-1B is found naturally and comprises 20-60% of SK3 channels in the brain (Tomita et al., 2003). Furthermore, a different truncation of the SK3 channel with a similar effect to SK3-1B, known as SK3-$\Delta$ has been found in patients with this disease (Tomita et al., 2003). A tentative association has also been found between expanded alleles of SK3 and patients with bipolar disorder I (a manic-depressive disorder) (Chandy et al., 1998). Although the association was not significant, there was an overrepresentation of expanded alleles in patients with the neuropsychiatric disorder.

### 1.3.5 Extracellular blockers of SK channels

SK channel blockers can be broadly classified into either natural peptidic toxins or small synthetic compounds.

#### Natural peptidic toxins

The most commonly used natural peptidic toxin blockers of SK channels are apamin, and scyllatoxin (leiurotoxin I), both of which have nanomolar affinity for all the channel subtypes.

**Apamin** The first toxin to be characterized on clonal SK channels was apamin (Kohler et al., 1996). This SK channel blocker has a high potency ($IC_{50}$ = 60 pM for

rSK2) and exquisite blocking selectivity of certain types of SK channel (compared with other calcium-activated potassium channels; see Blatz and Magleby (1986); Burgess et al. (1981). Although highly selective for SK channels, apamin has been found to additionally block L-type cardiac calcium channels (Schetz & Anderson, 1995). Nevertheless, it has proved to be a useful tool for studying SK channel pharmacology, and has been used considerably in structure-activity relationships in various tissues in the past. Further, studies involving radiolabelled apamin have demonstrated the neuroanatomical distribution of SK channels in brain slices (Gehlart & Gackenheimer, 1993).

The octadecapeptide is held in a rigid cyclic conformation resistant to denaturing conditions by two disulphide bridges (Habermann, 1984) at $Cys_1 \rightarrow Cys_{11}$ and $Cys_3 \rightarrow Cys_{15}$ (toxin residue numbers are denoted by the subscript throughout this thesis). The overall charge on the molecule is conferred by five residues, four of which are positive ($Cys_1$, $Lys_4$, $Arg_{13}$, $Arg_{14}$), and one which is negative ($Glu_7$), resulting in a basic molecule.

Attempts to identify the pharmacophore have shown that apamin binding is complex. The guanidium groups of the two contiguous arginine residues at positions 13 and 14 are thought to represent at least part of the pharmacophore of the toxin (Vincent et al., 1975; Hugues et al., 1982). However, the positive charges *per se* of the arginines are not responsible for the interaction with SK channels as it has been shown that substitution of either $Arg_{13}$ or $Arg_{14}$ (but not both arginines) with a cationic lysine residue hardly affects toxin binding (Granier et al., 1978). The role of the arginine residues has been further elucidated by creating partial apamin structures which have been used to assess the importance of the congruent guanidium groups to blocking activity (Demonchaux et al., 1991). The results of these selective analogues suggest that congruent guanidium groups are required for blocking activity but that they provide a permissive rather than a direct interaction role *per se*. C. Vergara et al. (1998) have created a model of apamin binding in rSK2

based on two interaction points, the first between $Glu_7$ in apamin and asparagine at position 555 in the channel, and the second between $Arg_{13}$ in apamin and aspartic acid at position 528 in the channel. These interaction points had previously been found to be responsible for high affinity apamin binding to SK channels (Ishii et al., 1997). However, the interaction of apamin with SK channels is undoubtedly much more complicated than this and probably involves residues between S1 and S6, both inside and outside the pore region (D'hoedt et al., 2004).

Expression of SK clones was initially performed using *Xenopus laevis* oocytes. It became accepted for a few years that hSK1 was an apamin-insensitive channel whereas SK2 and SK3 form apamin-sensitive channels (Kohler et al., 1996; Ishii et al., 1997). However, recent studies have contradicted such findings (Dale et al., 2002; Shah & Haylett, 2000). In particular, the expression system of the cloned channel has been proposed to be the cause of the disparate results (Shah & Haylett, 2000; Strobaek et al., 2000). This led to a re-examination of the apamin pharmacology in *Xenopus laevis* oocytes which demonstrated that *all* three subtypes are inhibitable by apamin (Grunnet, Jensen, et al., 2001). In particular, the dose-response curve for hSK1 (obtained through voltage-clamping the oocytes) may be fitted best to a biphasic curve as if apamin is able to bind competitively at two distinct sites on the channel (Grunnet, Jensen, et al., 2001). The authors suggest that the data are not too different from that in mammalian cell lines such as HEK 293 (Shah & Haylett, 2000), although they still conclude that the kinetics of block require further clarification. However, $I^{125}$-radiolabelled binding experiments in *Xenopus* oocytes confirm that all three subtypes bind apamin with $K_d$'s of approximately 390 pM for hSK1, 4 pM for rSK2, and 11 pM for rSK3 (Grunnet, Jensen, et al., 2001).

### Scorpion toxins

Scyllatoxin (also known as Leiurotoxin I) is one of a family of scorpion toxins isolated from the venom of the scorpion, *Leiurus quinquestriatus hebraeus*. It is

highly cationic (+3) and possesses three disulphide bridges between $Cys_3$-$Cys_{21}$, $Cys_8$-$Cys_{26}$, and $Cys_{12}$-$Cys_{28}$ (Calabro et al., 1997). Structure-activity studies have shown that reduction or S-alkylation of these disulphide bridges causes a loss of biological activity (Martins et al., 1995). Its 3-D structure has been determined by NMR (Martins et al., 1995) showing, at the tertiary level, an $\alpha$-helix between residues 6→16 linked to antiparallel $\beta$-sheets between residues 18→29 by the disulphide bonds at $Cys_8$-$Cys_{26}$ and $Cys_{12}$-$Cys_{28}$ (Q. Zhu et al., 2002; Martins et al., 1995) (the remaining disulphide bridge is not thought to stabilize the conformation or to be necessary for activity of the toxin (Calabro et al., 1997)). The resultant protein is a compact, roughly ellipsoidal (25Å by 11Å) molecule where all the residues, except for the cysteines, are exposed to solvent (Martins et al., 1995). $Arg_6$ and $Arg_{13}$ of scyllatoxin have been proposed to be analogous to $Arg_{13}$ and $Arg_{14}$ on apamin due to the conformational mobility of their side chains (Martins et al., 1990). All the scorpion toxins generally block $K^+$ channels by physically occluding the pore and leaving gating unaffected (Giangiacomo et al., 1992; MacKinnon & Miller, 1988).

The peptide toxin, scyllatoxin, is a potent SK channel blocker (Shakkottai et al., 2001; Strobaek et al., 2000; Hosseini et al., 2001). In particular, it blocks hSK2 with an $IC_{50}$ of 0.2 nM in Jurkat cells (Hanselmann & Grissmer, 1996), cloned hSK3 channels with an $IC_{50}$ of ~1 nM (Shakkottai et al., 2001), but SK4 is completely insensitive to scyllatoxin up till 1 μM (Logsdon et al., 1997). Substitution of $Met_7$ with the unnatural, cationic diaminobutanoic acid (DAB) generates a toxin molecule (Lei-$DAB_7$) with a much higher selectivity for SK2 over SK3 channels compared to unmutated scyllatoxin (Shakkottai et al., 2001). Lei-$DAB_7$ has been used to demonstrate a strong interaction between channel residue 555 and $DAB_7$ of this mutated toxin (Shakkottai et al., 2001) using a point mutant of the SK channel which significantly increases apamin affinity compared to the WT channel (Ishii et al., 1997). $DAB_7$ is residue X in the RXCQ motif of Lei-$DAB_7$. This RXCQ sequence is also present in apamin, with X being arginine ($Arg_{14}$), and superposition

of this structural motif from apamin onto the RXCQ motif of scyllatoxin (from which Lei-$DAB_7$ is generated) demonstrates a similar spatial arrangement (Shakkottai et al., 2001). This sequence is important for determining the binding properties of both scyllatoxin and apamin; $Arg_{13}$ and $Arg_{14}$, which form the first two amino acids of apamin's RXCQ motif, are important for apamin's blocking activity, and $Arg_6$ (adjacent to X in the RXCQ motif) of scyllatoxin contains a necessary charge and is an optimal size for binding to SK channels (Shakkottai et al., 2001). Therefore, these toxins not only share a good degree of structural homology with each other, but also share some molecular similarities regarding their binding to SK channels.

### Small synthetic compounds

Tubocurarine, atracurium, and pancuronium are all synthetic compounds that block SK channels with an $IC_{50}$ in the micromolar range (Cook & Haylett, 1985; Nohmi & Kuba, 1984; Jenkinson et al., 1983). Another such compound, dequalinium (Figure 1.7 on the following page), is a relatively potent ($\mu$M affinity on hSK1 (Shah & Haylett, 2000)) non-peptidic blocker of SK channels. Dequalinium contains two quinolinium groups joined by an aliphatic linker. The quinolinium group gives optimal blocking potency compared with other charge configurations, and this probably arises as a result of the ring-shaped electrostatic field around this group (Galanakis, Davis, et al., 1995). A methyl group on each of the quinoliniums (position 2) is not thought to contribute to its potency on SK channels (Galanakis et al., 1995), whilst an amino group on the heterocyle (position 4) has been found to produce a substantial contribution suggestive of an important role for the delocalized charge in binding (Galanakis et al., 1995). In an effort to make more potent and selective synthetic blockers, a series of UCL compounds based on the structure of dequalinium have been synthesized, with differing chemical properties. The linker region of these UCL compounds is not thought to interact with the channel but has been manipulated in an effort to alter the relative positions of the charged heterocycles,

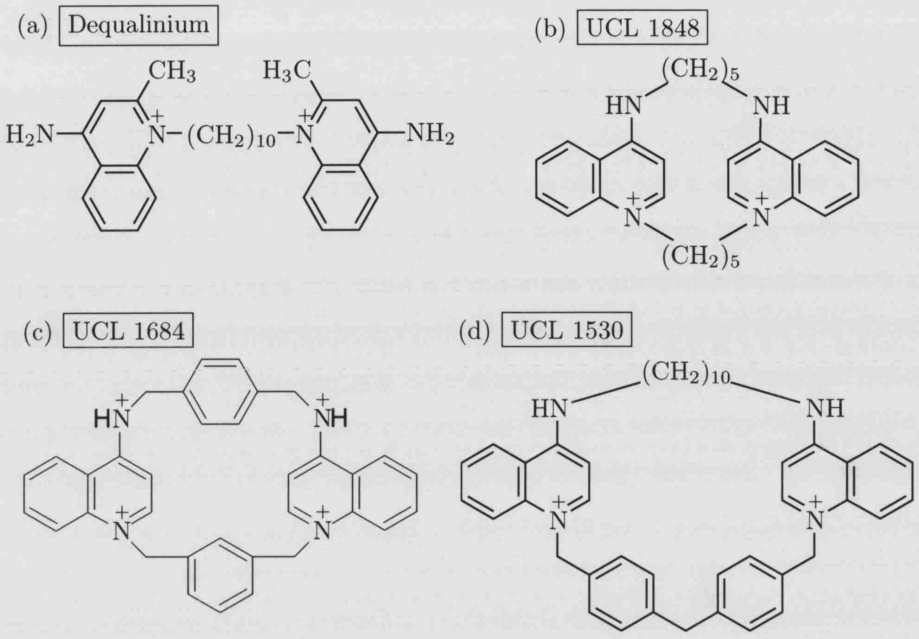


**Figure 1.7:** The structure of dequalinium and related UCL compounds (a)-(d). Double-ringed structure in each compound and carrying the charged nitrogen is the quinolinium

resulting in an optimal aliphatic chain length of 5 carbon atoms (for block of the apamin-sensitive AHP in rat SCG neurones) (Galanakis et al., 1996). It is believed that the 5 carbon atom linker holds the quinoliniums an optimal distance apart for SK channel interaction (Chen et al., 2000). Further modifications to the linker that force the quinoliniums to occupy more stricter spatial positions are described next.

**Rigidification of the linker** Rotation about the single bonds of the aliphatic linker may occur which can lead to stereoisomerism. Thus quinoliniums of, for example, dequalinium may occupy cis-(synperiplanar) or trans-(antiperiplanar) positions (Chen et al., 2000). A few structural modifications are necessary in order to rigidify the molecule so that the quinoliniums occupy stricter spatial positions. These include introducing double or triple bonds into the linker. Briefly, a single bond ($\sigma$ bond) has cylindrical symmetry whereas a double bond ($\Pi$ bond) needs to be broken in order for the carbon atom to rotate. The introduction of a benzene ring into the linker, as in UCL 1684 (Rosa et al., 1998), will also reduce the number

of freely rotatable bonds. Further rigidification can be achieved by generating cyclophane structures through the addition of two linkers between the quinoliniums. These linkers are attached to both the ring N atoms and exocyclic N atoms in order to constrain the quinoliniums. This would be most rigid if both linkers were of similar lengths, as they are in UCL 1848 and UCL 1684, but in any case conformational changes should be preventable even if they are not, as is the case for UCL 1530.

**UCL 1684** This is one of the most potent non-peptidic blockers of SK channels. It blocks hSK1 with an $IC_{50}$ of ~1 nM, rSK2 ~0.36 nM, and rSK3 ~6 nM when expressed in CHO cells (Hosseini et al., 2001). The conformational stability resulting from the benzene linkers is believed to induce the low-energy conformation that binds to SK channels most potently. However, it has very little blocking action on the intermediate conductance calcium-activated $K^+$ channel in rabbit red blood cells (Malik-Hall et al., 2000).

**UCL 1530** The interesting fact about UCL 1530 is its relative selectivity compared to apamin and UCL 1684 on sympathetic SCG neurones and hepatocytes. Whereas UCL 1684 is not able to discriminate between different subtypes of SK channel in these cells, UCL 1530 and apamin can (Dunn et al. (1996), personal communication with Dr Benton). Therefore, it might be possible to shed some light on the mechanism of apamin binding to SK channels by understanding the mechanisms of UCL 1684 and UCL 1530 binding to SCG neurones and hepatocytes.

**UCL 1848** UCL 1848 blocks the clonal SK channels with similar affinities to apamin. An $IC_{50}$ value of ~1 nM has been demonstrated in hSK1 (Shah & Haylett, 2000), ~0.1 nM in rSK2 (Hosseini et al., 2001), and ~2 nM in rSK3(Hosseini et al., 2001). The 5 carbon atom aliphatic linker is believed to hold the charges an optimal distance apart for SK channel interaction (Galanakis, Ganellin, et al., 1995). Together with UCL 1684, this is one of the most potent, selective non-peptidic

blockers of clonal SK channels (Chen et al., 2000).

## 1.4 Expression systems

It was decided to express the rSK3 channel in a mammalian cell line, since all the SK channels used in this study had been cloned from either rat or human libraries. Cell lines derived from human embryonic kidney (HEK 293) cells and Chinese hamster ovary (CHO) cells were chosen for this reason as well as due to their availability and well characterized endogenous currents. HEK 293 cells have been reported to contain endogenous calcium channels (Berjukow et al., 1996), chloride channels (G. Zhu et al., 1998) and potassium channels (Yu & Kerchner, 1998). Single channel data indicate the presence of five types of chloride conductances, two types of potassium conductances and a 50 pS calcium-dependent cation conductance. Yu and Kerchner (1998) suggested the majority of the conductance is a delayed rectifier type with a small contribution from inward rectifier channels. Furthermore, a low density tetradotoxin-sensitive sodium channel has been identified (Ukomadu et al., 1992). This heterogenic mix of currents has the ability to "contaminate" transfected SK channel currents and so it is desirable that they are minimal. The CHO cell line on the other hand is thought to only contain sodium channels (Lalik et al., 1993), but no endogenous potassium current. The latter may therefore be a better choice for expressing SK channels.

## 1.5 The present study

### 1.5.1 Main Aim

- To design, produce, and characterize a series of point mutations to investigate SK channel structure and pharmacology

### 1.5.2 Rationale

UCL compound interactions with residues of SK channels are not very well understood at present. Identifying these residues would help to facilitate this understanding and lead to the development of even more potent and selective blockers. This study is aimed at identifying these residues, as well as addressing several other issues concerning SK channels, that require investigation or further clarification:

Ishii et al. (1997) demonstrated a high affinity TEA site through a V553Y–rSK2 mutant. This data demonstrated that the pore of SK channels may have a similar structure to Shaker channels, amongst others, that also contain analogous residues responsible for high TEA affinity. It remains to be clarified in the remaining subtypes, SK1, SK3, and SK4, whether this is the case.

Ishii et al. (1997) have determined that two pore residues can account for almost all the high affinity apamin binding to SK channels expressed in oocytes. Since the affinities of UCL 1848 on SK1-3 appear to be very similar to apamin, the hypothesis that these two residues may produce a high affinity interaction with UCL 1848 will be investigated in this study.

The region of the channel to which UCL compounds bind has not been confirmed. It is not yet known whether UCL compounds bind to the pore or to some allosteric site.

The capacity for the SK subunits to heteromerize has not been fully investigated. Ishii et al. (1997) showed that SK1 could assemble with SK2 in co-expression experiments, whereas Fanger et al. (2001) demonstrated that SK2 could not assemble with SK4. M. Miller et al. (2001) have shown that a concomitantly mutated and truncated SK3 dominant negative can suppress endogenous SK2 currents in human Jurkat cells. It is not known whether assemblies of SK1–SK3, SK1–SK4, and SK3–SK4 are possible.

These issues have been addressed by creating and testing point mutations of residues in the pore of the rSK3 channel, with the dual aim of comparing the pharmacology of UCL compounds and other drugs. The next section provides a brief summary of these mutants.

### 1.5.3 General design of mutants and selection of blockers

Generally all point mutations were designed on the basis of relevant findings in Shaker and other potassium channels or due to their likely position based on similarity to the KcsA channel structure (Figure 1.8 on page 66). The numbering system used for SK1-4 in Figure 1.8 on page 66 is the same as that shown in Figure 1.4 on page 40, and has been used throughout this thesis. The remaining channels shown in Figure 1.8 on page 66 have been numbered conventionally. All point mutants have been named using the abbreviated form of the amino acid found in the WT channel, followed by the position of this residue in the channel's amino acid sequence shown in Figure 1.8 on page 66, and then by the abbreviated form of the mutated amino acid. Finally, the channel in which the mutation has been created is identified following a hyphen after the mutated amino acid. This nomenclature has been used throughout this thesis, not only for rSK3 but all the other channels which are mentioned. The abbreviated forms of the amino acids used in this thesis can all be found in Appendix C. Figure 1.9 on page 67 shows the positions of the mutated amino acids in a model of the rSK3 channel. This model is the crystal structure of KcsA in which equivalent residues in SK have been highlighted. Broadly speaking two types of mutation were created; those designed to alter the channel pharmacology ("pharmacology" mutants) and those designed to potentially create dominant negative constructs ("dominant negative" mutants) which might be useful in assessing the co-assembly of channel subunits. The V529K-rSK3, D528K-rSK3, H555K-rSK3 and V529L-rSK3 mutants fell into the former category, whereas the G548R-rSK3 and W538F-rSK3 mutants, together with the double point mutant,

H555N,G559A-rSK3, fell into the second. Some "structural" mutants were created to probe similarities to the Shaker and KcsA channel. These were the V553F-rSK3 and G535D-rSK3 mutants. UCL compounds have been predominantly used to determine the pharmacological effects of these mutations. UCL 1848 was chosen due to its high affinity on SK channels and its similar affinities to apamin on each subtype that may provide an insight into possible apamin/channel interactions. UCL 1684 was chosen, again due to its nanomolar affinity on rSK3, but in combination with UCL 1530 may provide some insight into why these two compounds differ in their effects on SCG neurones and hepatocytes (Dunn et al., 1996). This may facilitate the understanding of apamin as well as UCL compound selectivity. Finally, although apamin is the classical blocker of SK channels, it has been reported to take lengthy times for its application and washout from SK channels (Ishii et al., 1997). Therefore, it was decided not to use this toxin for experiments in this study, because it may prove comparatively difficult to obtain reliable pharmacological data.

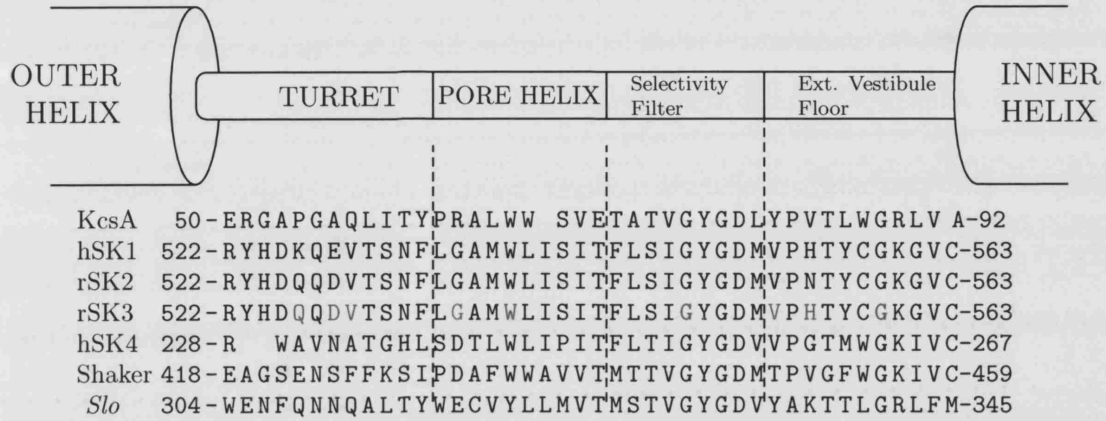


**Figure 1.8:** An alignment of the P-loop amino acid sequences of KcsA, hSK1, rSK2, rSK3, hSK4, Shaker and *Slo*. The positions of the putative pore regions are shown. Dotted lines indicate the division of aligned sequences into these pore structures. The amino acids which have been highlighted in blue are the "pharmacology" mutants, those highlighted in red are the "dominant negative" mutants and those highlighted in green are the "structural" mutants. The valine residue at position 519 in the rSK3 sequence is out of the range of the pore region shown. Numbers represent residue position at either end. The SK numbering system used above is the same as that shown in Figure 1.4 on page 40 and has been used throughout this thesis. The full names of the amino acids represented by each of these symbols in the above sequences can be found in appendix C.

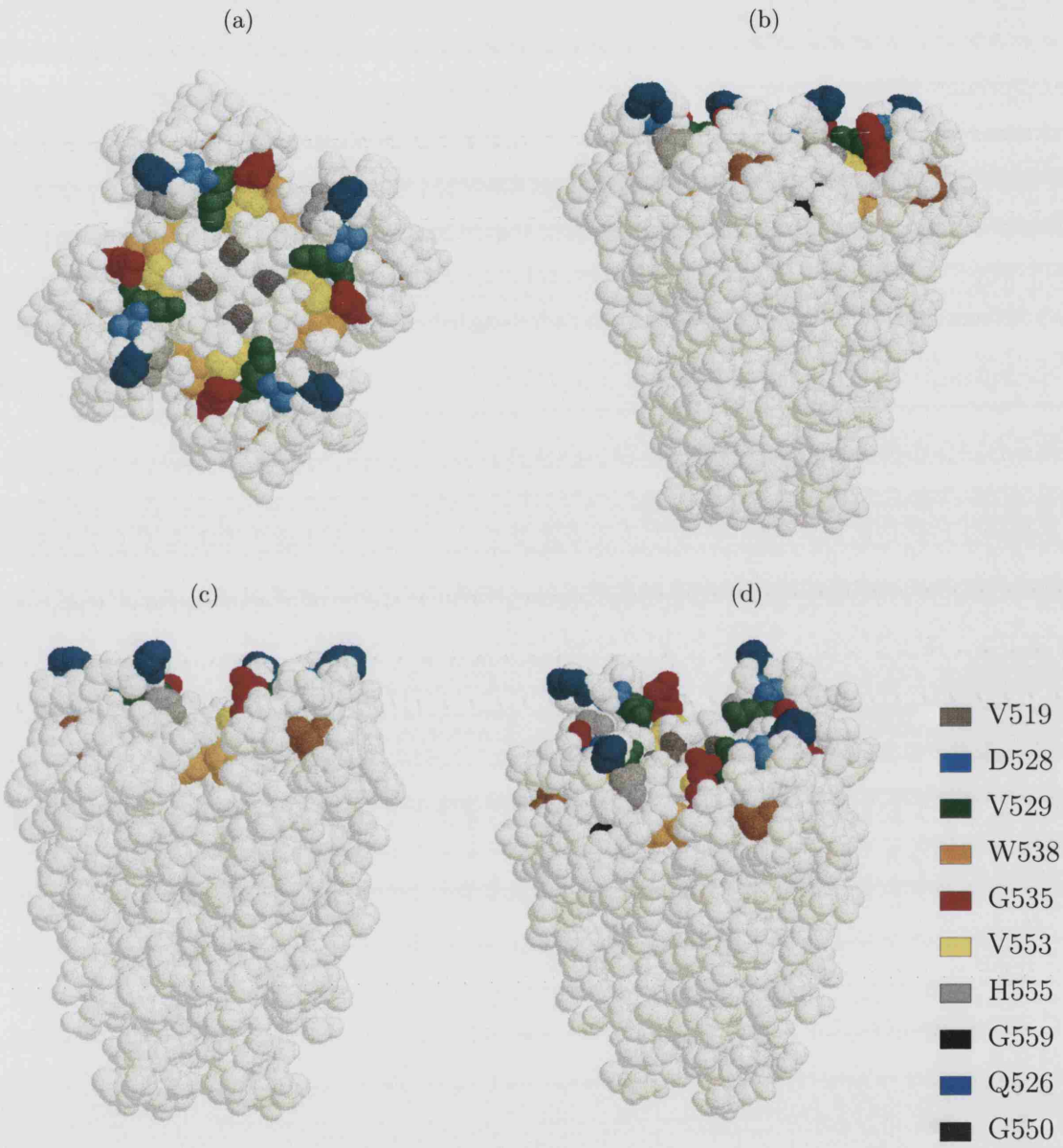


**Figure 1.9:** Spacefill diagram showing a 3-D 'map' of the point mutations used in this study on a hypothetical model of the pore region (last two transmembrane elements and P-loop) of rSK3 as estimated from the crystal structure of KcsA. The top view of the model channel is shown in (a), side views in (b) and (c), while (d) is an oblique view. Colour code is shown in the key on the right. Pictures were generated in Protein Explorer.

# Chapter 2

# Methods

## 2.1 Molecular Biology

Thirteen point mutations of the amino acid sequence in the pore of the rSK3 channel were designed in order to investigate structure-pharmacology relationships. Two methods of producing these point mutants have been used. One is a commercially available kit (QuikChange, Stratgene Ltd) whereas the other uses a simple overlap extension PCR protocol.

### 2.1.1 Method 1: QuikChange XL (Strategene) site-directed mutagenesis

The basis of this kit is to produce mutated copies of the gene and its plasmid from a WT template by PCR. The oligomers used overlap perfectly so that when they are extended, the copies will form a replica plasmid with staggered nicks (Figure 2.1 on the next page). Then, because the template DNA has been purified from bacteria, it will be methylated. The subsequent use of enzyme, DpnI, which digests only methylated (WT) DNA strands is the basis of selection for this kit. A schematic of procedure is shown in Figure 2.1 on the following page.

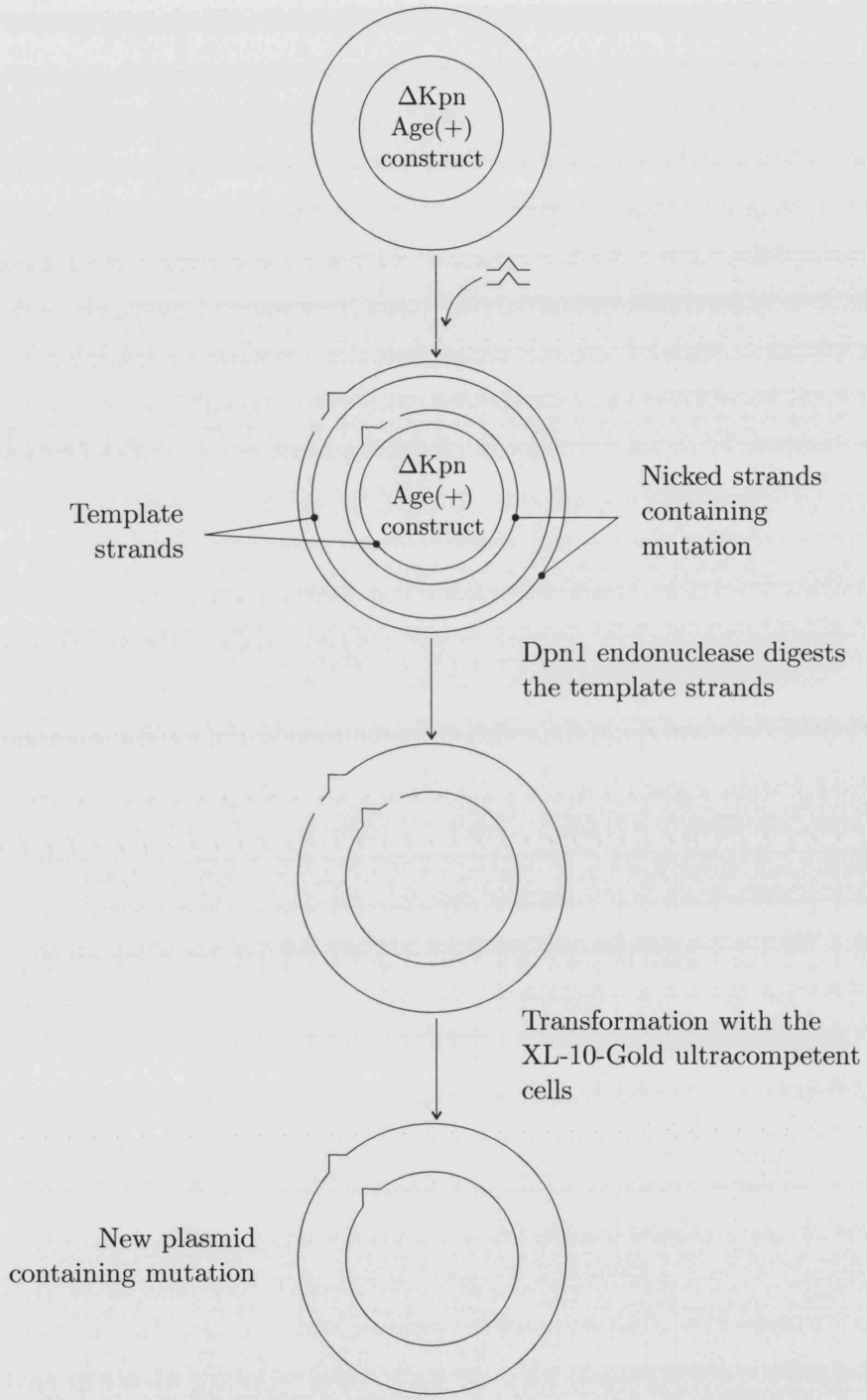


**Figure 2.1:** Overview of the principle steps in the production of point mutants using the Quikchange mutagenesis kit. First, double-stranded plasmid DNA is used as a PCR template to produce unmethylated, nicked cDNA. DpnI cuts only the methylated (WT) DNA leaving nicked mutated copy strands that are resealed by transformation. In this way, all the transformation colonies should be mutant ones. The indentations in the nucleotide strands indicate the site of the point mutation.

### Primer design

Primers were between 24 and 39 bases long, containing the mutation in a centralized position. They had a minimum two-fifths glycine and cysteine (GC) content, and a melting temperature ($T_m$) of at least 78 °C when calculated using the following formula:

$$T_m = 81.5 + 0.41(\%\text{GC}) - \frac{675}{N} - \%\text{mismatch}$$

where $N$ is the number of bases and "%mismatch" is the percentage change in the base sequence. By taking advantage of the degeneracy of the genetic code, it was possible to choose codons which made the required amino acid change but involved creating the fewest nucleotide changes to the WT DNA sequence. All primers were ordered from MWG Biotech or Sigma and came purified by fast polynucleotide liquid chromatography (MWG) or by polyacrylamide gel electrophoresis (Sigma).

### DNA constructs used in generation of point mutants

Two plasmids were constructed to facilitate the manufacture of pore mutations (Figure 2.2 on the next page). Both are based on the construct described by Hosseini et al. (2001) where the rSK3 gene was subcloned into pcDNA3.1 for expression under control of the CMV promoter. The first eliminates a KpnI site in the pcDNA3.1 polylinker and the second introduces a silent AgeI restriction site at the 3' end of the pore sequence. The elimination step reduced the KpnI sites in the plasmid to a single locus around the pore, allowing mutated pore sequences to be subcloned into the WT using this remaining KpnI site (see later). The silent AgeI site was used mainly for diagnostic purposes (discussed later). The latter allowed a fast and effective means of identifying mutant colonies as outlined in Figure 2.5 on page 79.

### Protocol

A basic QuikChange PCR reaction consisted of the following:

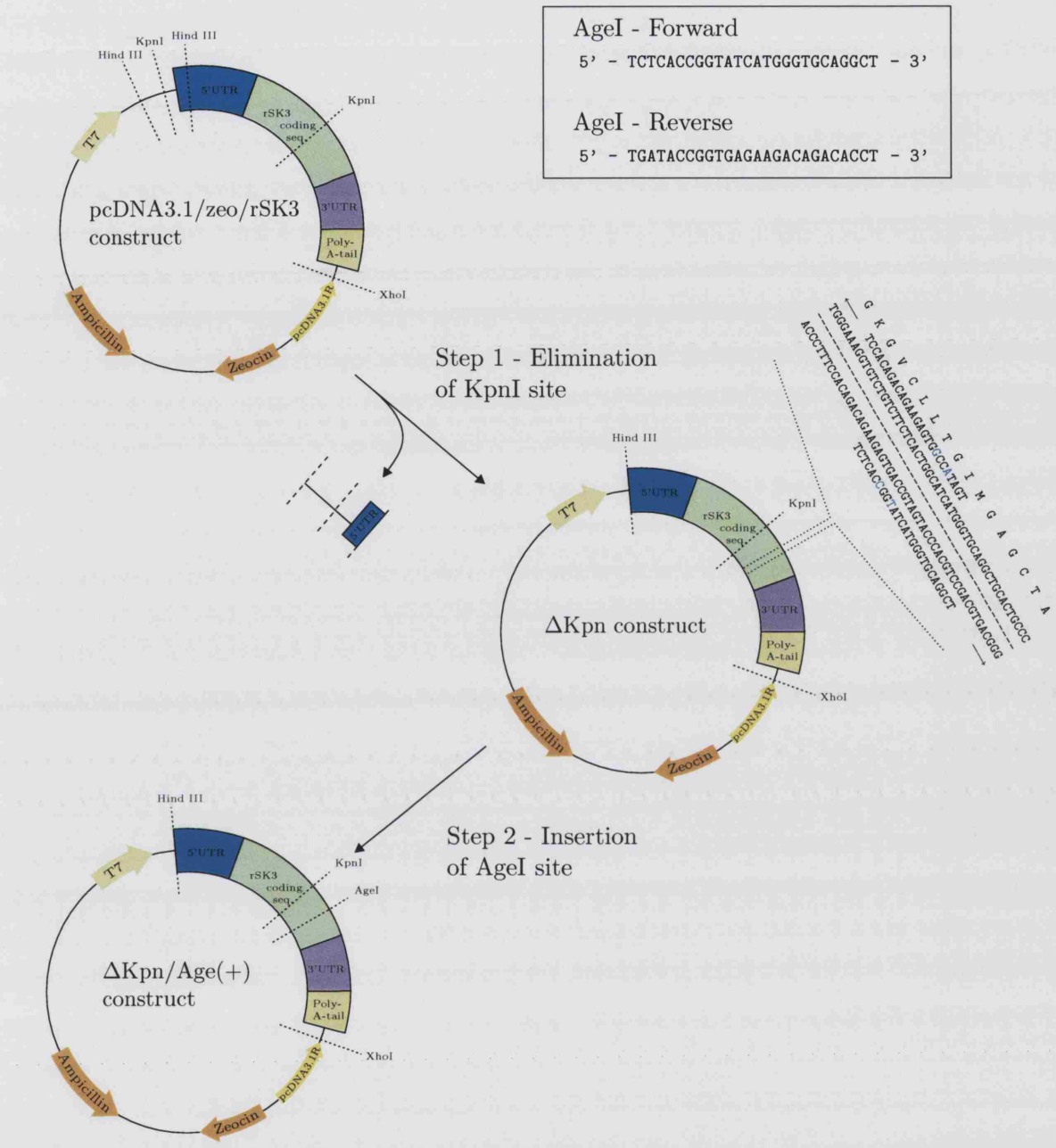


**Figure 2.2:** Schematic showing the production of the ΔKpn and ΔKpn/Age(+) constructs from the pcDNA3.1/zeo/rSK3 plasmid. For the ΔKpn construct a KpnI site in the polylinker was removed by digesting with Hind III at sites in the polylinker of pcDNA3.1 and the 5' untranslated sequence of rSK3. The ΔKpn/Age(+) construct was subsequently made by introducing a silent AgeI site into the SK3 sequence. The sequence of the AgeI forward and reverse primers is shown in the box at the top, and the alignment with the rSK3 sequence results in an overlapping region that contains the silent AgeI mutation. Approximate positions of restriction sites on the rSK3 gene (5'UTR (blue), coding sequence (green), 3' UTR (purple), and poly A-tail (light green)) are shown. Green arrows represent pcDNA3.1/T7 primer sites, orange arrows represent antibiotic resistance genes; the zeocin resistance allows one to create stable cell lines while the ampicillin resistance is for the selection of transformed bacteria.

125 ng of forward primer

125 ng of reverse primer

10 ng of WT ΔKpn/Age(+) plasmid

5 μl of 10× reaction buffer

1 μl of dNTP mix (2.5 mM of each nucleotide)

3 μl of QuikSolution

The mix was made up to a volume of 50 μl with Milli-Q water, and then 1 μl of PfuTurbo DNA polymerase (2.5 U/μl) was added in a PCR tube. Temperature cycling was performed using a Techne THC-3 PCR machine under the following conditions; 1 cycle at 95 °C for 1 minute, then 18 cycles consisting of three steps. First, 95 °C for 50 seconds to denature the plasmid, then 60 °C for 50 seconds to anneal mutant primers, and thirdly 68 °C for 16 minutes to extend the nucleotide chain (≈ 2 minutes/Kb of plasmid). Finally 1 cycle at 68 °C for 7 minutes was used to complete extensions. Following the reaction, tubes were placed on ice for 2 minutes to cool before 1 μl of DpnI restriction enzyme (10 U/μl) was added and the sample incubated at 37 °C for 1 hour to digest the WT DNA.

**Transformation of DpnI-treated PCR reaction products** 45 μl of XL-10-Gold ultracompetent cells were thawed from frozen stocks and placed in pre-chilled Falcon 2057 tubes on ice. 2 μl of $\beta$-Mercaptoethanol (provided with QuikChange kit) were added to the cells which were swirled gently every 2 minutes for a period of 10 minutes. 2 μl of DpnI-treated DNA was added to the mix and incubated with the cells on ice for 30 minutes. Cells were then heat shocked at 42 °C for 30 seconds and incubated on ice for a further 2 minutes. 0.5 ml of preheated (42 °C) $NZY^+$ broth was added to each reaction and bacteria were then incubated at 37 °C for 1 hour with shaking (225 rpm). At the end of the incubation, cells were collected

by centrifugation, then resuspended in 100 µl of broth and plated on LB-agar plates containing ampicillin at a concentration of 50 µg/ml (diluted from 50 mg/ml frozen ampicillin stocks). Plates were inverted and grown overnight at 37 °C. The following day, single colonies were picked with a sterile pipette tip and grown overnight (~ 16 hours) in LB Broth containing 50 µg/ml ampicillin. These cultures were then miniprepped as described later. All mutants (except V519A–rSK3) made by this method were sequenced from the KpnI site to the end of the rSK3 clone and this fragment was subcloned into WT rSK3 between KpnI and XhoI sites. V519A–rSK3 was sequenced in its entirety instead of being subcloned, due to the lack of single cutter restriction sites before position 519.

### 2.1.2 Method 2: Overlap extension-based site-directed mutagenesis

An overview of the principle steps is shown in Figure 2.3 on page 76. Briefly, as with any PCR reaction the WT DNA strands are separated by heating and then cooled so that the primers (carrying the mutation in this case) can be annealed to it. DNA polymerase then extends a fragment containing this desired mutation. Two reactions of this sort are carried out; one towards a convenient site in the 5' direction and another towards a second convenient site in the 3' direction (pcDNA3.1 reverse and SK3 MidForward were used as the flanking primers respectively (see Figure 2.6 on page 88 for approximate positions of these sites)). Following amplification, the two fragments are gel purified and placed in a new overlap extension PCR reaction where the sense strand of one reactant can anneal to the antisense strand of the second reactant. Extension of these chains and digestion with appropriate restriction endonucleases generates "sticky ends" thus allowing the subcloning of fragments. Overlapping forward (5' direction) and reverse (3' direction) primers carrying the mutation of interest were designed using similar criteria to that mentioned above.

Pairs of purified forward and reverse primers were ordered from Gibco.

### Primer stock solutions

Initially, primer stock solutions were prepared by adding enough Milli-Q water to dissolve each dried primer to a concentration of 1 μg/μl. Solutions were then left to sit on the bench at room temperature for a couple of minutes before being vortexed for 30 seconds to ensure all the dried material was dissolved. Aliquots were then taken and diluted stocks (at a concentration of 10 μM) were made in 1.5 ml Eppendorf tubes. Primer stock solutions were all labelled and then stored at −20 °C.

### PCR generation and overlap extension of mutant fragments

High fidelity Pfu polymerase was used to extend the cDNA strands. Multi-ultra thin-walled PCR tubes were used for the reactions. Typically, each reaction tube consisted of the following:

5 μl of Pfu buffer (10×)

0.4 μl of 25 mM dNTP (Final concentration of 0.2 mM of each nucleotide)

1 μl of diluted ΔKpn/Age(+) template plasmid (≈ 10 ng)

2.5 μl of each forward/reverse and SK3 MidForward/pcDNA3.1R primers

38.1 μl of Milli-Q water (to make the mix up to 50 μl)

0.5 μl of polymerase

Each reaction was subjected to 3 minutes at 96 °C in a PCR machine during which time 0.5 μl of Pfu polymerase was added to each reaction (i.e. a "hot start" protocol was used). This was followed by a programme of:

96 °C for 30 seconds to part the dsDNA template

57 °C for 15 seconds allowing the primer to anneal to ssDNA

72 °C for 4 minutes providing the optimum temperature for the polymerase activity

The cycle was repeated 30 times using a Techne PHC-3 Thermal Cycler. Figure 2.4 on page 77 is a representative gel of fragments generated in this way.

Appropriate forward and reverse fragments were co-purified using a Geneclean DNA purification kit (Bio101, Inc.) according to the manufacturer's instructions. Briefly, bands were excised from the gel and the volume of gel was estimated from its weight. It was then dissolved at ~46 °C in 3 volumes of NaI solution. 10 µl of GLASSMILK® was added and the tubes were gently mixed every minute to bind the dissolved DNA over a period of approximately 5 minutes. The GLASSMILK® was collected by centrifugation (spun at maximum speed, 14000 rpm, for 30 seconds in an Eppendorf model 5415C microfuge) and the supernatant was discarded. The GLASSMILK® was then washed by being resuspended in 500 µl of wash solution. The wash procedure was repeated a further two times and the GLASSMILK® collected again, before the DNA was eluted from the GLASSMILK® beads by resuspending them in 20 µl of sterile Milli-Q water. Finally, this solution containing the amplified DNA fragment was separated by centrifuging and removed for subsequent reactions or stored at −20 °C for later use.

Purified fragments were then used in overlap extension PCR (Figure 2.3 on the following page) under identical conditions to the above. Fragments of the correct size were purified from these overlap extension reactions by running them on a gel and purifying using the Geneclean kit as described above.

### 2.1.3 Subcloning of DNA fragments

Mutated cDNA fragments were subcloned into a WT rSK3 gene to minimize the amount of sequencing required in the final construct. Sequencing is necessary because the fidelity of nucleotide incorporation during DNA lengthening with poly-

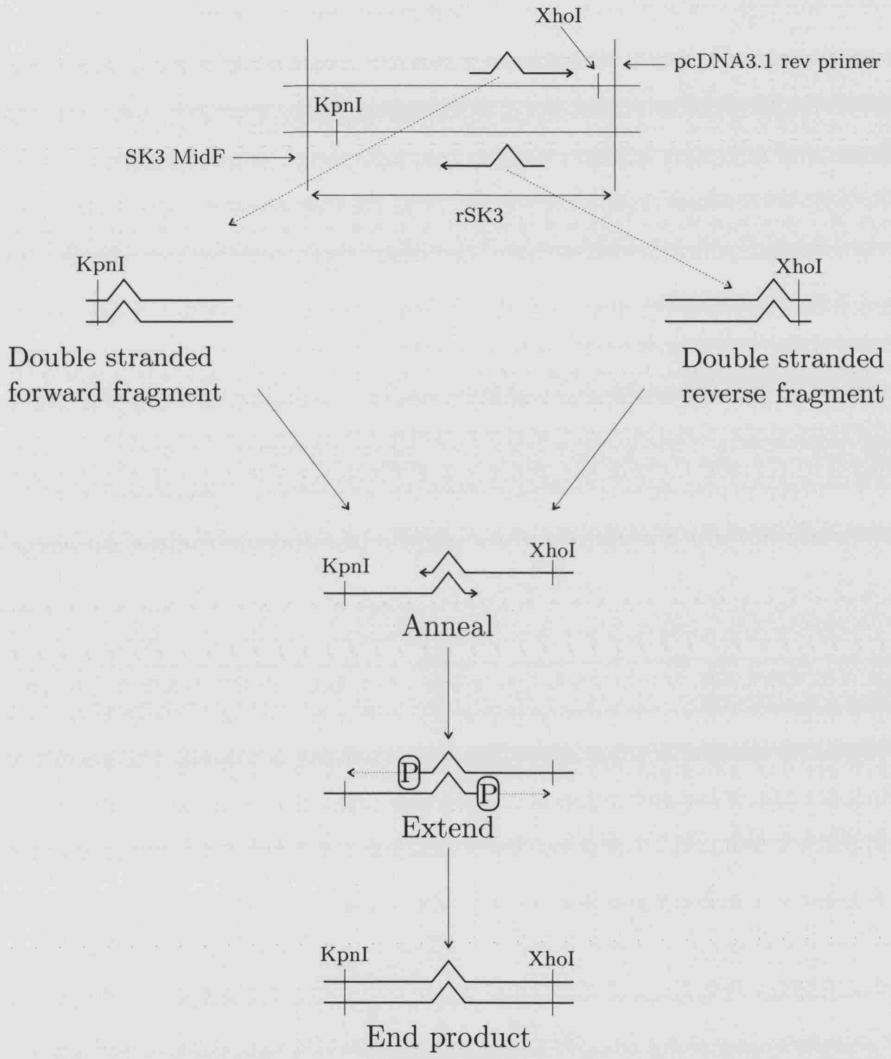


**Figure 2.3:** An outline of the overlap extension procedure. First two separate PCR reactions create overlapping forward and reverse fragments. These are then purified and annealed to each other in a second round of PCR reactions. Each strand is then extended with DNA polymerase. The cycle is repeated 30 times. P in the diagram denotes DNA polymerase. The indentations in the nucleotide strands indicate the site of the point mutation.

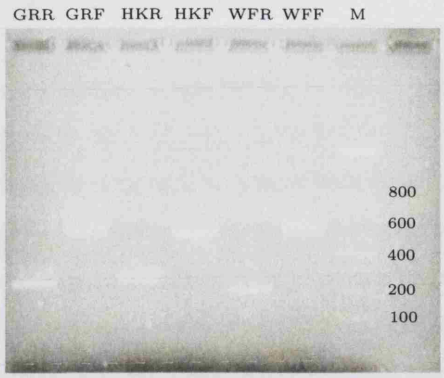


**Figure 2.4:** Representative gel showing the generation of forward and reverse mutant fragment pairs which were subsequently used in overlap extension reactions in order to generate the G548R-rSK3, H555K-rSK3 and W538F-rSK3 mutants. 100 bp marker (M) was used. GRR = Reverse fragment of G548R-rSK3, GRF = Forward fragment of G548R-rSK3, HKR = Reverse fragment of H555K-rSK3, HKF = Forward fragment of H555K-rSK3, WFR = Reverse fragment of W538F-rSK3, WFF = Forward fragment of W538F-rSK3.

merases is not 100%. Thus, small fragments (<1000 base pairs) were subcloned into the previously sequenced ΔKpn construct. A typical digestion reaction was carried out in a PCR tube containing:

14 μl of gel purified PCR reaction product containing a dsDNA fragment produced by the overlap extension method

1 μl of restriction enzyme

2 μl of the appropriate buffer (2×)

3 μl of Milli-Q water

The mix was placed in a water-jacketed incubator at 37 °C for three hours. At first, the efficiency with which the restriction enzymes cut sites located near the end of such small fragments of DNA was variable and it was decided that a more sensible strategy would be to subclone into a shuttle vector (pGEM-EZT), to improve digestion by restriction enzymes (several mutants were already made by the less efficient direct subcloning method (see figure 2.6 on page 88)). This procedure was

performed by "A-tailing" of the PCR fragments that were then subcloned in pGEM-EZT, which is supplied as a "cut" plasmid with overhanging thymidine (T) bases. The appropriate AgeI/KpnI or KpnI/XhoI fragments were cut from pGEM vectors and purified from gels. All purifications were carried out using the Geneclean kit as described above with one exception. A Mermaid Kit (purification for < 200 bp) (Anachem) was used to purify the 125 bp V529K fragment. It was purified following the manufacturer's instructions. Briefly, agarose gel slices containing the DNA were dissolved in 3 volumes of High Salt Binding Solution and the DNA purified with 10 µl of GLASSFOG®. The GLASSFOG® was collected by centrifugation (maximum speed, 14000 rpm, for 30 seconds in an Eppendorf model 5415C microfuge) and the supernatant discarded. The pellets were washed three times in 300 µl of Ethanol Wash solution in order to remove salts or other compounds that may inhibit enzymes, and the DNA was subsequently dried and eluted by adding 10 µl Tris buffer (pH 8). The eluted supernatant was then collected by centrifugation and the elution step repeated. Samples were run on a 2% agarose gel in 1 × TBE buffer. Fragments that were purified with this kit could not be co-purified with cut "backbone" ΔKpn plasmid (about 8000 bp) and were done separately using the Geneclean III kit and then ligated.

### Diagnostic analysis of subcloning

In order to side step sequencing on constructs which did not carry the mutation because the subcloning step was unsuccessful, a quick and effective diagnostic analysis was used. The basis of the procedure is shown in Figure 2.5 on the following page. In essence, one plasmid, lacking the AgeI site had the mutant fragment containing the AgeI site subcloned into it. Digestion with AgeI and observing the banding pattern on a diagnostic gel provided enough information on whether the subcloning was successful.

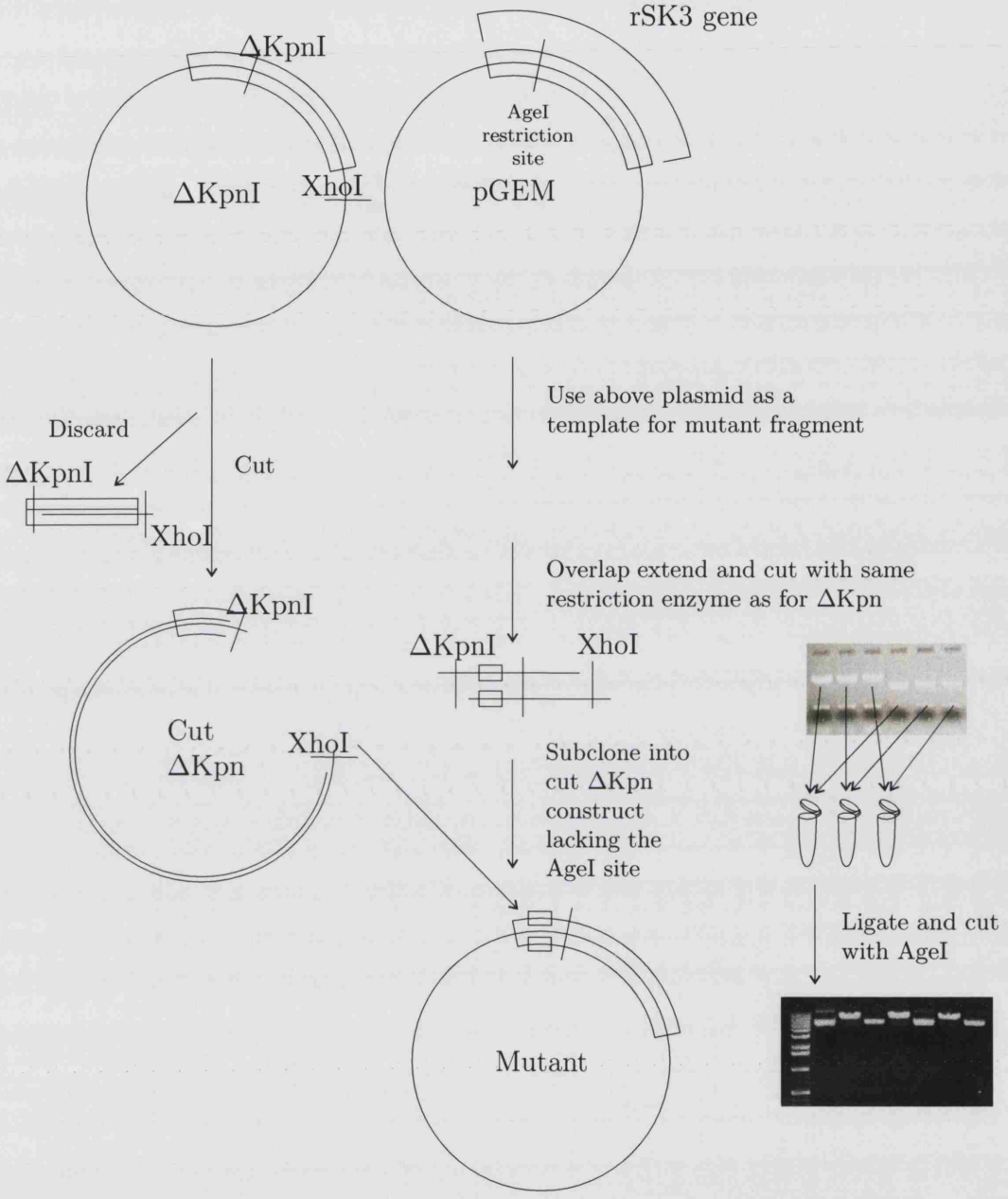


**Figure 2.5:** Schematic depicting the basis for quick identification of PCR clones carrying their intended mutations; mutant fragments were generated from WT rSK3 template plasmid containing an AgeI site and then subcloned into "backbone" WT rSK3 plasmid (cut ΔKpn) that originally lacked the AgeI site. The upper representative gel (inset) shows cut WT rSK3 plasmid co-purified with the cut mutant fragments. Positive clones are then identified by cutting with AgeI enzyme, and sequenced. The lower gel is a representative diagnostic gel showing plasmids cut with AgeI only. Alternative lanes represent cut, linearized DNA of putative mutants (single band lanes), and uncut, circular ΔKpn control plasmid (multi band lanes).

### 2.1.4 Ethanol precipitations

For some procedures, DNA had to be concentrated or cleaned by ethanol precipitation. This was done as follows. DNA solutions to be ethanol precipitated were made up to 100 µl with Milli-Q water. 10 %v/v of 3 M Sodium Acetate (pH 5.2) was added (10 µl) followed by approximately 2–2.5 volumes of pure ethanol (200–250 µl). The mix was left in the freezer for 10 minutes or the fridge for half an hour to precipitate. Reactants were then spun down for 5 minutes in a microfuge (Eppendorf model 5415C) at maximum speed (14000 rpm) to pellet the dsDNA. The supernatants were either carefully and promptly decanted, or aspirated off and discarded. Pellets were subsequently washed gently with 70% ethanol (200 µl) and then air-dried until glassy. Samples were resuspended in a suitable amount of buffer, left for 5 minutes and pipetted up and down a few times to ensure complete mixing.

### 2.1.5 Phenol-chloroform extractions

Phenol-chloroform extractions were performed to prevent "carryover" of enzymes from some manipulations (e.g. phosphatase treatment, see below) or during plasmid purification. As a first step, the volume of plasmid solution was estimated and to this twice the volume of Phenol:Chloroform:Isoamylalcohol (25:24:1) Tris-saturated (pH 8) was added. The mixture was then vortexed for about 20 seconds and spun down in an Eppendorf model 5415C centrifuge at 14000 rpm. The supernatants were removed into a fresh tube. This step denatures any proteins present and extracts them to the organic phase. One volume of chloroform was then pipetted onto the supernatant, vortexed and spun in a microfuge (Eppendorf model 5415C) for 2 minutes at maximum speed (14000 rpm) to remove phenol from the aqueous phase. The supernatant was removed and ethanol precipitated (as above).

### 2.1.6 Ligations and transformations

Typically, 17 µl of co-purified plasmid and insert, 2 µl of 10× ligation buffer and 1 µl of T4 DNA Ligase were gently mixed and placed at 4 °C overnight. 5 µl of this ligated DNA mix was then used for transformation. Transformations were performed in Falcon 2057 tubes using JM109 competent cells (efficiency of $10^7$ cfu/$\mu$g) following the manufacturer's instructions. Briefly, 5 µl of ligation mix was added to 50 µl of competent cells and incubated on ice for 10 minutes. The mixture was heat shocked at exactly 42 °C for 45–50 seconds before being returned to ice for another 2 minutes. 900 µl of sterile Lurea-Bertani (LB) medium (10 g/l bacto-tryptone, 5 g/l bacto-yeast extract, 10 g/l NaCl, titrated to pH 7.0 with 5 N NaOH) was added and the cells were subjected to an hour of shaking (225 rpm) at 37 °C to allow time for expression of antibiotic resistant genes. Cells were then spun down for 2 minutes at maximum speed and resuspended in 100 µl of LB medium before being spread on LB agar plates containing ampicillin (50 µg/ml of LB agar). Plates were inverted and placed in a 37 °C incubator overnight to allow colonies to grow.

### 2.1.7 Miniprepping

#### Alkaline lysis minipreps

Single colonies were picked from plates grown overnight using a flame-sterilized pipette tip. Cultures were then grown in 2–4 ml LB-ampicillin (50 µg/ml) at 37 °C for at least 8 hours with shaking at 225 rpm in a Model G25 Shaker Incubator (New Brunswick Scientific). Bacteria were then harvested by the alkaline lysis method: Cells were pelleted by centrifugation at 14000 rpm in an Eppendorf model 5415C centrifuge and resuspended in 100 µl cold Solution I (50 mM glucose, 25 mM Tris.Cl, 10 mM EDTA, pH 8.0), vortexed to disperse the bacterial pellet and lysed by the addition of 200 µl of freshly prepared Solution II (0.2 N NaOH, 1% SDS). Tubes were inverted 4–6 times to mix the lysis solution. Finally the genomic DNA, as well

as some protein and membranes were precipitated out of solution by adding 150 µl of ice-cold Solution III (5 M potassium acetate, 1 M glacial acetic acid). Again tubes were inverted to mix and this time they were incubated on ice for 5 minutes. The tubes were then centrifuged at 14000 rpm in an Eppendorf 5415C centrifuge to pellet the precipitate. The supernatant was removed and cleaned by phenol-chloroform extracting and ethanol precipitating (as described earlier) thus ensuring a relatively pure nucleic acid product. Precipitated DNA was resuspended in 50 µl of 10 mM Tris HCl (pH 8.0) and stored at 4 °C. 1 µl of RNAase was added to digest co-purified RNA. Plasmids were then cut with AgeI and positive clones were identified by the presence of the AgeI restriction site (Figure 2.5 on page 79). DNA for sequencing was PEG precipitated to ensure a higher quality DNA necessary for sequencing reactions. This was done by adding 60 µl of 20% polyethylene glycol (PEG6000 and 2.5 M NaCl) to the pure DNA suspension, and leaving the mix for 1 hour at 4 °C. Tubes were then spun for 15 minutes at 14000 rpm in an Eppendorf 5415C centrifuge and then the pellets were washed with 1 ml of 70% ethanol and air-dried for about 10 minutes. DNA was resuspended in 50 µl of Tris-HCl (pH 8.0) and stored at −20 °C.

### Qiaprep minipreps

For some mutants, capillary sequencing was performed which requires a very pure, low salt plasmid preparation for optimal results. For this reason some minipreps were performed using a Qiaprep Spin protocol. Cells from 2 ml of overnight bacterial cultures were pelleted and resuspended in 250 µl of Buffer P1 (Resuspension Buffer: 50 mM Tris-HCl, pH 8, 10 mM EDTA, 100 µg/ml RNase A). A similar amount of Buffer P2 (Lysis Buffer: 200 mM NaOH 1% SDS (w/v) ) was added and mixed by gentle inversion. To this, 350$\mu$l of Buffer P3 (Neutralization Buffer: 3 M potassium acetate, pH 5.5) was pipetted in and mixed by gently inverting the tubes 4–6 times. Following a 10 minute centrifugation (at 14000 rpm in an Eppendorf

5415C centrifuge), supernatants were pipetted into a QIAprep spin column placed in a 1.5 ml eppendorf tube, and re-centrifuged for 30 seconds. The flow-through was discarded and the spin columns were washed by applying 0.5 ml of Buffer PB in order to remove trace nuclease activity associated with the JM series competent cells. The columns were then re-centrifuged for 30 seconds and the flow through was again discarded. The columns were again washed by applying 0.75 ml of Buffer PE, centrifuging for 30 seconds and discarding the flow-through. Finally spin columns were transferred to a clean eppendorf tube and DNA was eluted with 50 µl of 10 mM Tris-Cl (pH 8.5). This buffer was used for elution purposes because the pH range of Milli-Q water was outside of a 7–8.5 pH range, where there is a great drop in the efficiency of elution.

### 2.1.8 Alkaline phosphatase treatment

To reduce the background in mutant cDNA ligations (Method 2), the plasmids were occasionally dephosphorylated at the 5' end using alkaline phosphatase. This was to prevent recircularization of singly-cut (linearized) DNA. To treat the plasmids they were first ethanol precipitated and resuspended in 40 µl 10 mM Tris-HCl, pH 8.0. 5 µl of Calf Intestinal Alkaline Phosphatase (CIAP), 10× reaction buffer and 3 µl of CIAP (0.01 U/1 µl, diluted in 1× reaction buffer) were added. The mix was incubated for half an hour at 37 °C after which time another 3 µl aliquot of diluted CIAP was added. Following incubation at 37 °C for another half hour period, 300 µl of STOP buffer (10 µM Tris-HCl (pH 7.5), 1 µM EDTA (pH 7.5), 200 mM NaCl, 0.5% SDS) was added to prevent any further CIAP activity. This halts the reaction by inactivating alkaline phosphatase through the chelation of magnesium ions from the reaction buffer. The mix was subsequently phenol-chloroform extracted to remove any CIAP that would dephosphorylate fragments during the ligation reaction.

### 2.1.9 Agarose gel electrophoresis

Fragments of between 100 and 200 base pairs (bp) were run on a 2% agarose (ultra-pure agarose Gibco) gel. All other DNAs were longer and were therefore run on 1% gels to allow greater resolution of bands and shorter run times. Low melting point agarose was used to facilitate DNA purification in subsequent steps. Agarose was made up in a 1× TAE buffer (2 mM Tris-Acetate, 0.05 M EDTA. pH 8.3 in Milli-Q water), heated to cause dissolution and cooled until it was just warm enough to prevent solidification so that ethidium bromide vaporization did not occur at the next step. 4 µl of ethidium bromide (10 mg/ml) was added to 30 ml of the cooled gel solution and mixed by gentle swirling of the solution. Gels were then poured into a caste and allowed to set. Solidified gels were immersed in 1× TAE buffer solution and voltage gradients used were generally 10 V/cm (PowerPac 300). Bands were visualized on a UV light box (IDI, Kodak) and recorded on a Sony system (Video Graphic Printer (UP-860CE). Scalpel blades were used to excise bands from these gels for purification.

### 2.1.10 Sequencing

Most sequencing was performed using the ABI PRISM Big Dye$^{TM}$ Terminator Cycle Sequencing Kit II (PE Applied Biosystems). Essentially polymerase fragments that have been prematurely terminated through the incorporation of ABI sequence terminating dyes are generated in a reaction and run on a gel. A mix was provided with the ABI dye terminator kit that contained AmpliTaq DNA Polymerase, $MgCl_2$, deoxynucleoside triphosphates, and A, C, G, T-dye terminators in Tris-HCl buffer (pH 9.0). 4 µl of this mix was added to 4 µl of dye dilution buffer in a PCR tube. Approximately 300 µg of dsDNA was added in a volume of 10 µl and 3.2 µg of the appropriate primer (primers were kept at 4 °C in 10 µM stocks). Samples were made up to 20 µl with Milli-Q water and placed in a PHC-3 Thermal Cycler (Techne).

Reactions were cycled under the following conditions: 96 °C for 30 seconds, 50 °C for 15 seconds, and 60 °C for 4 minutes. The cycle was repeated 25 times and the extension products were precipitated using 10% v/v 3 M Sodium Acetate (pH 4.6) and 2 volumes of 95% ethanol to remove unincorporated dyes. Tubes were vortexed and left at room temperature for 15 minutes to complete the precipitation before being spun (14000 rpm) in a microfuge for 20 minutes. The supernatants were aspirated off and the pellets were rinsed with 70% ethanol (1 ml). After a further 5 minute spin in the microfuge (14000 rpm) the supernatants were again aspirated away and the pellet was dried in a vacuum centrifuge for 10 minutes. The dried DNA pellet was stored at 4 °C until the day of the sequencing when it was resuspended in sequencing buffer and run on the sequencer gel.

Some mutants were sequenced on a Beckman Coulter CEQ2000XL capillary sequencer. As mentioned earlier, this sequencing required the DNA to be suspended in water, so the Qiaprep minipreps were ethanol precipitated and resuspended in Milli-Q water. Each reaction required $50 - 100$ fmol of dsDNA (determined by agarose gel electrophoresis assuming that the ΔKpn/Age(+) construct has a molecular weight of approximately 4650000). Sequenced colonies carrying plasmids of the correct sequence were grown in either 25 ml or 100 ml cultures for large scale maxi or midi-preparations (Qiagen) respectively (see next section). The amount and purity of the prepped DNA was determined by using a spectrophotometer (Bio-Rad SmartSpec 3000) and measuring the $A_{260} : A_{280}$ ratio. Zero absorbance was set using a cuvette filled with 1 ml of Milli-Q water and the subsequent reading containing a known volume of the DNA prep was made up to 1 ml with Milli-Q water. Preps with $A_{260} : A_{240}$ ratios that were close to 1.8 were used to calculate DNA concentrations, since this ratio is indicative of pure DNA i.e. pure ds DNA absorbs 1.8 times more light of wavelength 260 nm, than light of wavelength 280 nm. Contaminants such as proteins and phenol (which absorb strongly at 280 nm) that were present gave lower ratios and these preps were discarded. Likewise any preps where the recorded

$A_{260} : A_{280}$ ratio was above 2.0 were discarded, as these may have been contaminated with RNA.

Pore sequencing was performed using the sma-SK3 oligonucleotide (see below). The endogenous plasmid, pcDNA3.1, contains a primer site for the pcDNA3.1Reverse primer (Figure 2.6 on page 88). The list below shows the primers that were used to sequence mutant constructs.

| | |
|---|---|
| sma-SK3: | 5' - ACG CTC ATG ACC ATC TGC - 3' |
| AgeI-Forward: | 5' - TCT CAC CGG TAT CAT GGG TGC AGG CT - 3' |
| pcDNA3.1Reverse: | 5' - CCT CGA CTC TGC CTT CTA - 3' |

For full length sequencing of SK3, the following oligos were used in addition:

| | |
|---|---|
| SKCa3MidR: | 5' - ACA CCA GCA TCT CCA GGC TGA - 3' |
| SK3 3'GLU: | 5' - GCC TCC ACC AGG CCC ACT TG - 3' |

Primers recognized a specific base sequence of the rSK3 gene or pcDNA3.1/zeo plasmid. All custom primers above were ordered from GIBCO BRL, or MWG Biotech.

### 2.1.11 QIAGEN midipreps and maxipreps

In order to obtain large quantities of pure DNA plasmid for transfection purposes, DNA was amplified using QIAGEN midiprep and maxiprep kits. Briefly, cells from 25 ml (midi) or 100 ml (maxi) of overnight bacterial cultures were pelleted and resuspended in 4 ml (midi) or 10 ml (maxi) of Buffer P1. A similar amount of Buffer P2 was added and mixed by gentle inversion. To this, 4 ml (midi) or 10 ml (maxi) of Buffer P3 was pipetted in and mixed by gently inverting the tubes 4–6 times. This was immediately followed by placing the tubes on ice for 15 minutes (midi) or 20 minutes (maxi). Lysates were centrifuged for 30 minutes at 4 °C (Beckman

J2-MI model JA-14 rotor at 6000 rpm), and the supernatant was re-centrifuged for 15 minutes at 4 °C (Beckman J2-MI model JA-14 rotor at 6000 rpm), in order to prevent any particulate matter from clogging up the QIAGEN-tip. Equilibration of QIAGEN-tip 100 (midi) or QIAGEN-tip 500 (maxi) was performed by passing 4 ml (midi) or 10 ml (maxi) of Buffer QBT (750 mM NaCl, 50 mM MOPS (pH7.0), 15% isopropanol (v/v), 0.15% Triton® X-100 (v/v)) through the columns. Next, the supernatants containing the DNA was passed through the appropriate columns. QIAGEN-tips were washed with 2×10 ml (midi) or 2×30 ml Buffer QC (1 M NaCl, 50 mM MOPS (pH7.0), 15% isopropanol (v/v)), and then eluted with 5 ml (midi) or 15 ml (maxi) Buffer QF (1.25 M NaCl, 50 mM Tris-Cl (pH8.5), 15% isopropanol (v/v)). The DNA was precipitated out with isopropanol (0.7 volumes) at room temperature. Tubes were inverted 4–6 times and immediately centrifuged for 30 minutes at 4 °C (Beckman J2-MI model JA-17 rotor at 10500 rpm). The resulting pellet was washed with 70% ethanol, centrifuged (Beckman J2-MI model JA-17 rotor at 12500 rpm), and the new pellet was air dried and resuspended in 10 mM Tris-HCl (pH 8.5).

### 2.1.12 Preparation of glycerol stocks for storage of plasmids

For long-term storage, glycerol stocks of bacteria carrying rSK3 plasmids (WT and mutants) were made rather than propagating overnight cultures to eliminate the possibility of rogue, ampicillin-resistant bacterial growth in cultures that are carried long-term. To make these stocks, 150 µl of sterile glycerol was added to a 1 ml cryotube (Nunc) in a class II hood. 0.85 ml of bacterial overnight culture (grown for approximately 12–16 hours overnight) was subsequently pipetted in and vortexed to mix. Cryotubes were snap frozen in liquid nitrogen and stored in a −80 °C freezer. To restart cultures, glycerol stocks were taken from the −80 °C freezer, put on ice until the top layer of cells had thawed out, at which point the bacteria were streaked on an LB-agar plate containing ampicillin (50 µg/ml).

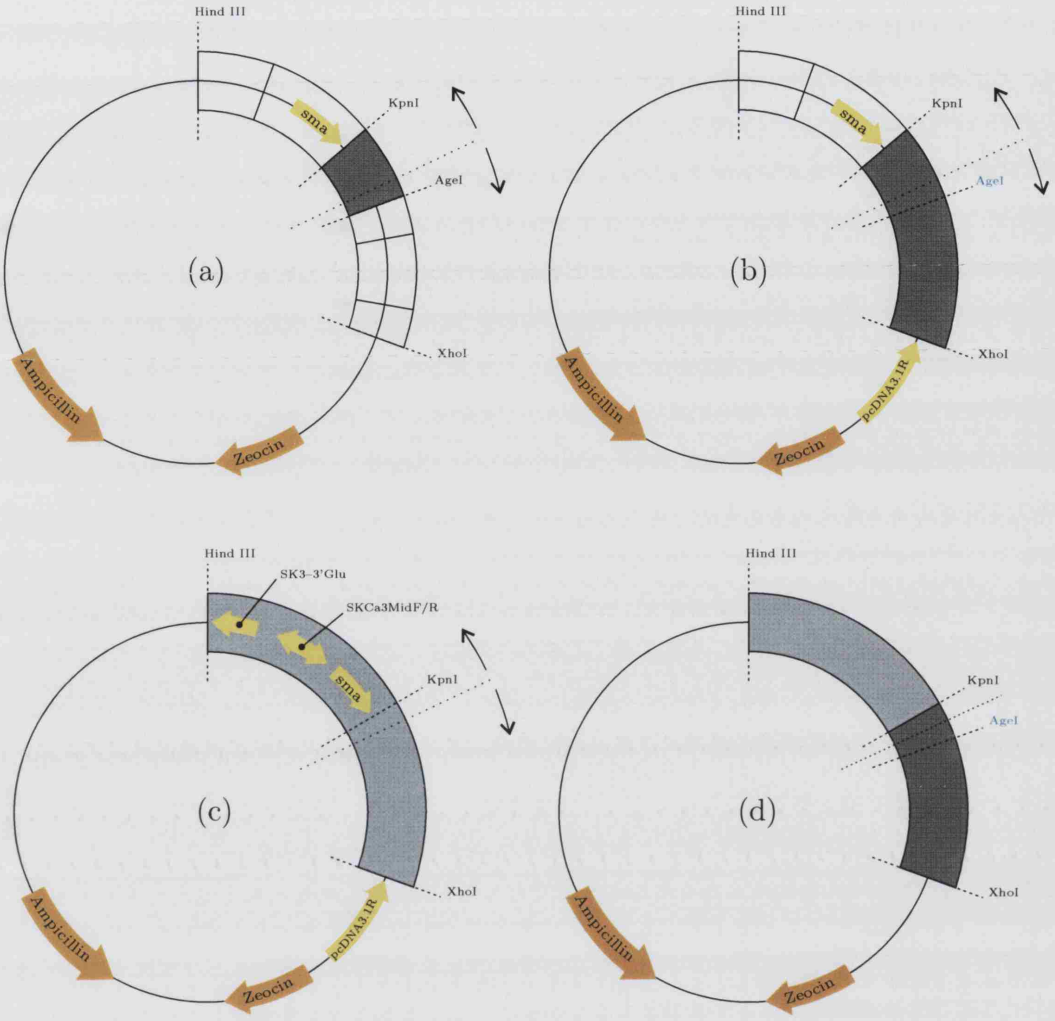


**Figure 2.6:** Plasmid maps showing the construction of mutants. V529K–rSK3 was constructed as in (a), G535D–rSK3, D528K–rSK3, W538F–rSK3, H555K–rSK3, G548–rSK3, V553F–rSK3, Q526K–rSK3, V529L–rSK3, H555N, G559A–rSK3, H555N–rSK3, were constructed as in (b), V519A–rSK3 was constructed as in (c), and V519A, H555N–rSK3 was constructed as in (d). Subcloned fragments are represented by gray bands and are scaled approximately according to size. The light blue band in (c) shows that the plasmid was copied with DNA polymerase in its entirity. H555N-rSK3 fragment was subcloned into V519A–rSK3 in (d). Sequencing was not required in (d) since both H555N-rSK3 and V519A-rSK3 had both been previously sequenced. Diagnostic enzymes are shown in blue lettering. Yellow arrows indicate approximate locations of primers used for sequencing. Black arrows indicate approximate region where mutant primers anneal and extend to generate mutated fragments. Colourless parts of rSK3 gene are regions from the original ΔKpn plasmid (i.e. Regions that were not copied using DNA polymerase.)

## 2.2 Immunocytochemistry

### 2.2.1 Antibodies for staining

A rabbit anti-rSK3 polyclonal antibody raised against amino acids 2–21 of the SK3 sequence was obtained from Chemicon International, Inc and kept in storage at −20 °C until use. TRITC (tetramethyl rhodamine isothiocyanate) conjugated to a goat-anti-rabbit secondary antibody was obtained from Molecular Probes.

### 2.2.2 Preparation of transfected cells for staining

Glass coverslips were placed centrally in 35 mm petri dishes, washed with double processed tissue culture water (Sigma), and coated with poly-D-lysine (0.05 mg/ml) for half an hour. After washing with tissue culture water again, the petri dishes and coverslips were sterilized under UV light using a UV light box (UVP transilluminator) for 30 minutes. HEK 293 cells, were transfected (see later) on the previous day with either

5 μg rSK3 WT and 5 μg GFP or

5 μg W538F–rSK3 and 5 μg GFP or

5 μg G548R–rSK3, and 5 μg GFP or

5 μg H555N,G559A–rSK3, and 5 μg GFP or

10 μg GFP only

These cells were then split and plated down onto these sterile petri dishes and coverslips, then incubated overnight in a Nuaire H autoflow $CO_2$ air-jacketed incubator at 37 °C providing a 5% $CO_2$, 95% $O_2$ environment.

### 2.2.3 Anti-rSK3 staining of transfected HEK 293 cells

Cells were washed three times with 1 ml of 1× Phosphate Buffered Saline (PBS) (NaCl (8 g/l), KCl (0.2 g/l), $NaHPO_4$ (1.44 g/l), $KH_2PO_4$ (0.24 g/l), pH 7.4), fixed by incubation in 4% paraformaldehyde (in 1× PBS) for 10 minutes at room temperature and washed once again with 1 ml of 1×PBS. The PBS was then removed and approximately 1 ml of methanol was added to permeabilize the cells by incubation for 10 minutes at room temperature. Cells were then washed twice with 1 ml of 1×PBS. Cover slips were then incubated for an hour at room temperature in 2 ml of blocking buffer (1% ovalbumin, 1% bovine serum albumin, 2% goat serum). The anti-rSK3 antibody (Chemicon, 0.3 µg/µl) was thawed and diluted 1:200 in blocking buffer solution ready for use. PBS was then completely removed from the cells using a tissue to absorb any solution around the coverslip, and a drop of the anti-rSK3 antibody solution was added. This created, through surface tension, a thin film of antibody solution over the coverslip which minimized antibody usage. Cells were incubated for 4 hours at room temperature and then washed five times with 1 ml PBS containing 0.1% Tween-20 (used to suppress unspecific reactions between antibodies and antigens). Dishes were placed on a shaker (Orbital Shaker SO3, 120 rpm) for 3 minutes during each wash. At the end of the four hour incubation and wash, the TRITC-labelled secondary antibody was thawed and diluted 1:100 with blocking buffer. Again, this was spread over the cells in a thin film to conserve materials and left for 1 hour at room temperature. Cells were then washed five times, again with shaking using 1 ml of 1×PBS containing Tween-20 (0.1%). A small drop of antifade mount (Vector laboratories) was placed onto labelled slides. Coverslips were removed from PBS with forceps, dipped in Milli-Q water, dried using a tissue placed at the edge of the coverslip, and mounted cell-side down on the drop of antifade mount. Slides were coated with nail varnish on the edge to attach them to the coverslips, covered with aluminium foil (to help preserve fluorescence)

and stored at 4 °C before viewing under a Leica confocal microscope. Images were recorded with a ×40 oil immersion objective.

## 2.3 Tissue Culture

### 2.3.1 Cell Maintenance

HEK 293 cells were routinely maintained in 50 ml cell culture flasks (Gibco) in a growth media of Dulbecco's Modified Eagles Medium (DMEM) supplemented with 10% Foetal Calf Serum (FCS), penicillin-streptomycin (5000 Iunits/ml (penicillin) per 5000 µg/ml (streptomycin)), 1% L-glutamine (2 mM, final concentration). Cells were split at about 80–90% confluency as follows. The media was decanted off and cells were carefully washed with 3 ml Hanks's Balanced Salt Solution (HBSS: 0.40 g/l KCL, 0.06 g/l $KH_2PO_4$, 0.35 g/l $NaHCO_3$, 8 g/l NaCl, 0.048 g/l $Na_2HPO_4$) before that too was discarded. Cells were then lifted by adding approximately 600 µl of trypsin-EDTA (1×) in HBSS (Gibco, now Invitrogen) onto the cells and waiting for a minute whilst gently tapping the flask. Cells were checked periodically to determine whether they had begun to lift (usually, the "sheen" by which cells can be visualized is disrupted as they begin to lift). At this point, 6 ml of HEK293 cell medium was added and then cells were triturated using a syringe with a sterile quill tip in order to disrupt larger clumps of cells. The cell suspension was then removed and pelleted. Supernatants were then decanted and cells were resuspended in approximately 5 ml of HEK293 cell growth medium. Cells were plated out at a dilution of approximately 1 in 3, and returned to the incubator. CHO cells were maintained similarly except that alpha minimal essential medium (alpha MEM) was substituted for DMEM in the growth media.

### 2.3.2 Transfection method

#### Cells were transiently transfected using the Calcium Phosphate method

Cells that had been maintained in a 95% $O_2$, 5% $CO_2$, incubator at 37 °C, were grown to ~ 30% confluency in two 35 mm petri dishes. The medium was decanted off and cells were washed twice with 1 ml of HBSS. This was then replaced with 1 ml of fresh medium and left to incubate while the DNA was prepared. GFP or channel plasmids that had either been maxi- or midi-prepped were unfrozen and 5 µg of each were placed in a 10 ml tube. 18.75 µl of 1 M $CaCl_2$ was added to the same tube and the volume made up to 75 µl with 1× TE buffer (10 mM Tris-HCl, 1 mM EDTA, pH 8). The resulting mix was added dropwise to 75 µl of 2× HBS (280 mM NaCl, 50 mM Hepes, 2.8 mM $Na_2HPO_4$, pH 7.2) to form a slightly cloudy precipitate. This precipitate was then added drop-wise onto the cells in an even manner around the petri-dish (a fine black-specked precipitate could be seen on top of the cells within 5 minutes of adding the precipitate mix (using a light microscope (×40)). The dish was returned to the incubator for 3 hours after which time the cells were glycerol shocked for 1 minute with 1 ml of 15% glycerol (in HBSS). Osmotic shocks using glycerol have been found to improve transfection efficiencies (Ahn et al., 1995). The cells were then washed twice with HBSS, and 2 ml of fresh medium was added, before they were returned to the incubator for use the following day. Generally, the transfection efficiency based on GFP staining was found to be between 10% and 35%, using this method. Exactly the same method was used to transfect cells for transient channel co-expression experiments, except that only 2 µg of GFP was added, and 4 µg of each channel plasmid.

#### Creation of a stable rSK3-expressing HEK 293 cell line

Cells were transiently transfected as described above with rSK3 WT construct in pcDNA3.1 carrying the zeocin resistance gene. Cells were incubated for 24 hours

and filter-sterilized (0.22 μM Nalgene filter) zeocin growth medium was prepared containing the normal HEK 293 cell growth medium supplemented with 1 μg/ml zeocin. These cells were then split in the usual way and a drop of the suspension was placed in a 145 mm petri dish to which was added the zeocin medium. Dispersed cells were grown for about 10 days. Once stable colonies were established, isolated colonies were marked out with a pen on the underside of the 145 mm petri dish and removed by placing the tip of a sterile glass pasteur pipette over the mark and sucking cells and surrounding solution into the pipette (most of the medium from the petri dish was removed to reduce optical distortion that occurs when the pipette tip is placed on the colony markers). Colonies were then placed in 3 ml of zeocin medium in a 6 well plate and grown to confluency before being split into flasks and maintained as described earlier. Healthy colonies expressing SK-like currents were frozen and stored in liquid nitrogen. Briefly, frozen stocks were made by lifting confluent cells with 600 μl of 0.005% trypsin/EDTA (Gibco, now Invitrogen), centrifuging to collect the cells (at 1000 rpm in a Denley BR401 refrigerated centrifuge), aspirating off enzyme/media, and resuspending in growth media supplemented with 10% DMSO. About 0.5 ml of cell suspension was quickly transferred to a cryotube and snap frozen in liquid nitrogen. Tubes were then stored in liquid nitrogen until subsequent use.

## 2.4 Electrophysiology

### 2.4.1 Electrodes and solutions

Electrodes were pulled from thin-walled borosilicate glass (Clark electromedical, catalogue no. GC15OTF-15) with a two-stage vertical puller (List Medical L-MP-30). Pipettes were coated with Sylgard (Dow Corning), and cured by rotating the tip of each pipette in a heating coil. Pipettes were then fire-polished to smooth

their ends using a microforge (Narishige, MF-9). These pipettes were backfilled with either bath or pipette solutions using a cannula. Air bubbles were removed by gently tapping the sides of the pipettes. Generally, for electrophysiological recording, the standard intracellular solution contained 130 mM KCl, 10 mM HEPES, 1 μM free $Ca^{2+}$, 3 mM $MgCl_2$ (50 μM free $Mg^{2+}$), 5 mM HEDTA and 2 mM $Na_2ATP$ (1 mM MgATP). The pH was adjusted to a typical intracellular physiological value of 7.2 with KOH. Some solutions contained ATP, no MgATP or different concentrations of magnesium in which case free concentrations of calcium, magnesium and ATP in electrode solutions were calculated according to the method of Tsien (1989) (stability constants were obtained from Martell and Smith (1976)). Cells were normally bathed in a standard solution containing 150 mM NaCl, 5 mM KCl, 1 mM $MgCl_2$, 2 mM $CaCl_2$, 10 mM HEPES (adjusted to a normal extracellular fluid pH of 7.4 with 1 N or 5 N NaOH). For bath solutions required to contain high concentrations of blockers (e.g. TEA at >100 mM), equimolar concentrations of NaCl were substituted for the drug to maintain osmolarity. The morphology of cells did not change for up to 3 hours in this medium and cells appeared healthy and remained stuck to the floor of the dish. Blockers were stored as stock solutions in dimethyl sulphoxide (DMSO) (UCL compounds) or Milli-Q water, as appropriate.

### 2.4.2 Patch clamp set-up

A Nikon inverted microscope (Eclipse TE200), with a fluorescent mercury lamp (Nikon-super high pressure), was mounted on an air-table (Barry Mount) inflated to approximately 35 psi to reduce vibrations. An earthed Faraday cage was placed on the air table to reduce electrical noise. Where possible all components were earthed using steel wire and banana plugs attached to a connector box on the Faraday cage. The pipette was positioned using a Narishige hydraulic 3-axis micromanipulator (MW3) to control fine movements after approximate localization with a coarse manipulator (Narishige, MMN-1). A perfusion system was manufactured

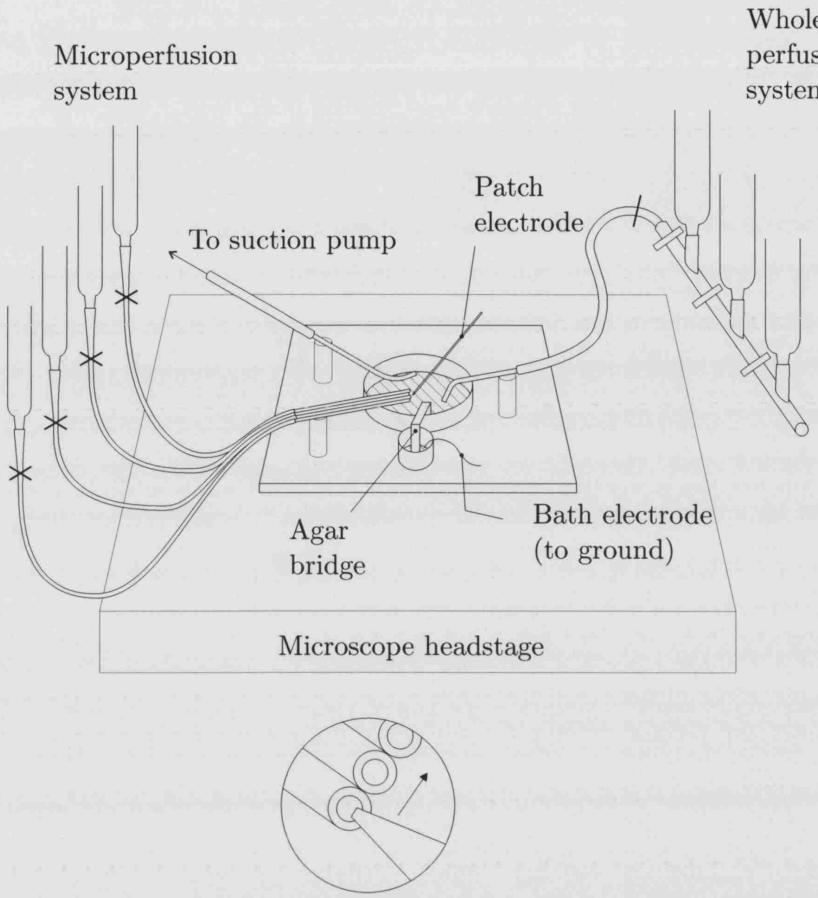


**Figure 2.7:** Schematic representation of patch-clamp setup. The inset is a cartoon of the view through the microscope eyepiece showing a pipette containing an excised patch that has been positioned in the mouth of a microperfusion tube. This part of the barrel system was submerged below the surface of the bath solution. The arrow indicates that the pipette tip was moved along the bores of each tube.

from standard laboratory plasticware to the style illustrated in Figure 2.7. A suction tube was connected to a Hy-Flow suction pump (Medcalf Bros Ltd). Both the bath electrode and pipette electrode were regularly chlorided in bleach for half an hour to maintain the AgCl coating. To spare the cellular environment from any silver ions, agar bridges (filled with 3% agar and standard intracellular solution) were used to connect between the culture dish and the chlorided ground electrode (placed in an intermediate bath solution compartment). This was connected through a signal ground connector mounted on the probe.

An EPC-9 patch clamp amplifier (HEKA electronik) was used to voltage-clamp

cells. The data was digitized at 5 kHz and filtered with an 8-pole low-pass Bessel filter at 2 kHz. The acquired current traces were analyzed with the HEKA online analysis. Liquid junction potential (LJP) changes were not corrected for when new solutions were being applied because the associated changes are likely to be very small (<5 mV). The very large currents recorded from some of the SK transfected cells can cause problems when the slow capacitance transient gets too small as described in Appendix B. These cells were identified by their uncompensatable slow capacitances and were discarded. Series resistance compensation was not employed. Instead, the data to be used in subsequent analysis was taken from potentials that generated small currents. In most cases, drug inhibitions would cause less than 10 mV potential drop across the series resistance (around 12 MΩ) at -40 mV, and so generally currents generated at this command voltage were selected for analysis. Finally, when recording from cells the gain was not changed between values that would switch feedback resistors as this was found to introduce an artifactural offset on the baseline current.

### 2.4.3 Voltage-clamp procedures

Cells were recorded under whole-cell voltage-clamp typically with a 'step' protocol, as described below:

#### Voltage protocol

The voltage step protocol could be divided up into three phases. Generally, during a recording cells were held at −80 mV for approximately 10 ms, stepped between potentials of −100 mV and +40 mV in 10 mV intervals for approximately 40 ms, and finally restored for 10 ms to a holding potential of −80 mV. The average current recorded over the whole of the -40 mV step phase was generally, but not always, used for subsequent analyses to keep series resistance errors to a minimum; when currents have been analyzed either at other step potentials or not over the full step

phase, the relevant potential or recording interval position have been specified. Since the large SK currents appear superficially to be similar to 'leak' currents, recordings were continuously checked to ensure that the reversal potential was $\sim$−80 mV ($E_k$). A reversal potential close to this value was taken to indicate a good seal.

### Practical procedures for patch clamping

A good cell-attached seal was taken to be when the pipette resistance increased to at least 1 GΩ. The resting potential for the pipette was then set to −80 mV. Fast capacitive transients ($C_{fast}$) were compensated for or cancelled and further gentle suction was used to rupture the cell membrane. The large whole-cell capacitive transients were cancelled and voltage protocols (as above) were used to study the currents. Pipette resistance, series resistances and slow capacitative compensation values were noted for all recordings. Whole-cell currents were usually given about five minutes to stabilize. Cells in which the whole-cell currents took longer than 5-10 minutes to stabilize (after going whole-cell) were discarded, as were those with persistently unstable currents (>10% current fluctuation). For experiments requiring outside-out patches, these were pulled approximately 30–50 seconds after going whole-cell using the fine manipulator to zig-zag the pipette in the vertical plane. Inside-out patches were "snapped off" from cell-attached patches using the y-axis coarse adjuster. The same cell-selection criteria applied to whole-cells was applied to patches.

## 2.4.4 Drug application

For whole-cell recording, the bath was superfused with drug solutions under gravity from a row of raised 50 ml syringes connected to a single perfusion line via 3-way taps at their bases. Perfusion rates were approximately 0.25 ml/s. Drugs were only applied after whole-cell currents had stabilized (to within 10%) for a five minute period. This "window" for drug application occurred following a period of initial

run down in most whole-cell recordings.

For patch recordings, a microperfusion system was used that is also gravity driven (Figure 2.7 on page 95). Following patch excision, the magnification was changed to low power (×40), and the pipette tip moved carefully towards the barrel system using the coarse manipulator. Patches were usually robust enough to tolerate fairly abrupt movements in solution and were placed just in front of the mouth of the appropriate capillary. Calcium-free solutions were applied to all patches to assess the contribution of non-calcium-activated currents. Drugs (and blocking ions) were were applied after patch currents had been stable (to within 10%) for a one minute period. The reduced time selection criteria for patches (one minute) compared with whole-cells (five minutes) was necessary since they were not as robust as the whole-cells.

## 2.5 Data quantification and statistical analysis

In experiments on both stably and transiently transfected cell lines, current run down was quantified by measuring the current loss over the run down phase (in whole-cells, this was defined by the interval between going whole-cell and the point at which the current, having run down, stabilizes or begins to run up). In order to quantify the current stability during the post-run down phase in these cell lines, the maximal positive or negative deviation from the current at the end of the run down phase was expressed as a percentage of the current at the end of the run down phase. All values are given as the mean±standard error of the mean (SEM). The differences between mean values were compared using a two-sample, unpaired t-test (P values of less than 0.05 were considered significant). The "n" number gives the number of experimental repetitions.

In experiments involving the application of blockers, drug effects were quantified as the percentage current block at -40 mV. Drug blocks were all measured during

the post-run down phase. In most cases, unblocked SK currents fluctuated slightly (maximal current fluctuation permitted in the absence of blockers was 10% of the control value) between the time that control recordings were made and the time that the drug was washed out; the unblocked current was taken to be the average between the control and washout currents;

$$\left(\text{Current block} = \frac{\text{Average of control and washout currents - Current remaining in the presence of the blocker}}{\text{Average of control and washout currents}}\right)$$

Due to the presence of current fluctuations in recordings, drug blocks that were within the limits of current instability (<10% block) needed to be distinguished. To do this, currents produced following blocker application and following washout were firstly normalized to the control currents, and means together with SEM values were calculated for each. Next, a one-sample t-test (one-tailed) was used to determine whether the application of the blocker significantly reduced the average current compared with the mean control current (the mean control current always had a value of 1 since it was normalized). A two-sample t-test was used to determine whether the mean current present following blocker application was significantly reduced compared to the value obtained following drug washout. If both tests showed that the normalized mean current remaining after blocker application was significantly lower ($P<0.05$) than the control and washout currents, then such current was deemed to be blocked. Once block had been established, the amplitude of current block was worked out as normal. In some cases drug washout was not achieved, so the normalized currents were compared to the control currents only using a one-sample t-test (one-tailed). The "n" number gives the number of experimental repetitions.

Dose-response curves were plotted using the mean current at -40 mV in the presence of the blocker as a percentage of that in its absence (% control). The methods of curve fitting to such data as well as to determine voltage-dependent block are now described.

## 2.6 Curve Fitting

### 2.6.1 Dose-response curves

All dose-response curves were fitted to the sum of the Hill equation (2.1) and a constant term, added to allow for any uninhibitable component. However, for these experiments, this uninhibitable component was zero.

$$y = 100 - \left( (B_{max})(\frac{[X]^{n_H}}{(\mathrm{IC}_{50})^{n_H} + [X]^{n_H}}) \right) \tag{2.1}$$

where $B_{max}$ = maximum unblocked current
$y$ = Percentage current remaining after drug application
$[X]$ = concentration of blocker
$\mathrm{IC}_{50}$ = drug concentration which produces 50% block
$n_H$ = Hill coefficient

All dose-response curves were constrained to values of 100% for $B_{max}$. This value was not allowed to vary during the procedure of curve-fitting.

### 2.6.2 Voltage-dependent block analyses

Voltage-dependency of block by magnesium or TEA was fitted to the Woodhull equation (Woodhull, 1973):

$$\ln IC_{50} = \ln {IC_{50}}^{0\,\mathrm{mV}} + \frac{z\delta FV}{RT}$$

where $\ln IC_{50}$ = natural log of $IC_{50}$ of block at potential, V
$\ln IC_{50}{}^{0\,mV}$ = natural log of $IC_{50}$ in absence of a transmembrane voltage
$R$ = Gas constant (8.314 J $mol^{-1}$ $K^{-1}$)
$F$ = Faraday's constant (9.6485 $\times$ $10^4$ C)
$z$ = valency of blocking ion
$V$ = transmembrane voltage
$T$ = absolute temperature (K)
$\delta$ = fraction of electric field experienced by ion

Curve fitting was performed using Gnuplot software (Gnuplot version 3.7.1, (T. Williams et al., 1999)). A non-linear least squares Marquardt-Levenberg algorithm was used for the curve fitting, with points weighted by the inverse of their variance. Parameter estimates are given together with an approximate standard deviation (SD). All other values are given as the mean±SEM.

## 2.7 Drugs and Reagents

Restriction enzymes and buffers were all obtained from PROMEGA except for AgeI which was from New England Biolabs.

All the tissue culture materials were obtained from Gibco, except for Zeocin (Cayla, Toulouse, France) and trypsin-EDTA (1×) in HBSS (Gibco). The poly-D-lysine was obtained from Sigma.

UCL 1848 (8,14-diaza-1.7(1,4)-diquinolinacyclotetradecaphanedium ditrifluoroacetate), UCL 1684 (6,10-diaza-1,5(1,4)-diquinolina-3(1,3),8(1,4)-dibenzenacyclodecaphanedium tritrifluoroacetate hydrate) and UCL 1530 (8,19-diaza-1,7(1,4)-diquinolina-3,5(1,4)-dibenzenacyclononadecanephanedium tetratrifluoroacetate hydrate) were synthesized in the department of Chemistry, UCL , by Professor Ganellin's group, as previously described (Rosa et al., 1998; Campos-Rosa et al., 2000; Chen et al., 2000). Apamin and gallamine were purchased from Sigma, HEPES, EDTA and HEDTA were obtained from Calbiochem. All other reagents were obtained from

Merck unless stated.

# Chapter 3

# Regulation of rSK3 channels

## 3.1 Aims

- To create a stable cell line for routine recordings of the WT channel
- To characterize the WT rSK3 current
- Establish suitable recording conditions

## 3.2 Introduction

Ion channel run down has been demonstrated in several types of channel, including $K^+$ channels (Vasilyev et al., 2002; Berdiev et al., 1996; Lukyanetz et al., 2002; Hattori et al., 2003). For example, P/Q- and N-type calcium channels have been shown to run down (Zeilhofer et al., 2000; Wu et al., 2002), as have L-type calcium channels (Hadley & Lederer, 1991). Rundown in these channels has been shown to be reduced by phosphatidylinositol-3,5-bisphosphate ($PIP_2$) (Wu et al., 2002), and intracellular calmodulin application together with ATP (Xu et al., 2004), respectively. There clearly is no universal source which causes run down of all these channel currents. For example, in the KAT1 channel, ATP can slow down the rate of channel run down, whereas the same molecule is without effect on the run down

of EAG channels (Hoshi, 1995). The sources of channel run down can vary from extrinsic factors (e.g. cellular factors) to intrinsic ones (e.g. molecular factors of the channel *per se*). Extrinsic factors will be examined in the main body of this chapter, although intrinsic factors may also modulate run down, as have been proposed in SK channels (Khawaled et al., 1999).

This chapter initially characterizes the WT rSK3 currents recorded in response to a step protocol under voltage-clamp and then looks at the possible causes of SK current run down and instability. Run down of SK current refers to the spontaneous loss of SK channel activity upon calcium entry, as has been demonstrated in inside-out oocyte patches expressing the SK1 channel (Ishii et al., 1997). Instability refers to time-dependent current fluctuations during the post-run down period. These are common phenomena in ion channel electrophysiology and are substantial hurdles in the pursuit of reliable pharmacological data. For example, Strobaek et al. (2000) had to interpolate currents that were running down and up during blocker application, in order to obtain pharmacological data from HEK 293 cells that were producing highly unstable SK currents. Interpolating currents in order to quantify block of channels that are producing unstable currents is potentially very unreliable, especially when recording block from whole-cells due to the lengthy times required to wash drugs out from extracellular solutions. Usually a minimum washout period of 1 minute would be required to remove fast-acting drugs from the bath solution, and potentially unstable recordings made during this time may lead to inaccurate drug block data. Therefore, it was necessary to minimize current run down, and particularly instability as much as possible. These issues provide the focus of this chapter.

## 3.3 Results

### 3.3.1 Characterization of endogenous currents in HEK 293 cells and CHO cells

Endogenous currents in untransfected WT HEK 293 and CHO cells, were characterized in order to establish the suitability of these cells for studying SK channel activity. These recordings thus serve as a control to confirm that there are suitably small background currents. They are also important to ensure that endogenous potassium currents are not of the SK type. To do this, whole-cell recordings were made first with nominally zero free calcium (5 mM HEDTA, no added calcium) and then with high intracellular calcium (1 μM free calcium) under voltage-clamp conditions, with a standard physiological bath solution. All the cells that were selected for analysis were representative (in size and shape) of the majority of the same type of cells. Immediately (<20-30 seconds) after going into whole-cell mode, a pulse protocol was applied, starting from a holding potential of −80 mV and stepping to a series of incremented voltages beginning at −100 mV and increasing in 10 mV intervals to +70 mV before returning to −80 mV. Figure 3.1 on page 107 shows the endogenous currents present in HEK 293 cells and CHO cells recorded in this way. CHO cells contain very little endogenous current. A calcium-free intracellular solution evoked 9.6±1.6 pA (mean±SEM) at +40 mV in CHO cells (n=4 recordings), whereas 1 μM free calcium internal solutions produced 12.6±3.4 pA (mean±SEM) at the same potential (n=4 recordings). WT HEK 293 cells produced a voltage-dependent current that reached 417±72 pA (mean±SEM) using calcium-free intracellular solutions (n=4 recordings) at +40 mV, whereas 1 μM free calcium internal solutions produced 311±43 pA (mean±SEM) at the same potential (n=4 recordings). These values are similar to those reported in a previous study that demonstrated 296±38 pA (n=35 recordings) of endogenous current at +40 mV

(Yu & Kerchner, 1998). The presence of a significant endogenous current whilst recording drug inhibitions at positive potentials could potentially produce highly inaccurate $IC_{50}$ values in future whole-cell recordings of SK current block. Since the endogenous currents in HEK 293 cells were voltage-dependent with very little current produced at negative potentials, the recording and measurement of transfected currents at fairly negative potentials would avoid this potential problem, together with errors induced by a high voltage drop across the series resistance. It was therefore important to make sure there were no calcium-activated currents or significant endogenous currents at negative potentials. Analysis of the same four HEK 293 and CHO cells mentioned above, demonstrated 15.4±2.9 pA (mean±SEM) of whole-cell current in untransfected WT HEK 293 cells using calcium-free intracellular solutions (n=4 recordings) at -40 mV, whereas 1 μM free calcium internal solutions produced 20.2±2.8 pA (mean±SEM) at the same potential (n=4 recordings). A calcium-free intracellular solution evoked 3.1±0.5 pA (mean±SEM) at -40 mV in CHO cells (n=4 recordings), whereas 1 μM free calcium internal solutions produced 4.2±1.1 pA (mean±SEM) at the same potential (n=4 recordings). Therefore, the magnitudes of the currents recorded at the same potential in both high (1 μM) calcium and calcium-free internal solutions were essentially identical in each untransfected cell line . From these results, there is 1) no significant endogenous current at -40 mV in either CHO or HEK 293 cells and 2) no evidence of calcium-activated currents at positive or negative potentials.

### 3.3.2 Stable cell line expression

To facilitate routine recording, stable cell lines expressing the rSK3 gene were created using HEK 293 cells. In all, 12 clonal colonies were selected (1A to 12A), and screened for rSK3 expression. After patch-clamping 7A cells with high (1 μM) intracellular calcium in the whole-cell configuration, only typical endogenous currents were observed when a standard voltage step protocol was applied as described in

(a) Untransfected HEK 293 cell with zero pipette calcium

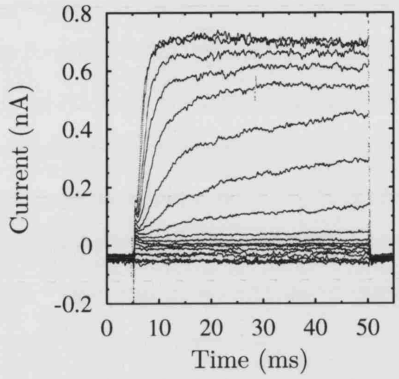


(b) Untransfected CHO cell with zero pipette calcium

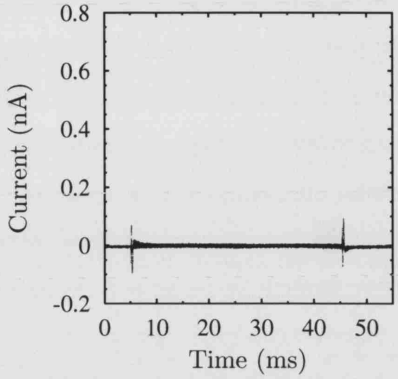


(c) Untransfected HEK 293 cell with 1 μM free calcium in the pipette

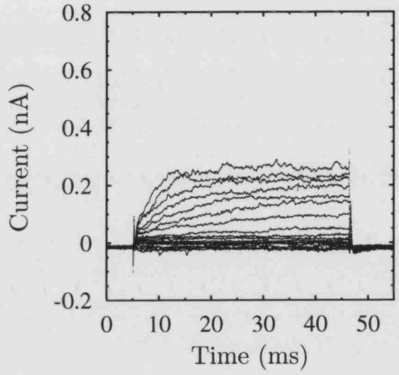


(d) Untransfected CHO cell with 1 μM free calcium in the pipette

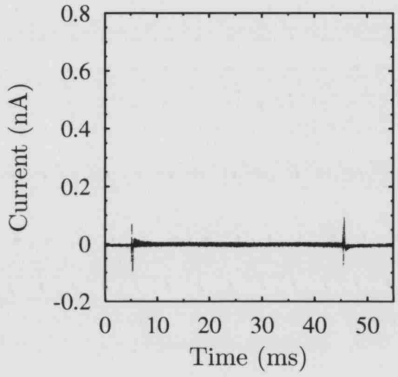


**Figure 3.1:** Characterization of endogenous currents in HEK 293 and CHO cells in both high and low calcium. Recordings were made immediately (<20-30 seconds) after going whole-cell by applying a voltage step protocol. Cells were voltage-clamped and held at −80 mV, before being stepped to voltages between −100 mV and +70 mV (in 10 mV increments). After 40 ms at the appropriate potential, the cells were returned to −80 mV. (a) is recorded from a HEK 293 cell with nominally zero intracellular calcium, showing an endogenous, voltage-dependent current which rectifies (outwardly). In four such recordings, the average current at -40 mV was 15.4±2.9 pA (mean±SEM), and at +40 mV it was 417±72 pA (mean±SEM). (b) is recorded from a CHO cell with nominally zero intracellular calcium. In four such recordings, the average current at -40 mV was 3.1±0.5 pA (mean±SEM), and at +40 mV it was 9.6±1.6 pA (mean±SEM). (c) is recorded from a HEK 293 cell with 1 μM free calcium in the intracellular solution, showing no activation besides the endogenous currents seen in (a). In four such recordings, the average current at -40 mV was 20.2±2.8 pA (mean±SEM), and at +40 mV it was 311±43 pA (mean±SEM). (d) is recorded from a CHO cell in 1 μM free calcium (pipette solution) and again shows no further activation other than the endogenous currents seen in (b). In four such recordings, the average current at -40 mV was 4.2±1.1 pA (mean±SEM), and at +40 mV it was 12.6±3.4 pA (mean±SEM).

the Methods (section 2.4.3). However, a large, voltage-independent (SK-like) current was found in both the 4A and 6A cell lines when recording with high (1 μM) intracellular calcium in the whole-cell configuration, using the same standard voltage step protocol. Because of its robust currents, the 6A cell line was selected for further study.

### 3.3.3 Characterization of WT rSK3 currents in the 6A cell line

To confirm functional expression of the rSK3 channels in the 6A cell line, whole-cell currents were recorded in the presence and absence of calcium (under similar conditions to the above endogenous current recordings (section 3.3.1)). In the calcium-free condition, as expected, a voltage-dependent endogenous HEK 293 current was seen when a standard voltage step protocol was applied as described in the Methods (section 2.4.3). However, when recording in 1 μM free calcium, a large voltage-independent current was seen using the same step protocol (Figure 3.2 on the following page). Due to the presence of endogenous currents at positive potentials, all the data to be analyzed were measured at -40 mV. Recordings made immediately (<20-30 seconds) after going whole-cell in the presence of 1μM intracellular calcium, produced an average current of 1.9±0.5 nA (mean±SEM) at -40 mV (n=5 recordings). The current-voltage (I–V) graph for this current was linear in each case, and reversing at a potential of approximately −80 mV. This is close to the theoretical value of a perfectly selective potassium conductance, −82 mV, in the recording solutions used as predicted by the Nernst equation (with 5 mM external $K^+$ and 130 mM internal $K^+$).

These results are therefore consistent with current largely being carried by small conductance calcium-activated potassium channels (SK channels) (Kohler et al., 1996; Grissmer et al., 1992; Lancaster et al., 1991; Hirschberg et al., 1998).

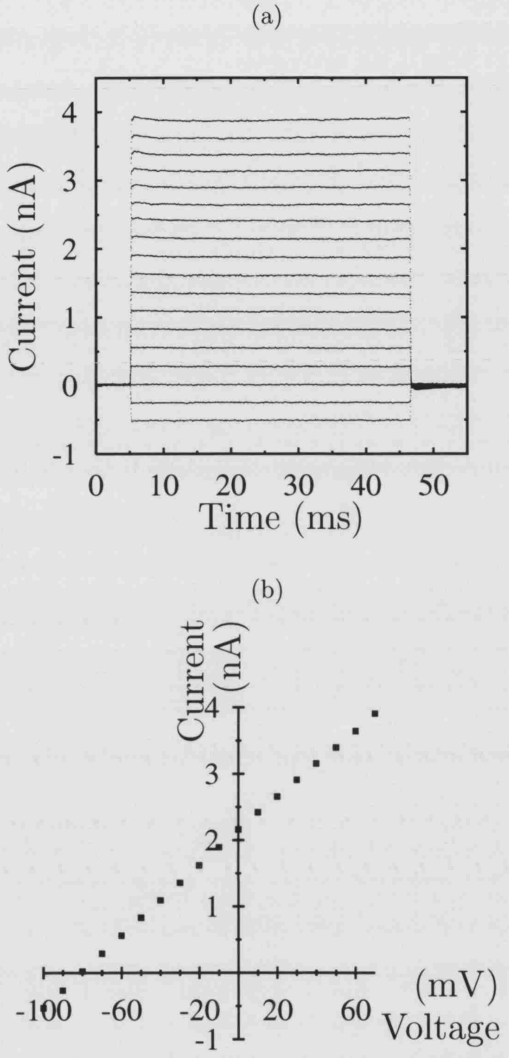


**Figure 3.2:** SK current recorded from a 6A cell. The cell was voltage-clamped and the currents shown were evoked immediately (<20-30 seconds) after going whole-cell by applying a standard voltage step protocol; the cell was held at −80 mV, before being stepped to voltages between −100 mV and +70 mV (in 10 mV increments). After 40 ms at the appropriate step, the cell was returned to −80 mV. (a) shows the whole-cell trace and (b) shows the corresponding current-voltage relationship. The average current at each potential over the 40 ms step phase has been plotted in (b). Standard $K^+$ ion concentrations were used consisting of 130 mM intracellular $K^+$, and 5 mM extracellular $K^+$ to give a reversal potential of −80 mV, close to the theoretical reversal potential of -82 mV for a perfectly selective $K^+$ channel. Further recordings from 6A cells that were made immediately (<20-30 seconds) after going whole-cell using a similar voltage step protocol, produced an average current of 1.9±0.5 nA (mean±SEM) over the -40 mV step (n=5 recordings). All the pipette solutions included 1 μM free calcium.

### 3.3.4 Run down and instability of WT rSK3 current

At the start of each recording, following channel activation, the stably transfected 6A cells expressing WT rSK3 channels exhibited run down, as demonstrated in plots of the time-dependency of 6A whole-cell currents. The empirical data for these plots were generated in the following way. SK channels were activated upon calcium entry into the intracellular side of the membrane. At this point (defined as time zero), whole-cell currents were evoked by applying a standard voltage step protocol; the whole-cell was held at −80 mV and then stepped to a series of incremented voltages which began at −100 mV and increased in 10 mV intervals to +70 mV before the cell was returned to −80 mV. Similar step protocols were applied every minute after time zero and the average current at -40 mV was recorded and subsequently plotted for each minute as shown in Figure 3.3 on page 112. The run down phases of two cells, each defined by the interval between time zero and the time-point at which the whole-cell current, having run down, stabilizes for two to three minutes or begins to run up, are shown in Figure 3.3 on page 112. In four 6A cells that were recorded and analyzed in this way, the average whole-cell current ran down to 33.7±4.2% (mean±SEM) of their original value recorded at time zero. In addition, after the initial run down there was frequently a period of instability which, for the purposes of discussion, will be considered as distinct from the initial run down phase (although the two phenomena may be related). This instability phase consisted of both current run up and run down. Following the initial run down phase, the average current from the same four 6A cells from which the mean amplitude of run down was derived, was stable to within 97.1±23.2% (mean±SEM). Clearly, the 6A cell line was too unstable to use for recording purposes and it was frozen and stored.

Run down was seen in virtually all whole-cell recordings including those from cells which had been transiently transfected with WT rSK3 DNA. In HEK 293 cells, which had been transiently transfected with this DNA, the average current

amplitude at the end of the run down phase fell to 39.2±10.6% (mean±SEM) of its original value recorded immediately after going whole-cell (n=3 recordings). In transiently transfected HEK 293 cells, the average current during this instability phase fluctuated by 44.3±16.0% (mean±SEM) (n=3 recordings) from the value recorded at the end of the run down phase. This designated the vast majority of whole cells to be unsuitable for recording. This made it very difficult to collect meaningful pharmacological data, and a variety of experiments were undertaken to try to circumvent this problem.

### 3.3.5 A comparison of run down and instability of WT rSK3 currents in different cell expression systems

WT rSK3 DNA was transiently transfected into three different cell types to determine whether run down was produced by some cellular factor that was present in variable amounts in different cell lines. Three well-characterized heterologous expression systems, HEK 293, CHO, and tsa201 were chosen. SK channels that were expressed in each cell type, were activated upon calcium entry into the intracellular side of the membrane. At this point (defined as time zero), whole-cell currents were evoked in each cell by applying a standard voltage step protocol; whole-cells were held at −80 mV and then stepped to a series of incremented voltages which began at −100 mV and increased in 10 mV intervals to +70 mV before the cells were returned to −80 mV. Similar step protocols were applied every minute after time zero for each cell type, and the average current at -40 mV was recorded and subsequently plotted for each minute as shown in Figure 3.4 on page 114. Expression of SK channels in all three cell types produced whole-cell rSK3 currents which ran down (Figure 3.4 on page 114). In CHO cells, which had been transiently transfected with WT rSK3 DNA, the average current amplitude at the end of the run down phase (for definition see Methods or section 3.3.4) fell to 15.3±1.8% (mean±SEM)

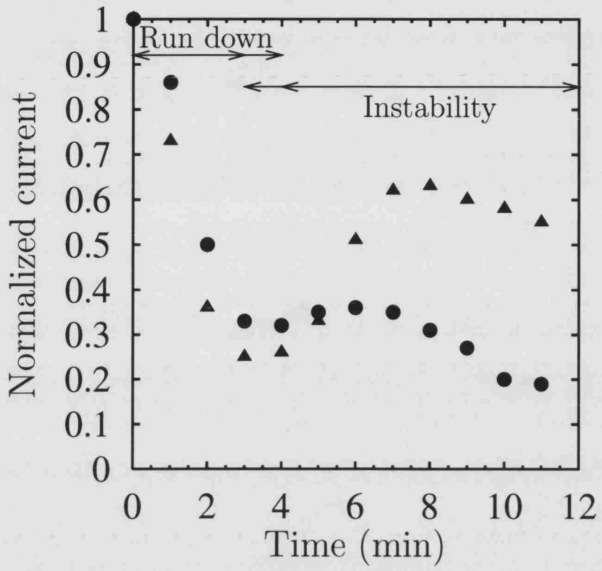


**Figure 3.3:** Representative examples of the time-dependency of normalized rSK3 currents as seen in two cells (*triangles* and *circles*) from the stably transfected 6A cell line. Each cell was voltage-clamped (held at -80 mV) and the whole-cell current amplitudes that were generated at -40 mV were normalized and plotted every minute as shown (cells entered the whole-cell mode at time zero). The phases of run down and instability are shown. Currents from the cell represented by circles took longer to run down (corresponding to the extended arrow over the run down interval), whereas the instability phase began earlier in the cell represented by triangles (corresponding to the extended arrow over the instability interval). In four cells, the average whole-cell current ran down to 33.7±4.2% (mean±SEM) of the original value recorded at time zero; following run down, the average current from the same four cells was stable to within 97.1±23.2% (mean±SEM). A standard intracellular pipette solution with 1 μM free $Ca^{2+}$ but lacking MgATP was used to make these recordings in the whole-cell configuration.

of its original value recorded immediately after going whole-cell (n=3 recordings). In tsa201 cells, which had also been transiently transfected with WT rSK3 DNA, the average current amplitude at the end of the run down phase fell to 7.0±1% (mean±SEM) of its original value recorded immediately after going whole-cell (n=3 recordings). Both these values are not significantly different (P>0.05) from the reduction in SK current following run down in transiently transfected HEK 293 cells (39.2±10.6% (mean±SEM), Figure 3.4 on the next page). The number of passages of the cell line appeared to make no discernible difference to the run down either. Following run down, SK currents in tsa201 cells were stable to within 52.7±23.8% (mean±SEM) (n=3 recordings), whereas SK currents in CHO cells were stable to within 60.3±28.0% (mean±SEM) (n=3 recordings). Again, neither of these values were significantly different (P>0.05) from the instability found in transiently transfected HEK 293 cells (44.3±16.0% (mean±SEM), Figure 3.4 on the following page).

In general, the stability of SK currents in transiently transfected HEK 293 cells after the run down phase was greater than for the other cell lines, and so this cell line was selected for the majority of future whole-cell experiments (additionally, less current run down in these transfected cells meant that more current was usually present during the post-run down phase). However, CHO cells were used in some instances, such as excised patch recordings, due to their lack of endogenous currents. This permitted data from patches to be analyzed at positive potentials, since series resistance errors are not an issue in patch recordings.

### 3.3.6 Can poor calcium buffering account for apparent SK current instability?

As the calcium dose-response curve for SK channels is very steep with a peak plateau at ~1 μM free calcium (Kohler et al., 1996; Xia et al., 1998), any perturbations that

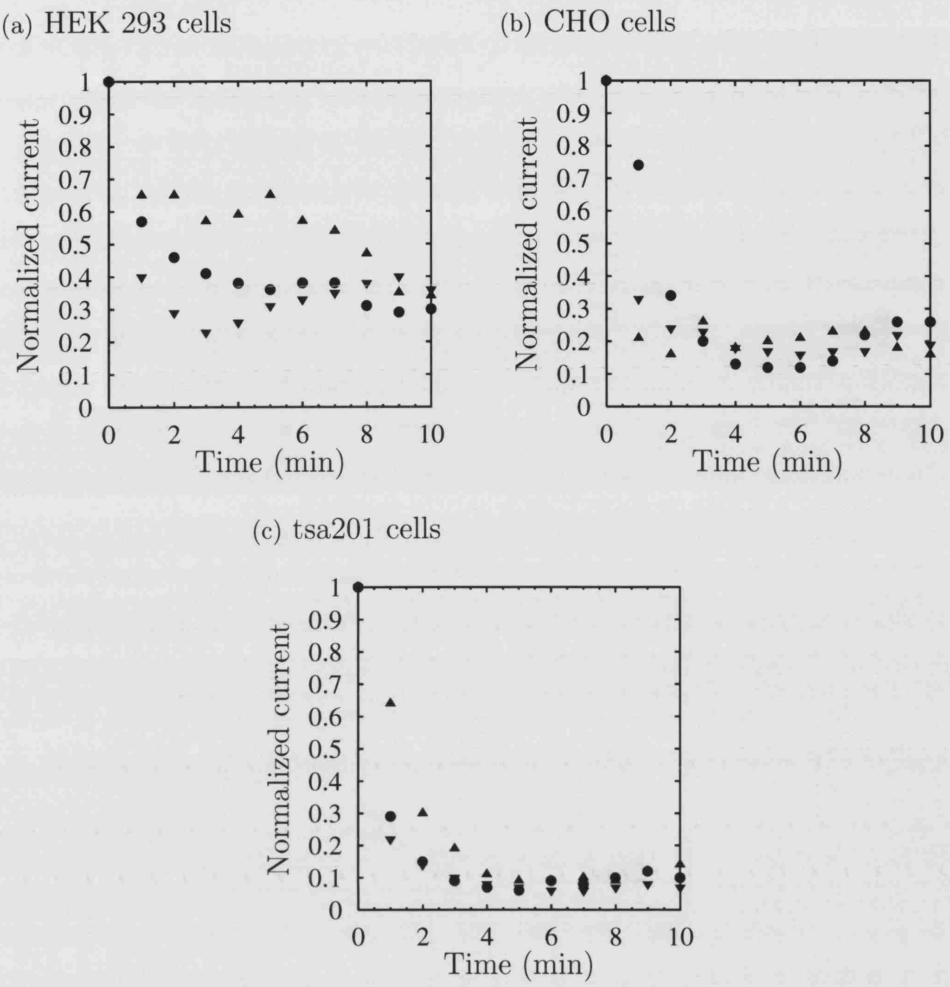


**Figure 3.4:** Examples of normalized rSK3 current run down and instability seen in HEK 293 (a), CHO (b), and tsa201 cells (c). Each cell (*circles*, *upright triangles*, *inverted triangles*) had been transiently transfected with WT rSK3 DNA. Upon expression of the WT rSK3 channels, cells were voltage-clamped and the whole-cell current amplitudes that were generated at -40 mV were normalized and plotted every minute as shown (cells entered the whole-cell mode at time zero). In the three transiently transfected HEK 293 cells shown, the average whole-cell current after run down fell to 39.2±10.6% (mean±SEM) of the original value recorded at time zero. Following run down, the average current from these three cells was stable to within 44.3±16.0% (mean±SEM). In the three transiently transfected CHO cells shown, the average whole-cell current after run down fell to 15.3±1.8% (mean±SEM) of its original value that was recorded at time zero, and was stable to within 60.3±28.0% (mean±SEM) during the period of instability. Finally, in the three transiently transfected tsa201 cells shown, the average whole-cell current following run down fell to 7.0±1% (mean±SEM) of its original value recorded at time zero, and was stable to within 52.7±23.8% during the instability phase. A standard intracellular pipette solution with 1 μM free $Ca^{2+}$ but lacking MgATP was used to make these recordings in the whole-cell configuration. A standard extracellular solution containing 5 mM KCl was also used.

| Dissociation equilibrium constant | 18 °C | 25 °C |
|---|---|---|
| $K^{Ca}_{HEDTA}$ | 2.63 μM | 2.03 μM |
| $K^{Mg}_{HEDTA}$ | 36.82 μM | 32.17 μM |
| $K^{Ca}_{ATP}$ | 97.3 μM | 81.4 μM |
| $K^{Mg}_{ATP}$ | 165.3 μM | 158.9 μM |

**Table 3.1:** Table showing calculated values of dissociation equilibrium constants for calcium and magnesium-chelating molecules in the pipette solution at both 25 °C and 18 °C. The method of Tsien (1989) has been used in all calculations. $K^{Ca}_{HEDTA}$ is the dissociation equilibrium constant of CaHEDTA. $K^{Mg}_{HEDTA}$ is the dissociation equilibrium constant of MgHEDTA. $K^{Ca}_{ATP}$ is the dissociation equilibrium constant of CaATP. $K^{Mg}_{ATP}$ is the dissociation equilibrium constant of MgATP. $K_d$ values at 25 °C were obtained from Martell and Smith (1976), and were used to calculate the $K_d$ values at 18 °C, as shown in Appendix A.

reduce the concentration of the unbound cation would produce a sharp decrease in channel activation (all calcium-containing pipette solutions theoretically provided 1 μM free calcium). However, bath solution temperature could, for example, fluctuate around the typical recording value, 25 °C, as a result of heating due to the close proximity of the microscope lamp. This introduces a potential source of error in intracellular free calcium buffering. It was therefore important to assess through calculation, the likely extent of free calcium change with temperature. There are two calcium-buffering molecules in the intracellular solutions used, namely HEDTA, and ATP. Table 3.1 shows the theoretical change in $K_d$ values for both these molecules as a result of a 7 °C change in temperature (full calculations are shown in Appendix A).

Table 3.1 shows that all the calcium and magnesium dissociation equilibrium constants increase as a result of reducing the temperature by 7 °C. This would mean dissociation is favoured in every case. This would cause an increase in the amount of free calcium present in the pipette solution and channels should remain saturated with sufficient calcium for maximal activation. It would appear that only when temperature levels increase above 25 °C, do intracellular free calcium levels become reduced. This rarely happens even in summertime and is unlikely to account

for the minute by minute fluctuations seen. It thus seems likely that submaximal channel activation is not a cause of the run down or current instability.

### 3.3.7 Do series resistance changes account for SK current instability?

Some of the currents recorded from transfected cells were so large that there was a slight concern that changes in the series resistance of the pipette, $R_{series}$, might have caused the apparent current fluctuations (Figure 3.5 on the next page). This could have arisen through a gradual resealing of the whole-cell membrane, but the application of gentle suction to the pipette (which might clear the pipette-cell interface), did not prevent run down. The following derivation predicts the relationship between current through the membrane and the series resistance.

Given that $R_s$ and $R_m$ may be considered as two resistances in series with each other (Figure 3.5 on the following page), the voltage drop across each will bear an inverse relation; as one increases the other will decrease, as shown in the derivation below:

$$
\begin{aligned}
V_m + V_s &= V_{command} \\
I_m R_m + I_s R_s &= V_{command} \\
R_s + R_m &= \frac{V_{command}}{I} \qquad (I = I_m = I_s) \\
& \quad V_{command} \text{ is constant and so } I \text{ must decrease as } R_s \text{ increases}
\end{aligned}
$$

The graph shown in Figure 3.6 on page 118 demonstrates there is no correlation between current fluctuations and changes in $R_s$. It therefore seems unlikely that time-dependent series resistance changes are a major factor that leads to current instability in recordings.

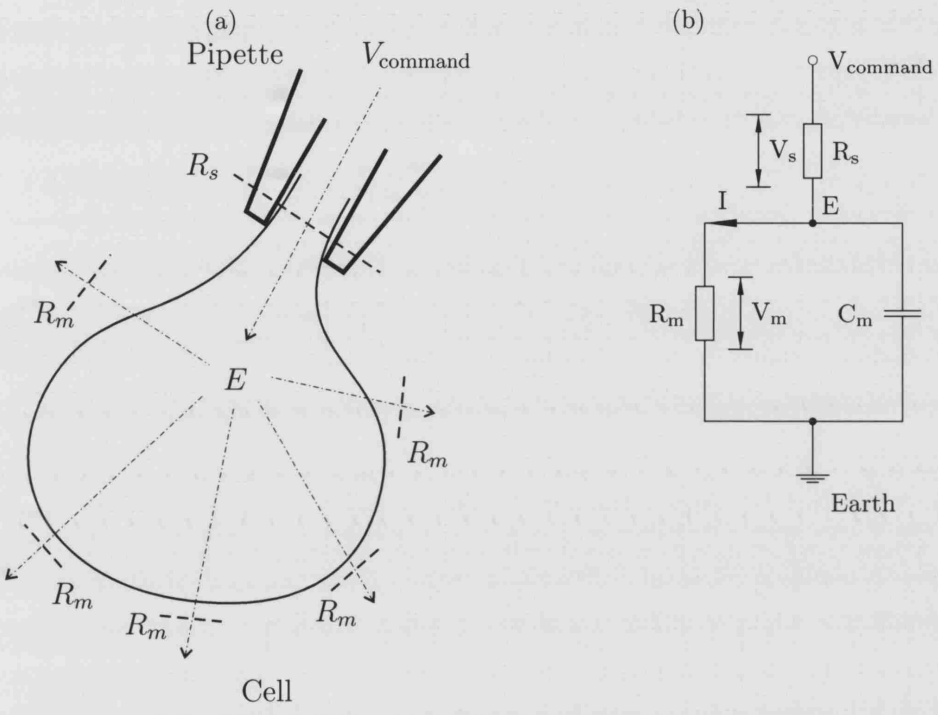


**Figure 3.5:** Series resistance is produced as a result of the geometry of the pipette (a) Broken arrows indicate flow of current, dashed lines show points where resistance to current flow exists. (b) shows the equivalent circuit for the setup in (a) with earth being analogous to the grounding of the bath solution and E being equivalent to the potential of the intracellular solution. $V_s$ is the voltage drop across the series resistance, $R_s$, and $V_m$ is the voltage drop across the membrane resistance, $R_m$. $V_{command}$ is the pipette potential, and $C_m$ is the membrane capacitance.

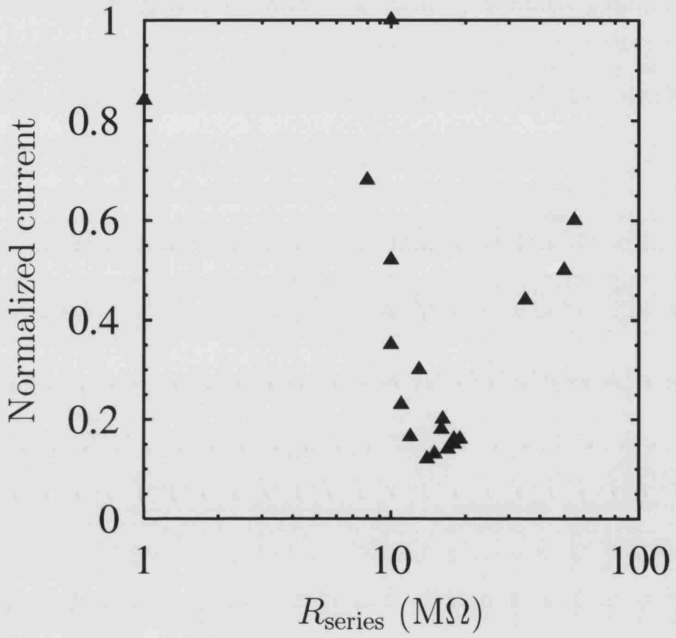


**Figure 3.6:** Fluctuations in SK channel current do not correlate inversely with changes in series resistance, $R_{\text{series}}$. The current fluctuations with $R_{\text{series}}$ were measured in a single HEK 293 cell transiently expressing WT rSK3 channels and voltage-clamped in the whole-cell configuration. The extreme variations in $R_{\text{series}}$ seen in this graph could be artifactual, since the amplifier circuitry cannot compensate for very large currents (see Appendix B). Each point in the graph represents $R_{\text{series}}$ and normalized currents from recordings taken every minute after going whole-cell. The experiment was repeated in three other cells and no correlation was found each time.

### 3.3.8 SK current run down and instability are not modulated by elevated concentrations of extracellular permeant ions

The effect of augmenting the external permeant ions was investigated since this has been shown to reduce run down of small conductance calcium-activated $K^+$ channels in chromaffin cells (Y. Park, 1994). This was tested by raising the extracellular $K^+$ ion concentration from 5 mM to 30 mM whilst maintaining the ionic strength of the solution. In order to achieve this, an equivalent amount of NaCl (25 mM) was removed from the external solution. The control solution, therefore, had 5 mM KCl and 150 mM NaCl (low external $K^+$), whereas the high external $K^+$ ion bath solution had 30 mM KCl and 125 mM NaCl (30 mM extracellular $K^+$ was chosen in order to reproduce the extracellular potassium ion concentration used by Y. Park (1994)). This resulted in a $K^+$ reversal potential of -37 mV in high external $K^+$, and so currents were recorded at 0 mV since their magnitude was around 1 nA at this potential. The conditions under which chromaffin cells were recorded (Y. Park, 1994) included the presence of intracellular MgATP and this was also added to the pipette solution (1 mM). SK channels were transiently expressed in HEK 293 cells, and subsequently voltage clamped. Upon entry into the whole-cell mode (defined as time zero), currents were evoked from cells by applying a standard voltage step protocol; whole-cells were held at $-80$ mV and then stepped to a series of incremented voltages which began at $-100$ mV and increased in 10 mV intervals to $+70$ mV before the cells were returned to $-80$ mV. Similar step protocols were applied every minute after time zero, and the average current at -40 mV was recorded and subsequently plotted for each minute as shown in (Figure 3.7 on the following page). The average current amplitude at the end of the run down phase in transiently transfected HEK 293 cells, fell to 33.7±3.9% (mean±SEM) of its original value recorded immediately after going whole-cell at 0 mV (n=3 recordings). This value was not significantly

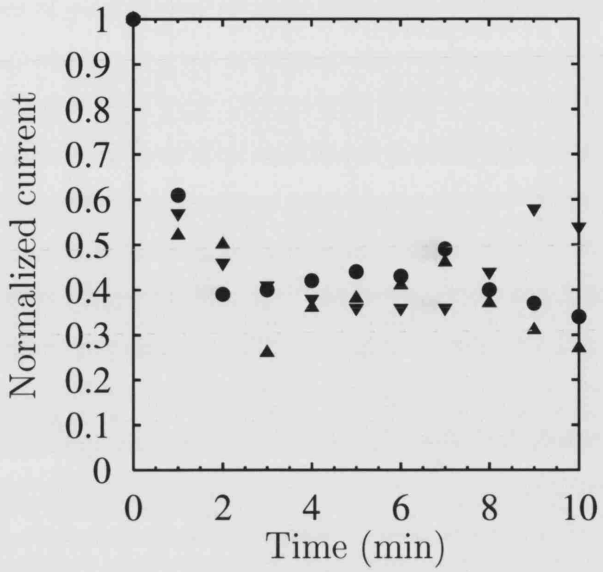


**Figure 3.7:** Graph showing run down of normalized rSK3 current in three transiently transfected HEK 293 cells (*circles*, *upright triangles*, *inverted triangles*) which were bathed in elevated extracellular $K^+$ ion solution (30 mM). Each cell was voltage-clamped and the whole-cell currents that were generated at 0 mV were normalized and plotted every minute as shown (cells entered the whole-cell mode at time zero). The run down component is still present in these recordings. In the three recordings shown, the average whole-cell current ran down to 33.7±3.9% of its original value recorded at time zero. Additionally, following run down the average current from these three recordings was stable to within 54.3±14.9%. A standard intracellular solution containing 130 mM KCl, 1 μM free $Ca^{2+}$ and 1 mM MgATP was used to make these recordings, together with a standard extracellular solution containing 5 mM KCl.

different (P>0.05) from the current reduction seen over the run down phase when using 5 mM extracellular $K^+$ ion solutions (39.2±10.6% (mean±SEM), Figure 3.4 on page 114). This indicates that run down of cloned SK channels is not modulated by extracellular $K^+$. Additionally, whole-cell current stability was not affected by the elevated extracellular $K^+$: following run down, currents were stable to within 54.3±14.9% (n=3 recordings), which is not significantly different (P>0.05) from the instability value obtained under similar conditions, but in low extracellular $K^+$ (44.3±16.0% (mean±SEM), (Figure 3.4 on page 114)).

### 3.3.9 Modulation of rSK3 channels by intracellular MgATP

Next, the idea that MgATP might help alleviate run down was investigated since the intracellular application of MgATP to C6 Glioma cells (which endogenously express apamin-sensitive SK channels) has been reported to eliminate run down of these channels (Manor & Moran, 1994). SK channels were transiently expressed in HEK 293 cells, and subsequently voltage clamped. Upon entry into the whole-cell mode (defined as time zero), currents were evoked from cells by applying a standard voltage step protocol; whole-cells were held at −80 mV and then stepped to a series of incremented voltages which began at −100 mV and increased in 10 mV intervals to +70 mV before the cells were returned to −80 mV. Similar step protocols were applied every minute after time zero, and the average current at -40 mV was recorded and subsequently plotted for each minute as shown in Figure 3.8 on page 124. Some further data showing the time-dependency of SK currents expressed in inside-out patches exposed to 1 mM intracellular MgATP is also shown in Figure 3.8 on page 124. These plots were generated using the same voltage step protocol as for the whole-cell data, except currents were analyzed at +70 mV (as series resistance errors are negligible in patches), and CHO cells were chosen to express the rSK3 channels (since this cell line has negligible endogenous current which would not be able to modulate small patch currents). The time-dependency of whole-cell currents shown in Figure 3.8 on page 124 demonstrates that the inclusion of 1 mM MgATP to the recording solution did not stop the run down *per se*; it merely stabilized the SK current level following run down, which was a substantial aid in producing reliable pharmacological data. Currents during the instability phase which had fluctuated as much as 44.3±16.0% (mean±SEM) in whole-cells that were recorded without 1 mM MgATP (Figure 3.4 on page 114, n=3 recordings), only deviated 20.4±14.4% (mean±SEM) with 1 mM intracellular MgATP (n=3 recordings). Although this improved the percentage of whole-cells which were

acceptable for obtaining pharmacological data to about 1 in every 3 or 4 cells, there were usually only 5 or 10 minute windows when drugs could be applied and washed off. Fortunately, the future use of UCL compounds would make recordings feasible since a 5 minute interval would normally be sufficient to apply this drug and wash it off (apamin on the other hand would take much longer (Ishii et al., 1997)).

In these experiments, the amplitude of whole-cell SK currents also appeared to be raised during the post-run down instability phase, as a result of the inclusion of 1 mM MgATP intracellularly. For this reason it was decided to investigate the possibility that intracellular MgATP activates the rSK3 channel. The stimulatory effect of MgATP on the rSK3 channel can be best seen in inside-out patches by varying the intracellular MgATP (Figure 3.9 on page 125 and 3.10 on page 126). These patches had been excised from CHO cells as they contain very little endogenous current. Application of 1 mM MgATP in the first minute after excising the patch, caused the current amplitude to increase to 248±36.6% (mean±SEM) (n=4 recordings) of the value recorded in intracellular solution which lacked MgATP (Figure 3.9 on page 125). This is equivalent to 1 mM MgATP inducing nearly a two and a half fold increase in rSK3 current. However, the ability to activate SK channels using MgATP was clearly time-dependent (Figure 3.10 on page 126). These plots, which demonstrate the time-dependency of MgATP efficacy on inside-out patches expressing rSK3 channels, were created with the same voltage step protocol used to generate previous time-dependency plots, except that currents were analyzed at +70 mV. Briefly, upon entering into the inside-out patch mode (defined as recording number zero in Figure 3.10 on page 126 (time zero)), currents were evoked from patches by applying the following voltage step protocol; patches were held at −80 mV and then stepped to a series of incremented voltages which began at −100 mV and increased in 10 mV intervals to +70 mV before they were returned to −80 mV. Similar step protocols were applied at various time intervals after time zero, as described in Figure 3.10 on page 126, and the average current at +70 mV

was recorded and subsequently plotted. In these recordings, the existence of leak currents and non-calcium-activated conductances were checked by performing patch recordings in calcium-free intracellular solutions.

### rSK3 channels are not modulated by 1-naphthylphosphate, a general phosphatase inhibitor, in the whole-cell configuration

In order to test whether the activation of endogenous phosphatases under the whole-cell configuration caused run down, a phosphatase inhibitor was included in the pipette solution. Upon entry into the whole-cell mode (defined as time zero), currents were evoked from cells by applying a standard voltage step protocol; whole-cells were held at −80 mV and then stepped to a series of incremented voltages which began at −100 mV and increased in 10 mV intervals to +70 mV before the cells were returned to −80 mV. Similar step protocols were applied every minute after time zero, and the average current at -40 mV was recorded and subsequently plotted for each minute as shown in (Figure 3.11 on page 127). The inclusion of 1-naphthylphosphate, a general phosphatase inhibitor (type1/2a) (Wagner & Wu, 1990), in a standard pipette solution lacking any MgATP produced a current which fell to 25.3±8.8% (mean±SEM) (n=3 recordings) of its original value over the run down phase. Following run down, currents were stable to within 58.3±42.0% (mean±SEM). These values compared to a reduction to 39.2±10.6% (mean±SEM) over the run down phase (n=3 recordings), followed by an instability phase in which currents were stable to within 44.3±16.0% (mean±SEM), using a pipette solution lacking both MgATP and this phosphatase inhibitor (Figure 3.4 on page 114). The reductions in current over the run down phase and the magnitudes of current instability between recordings generated using intracellular solutions containing 1-naphthylphosphate and those lacking it, are not significantly different from each other ($P>0.05$). This suggests that type 1/2a phosphatases are either not present or that they do not regulate the rSK3 channel.

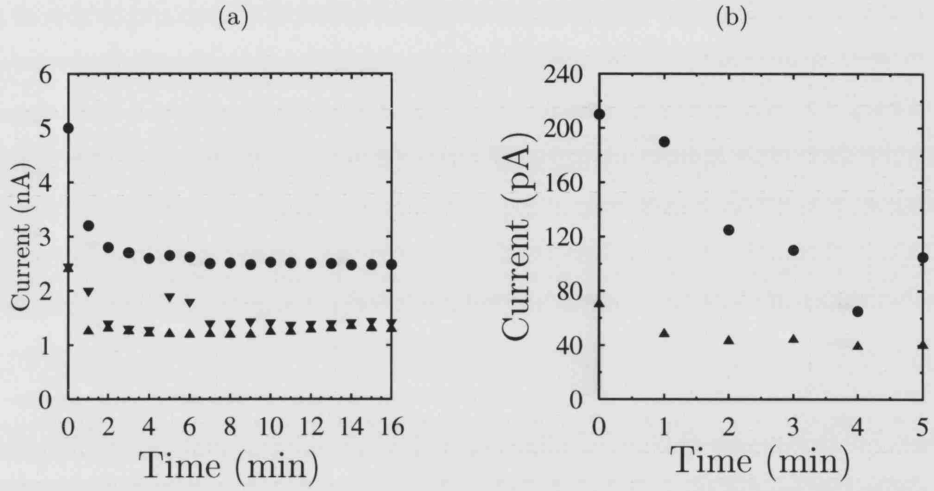


**Figure 3.8:** Graphs showing time-dependency of SK currents from whole-cells and inside-out patches when the intracellular solution contains 1 mM MgATP. (a) Time-dependency of WT rSK3 currents in 3 transiently transfected HEK 293 cells (*circles*, *upright triangles*, *inverted triangles*) under the whole-cell configuration, which were exposed to 1 mM intracellular MgATP. Each cell was voltage-clamped and the whole-cell currents that were generated at -40 mV were plotted every minute as shown (cells entered the whole-cell mode at time zero). In these three transiently transfected HEK 293 cells, the average whole-cell current fell to 50.7±6.7% (mean±SEM) of the original current over the run down phase. Following run down, the average current in these three cells was stable to within 20.4±14.4% (mean±SEM). Currents at -40 mV during the post-run down phase were more stable with 1 mM MgATP in the intracellular solution than without (e.g. Figure 3.4 on page 114). (b) Time-dependencies of WT rSK3 currents in two inside-out patches excised from CHO cells that had been transiently transfected with WT rSK3 DNA. Each patch was voltage-clamped and the currents that were generated at +70 mV were plotted every minute as shown. Run down was virtually absent in one patch but occurred in the other. In the two cells shown in (b), the average patch current fell to 45% of its original value recorded immediately following excision (patches were both excised at time zero). *Circles* and *upright triangles* each represent separate patches. The intracellular solution contained 1 mM MgATP and 1 μM free $Ca^{2+}$ for each recording. A standard bath solution containing 5 mM KCl was used extracellularly in each case.

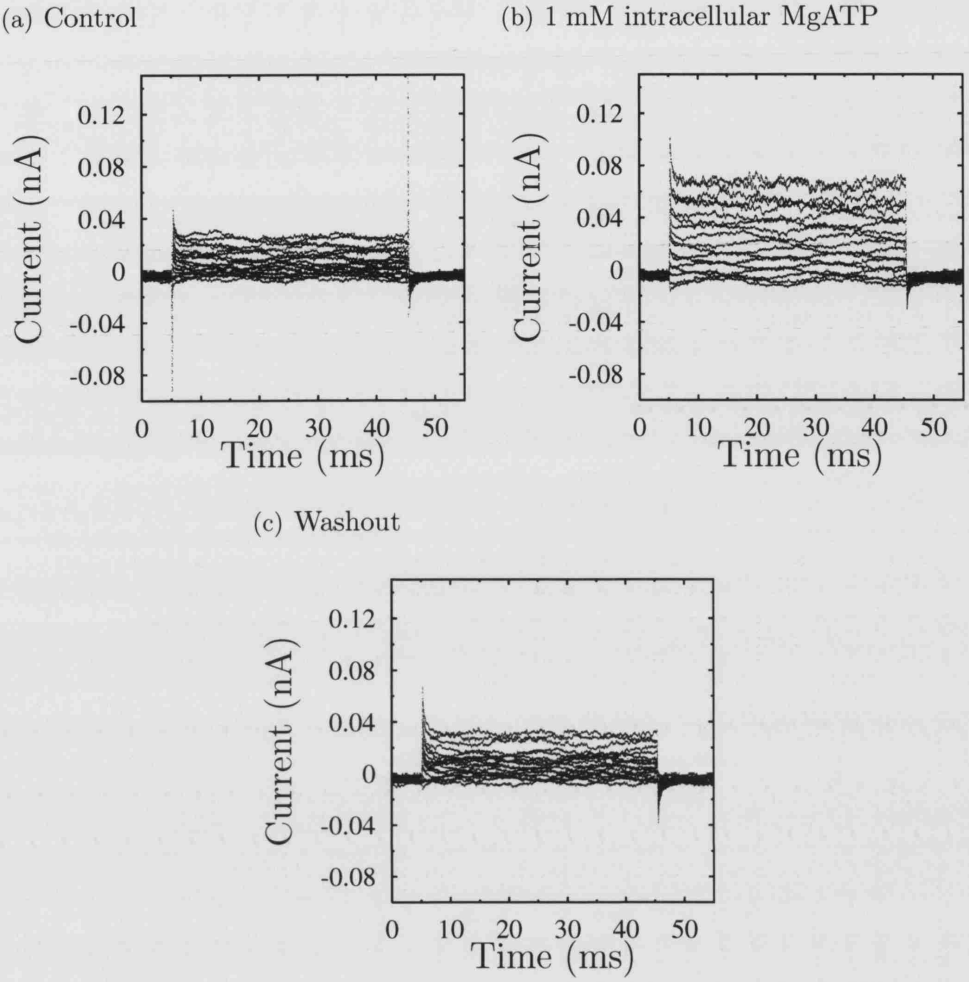


**Figure 3.9:** Representative current traces showing the activation of WT rSK3 channels by 1 mM intracellular MgATP in an inside-out patch that had been excised from a transiently transfected CHO cell. This patch was voltage-clamped and held at −80 mV, before being stepped to voltages between −100 mV and +70 mV (in 10 mV increments). After 40 ms at the appropriate potential, the patch was returned to −80 mV. Using this voltage-clamp protocol, current traces were obtained by perfusing the intracellular side of the patch with; (a) Control (intracellular solution containing 130 mM KCl, 1 μM free $Ca^{2+}$, 5 mM HEDTA, 10 mM HEPES, but no added $Mg^{2+}$ or ATP) (b) 1 mM intracellular MgATP (intracellular solution contained 130 mM KCl, 1 mM MgATP, 1 μM free $Ca^{2+}$, 5 mM HEDTA, 50 μM free $Mg^{2+}$), (c) Washout (intracellular solution was same as control solution). (b) was recorded half a minute after (a), and (c) was recorded half a minute after (b). In four such recordings, application of 1 mM MgATP caused the current amplitude to increase to 248±36.6% (mean±SEM) (n=4 recordings) of the value recorded in intracellular solution which lacked MgATP. The standard bath solution (containing 5 mM $K^+$) was used to fill the pipette.

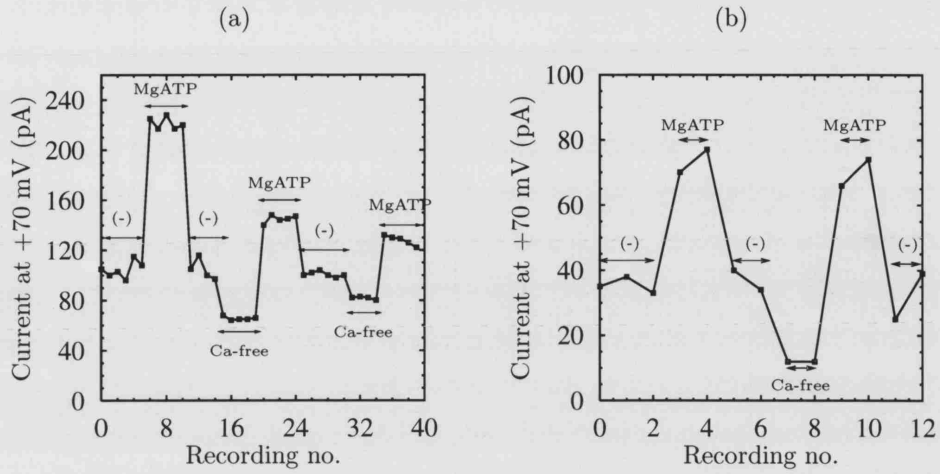


**Figure 3.10:** Effect of 1 mM intracellular MgATP on excised inside-out CHO cell patches expressing WT rSK3 channels. Each patch was voltage-clamped and the currents that were generated at +70 mV were plotted as shown (both patches were excised at recording number zero). Each recording number is separated by 10 seconds except when shifting between barrels of the microperfusion system (30 seconds to reposition the pipette tip) (a) Shows activation by 1 mM intracellular MgATP and time-dependent loss in efficacy of this activation. Activation by intracellular MgATP can clearly be seen, whilst run down was present when the intracellular solution contained MgATP, but not when the intracellular solution did not. "(-)" recordings were made using an intracellular solution lacking MgATP but containing 130 mM KCl, 5 mM HEDTA, 10 mM HEPES, and 1 μM free calcium (pH 7.2 with KOH), "Ca-free" recordings were made using an intracellular solution lacking MgATP and $Ca^{2+}$ but containing 130 mM KCl, 5 mM HEDTA and 10 mM HEPES (pH 7.2 with KOH), "MgATP" recordings were made using an intracellular solution containing 130 mM KCl, 5 mM HEDTA, 10 mM HEPES, 1 mM MgATP (3 mM $MgCl_2$, 2 mM $Na_2ATP$) and 1 μM free calcium(pH 7.2 with KOH) as described in the method. Patches were perfused using the multi-barrel system. The seal on CHO cells tended to be in the range 1–10 GΩ suggesting approximately 7–70 pA of leak current at +70 mV. A 70 pA leak current would account for the current in the first $Ca^{2+}$-free application suggesting all the channels are $Ca^{2+}$-activated. (b) Different excised inside-out patch showing activation of rSK3 channels by 1 mM intracellular MgATP. As in (a), there is no evidence of run down in this patch when using a MgATP-free intracellular solution, and in addition when using 1 mM MgATP in the intracellular solution. In four such recordings, application of 1 mM MgATP in the first minute after excising the patch, caused the average current amplitude to increase to 248±36.6% (mean±SEM) of the value recorded in intracellular solution which lacked MgATP (e.g. Figure 3.9 on the preceding page). A standard bath solution (containing 5 mM $K^+$) was used to fill the pipette.

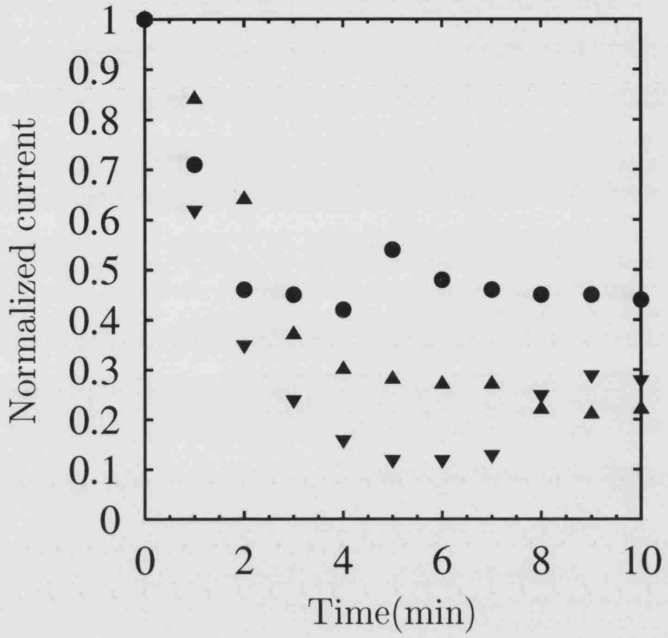


**Figure 3.11:** Time-dependency of whole-cell SK currents recorded with a pipette solution containing the general phosphatase inhibitor, 1-naphthylphosphate (1mM). HEK 293 cells that had been transiently transfected with WT rSK3 DNA were used for this experiment. Each cell, represented by *circles*, *upright triangles* and *inverted triangles*, was voltage-clamped and the whole-cell currents that were generated at -40 mV were normalized and plotted every minute as shown (cells entered the whole-cell mode at time zero). In these three recordings, whole-cell current amplitudes ran down to an average of 25.3±8.8% of their original value recorded at time zero. Following run down, the average current from these three cells was stable to within 58.3±42.0%. A standard intracellular solution with 1 μM free $Ca^{2+}$, 130 mM KCl, 10 mM HEPES, 1 mM 1-naphthylphosphate and 5 mM HEDTA (no added $Mg^{2+}$ or ATP) was used to make these recordings. A standard extracellular solution containing 5 mM KCl was also used.

### 3.3.10 Inward rectification of rSK3 currents occurs in patches

Although rSK3 channels appeared to be partially stabilized by the inclusion of MgATP in the pipette, the I–V curves in some patch recordings were found to show inward rectification, not seen in control (0 mM MgATP) recordings (Figure 3.12 on the next page). This could be the result of either free magnesium ion block or free ATP block, since both species cannot be reduced to zero if the MgATP complex is to be included in the intracellular solution. It was therefore important to look at the effect of both intracellular magnesium ions and intracellular ATP in turn. Although ATP may seem like an unlikely blocker, it was worth testing because in bullfrog erythrocytes, the calcium-activated permeability (known to be SK4) has been reported to be blocked with an inverted bell-shaped, biphasic inhibition curve in the range, 0.1⇒0.01 mM ATP (Shindo et al., 2000). No $Mg^{2+}$ was present in the recording solution and therefore block could not be attributable to this ion.

$Mg^{2+}$ ions are also known to block several channels and it has been reported in cultured hippocampal neurons, that application of 500 μM intracellular magnesium causes a substantial reduction of SK current in inside-out patches at positive potentials only (Lancaster et al., 1991). This is perhaps more likely to account for inward rectification than ATP and was also investigated.

#### Intracellular ATP does not block rSK3 channels

The effect of 1 mM intracellular ATP was investigated since this is known to produce approximately 50% block of SK4 currents (Shindo et al., 2000). Figure 3.13 on page 131 shows that 1 mM free intracellular ATP had no effect on rSK3 currents in patches that had been excised from CHO cells (CHO cell patches were used to express rSK3 channels because they contain very little endogenous current). Currents that were evoked using a standard voltage step protocol were not reduced by the application of 1 mM ATP intracellularly: the mean normalized current following

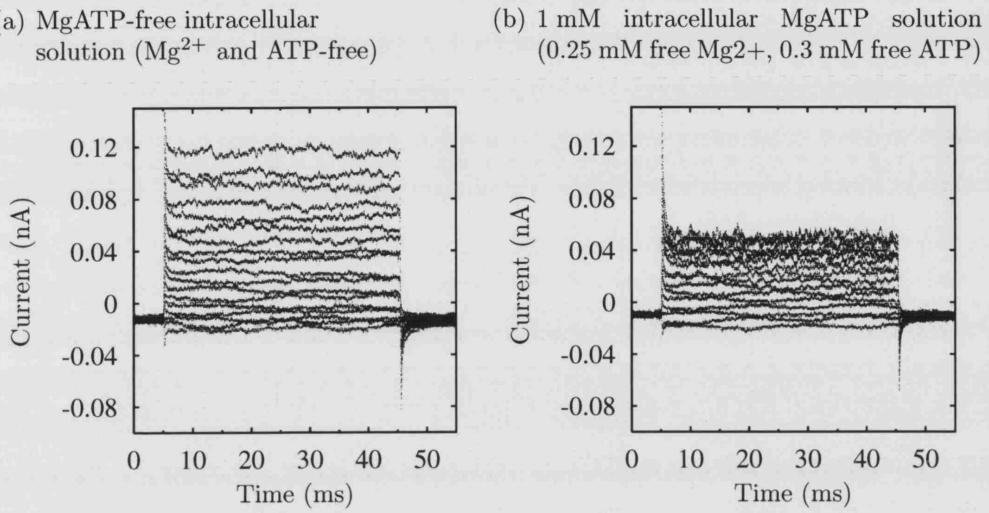


**Figure 3.12:** Recordings showing that the presence of intracellular MgATP (1 mM) does produce rectification of WT rSK3 currents in CHO cell inside-out patches. This patch was voltage-clamped and held at −80 mV, before being stepped to voltages between −100 mV and +70 mV (in 10 mV increments). After 40 ms at the appropriate potential, the patch was returned to −80 mV. Using this voltage-clamp protocol, current traces were obtained by perfusing the intracellular side of the patch with; (a) MgATP-free intracellular solution (containing 1 μM free $Ca^{2+}$, and (b) 1 mM intracellular MgATP solution (containing 0.25 mM free $Mg^{2+}$, 0.3 mM free ATP and 1 μM free $Ca^{2+}$). In three recordings made in this way, normalization of the average current over the 0 mV step to the average current at +70 mV, gave a figure of 0.35±0.03 (mean±SEM) for recordings that were made using intracellular solutions as in (a), whereas a figure of 0.71±0.04 (mean±SEM) was obtained for currents recorded with intracellular solutions as in (b). Pipette solutions were applied to the intracellular surfaces of patches, and contained 130 mM KCl. A standard bath solution (containing 5 mM $K^+$) was used to fill the pipette.

application of 1 mM intracellular ATP was 1.06±0.05 (mean±SEM) at -40 mV, and the mean normalized current after washout of the drug was 1.05±0.02 (mean±SEM) at -40 mV (n=3 recordings) (currents have been normalized to the control currents and then averaged). This demonstrates that the SK current is insensitive to the ATP ligand, at least up to a concentration of 1 mM.

### Intracellular $Mg^{2+}$ ions induce rectification of rSK3 currents

The inclusion of 0.25 mM intracellular $Mg^{2+}$ caused an inward rectification of SK current, in the absence of ATP (Figure 3.14 on page 132). The degree of rectification (defined by the normalization of the mean current at 0 mV to the mean current at +70 mV), is very similar to Figure 3.12 on the preceding page, suggesting that intracellular $Mg^{2+}$ may fully account for the inward rectification seen in the presence of MgATP. Furthermore, the extent of intracellular $Mg^{2+}$ inhibition appeared to be dose-dependent (Figure 3.15 on page 133). Such rectification was always observed in the patch configuration, but not in whole-cell (Figure 3.16 on page 134): normalization of the average current over the 0 mV step to the average current at +40 mV, gave a figure of 0.69±0.02 (mean±SEM) for whole-cell recordings that were made using 1 mM free $Mg^{2+}$ intracellularly (n=3 recordings), whereas a figure of 0.70±0.04 (mean±SEM) was obtained from whole-cells when intracellular solutions did not contain any free intracellular $Mg^{2+}$ (n=3 recordings). Next, dose-response curves were plotted for each voltage, and used in the next stage of analysis.

**Analysis of $Mg^{2+}$ block** Having obtained the $IC_{50}$ values at each step potential through fitting a Hill-Langmuir isotherm to the data (Table 3.2 on page 136), it was apparent that this block was voltage-dependent. The method of Woodhull (1973), first used to analyze a proton binding site in the sodium channel, predicts a voltage-dependent block by cations assuming a single blocking site. Therefore the Woodhull equation was used to fit the data in a plot of log[$IC_{50}$] against transmembrane po-

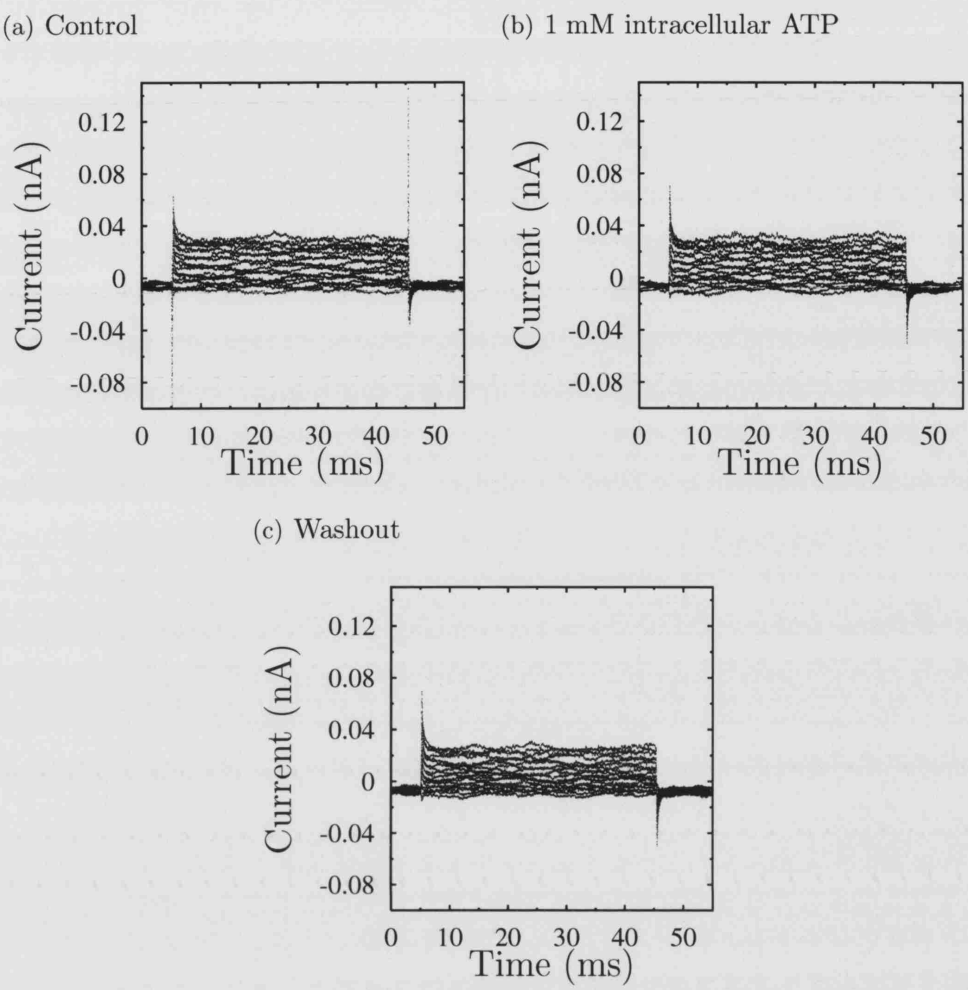


**Figure 3.13:** Lack of effect of 1 mM intracellular ATP on an excised inside-out CHO cell patch expressing rSK3 currents. In each trace, the transmembrane potential of the patch was held at −80 mV, before being stepped to voltages between −100 mV and +40 mV (in 10 mV increments). After 40 ms at the appropriate voltage, the potential was returned to −80 mV. Using this voltage-clamp protocol, the patch was perfused with (a) Control solution that lacked intracellular ATP, (b) 1 mM ATP solution that was applied to the intracellular surface of the patch, (c) Washout (same as control). No effect of 1 mM intracellular ATP application can be seen in this recording. In three such recordings, 1 mM intracellular ATP did not produce a significant block of WT rSK3 current: the mean normalized current following application of 1 mM intracellular ATP was 1.06±0.05 (mean±SEM) at -40 mV, and the mean normalized current after washout of the drug was 1.05±0.02 (mean±SEM) at -40 mV (currents have been normalized to the control currents and then averaged). An intracellular solution containing 130 mM KCl, 5 mM HEDTA, 10 mM HEPES, 1 μM free calcium, no added magnesium and no added ATP was used in the microperfusion system in recordings (a) and (c). An intracellular solution containing 1 mM free ATP (no added magnesium, 1 μM free calcium, 5 mM HEDTA, 10 mM HEPES, 130 mM KCl) was used for perfusing the patch in (b). A standard bath solution (containing 5 mM $K^+$) was used to fill the pipette in each case.

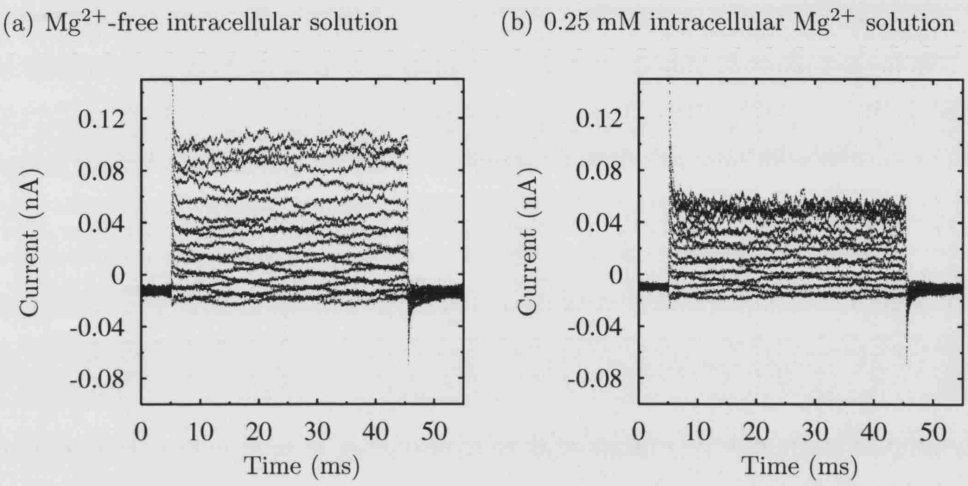


**Figure 3.14:** Current traces from an inside-out patch illustrating a voltage-dependent block by intracellular $Mg^{2+}$ ions. This patch had been excised from a CHO cell that had been transiently transfected with WT rSK3. It was voltage-clamped and held at −80 mV, before being stepped to voltages between −100 mV and +70 mV (in 10 mV increments). After 40 ms at the appropriate step, the patch was returned to −80 mV. Using this voltage-clamp protocol, the patch was perfused with intracellular solutions containing (a) 0 mM $Mg^{2+}$, 1 μM free $Ca^{2+}$, and (b) 0.25 mM free $Mg^{2+}$, 1 μM free $Ca^{2+}$. In three recordings made in this way, normalization of the average current over the 0 mV step to the average current at +70 mV, gave a figure of 0.37±0.03 (mean±SEM) for recordings that were made using intracellular solutions as in (a), whereas a figure of 0.68±0.02 (mean±SEM) was obtained for currents recorded with intracellular solutions as in (b). Solutions (intracellular) used in the microperfusion system all contained 130 mM KCl, but no ATP. A standard bath solution containing 5 mM KCl and 1 mM $MgCl_2$ was used in the pipette.

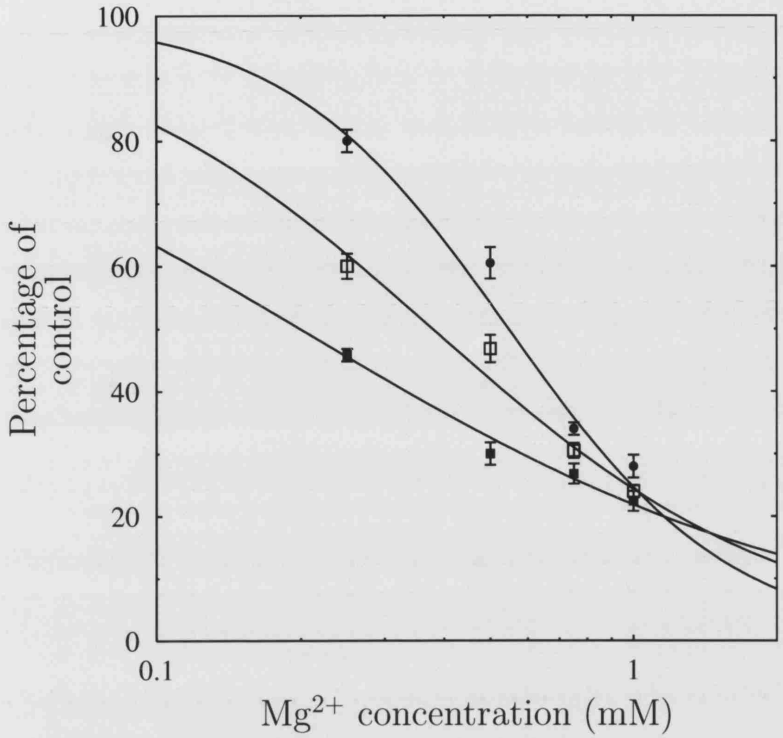


**Figure 3.15:** Dose-response curves for intracellular $Mg^{2+}$ block of WT rSK3 currents at different transmembrane potentials. All experiments were carried out using CHO cells that had been transiently transfected with WT rSK3 DNA. *Filled squares* represent current remaining at +70 mV at different intracellular $Mg^{2+}$ concentrations. *Open squares* represent current remaining at +30 mV and *Circles* represent the current remaining at 0 mV. $Mg^{2+}$ concentrations are plotted on a log scale. Each set of data has been fitted to the Hill equation and the $IC_{50}$s and Hill coefficients have been allowed to vary. In each case, $B_{max}$ has been fixed at 100. At +70 mV, the estimated $IC_{50}$ for magnesium block is 0.20±0.01 mM (mean±SD) with a Hill coefficient of 0.79±0.07 (mean±SD); this Hill isotherm is not a very good fit of the data, since the range of the data points obtained only covers the lower half of the dose-response curve. At +30 mV, the estimated $IC_{50}$ for magnesium block is 0.38±0.03 mM (mean±SD) with a Hill coefficient of 1.2±0.1 (mean±SD), and at 0 mV the estimated $IC_{50}$ is 0.55±0.03 mM (mean±SD) with a Hill coefficient of 1.9±0.3 (mean±SD); the Hill isotherm generated at 0 mV is the best of the three fits, since the range of the data points obtained at 0 mV covers the entire dose-response curve. Data points are the average current remaining at the various potentials shown after application of intracellular $Mg^{2+}$ to three different inside-out patches, and the vertical bars indicate the SEM. All cells were held at -80 mV between recordings, and current block was measured at +70 mV, +30 mV and 0 mV for each patch. Solutions used in the microperfusion system all contained 130 mM KCl, and 1 μM free $Ca^{2+}$, but no ATP. A standard bath solution containing 5 mM KCl and 1 mM $MgCl_2$ was used in the pipette.

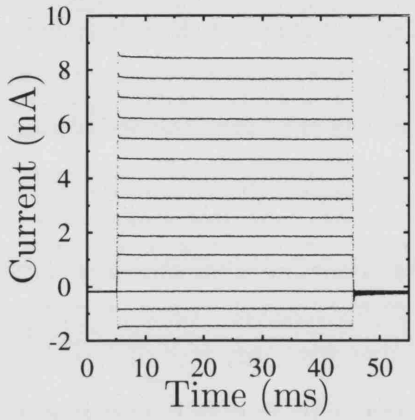


**Figure 3.16:** Representative recording showing that the presence of 1 mM intracellular $Mg^{2+}$ does not produce rectification of whole-cell WT rSK3 currents in transiently transfected HEK 293 cells. The cell was voltage-clamped and the currents shown were evoked immediately (<20-30 seconds) after going whole-cell by applying a standard voltage step protocol; the cell held at −80 mV, before being stepped to voltages between −100 mV and +40 mV (in 10 mV increments). After 40 ms at the appropriate step, the cell was returned to −80 mV. In three such recordings, a voltage-independent SK current was obtained each time: normalization of the average current over the 0 mV step to the average current at +40 mV, gave a figure of 069±0.02 (mean±SEM) for recordings that were made using 1 mM free $Mg^{2+}$ intracellular solutions as above. This figure is not significantly different from the value obtained using intracellular solutions not containing any free $Mg^{2+}$ ions (0.70±0.04 (mean±SEM)). For each recording, a pipette solution containing 130 mM KCl, 1 μM free calcium, and 1 mM free $Mg^{2+}$ was used. Additionally, a standard bath solution (containing 5 mM $K^{+}$) was used externally each time.

tential. Figure 3.17 on page 137 shows such a plot which has been fitted using the positive potentials only, since the negative potentials appear to have a distinct slope. The gradient of this fitted line is equal to the empirical $\frac{z\delta F}{RT}$ value (Figure 3.17 on page 137, symbols have been defined in section 2.6.2). $z\delta$ can therefore be worked out using this gradient as the remaining parameters are all constants. In the case of Figure 3.17 on page 137, $z\delta$ is 0.38±0.03 (mean±SD), or $\delta$ is 0.19. Hill coefficients increased as the $Mg^{2+}$ affinity decreased, suggesting rSK3 channels could have negative cooperativity of intracellular $Mg^{2+}$ ion binding. However, the accuracy of the dose-response curves obtained at each potential either side of 0 mV is questionable, since the range of the data points used did not provide a broad spread of values required to generate an accurate fit. The fitted data will need to be confirmed using more appropriate ranges of $Mg^{2+}$ concentrations to get more accurate dose-response curves for each potential.

## 3.4 Discussion

CHO cells did not express any significant endogenous or calcium-activated currents, consistent with previous reports (Yu & Kerchner, 1998). The endogenous currents seen under both low and high intracellular calcium conditions for untransfected HEK 293 cells were essentially identical suggesting that any calcium-activated conductances are insignificant. Both cell lines are therefore suitable for exogenous SK channel expression. However, the voltage-dependence of endogenous HEK 293 currents suggest that patch clamp data obtained from these cells should be used at negative potentials, where there are virtually no endogenous currents. Suppression of these endogenous currents is not possible because such currents have been found to be relatively insensitive to 4-aminopyridine (a 10 mM concentration produces ≈25% block), TEA (20 mM TEA produces nearly 60% block), and apamin (insensitive up till 1 μM) (Yu & Kerchner, 1998), and so these drugs cannot be used to

| Transmembrane potential | $IC_{50}$ (mM) | Hill coefficient |
|---|---|---|
| +70 mV | $0.20 \pm 0.01$ | $0.79 \pm 0.07$ |
| +60 mV | $0.23 \pm 0.04$ | $0.84 \pm 0.2$ |
| +50 mV | $0.22 \pm 0.05$ | $0.72 \pm 0.2$ |
| +40 mV | $0.33 \pm 0.03$ | $1.1 \pm 0.2$ |
| +30 mV | $0.38 \pm 0.03$ | $1.2 \pm 0.1$ |
| +20 mV | $0.49 \pm 0.03$ | $1.6 \pm 0.2$ |
| +10 mV | $0.53 \pm 0.05$ | $1.9 \pm 0.4$ |
| 0 mV | $0.55 \pm 0.03$ | $1.9 \pm 0.3$ |
| −10 mV | $0.59 \pm 0.04$ | $2.7 \pm 0.5$ |
| −20 mV | $0.51 \pm 0.03$ | $2.9 \pm 0.4$ |
| −30 mV | $0.62 \pm 0.03$ | $4.6 \pm 0.8$ |

**Table 3.2:** Table to show the variation of $IC_{50}$ for intracellular $Mg^{2+}$ block with transmembrane potential in inside-out patches pulled from CHO cells that had been transiently transfected with WT rSK3. A dose-response curve for intracellular $Mg^{2+}$ block of the WT rSK3 channel was generated at each potential shown using concentration-inhibition points at 0.25 mM, 0.50 mM, 0.75 mM and 1 mM free $Mg^{2+}$ concentrations. Each concentration-inhibition point was the average of three observations. Hill-Langmuir isotherms were fitted to the data with $B_{max}$ fixed at 100. The increasing Hill coefficients as transmembrane potentials become less negative and more positive, are probably due to inaccuracies involved in the generation of the fitted lines for each dose-response curve. The data points at 0 mV fitted well to a Hill isotherm Figure 3.15 on page 133, but the data at the extreme potentials (+70 mV and -30 mV) did not. For these experiments, a standard pipette solution was used externally which contained 130 mM KCl, and 1 μM free $Ca^{2+}$. Intracellular $Mg^{2+}$ concentration was varied between 0 mM and 1 mM as described. A standard bath solution, which was used to fill the pipette, contained 5 mM KCl, and 1 mM free $Mg^{2+}$.

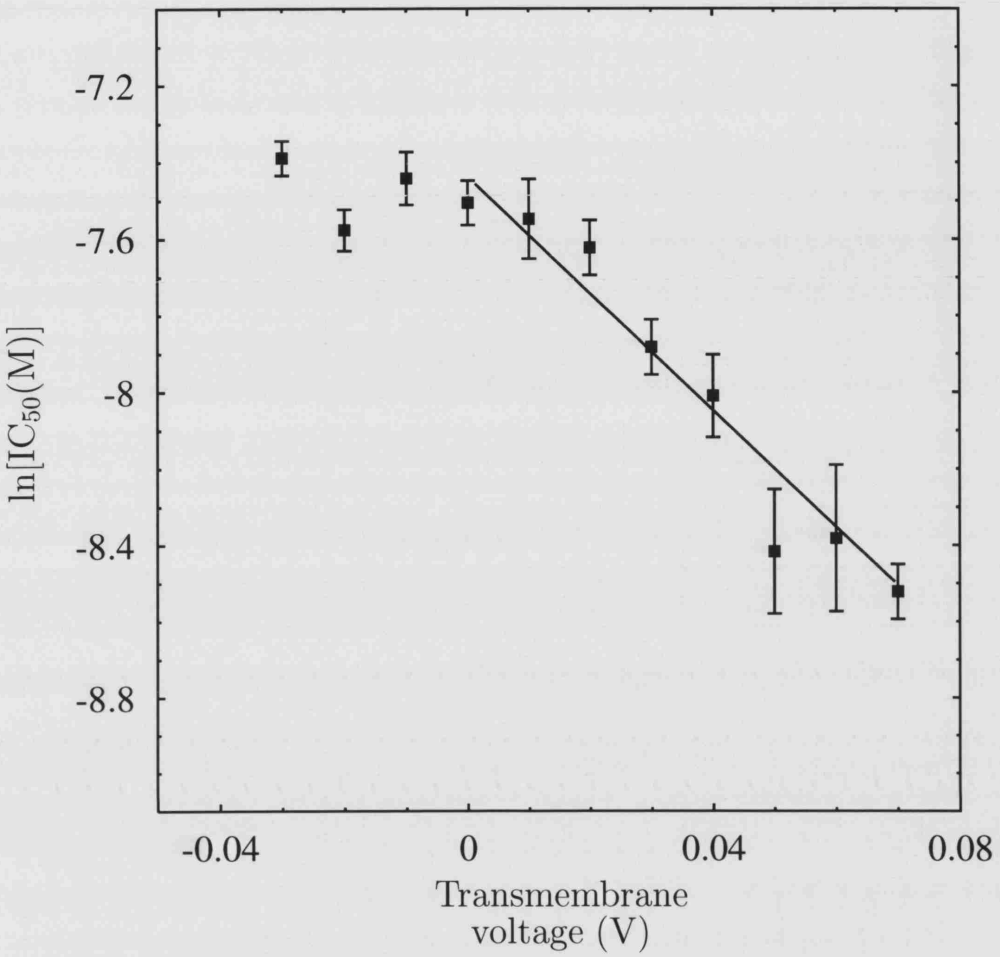


**Figure 3.17:** Natural logarithms of the $IC_{50}$ values for intracellular $Mg^{2+}$ ion block of WT rSK3 currents at different transmembrane potentials, recorded in transiently transfected HEK 293 cells. Each point is the natural log of the $IC_{50}$ value at each potential as estimated from the Hill equation, and the vertical bars indicate the natural log of the SD of each data point. The least squares fit line for values between +70 mV and 0 mV has been plotted using the Woodhull equation with the $z\delta$ and $\ln IC_{50}^{0\,mV}$ parameters allowed to vary. For this fit, $z\delta$ is 0.38±0.03 (mean±SD) ($\delta$=0.19) and $\ln IC_{50}^{0\,mV}$ is -7.4±0.05 (mean±SD) ($IC_{50}^{0\,mV}$ is 0.64 mM). A biphasic plot appears to fit all the data points best. The reason more negative potentials could not be plotted is because the block by magnesium at the concentrations used became too small for dose-response curves to be drawn. Due to the lack of data points at negative potentials, and the appearance of a distinct slope at the low negative potentials, the line of best fit using the Woodhull equation has been plotted for positive potentials only. Cells were held at -80 mV and the average current was measured over the entire voltage step interval in each experiment.

suppress endogenous HEK 293 currents without blocking SK channels (4-AP blocks SK3 channels with an $IC_{50}$ of 512 μM (Grunnet, Jespersen, et al., 2001), TEA blocks SK1 channels with an $IC_{50}$ of 14.6 mM (Ishii et al., 1997), and apamin blocks SK3 channels with an $IC_{50}$ of 1.4 nM (Hosseini et al., 2001)).

### 3.4.1 Run down of rSK3 channels

The rSK3 channel activity recorded in every cell line ran down. There could be a number of possible reasons for this reduction in current. Broadly speaking, run down of SK channels may be regulated by factors which are "extrinsic" to the channel protein or those which are "intrinsic", as described in the introduction to this chapter.

#### Extrinsic factors

**External ion concentrations** The lack of effect on run down of raising the external $K^+$ ion concentration contradicts an earlier finding in adrenal chromaffin cells which endogenously express SK channels (Y. Park, 1994). One possibility is that hetero-oligomeric assemblies involving non-SK $\alpha$-subunits may have formed the native channels that produced these SK-like currents, and the lack of effect of raising the external $K^+$ ion concentration on cloned SK channels, could be as a result of a lack of such heteromeric associations occurring. Alternatively, $\beta$-subunit expression may vary in the two cell types, causing one channel complex to be sensitive to the external $K^+$ ion concentration and the other not to be. It might be worth testing to see the effect of removal of extracellular $Mg^{2+}$, since this has been shown to prevent run down of ROMK1 $K^+$ channels (Kubokawa et al., 1995)

**MgATP** The application of exogenous MgATP did appear to reduce run down slightly. In $K_{ATP}$ channels, the hydrolysis of phosphatidylinositol-3,5-bisphosphate ($PIP_2$) has been found to underlie $Ca^{2+}$-induced run down, an effect which can

be completely reversed by the addition of MgATP (Ribalet et al., 2000). In such channels, MgATP probably increases $PIP_2$ levels through lipid (PIP) phosphorylation (Xie et al., 1999). It is possible that $PIP_2$ hydrolysis causes SK current run down, and it would be worth seeing the effect of exogenous $PIP_2$ on this run down. However, SK channel run down may have a complex underlying mechanism, since MgATP can only partially prevent run down (Figure 3.16 on page 134). Furthermore, inside-out patch recordings that displayed virtually no run down in the absence of MgATP, appeared to copiously run down in the presence of intracellular MgATP (Figure 3.10 on page 126), suggesting that the mechanism underlying SK current run down in the presence of MgATP might be distinct to run down in the absence of MgATP. This important result is described in more detail later.

**Inside-out patches/membrane phosphatases** Inside-out patches sometimes did not show any SK current run down in the absence of MgATP ($\approx$ 50% of inside-out patches behaved like this), whereas run down was nearly always present in whole-cell recordings in the presence or absence of MgATP. This result suggests that a procedural difference might account for run down in some cases. In C6 Glioma cells, where membrane disruption has been proposed to activate endogenous phosphatases causing SK current run down, it has been found that inside-out patches run down the least (Manor & Moran, 1994). Application of a general phosphatase inhibitor (of type 1/2a phosphatases) intracellularly did not prevent run down of cloned SK channels in this study suggesting that phosphatase activation does not account for procedural differences in run down, although the possibility that other classes of phosphatases are activated cannot be discounted.

### Intrinsic factors

The cloned rSK3 channels in this study ran down by 49% in HEK 293 whole-cells in the presence of MgATP, whereas cloned rSK2 channels only ran down by about

10% in oocyte patches (Ishii et al., 1997). Although the basis for this discrepancy might be differences in $\beta$-subunit expression or recording configuration differences, or both, it is also plausible that certain molecular factors of the channel *per se* are causing the rSK3 channel to run down to a greater extent than rSK2, based on two previous reports. Firstly, point mutations in the SK pore have been shown to affect the magnitude of run down (Khawaled et al., 1999) (one of these SK channel residues, D528-rSK3, has been mutated into a lysine in this study, and can be used to ascertain such molecular contributions to run down). Secondly, it has been shown that run down of the SK1 channel is temporally correlated with a reduced sensitivity to block with bicucculine (Khawaled et al., 1999). One explanation for the time-dependent change in bicucculine sensitivity of the channel might be that the external pore is physically changing with time, thereby concomitantly altering the affinity of drug block with time and the current flowing through the channel. It is possible that the SK2 pore is not as dynamic or "plastic" as the pore of SK1 following calcium activation. This loss of SK current associated with a changing outer vestibule might be due to C-type inactivation, since this is known to occur as a result of a change in the outer pore region of $K^+$ channels with time (Y. Liu et al., 1996; Yellen et al., 1994). However, this process should be modifiable by elevating the extracellular $K^+$ ion concentration (Pardo et al., 1992; Heginbotham et al., 1994; Lopez-Barneo et al., 1993; Yang et al., 1997), and this effect was not observed in this study.

### 3.4.2 Regulatory properties of rSK3 channels

It has been observed that 1 mM intracellular MgATP does not activate hSK1, or rSK2, or rSK3 in *Xenopus* oocytes (Gerlach et al., 2001). The contradictory finding with rSK3 in this study could be as a result of the different expression systems used. Shah and Haylett (2000) suggest that differential $\beta$-subunit expression may occur between mammalian and *Xenopus* expression systems based on SK channel pharmacology. Endogenous $\beta$-subunit expression in oocyte and mammalian cells could be

tested using photoaffinity labelling of cells expressing SK channels with the photoreactive apamin derivative, 4-azido-2-nitro-phenylaminoacetyl mono[$^{125}$]iodoapamin ($^{125}$I-ANPAA-apamin) followed by membrane solubilization and gel electrophoresis. The banding pattern could indicate the lack of a $\beta$-subunit in any of the different expression systems. Although one target of intracellular MgATP may be the channel *per se*, another may be such an endogenously expressed $\beta$-subunit that could, as described above, be expressed differently in the mammalian and *Xenopus* expression systems. For example, MgATP was found to activate hSK4 via membrane-delineated kinases though the channel *per se* was not directly phosphorylated (Gerlach et al., 2000). Membrane-delineated A-kinase anchoring proteins which bind protein kinase A, were suggested to be associated with hSK4 forming a complex that may be the target of MgATP in these channels. The inside-out patches which were stimulated by internal MgATP (Figure 3.10 on page 126) also suggest the presence of membrane associated kinases in CHO cells which are capable of phosphorylating the rSK3 channel.

Cofactors such as $Mg^{2+}$ are usually required in order for kinases to transfer phosphate groups from ATP (Mitsuda et al., 1975; Weller, 1979), and this may explain why ATP *per se* does not produce any activation of the rSK3 channel whereas MgATP does. However, it is also possible that MgATP is directly binding to the channel and activating it. The use of non-hydrolyzable ATP analogues complexed with $Mg^{2+}$, such as MgATP$\gamma$S, would establish whether MgATP hydrolysis or direct ligand binding is causing channel activation. If hydrolysis is found to occur, it might be worth testing the effect of adding intracellular wortmannin, an inhibitor of phosphatidylinositol 3- and 4-kinases, in order to determine whether lipid phosphorylation mediates the effects of MgATP, as has been found for MgATP reactivation of $K_{ATP}$ channels (Xie et al., 1999).

### The time-dependency of MgATP activation of rSK3 channels

The target of the aforementioned kinases, which may be activated by MgATP, could be the channel, some associated protein, or regulatory molecule. The mechanism by which such a kinase activates the rSK3 channel must account for the time-dependent loss in the efficacy of MgATP activation that was seen in excised patches. This loss in efficacy of MgATP activation of SK channels is not due to current run down or instability since currents generated with an intracellular solution lacking MgATP were stable when the efficacy loss occurred (Figure 3.10 on page 126). The initial loss of MgATP activation of rSK3 over the first 5-10 minutes shares similar characteristics to the ability of MgATP to activate $K_{ATP}$ channels in the presence of internal calcium. Following a brief (<1 minute) exposure to 10 μM calcium, it was found that $K_{ATP}$ channels could be activated by MgATP, but following a more sustained exposure (5 minutes), MgATP reactivation was lost (Ribalet et al., 2000). The loss of MgATP activation following SK channel opening (Figure 3.10 on page 126) might occur through a similar mechanism as this loss of calcium-induced MgATP reactivation in $K_{ATP}$ channels. It was proposed that the loss of MgATP reactivation of $K_{ATP}$ channels following five minutes exposure to calcium, was due to a dephosphorylation-induced uncoupling of the SUR subunit from the $K_{ATP}$ $\alpha$-subunit, $K_{ir}6.2$ (Ribalet et al., 2000). It is possible that the uncoupling of a $\beta$-subunit from the SK channel $\alpha$-subunit might be occurring in a time-dependent manner with the resultant loss of MgATP activation, but identification and characterization of a $\beta$-subunit is required before this hypothesis can be investigated.

## 3.4.3 Magnesium-induced SK channel rectification

Whole-cell recordings did not show any magnesium-induced SK channel rectification despite being recorded with similar ionic solutions as those patches which rectified. This is probably because at the very positive command potentials, large voltage

drops across the series resistance occur which reduce the transmembrane potential *per se* to a value at which rectification does not occur. So, for example, at +70 mV there can easily be a 36 mV ($V_s$) drop across the series resistance, $V_s$ ($V_s = [3\times10^{-}9] \times [12\times10^{6}]$, assuming a whole-cell current of 3 nA at +70 mV and typical series resistance of 12 MΩ). This would result in a pipette potential that is not positive enough to observe this rectification in the whole-cell configuration.

### The $Mg^{2+}$ binding site

$Mg^{2+}$ and barium ($Ba^{2+}$) behave as divalent $K^+$ ions which can enter the selectivity filter of $K^+$ channels. However, these alkaline earth metals get bound too tightly in the selectivity filter due to their high charge, thereby blocking the flow of $K^+$ ions. In rSK2, for example, evidence that the magnesium binding site is located in the selectivity filter has been demonstrated through "trans knock-off" by potassium ions (Soh & Park, 2001). In the well-documented case of $Ba^{2+}$, the high affinity barium ion binding site has been determined, through X-ray crystallography, to be located at around position 4 in the selectivity filter (Jiang & MacKinnon, 2000). This is also known as the "inner ion" location just to the intracellular aspect of the selectivity filter. In rSK2, a recent study identified a serine residue at position 546 (located at the intracellular aspect of the selectivity filter in the rSK3 channel model based on KcsA) to be important but not wholly accountable for $Mg^{2+}$ block (Soh & Park, 2002). Serine is a hydrophillic (polar) amino acid and substituting this for a hydrophobic (non-polar) but structurally conserved alanine residue reduced $Mg^{2+}$-based inward rectification in the rSK2 channel, and caused a significant reduction in several other divalent cation affinities, including that of $Ba^{2+}$. This suggested a common divalent cation binding site in rSK2 which was partly formed by residue 546 in SK channels. Assuming that most of the transmembrane potential falls across the open potassium channel selectivity filter, as modelled in the open MthK channel (Jiang et al., 2002), the empirical results from this study also suggest an rSK3 $Mg^{2+}$

binding site which is located at a very intracellular point of the selectivity filter, at an electrical distance of 0.19 (Figure 3.17 on page 137) from the intracellular side. The fact that 1 mM $Mg^{2+}$, present in the extracellular solution in each and every recording, failed to produce any rectification when the driving force on $Mg^{2+}$ ions was from extracellular to intracellular (for instance, no rectification was seen at -40 mV with 1 mM external $Mg^{2+}$, whereas at +40 mV, rectification was quite apparent in the presence of 1 mM internal $Mg^{2+}$), demonstrates the asymmetry of access to the rSK3 channel's $Mg^{2+}$ binding site.

As a starting point towards identifying the residues which form the $Mg^{2+}$ ion binding site in rSK3, an S546A-rSK3 point mutant could be made in order to determine the contribution of the hydroxyl group of this serine residue. This is likely to account for some of the $Mg^{2+}$-induced rectification, as in the rSK2 channel (Soh & Park, 2001, 2002). However, because the S546-rSK2 residue can only partially account for the divalent cation rectification in this channel, it is possible that interaction of these cations with the carbonyl oxygens or side chains of neighbouring amino acids occurs. The primary sequence of SK channels reveals that the residues which surround S546-rSK3 are leucine (545) and isoleucine (547). Both these amino acids have aliphatic, non-polar side-chains which would not interact with divalent cations, although it is possible that the backbone carbonyl oxygen of the I547-rSK3 residue contributes to coordinating $Mg^{2+}$ ions, since its carbonyl oxygens should be facing the pore passageway (Zhou & MacKinnon, 2004).

### 3.4.4 Comparison of rectification in SK channels and inward rectifiers

Physiological concentrations of magnesium are in the millimolar range, which would tonically inhibit rSK3 channels making them functional inward rectifiers. Inward rectifiers that are blocked by millimolar intracellular $Mg^{2+}$ (e.g. $K_{ir}2.1$) are usually

classed as weak (Nichols et al., 1994) (higher $Mg^{2+}$ sensitivity is seen only with strongly rectifying channels (Nichols & Lopatin, 1997)). Therefore $Mg^{2+}$ rectification may be classed as weak in SK channels (Figure 3.15 on page 133) and supports the notion that these channels should be classed pharmacologically as inward rectifiers, although structurally (*viz.* TM elements) they are completely different.

The elements of high affinity $Mg^{2+}$ block (strong rectification) in $K_{ir}$ are believed to be the presence of hydrophillic, negatively charged residues at positions 171 in the M2 region and 224 in the C-terminus (Kubo et al., 1993; Bond et al., 1994; Ho et al., 1993; Abrams et al., 1996; Henry et al., 1995). Neutralization of these residues in $K_{ir}2.1$, a strong inward rectifier, reduces the affinity of rectification almost to that seen in ROMK1 ($K_{ir}1.1$), a weak inward rectifier (Yang et al., 1997). The anionic nature of the aspartic acid and glutamic acid are thought to interact electrostatically with the cationic metal blocking ion (Lu & MacKinnon, 1994). On the other hand, the rSK2 residue, Thr-574, (see Figure 1.4 on page 40 for the numbering system used) which is at the equivalent position to residue 171 of $K_{ir}$, is not thought to contribute appreciably to SK rectification (Soh & Park, 2002). This suggests, assuming magnesium blocks rSK2 and rSK3 similarly (which is quite likely based on the primary sequence homology of their pore regions), that the mechanism of rectification observed in this study is not similar to high affinity $Mg^{2+}$ block in $K_{ir}$. Furthermore, the predicted location of these amino acids (171 in M2 and 224 in the C-terminus of $K_{ir}$ channels) is in the internal cavity of SK channels based on sequence alignments, and therefore $Mg^{2+}$ block would not be expected to be influenced by voltage (the electric field of the open channel is thought to fall mainly across the selectivity filter (Jiang et al., 2002), and the central cavity $K^+$ ion is flooded with water (Doyle et al., 1998), and therefore neither should exert much electrical influence over any surrounding $Mg^{2+}$ ions). This is consistent with SK channel $Mg^{2+}$ block being distinct from high affinity $K_{ir}$ $Mg^{2+}$ block.

### 3.4.5 Summary and future directions

A stably expressing WT rSK3 cell line was created, but due to current instability and excessive amounts of run down, preference, for future recording purposes, will be given to transiently transfected cells. In addition, WT rSK3 currents were successfully characterized, showing a large, voltage-independent current, as seen in other studies (Hosseini et al., 2001; Kohler et al., 1996). Another important result of this work with regards to future recordings from cloned SK channels, is that CHO cells might be better than HEK 293 cells for recording small currents, such as those that are present in patches, as they do not have any substantial endogenous currents, whereas HEK 293 cells do. Additionally, CHO cells would be more desirable when characterizing currents for the first time, such as those from the mutant SK channels, as there would be no chance of endogenous currents being a factor in any atypical current shapes. However, the HEK 293 cell line is probably better suited for recording large, well-characterized whole-cell SK currents, since transiently transfected HEK 293 cells show a bit more SK current stability during the post-run down phase in the whole-cell mode compared to other cell lines. In addition, it is worth using intracellular MgATP to record from whole-cells in future experiments since this molecule does also appear to stabilize SK currents during the post-run down phase when drugs would be applied. Approximately 1 in every 3 or 4 transiently transfected HEK 293 whole-cells that have 1 mM MgATP intracellularly, would possess 5 or 10 minute windows during the instability phase, when drugs could be applied and washed off (unblocked currents remaining stable to within 10%). This combination of transiently transfected HEK 293 cells with millimolar intracellular MgATP produced the most optimal conditions for drug application to whole-cells.

Due to the vast number of extrinsic variables that may cause current run down, a more general approach to identifying its source might be preferable which firstly identifies the type of molecule causing run down, as it appears that results regarding

regulation of SK channels in native cells or of cloned SK channels in non-mammalian cell lines are not reproducible in mammalian cell lines. For example, in order to identify whether kinases or phosphatases contribute to SK current run down or activation, a low concentration of trypsin (<0.5 mg/ml (Spreadbury et al., 2004)) could be used as an intracellular protease. If the extent of run down, for example, is reduced by this treatment, then it might be worth testing other phosphatases, such as types 2b and 2c, which were not tested in this study. Cyclosporin A (Matsuda & Koyasu, 2000)) or the recently synthesized 1,5-dibenzoyloxymethyl-substituted norcantharidin (Baba et al., 2003) are both inhibitors of type 2b phosphatases. Okadaic acid is a general phosphatase inhibitor of type 1, 2a, and 2b phosphatases but no potent inhibitors of type 2c phosphatases have as yet been discovered (Herzig & Neumann, 2000).

# Chapter 4

# CTX-sensitive and TEA-sensitive point mutants of rSK3 channels

## 4.1 Aim

- To determine whether structural features of the KcsA and Shaker channel pores provide an appropriate basis for comparison with the rSK3 pore

## 4.2 Introduction

A good starting point for understanding SK channel structure is to try to relate it to the known structure of KcsA. This structure has been shown to be similar to that of other $K^+$ channels in the pore region, particularly that of the Shaker $K^+$ channel for which there is a great deal of data concerning the residues that dictate its pharmacology. Two residues, which are important in the pharmacological profile of Shaker and other $K^+$ channels, have been shown to determine charybdotoxin (CTX) and tetraethylammonium (TEA) binding (Heginbotham & MacKinnon, 1992; Goldstein et al., 1994; Jensen et al., 2001; Ishii et al., 1997), and this chapter takes a look at the effects of two equivalent rSK3 point mutations (G535D-rSK3 and V555F-rSK3)

on the pharmacology of these two well known blockers. The benefit of using these two blockers is that their structures are well known and their mechanisms of action and binding interactions are well characterized for some channels. Hence the experimental designs are geared to test the validity of a comparison between SK channels and other channel structures.

### 4.2.1 Rationale for "structural" mutants considered in this chapter

#### V553F–rSK3

In Shaker, several pore residues appear to be involved in determining the affinity of the channel for extracellular TEA (Yokoyama et al., 1989; Stuhmer et al., 1989; Frech et al., 1989; MacKinnon & Yellen, 1990). Amongst these residues, position 449 (see Figure 1.8 on page 66 for numbering system used) appears most crucial, since threonine substitution with an aromatic amino acid at this point can cause a 100-fold increase in channel affinity for this blocker (MacKinnon & Yellen, 1990; Kavanaugh et al., 1991). An analogous mutation in rSK3, V553F-rSK3, will determine whether the rSK3 channel is capable of a similar interaction and thus can be used, in part, to confirm that the Shaker and SK channels share a similar general structural topology. The rationale for choosing phenylalanine over tyrosine is that it is closer to valine in size, so it is less likely to cause global structural changes and in addition, it creates a slightly higher affinity for TEA in Shaker channels (Heginbotham & MacKinnon, 1992; Yool & Schwarz, 1991).

#### G535D–rSK3

CTX is a peptide inhibitor of $K^+$ channels that for some channels can block ion movement through pore occlusion at nanomolar concentrations (C.-S. Park et al., 1991; MacKinnon & Miller, 1988; C. Miller, 1988) in a bimolecular reaction (Gold-

stein & Miller, 1993). Substitution of an aspartic acid (residue 431 (see Figure 1.8 on page 66 for the numbering system used)) by lysine in Shaker causes a reduction in CTX affinity (Goldstein et al., 1994). Similarly WT hSK4, which contains an aspartic acid at the equivalent position, can be blocked potently by this toxin (Jensen et al., 1998). The analogous residue in rSK3 is G535-rSK3, where an aspartic acid substitution would be expected to attract the cationic CTX molecule. If the CTX affinity were to increase, this would provide support for the idea of overall structural similarity between SK3 and Shaker channels, based on analogous point mutations producing similar effects in either channel. It might also provide a partial explanation of the SK4 channel's CTX sensitivity (Jensen et al., 1998), and the insensitivity of SK1, SK2 and SK3 channels to this toxin (Grissmer et al., 1992; Dale et al., 2002; Carignani et al., 2002; Castle, 1999), since only the SK4 channel has an acidic aspartic acid residue at position 535 in any of these WT channels.

Together, the V553F-rSK3 and G535D-rSK3 mutants provide a two-point calibration of the SK channel pore for comparison with the best studied channel structures available.

## 4.3 Results

### 4.3.1 Characterization of the "structural" mutants

In order to characterize the whole-cell currents from the "structural" mutants, CHO cells were initially used to express each mutant channel, since they produce virtually no endogenous current (Figure 3.1 on page 107) that might be a factor in potential atypical SK current shapes (subsequent experiments in this chapter were performed using transiently transfected HEK 293 cells since the stability of SK currents during the post-run down phase in these cells was generally greater than for the other cell lines). All the transfected CHO cells that were selected for analysis were represen-

tative (in size and shape) of the majority of other CHO cells that were plated down. Mutant G535D-rSK3 showed typical nanoampere, square SK currents (Table 4.1 on the following page). Recordings that were made immediately (<20-30 seconds) after going whole-cell in the presence of 1μM intracellular calcium displayed an average current of 2.3±0.3 nA (mean±SEM) at -40 mV from CHO cells transiently expressing this mutant under voltage-clamp conditions (n=5 recordings). This compared to an average current recorded immediately (<20-30 seconds) after going whole-cell of 2.4±0.5 nA (mean±SEM)(n=4 recordings) at -40 mV from CHO cells that were transiently expressing WT rSK3 channels.

Mutant V553F-rSK3 showed atypical, nanoampere SK currents (Table 4.1 on the next page), suggesting that results obtained with V553F-rSK3 should be obtained and interpreted cautiously. The currents were voltage-dependent over interval (ii), but not over interval (i), and no time-dependency in the amplitude of the average current at +40 mV was observed between these intervals (Figure 4.1 on page 153). Recordings made immediately (<20-30 seconds) after going whole-cell in the presence of 1μM intracellular calcium, displayed a whole-cell current of 0.74±0.1 nA (mean±SEM) at -40 mV when recorded over the whole of the step interval (n=4 recordings). This value is significantly less than the average whole-cell current recorded immediately (<20-30 seconds) after going whole-cell at the same potential from CHO cells transiently expressing WT rSK3 channels under the same conditions (2.4±0.5 nA (mean±SEM), n=4 recordings).

### 4.3.2 G535D-rSK3 is a CTX-sensitive channel

The effect of CTX on WT rSK3 currents was investigated first. Although SK4 is sensitive to CTX block in the nanomolar range (Jensen et al., 1998), the apamin-sensitive channels (SK1-3) have been reported to be unaffected by CTX (Carignani et al., 2002; Castle, 1999). Consistent with these observations, Figure 4.2 on page 155 shows that concentrations of up to 200 nM extracellular CTX had no effect on WT

| Mutation | Chromatogram | Current trace |
|---|---|---|
| V553F–rSK3 | 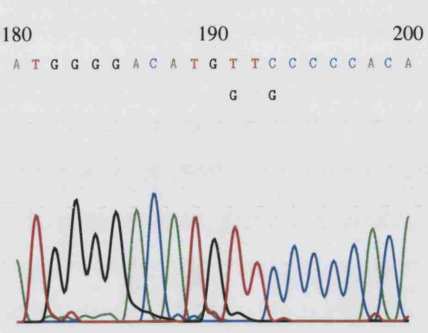  | 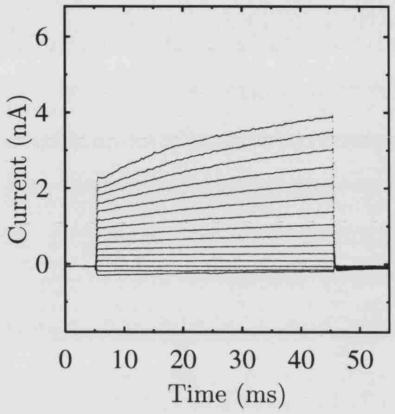  |
| G535D–rSK3 | 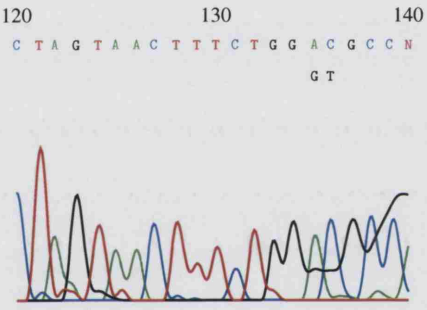  | 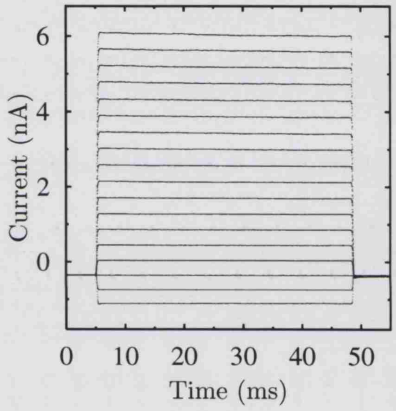  |

**Table 4.1:** Table showing sections of the sequencing chromatograms spanning the mutated bases of the V553F–rSK3 and G535D–rSK3 mutants and the representative current traces produced after their cellular expression. Representative current traces have been generated immediately (<20-30 seconds) after going whole-cell, and are from CHO cells that were transiently transfected with either G535D-rSK3 or V553F-rSK3. These cells were held at −80 mV, before being stepped to voltages between −100 mV and +40 mV (in 10 mV increments). After 40 ms at the appropriate step, the cells were returned to −80 mV. The time-dependency of the whole-cell currents shown in the V553F-rSK3 trace is illustrated in Figure 4.1 on the following page. The intracellular solutions all contained 1 mM Mg–ATP, 130 mM KCl, and 1 μM free calcium. A standard bath solution (containing 5 mM $K^+$) was used to bathe each cell. Bases below the main sequence in the chromatograms are the WT rSK3 bases at the equivalent positions to the mutated bases directly above them. Numbers above bases begin from the start of the read, and do not relate to the entire sequence for rSK3.

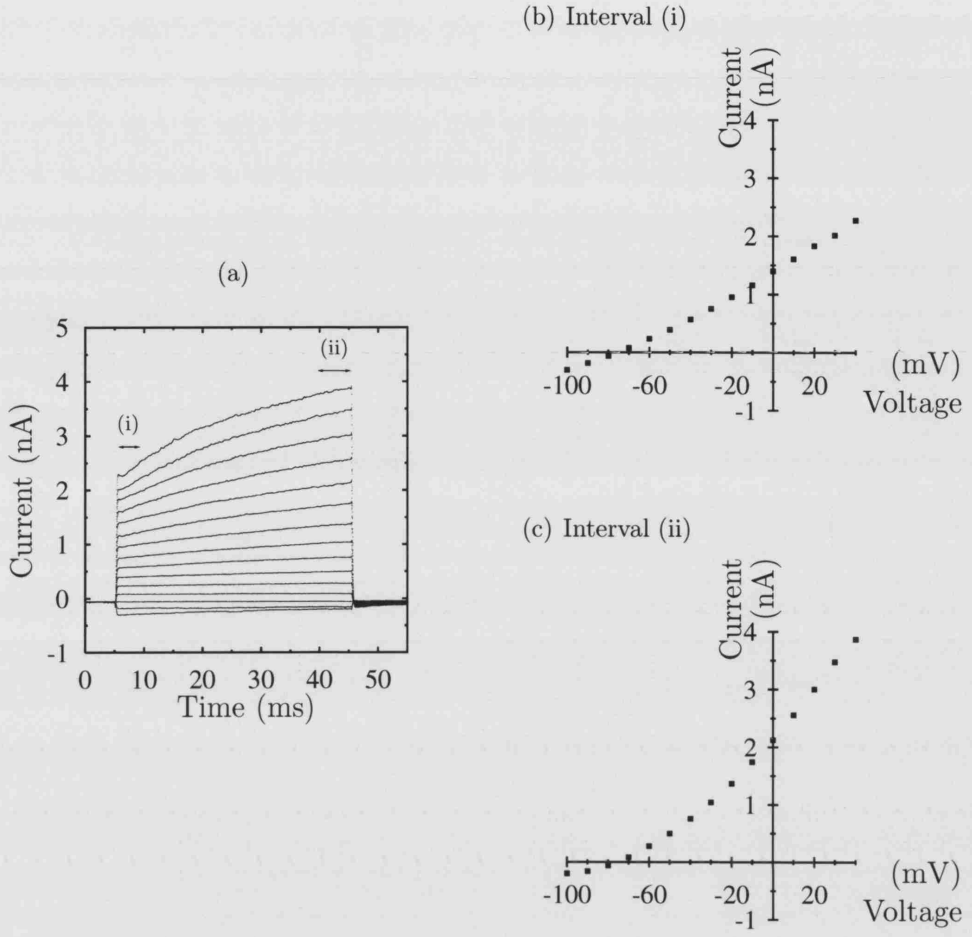


**Figure 4.1:** Time and voltage-dependency analysis of the V553F-rSK3 whole-cell current trace. Currents recorded immediately after going whole-cell are shown from a CHO cell that had been transiently transfected with V553F-rSK3. (a) Representative whole-cell trace of V553F-rSK3 currents generated by a step protocol (holding potential of −80 mV followed by 10 mV steps between −100 mV and +40 mV for 40 msec before returning to the same holding potential). (b) shows the I-V curve for the region labelled (i) in (a). (c) shows the I-V relationship for region (ii) in (a). Voltage-dependency was analyzed by expressing the slope of the tangent (voltage-dependence) generated at -90→-100 mV as a percentage of that at +30→+40 mV, firstly over interval (i) and then over interval (ii). In three whole-cell recordings analyzed in this way, the average voltage-dependence at -90→-100 mV was 87±7.2% of that at +30→+40 mV over interval (i), whilst over interval (ii), it was 32±8.2% (n=3 recordings). Only the latter figure (i.e. interval (ii)) is significantly different from 100%. In the same three whole-cell recordings, the average current recorded at +40 mV over interval (ii) was 137±16% bigger than over interval (i) at the same potential. This value is not significantly different from the figure of 100% (interval (i)). Standard bath solutions and intracellular solutions containing 1 mM Mg–ATP, 130 mM KCl, and 1 μM free calcium, were used for cell recordings.

rSK3 currents. The mean normalized current following application of 200 nM CTX was 1.01±0.03 (mean±SEM) at -40 mV, and the mean normalized current after washout was 0.99±0.02 (mean±SEM) at -40 mV (n=3 recordings)(currents have been normalized to the control currents and then averaged). However, a lower concentration of CTX, 100 nM, produced a significant block of the G535D–rSK3 channel (Figure 4.3 on page 156). Application of 100 nM extracellular CTX produced 62.0±3.5% (mean±SEM) block of G535D-rSK3 currents at -40 mV (n=3 recordings). The block was sufficiently potent to allow a full dose-response curve to be obtained for the mutant, and this is shown in Figure 4.4 on page 157. The data are well fitted to a single component Hill-Langmuir isotherm with a Hill coefficient of 0.85±0.1 (mean±SD) and an $IC_{50}$ for CTX block of 31.1±3.7 nM (mean±SD). The data was then analyzed for voltage-dependence of the CTX block of G535D-rSK3. A $z\delta$ value of 0.17±0.01 (mean±SD) ($\delta$=0.043 (net charge of +4 for CTX)) and $\ln IC_{50}^{0\,mV}$ of -17.0±0.01 (mean±SD) (41.4 nM)(Figure 4.5 on page 158) was found. This shows that CTX block of G535D-rSK3 is voltage-dependent, making it likely that the lysine residue at position 27 of the toxin is located above the selectivity filter, as has been postulated in Shaker channels and BK channels where CTX block is also voltage-dependent (Goldstein et al., 1994; C. Park & Miller, 1992).

### 4.3.3 Effect of raising the extracellular $K^+$ ion concentration on CTX sensitivity of the G535D-rSK3 channel

Next, to test for the possible presence of a $K^+$ coordination site on the external face of the channel, the extracellular $K^+$ ion concentration was increased whilst keeping the ionic strength constant. This was achieved by reducing the external sodium ion concentration (down to 25 mM) whilst substituting with $K^+$ ions (up till 130 mM). Thus CTX binding to G535D-rSK3 was assessed in the presence of symmetrical $K^+$ (130 mM extracellular and intracellular). The results are shown in Figure 4.6 on the

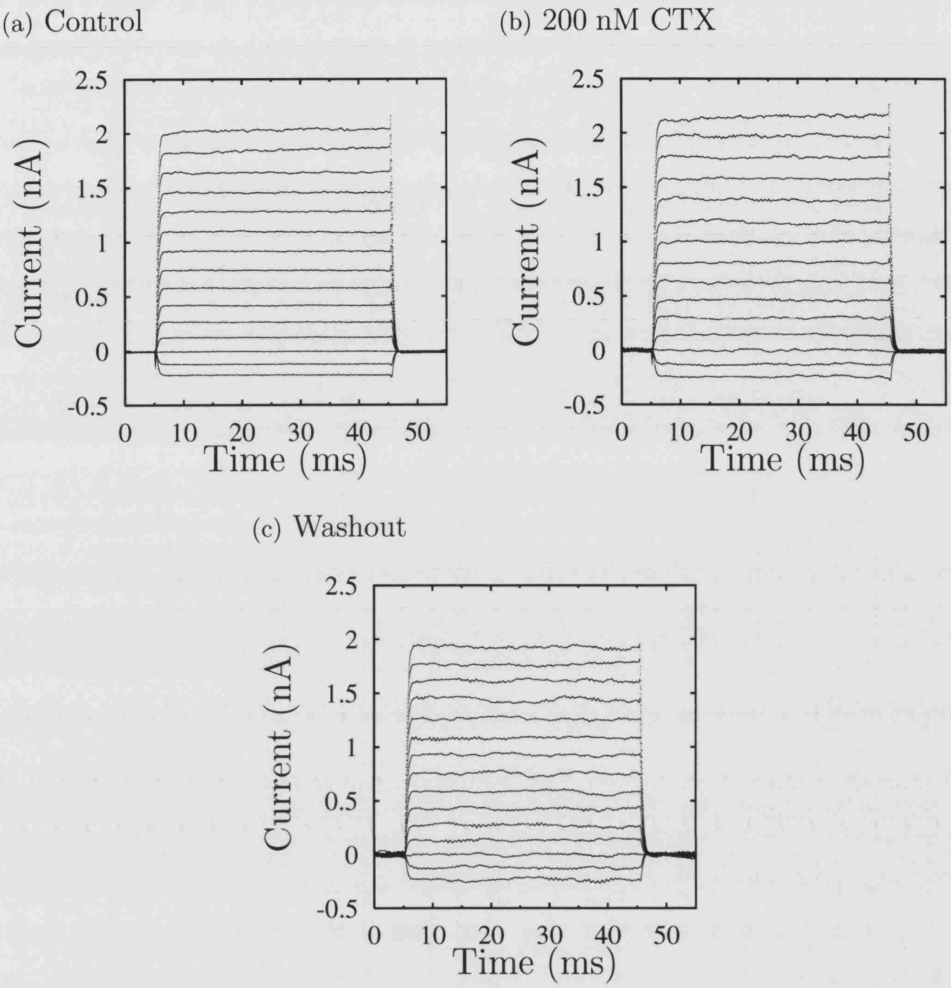


**Figure 4.2:** Effect of 200 nM extracellular CTX on WT rSK3 currents. Representative whole-cell currents from a HEK 293 cell which was transiently transfected with WT rSK3, are shown. In each trace, the transmembrane potential of the cell was held at −80 mV, before being stepped to voltages between −100 mV and +40 mV (in 10 mV increments). After 40 ms at the appropriate step, the potential was returned to −80 mV. Using this voltage-clamp protocol, the cell was perfused with standard bath solution (a), with standard bath solution supplemented with 200 nM CTX (b), and again perfused with standard bath solution (washout) (c). In three such recordings, 200 nM CTX produced no block of WT rSK3 current: the mean normalized current following application of 200 nM CTX was 1.01±0.03 (mean±SEM) at -40 mV, and the mean normalized current after washout was 0.99±0.02 (mean±SEM) at -40 mV (currents have been normalized to the control currents and then averaged). The intracellular solutions all contained 1 mM Mg–ATP, 130 mM KCl, and 1 μM free calcium. A standard bath solution (containing 5 mM $K^+$) was used for cell recordings.

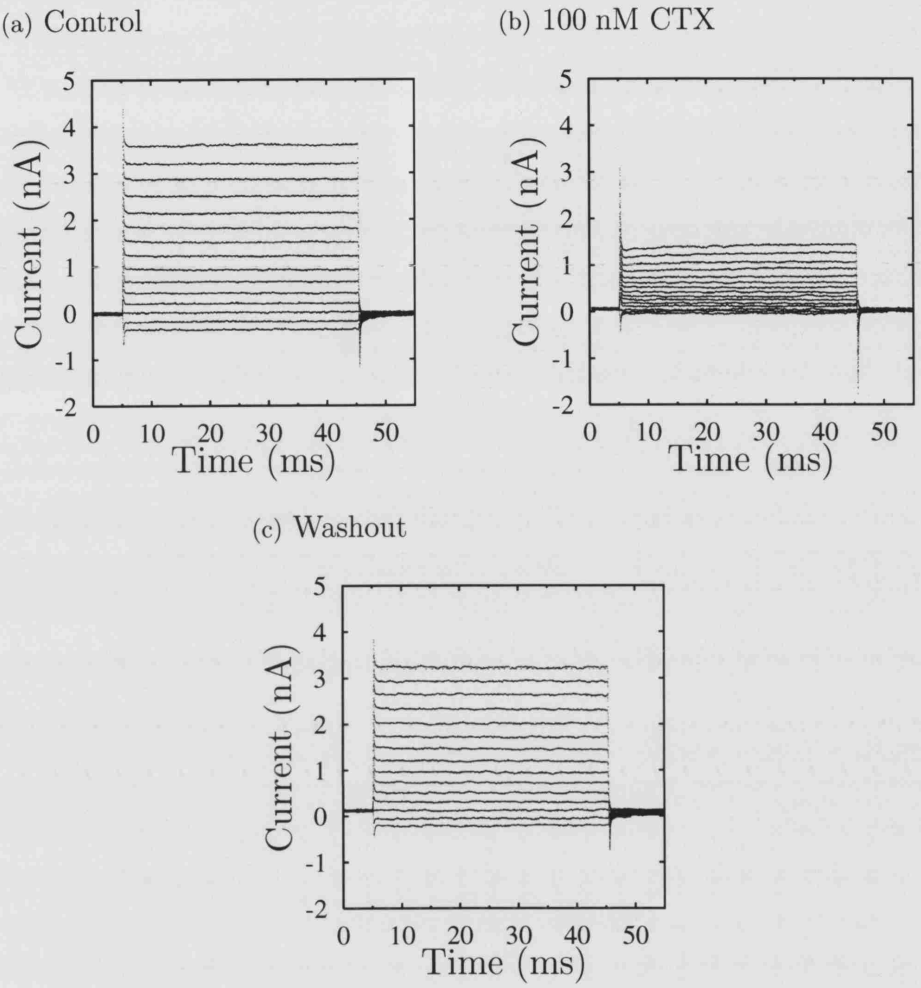


**Figure 4.3:** Effect of 100 nM extracellular CTX on G535D–rSK3 currents. Representative whole-cell currents from a HEK 293 cell which was transiently transfected with G535D–rSK3, are shown. In each trace, the transmembrane potential of the cell was held at −80 mV, before being stepped to voltages between −100 mV and +40 mV (in 10 mV increments). After 40 ms at the appropriate step, the potential was returned to −80 mV. Using this voltage-clamp protocol, the cell was perfused with standard bath solution (a), with standard bath solution supplemented with 100 nM CTX (b), and again perfused with standard bath solution (washout) (c). In three such recordings, 100 nM CTX produced 62.0±3.5% (mean±SEM) block at a step potential of -40 mV. The intracellular solutions all contained 1 mM Mg–ATP, 130 mM KCl, and 1 μM free calcium. A standard bath solution (containing 5 mM $K^+$) was used for cell recordings.

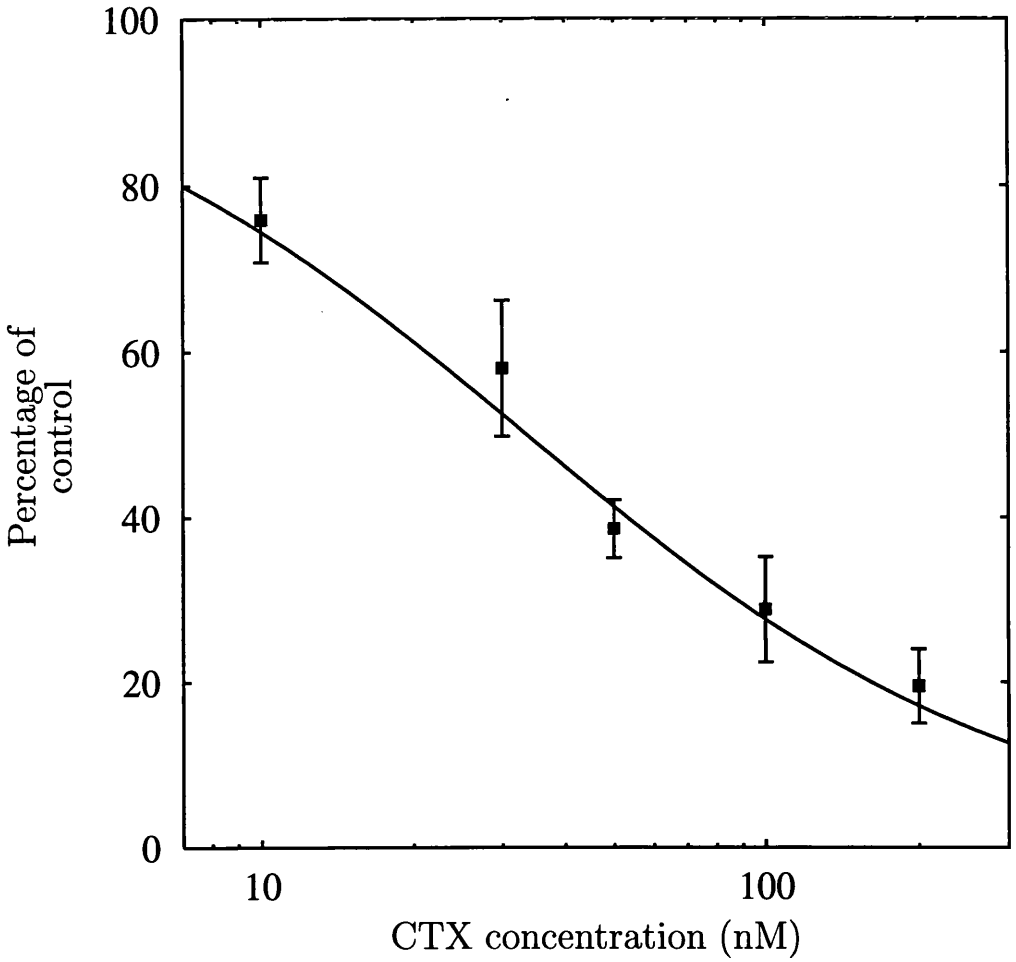


**Figure 4.4:** Dose-response curve for CTX block of G535D–rSK3 channels transiently expressed in HEK 293 cells. CTX concentrations are plotted on a log scale. The data are fitted to the Hill equation with an estimated $IC_{50}$ for CTX block of 31.1±3.7 nM (mean±SD) and Hill coefficient of 0.85±0.1 (mean±SD). $B_{max}$ was fixed at 100. Each data point is the mean of three observations and the vertical bars indicate the SEM. Cells were held at a potential of -80 mV and the percentage current remaining following the application of CTX was analyzed at -40 mV for each experiment.

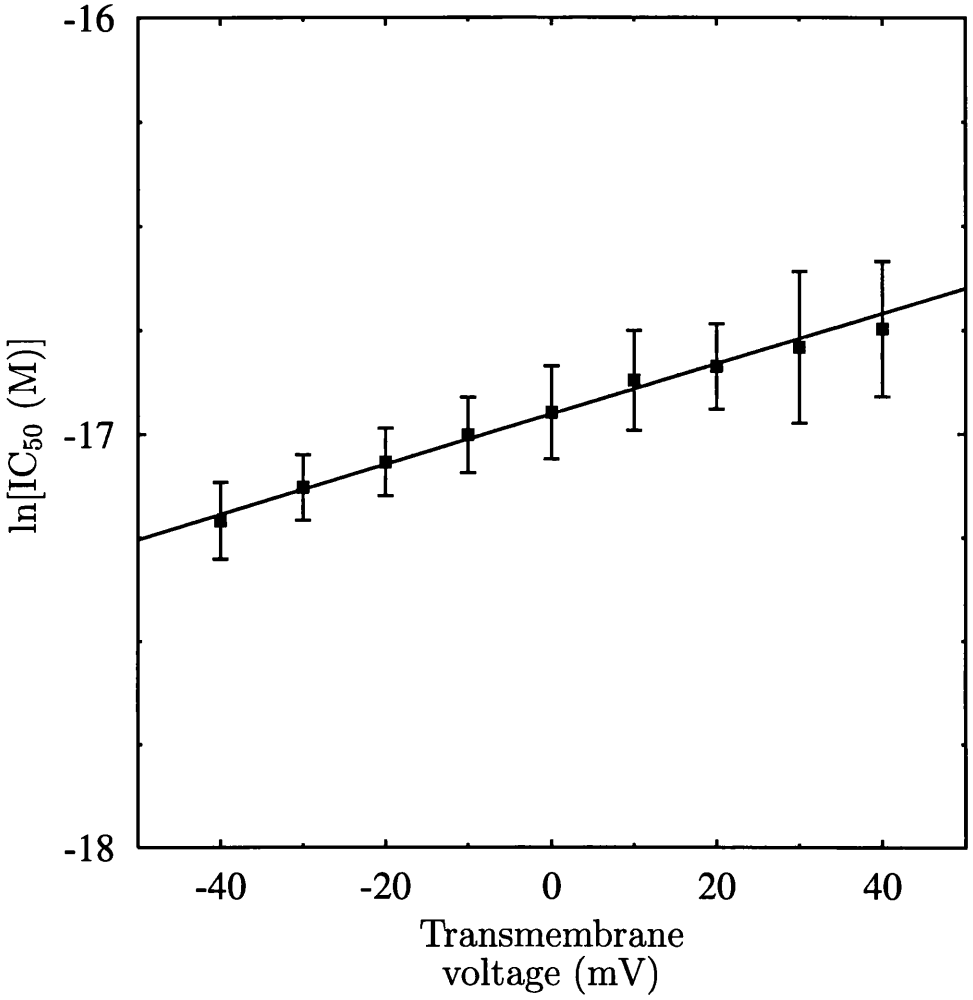


**Figure 4.5:** Natural logarithms of the $IC_{50}$ values for extracellular CTX block of G535D-rSK3 channels, which have been transiently expressed in HEK 293 cells, plotted against transmembrane potential. The data are fitted to the Woodhull equation with the $lnIC_{50}$ and $z\delta$ parameters allowed to vary. For this fit, $z\delta$ is 0.17±0.01 (mean±SD) ($\delta$=0.043 (net charge of +4 for CTX)) and $lnIC_{50}^{0\,mV}$ is -17.0±0.01 (mean±SD) (41.4 nM). Each point is the $lnIC_{50}$ at each potential as estimated from the Hill equation, and the vertical bars indicate the natural log of the corresponding SD. Cells were held at -80 mV and $IC_{50}$ values at each potential were generated using data points at 10 nM, 50 nM, 100 nM 200 nM.

next page. 200 nM CTX produced only 30.2% block (n=2 recordings) of mutant channel currents, which is considerably less than CTX block in low extracellular $K^+$ (100 nM CTX produced 62.0±3.5% (mean±SEM) block of G535D-rSK3 current in physiological $K^+$ (Figure 4.3 on page 156)). This suggests that a $K^+$-selective coordination site may be present in the outer vestibule of the rSK3 channel, similar to one that probably exists in SK4 (Malik-Hall et al., 2000) and in Shaker channels (Goldstein & Miller, 1993).

### 4.3.4 Effect of the V553F mutation on external TEA binding to the rSK3 channel

#### External TEA block of V553F-rSK3 channels is not time-dependent

V553F-rSK3 exhibits a non-square whole-cell current shape whilst voltage-clamped (Figure 4.1 on page 153). To test whether external TEA block depends on the interval over which the current is recorded (i.e. position (i) or (ii) in Figure 4.1 on page 153), 0.3 mM external TEA was applied and mean currents over intervals (i) and (ii) were measured (Figure 4.7 on page 161). This concentration of TEA was chosen because it produces 50% block of V553Y-SK1 (Ishii et al., 1997). At +40 mV, 35.9±4.7% (mean±SEM) block of the average V553F-rSK3 current over interval (i) was found (n=3 recordings), whilst the same concentration of external TEA blocked 48.8±6.2% (mean±SEM) over interval (ii) (n=3 recordings). These values were not significantly different to each other. This suggests that external TEA block of V553F-rSK3 is not time-dependent.

#### Dose-response curves for TEA block of WT rSK3 and V553F-rSK3 channels

The V553F–rSK3 channel was examined for changes to its external TEA affinity relative to the WT. In these preliminary experiments, there was no reason for giving

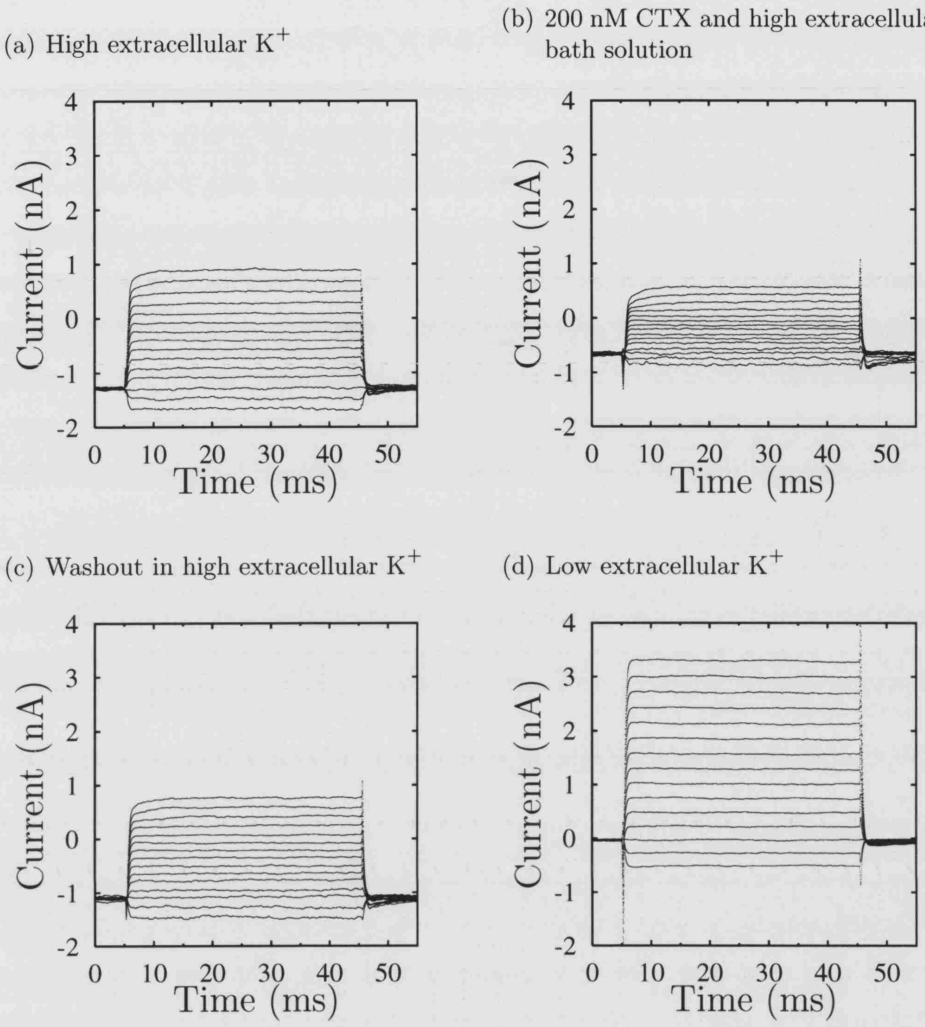


**Figure 4.6:** The effect of elevating the extracellular $K^+$ ion concentration (to 130 mM) on extracellular CTX block of G535D–rSK3 currents. Representative whole-cell currents from a HEK 293 cell which was transiently transfected with G535D–rSK3, are shown. In each trace, the transmembrane potential of the cell was held at −80 mV, before being stepped to voltages between −100 mV and +40 mV (in 10 mV increments). After 40 ms at the appropriate step, the potential was returned to −80 mV. Using this voltage-clamp protocol, the cell was perfused with bath solution containing high $K^+$ (130 mM KCl) (a), with high $K^+$ bath solution (130 mM KCl) supplemented with 200 nM CTX (b), with high $K^+$ bath solution only (130 mM KCl) (c), and with low $K^+$ bath solution (5 mM KCl) (d). In two such recordings, 200 nM CTX produced only 30.2% block at +40 mV, which is considerably less than in low $K^+$ (Figure 4.3 on page 156). Currents were analyzed at +40 mV in symmetrical $K^+$ solutions since they were all under 1 nA at this potential, thereby producing minimal series resistance errors. The high $K^+$ bath solution contained 130 mM KCl and 25 mM NaCl with the remaining constituents unaltered. The physiological (low) $K^+$ bath solution contained 150 mM NaCl and 5 mM KCl. A standard intracellular solution containing 130 mM KCl, 1 mM MgATP and 1 μM free calcium was used in each recording.

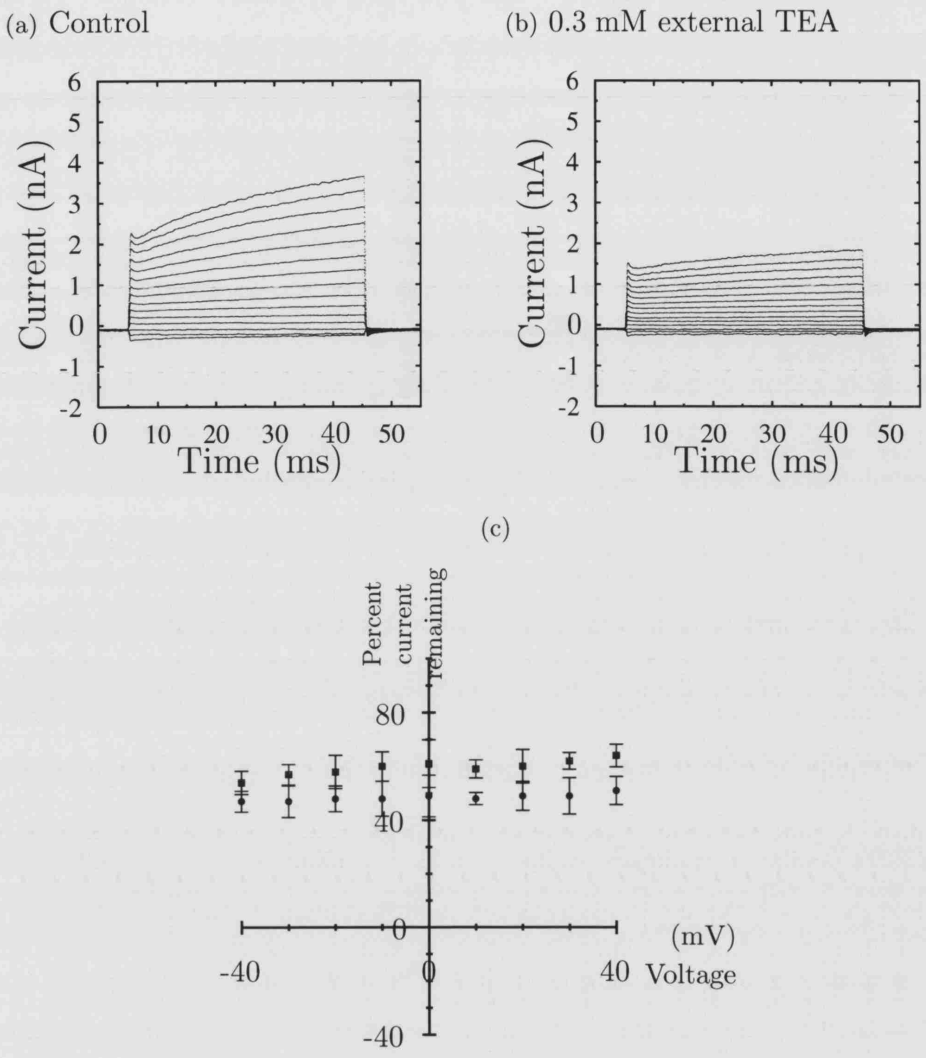


**Figure 4.7:** TEA block of V553F-rSK3 currents is time-dependent. (a) and (b) Representative whole-cell currents from a HEK 293 cell which was transiently transfected with V553F–rSK3, are shown. In each trace, the transmembrane potential of the cell was held at −80 mV, before being stepped to voltages between −100 mV and +40 mV (in 10 mV increments). After 40 ms at the appropriate step, the potential was returned to −80 mV. Using this voltage-clamp protocol, the cell was perfused with standard bath solution (a), with standard bath solution supplemented with 0.3 mM TEA (b). 0.3 mM TEA blocks a greater proportion of V553F-rSK3 current over interval (ii) compared to interval (i) as shown in (c) (region of the current trace corresponding to intervals (i) and (ii) are shown in Figure 4.1 on page 153). (c) Percentage current remaining after TEA block when measured over the intervals (i) *squares* or (ii) *circles*. The data points represent mean values±SEM (each data point represents the average of three experiments). The intracellular solutions all contained 1 mM MgATP, 130 mM KCl, and 1 μM free calcium. A standard bath solution (containing 5 mM $K^+$) was used for cell recordings.

preference to analyzing data over intervals (i) or (ii). However, it was clear that data should be analyzed over similar recording intervals, since the extent of TEA block is determined by the position of the recording interval (Figure 4.7 on the preceding page). Block was therefore consistently analyzed over the entire step recording interval (i.e. the interval between and inclusive of (i) and (ii) (Figure 4.1 on page 153)). TEA block of currents obtained from WT and mutant channels over the step recording interval were in the millimolar region and full dose-response curves were obtained for both. Figure 4.8 on the following page shows the data could be well fitted to a single component Hill-Langmuir isotherm in both cases: WT rSK3 with an estimated $IC_{50}$ for TEA block of 5.05±1.1 mM (mean±SD) and Hill coefficient of 0.87±0.08 (mean±SD), V553F–rSK3 with an estimated $IC_{50}$ for TEA block of 0.21±0.04 mM (mean±SD) and Hill coefficient of 0.90±0.07 (mean±SD). This demonstrates that the mutant channel, V553F–rSK3, has a greater affinity for TEA than WT rSK3.

### Voltage-dependence of TEA block of WT rSK3 and V553F-rSK3 channels

In Shaker channels, TEA block from the external side has been found to be voltage-dependent (Heginbotham & MacKinnon, 1992). Substitution of the WT threonine residue at position 449 (equivalent to residue 553 of rSK3) with an aromatic residue, has been shown to alter the voltage-dependency of external TEA blockade (Heginbotham & MacKinnon, 1992). To investigate the nature of TEA binding to the V553F-rSK3 and WT rSK3 channels, the voltage-dependency of channel blockade of each was analyzed in turn. Plots of the $\ln IC_{50}$ versus the transmembrane potential for TEA block of the WT rSK3 and mutant V553F-rSK3 channels are shown in Figure 4.9 on page 164. The lines superimposed on the data points have been fitted to the Woodhull equation. In contrast to the results found in Shaker (Heginbotham & MacKinnon, 1992), the fitted lines show that the voltage-dependency ($z\delta$) of TEA block increases from 0.15±0.02 in the WT channel to 0.26±0.02 in the highly TEA

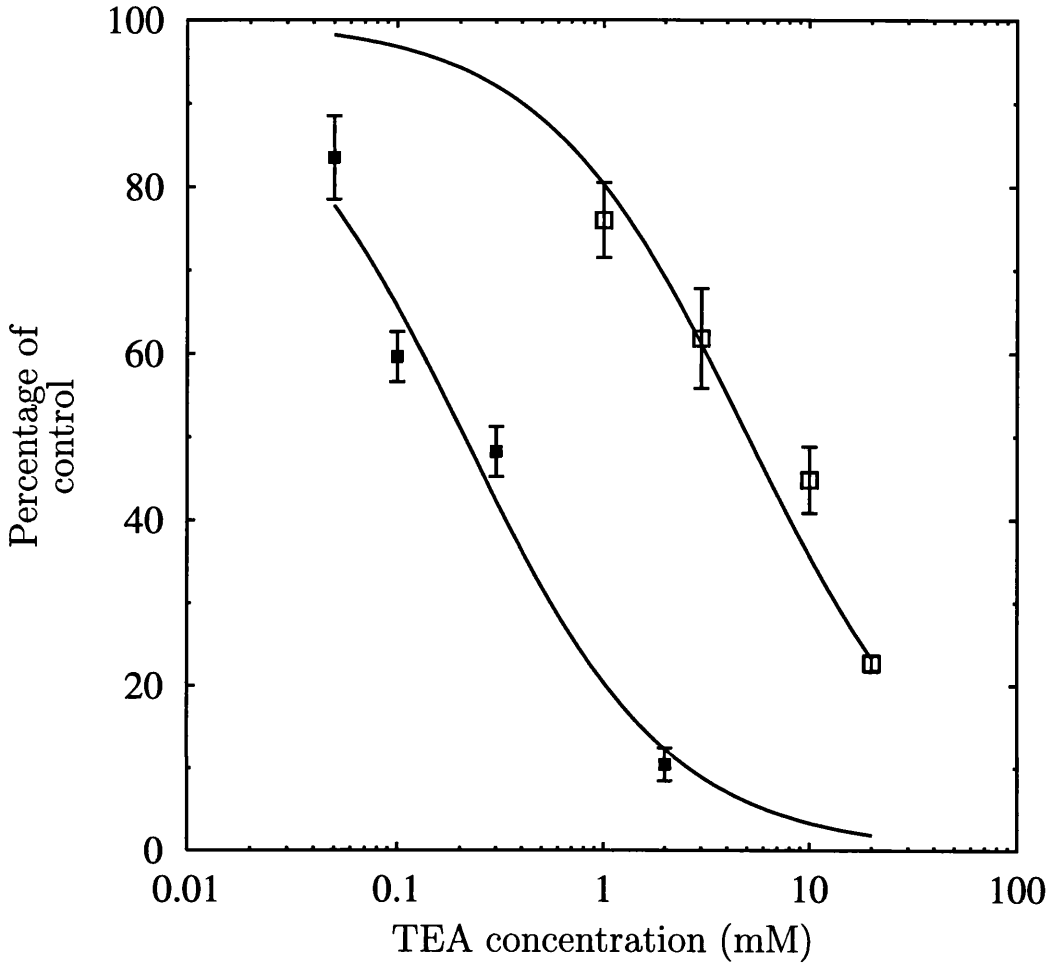


**Figure 4.8:** Dose-response curves for TEA block of WT rSK3 (*open squares*) and V553F–rSK3 (*closed squares*) currents. Block was measured over the whole of the 40 msec step recording interval in each experiment. TEA concentrations are plotted on a log scale. Data have been fitted to Hill equations with the $IC_{50}$s and Hill coefficients allowed to vary in each case. The estimated $IC_{50}$ for TEA block of the WT rSK3 channel is 5.05±1.1 mM (mean±SD), with a Hill coefficient of 0.87±0.08 (mean±SD). The estimated $IC_{50}$ for TEA block of the V553F–rSK3 channel is 0.21±0.04 mM (mean±SD) with a Hill coefficient of 0.90±0.07 (mean±SD). Each data point is the mean of three observations and the vertical bars indicate the SEM. Cells were held at a potential of -80 mV and percentage current remaining after application of TEA was analyzed at -40 mV for each experiment. All these experiments were carried out using HEK 293 cells that had been transiently transfected with either V553F-rSK3 DNA or WT rSK3 DNA.

sensitive channel. This shows that TEA interaction with the WT rSK3 channel is distinct from its interaction with the V553F-rSK3 channel.

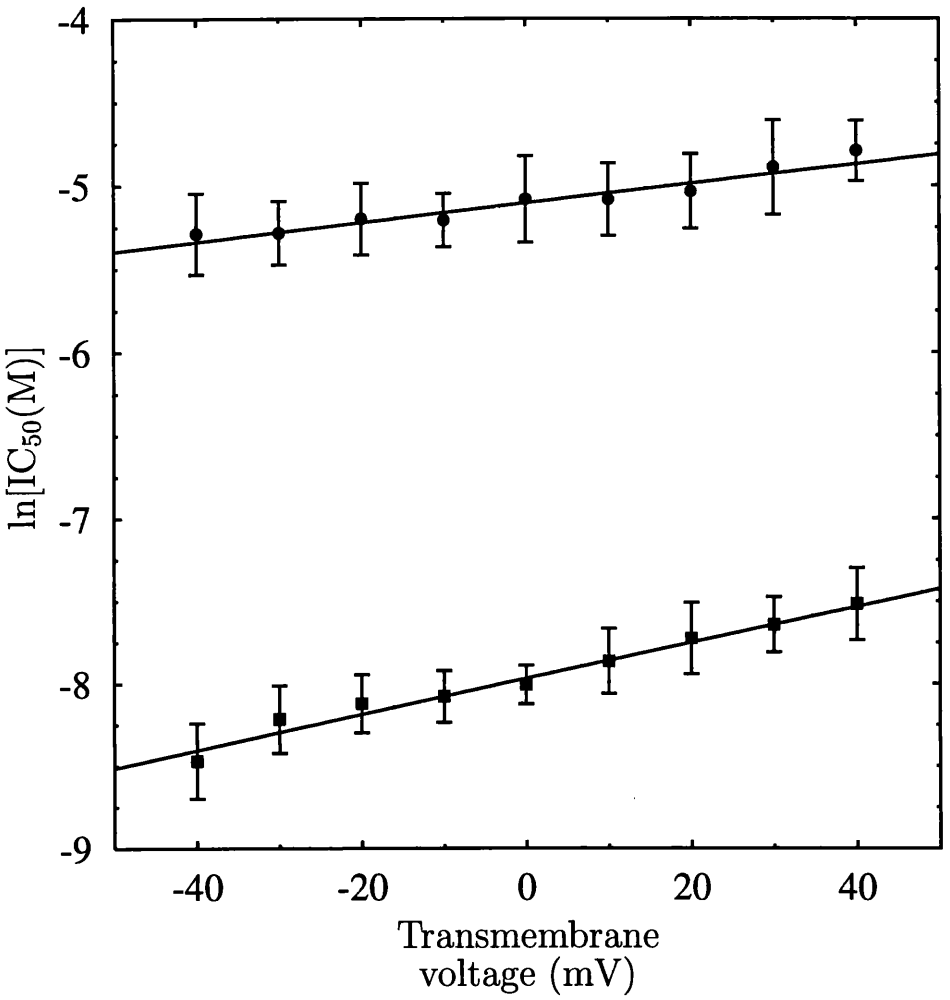


**Figure 4.9:** Voltage-dependencies of TEA blockade of WT rSK3 (*circles*) and V553F–rSK3 (*squares*) currents, recorded in the whole-cell configuration after transient transfection in HEK 293 cells. Each point is the natural log of the $IC_{50}$ value at each potential as estimated from the Hill equation, and the vertical bars indicate the natural log of the SD of each data point. The lines superimposed on the data points have been fitted to the Woodhull equation with the $z\delta$ and $\ln IC_{50}^{0\,mV}$ parameters allowed to vary. For this fit, the $z\delta$ value for WT rSK3 is 0.15±0.02 (mean±SD) with an $\ln IC_{50}^{0\,mV}$ value of -5.1±0.02 (mean±SD) ($IC_{50}^{0\,mV}$ = 6.10 mM). For V553F-rSK3, the $z\delta$ value for this fit is 0.26±0.02 (mean±SD), while the $\ln IC_{50}^{0\,mV}$ is -7.96±0.02 (mean±SD) ($IC_{50}^{0\,mV}$ = 0.35 mM). Cells were held a -80 mV and the average current was measured over the entire voltage step interval in each experiment. Transfected cells that expressed very high currents (>2 nA at +40 mV) were not included in these experiments due to the large voltage drops that would be incurred over the series resistance.

## 4.4 Discussion

The main aim set out at the beginning of this chapter was to compare the pore of the rSK3 channel with those of the Shaker and KcsA channels using the V553F-rSK3 and G535D-rSK3 mutations as a two-point callibration for the rSK3 structure. This was successfully done using TEA and CTX as blockers of the V553F-rSK3 and G535D-rSK3 point mutants respectively, and it was found that the rSK3 pore probably has a similar structure to the other Shaker and KcsA channel pores, otherwise the mutated residues would not interact with these toxins in the observed manner. For example, the hydrophobic "cage" (see the next section) that is thought to house TEA at the extracellular binding site would not be able to coordinate TEA as effectively in the V553F-rSK3 mutant as compared with the Shaker and KcsA channels (Heginbotham & MacKinnon, 1992), if the substituted aromatic phenylalanine residues are too far apart or are too close together. Together with the results obtained for the G535D-rSK3 mutant channel, these observations suggest the pores of the Shaker, KcsA, and rSK3 channels are probably similar and that the model rSK3 pore (Figure 1.9 on page 67) is a valid general structural representation of the rSK3 pore *per se*.

### 4.4.1 Non-ionic forces generated from an "aromatic bracelet" may produce a high affinity TEA binding site in V553F-rSK3 channels

Aromatic amino acids such as tyrosine and phenylalanine contain phenyl rings which create local hydrophobic environments. The substituted phenylalanine residues in the tetrameric V553F-rSK3 channel might perfectly coordinate the non-polar TEA ethyl groups within these hydrophobic regions, stabilizing the TEA molecule as has been proposed for KcsA and RBK1 binding to TEA (Luzhkov & Aqvist, 2001; Kavanaugh et al., 1991). The extent to which hydrophobic forces are responsible for the interaction between TEA and V553F-rSK3 could be examined using extracellular

tetrabutylammonium application to the mutant channel, since it has longer alkyl chains that might not be coordinated by the hydrophobic phenyl groups as effectively as the ethyl chains of TEA are.

### 4.4.2 The voltage-dependency of TEA blockade

The voltage-dependency of TEA block in KcsA and Shaker channels is thought to arise from the coupling between TEA and $K^+$ ions in the selectivity filter (Spassova & Lu, 1998; Crouzy et al., 2001; Molina et al., 1998). In KcsA, pyramidal TEA is thought to project a positively charged ethyl group into the selectivity filter, and the stablest $K^+$ ion configuration, when TEA is bound to the channel, has been predicted to be one in which only the fourth (most intracellular) binding site is occupied by a $K^+$ ion (Luzhkov & Aqvist, 2001). The stablest $K^+$ ion configuration in the WT rSK3 selectivity filter, with TEA bound, may produce less repulsion between the $K^+$ ions and the projecting ethyl group than in the V553F-rSK3 channel, which could result in the comparatively reduced voltage-dependency of TEA blockade of WT rSK3 channels.

### 4.4.3 A structural model of CTX binding to rSK3 channels

Any model for CTX block of the G535D-rSK3 channel would have to incorporate features that account for the observations of voltage-dependency of CTX block, and an increase of CTX affinity as a result of the glycine for aspartic acid substitution. The first observation has been found to occur with CTX block in several other channels, and mutational studies have suggested that the positively charged lysine residue at position 27 of the toxin is positioned over the selectivity filter in these channels (C. Park & Miller, 1992; Goldstein & Miller, 1993). The interaction between the negatively charged aspartic acid at position 535 in the channel and the positively charged CTX is probably electrostatic in nature, and this could be tested

by raising the ionic strength of the extracellular solution (not using $K^+$ ions since there might be an extracellular $K^+$ ion binding site on the rSK3 channel (Figure 4.6 on page 160)), and re-examining CTX block. Agitoxin (AGXN), another scorpion toxin, has a very similar quaternary structure to CTX (Figure 4.10 on the following page), and an ionic interaction underlies the strong coupling energy between the aspartic acid at Shaker position 431 (residue 431 in Shaker is analogous to residue 535 in rSK3) and the arginine at residue 24 in AGXN (Garcia et al., 2001). Further, the positioning of the lysine residue at position 27 centrally over the pore, would mean the arginine residue at position 31 of AGXN interacts with the diagonally opposite channel subunit's aspartic acid residue at position 431 (Garcia et al., 2001).

The nanomolar affinity of CTX for the G535D-rSK3 channel is probably also derived from the interaction between the positive charges on the toxin and the negatively charged aspartic acid residues of the channel. Based on the studies of AGXN block in Shaker, it could be that the equivalent cationic charges in CTX, $Lys_{31}$ and $Arg_{25}$, which are located on the "perimeter" of the toxin molecule, generate an interaction with the anionic residues at position 535 (rSK3) in two of the four channel subunits (Figure 4.11 on page 169). Thompson and Begenisich (2000) have proposed that these two amino acids form part of a triad of positively charged residues which interact with the basic environment surrounding the putative turret in Shaker channels, the source of which is the cationic lysine (position 427 of Shaker (Figure 1.8 on page 66)) residue located in this hypothetical turret region. In contrast, high affinity CTX block to the G535D-rSK3 channel is solely determined by residue 535, since the glycine for aspartic acid substitution confers the WT rSK3 channel with nanomolar sensitivity to CTX. It appears that the turret residues are not important for this high affinity interaction, and therefore another arrangement, which orientates the positively charged CTX residues towards the anionic aspartic acid residues at position 535 in the G535D-rSK3 channel, is probably more likely. Goldstein et al. (1994) have proposed that the two threonines at positions 8 and

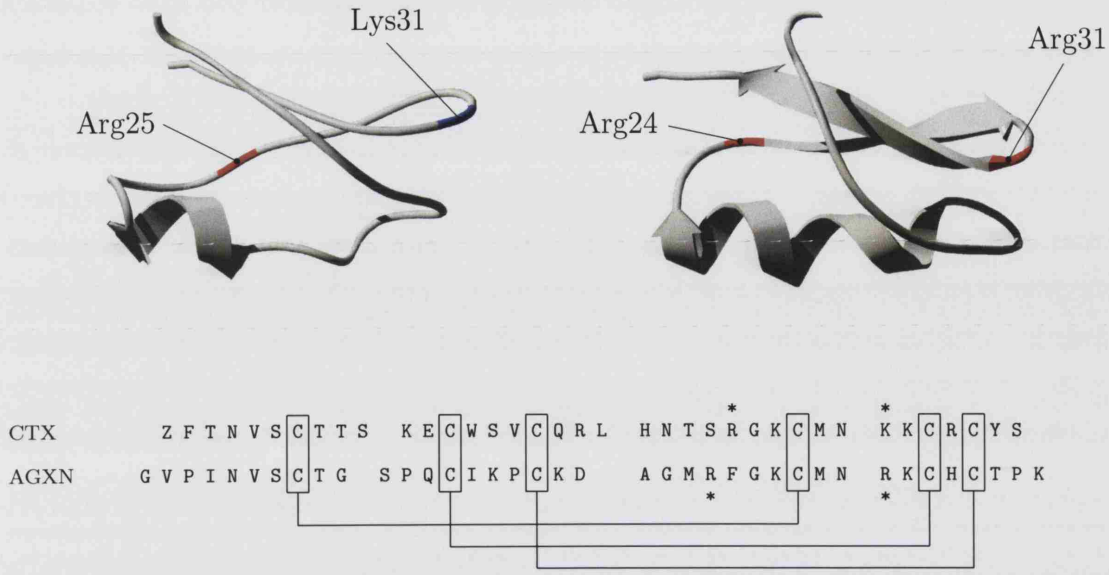


**Figure 4.10:** A comparison of the structures and peptide sequences of charybdotoxin (CTX) and agitoxin (AGXN). Both the CTX (left) and AGXN (right) structures are shown in cartoon display and were generated using Swisspdb viewer and Povray. Similarities can be seen in these 3-D structures and in the charge distribution and positions of cysteine bridges (lines joining boxed regions) within the peptide sequences. Boxed regions represent cysteine residues involved in producing cysteine bridges. Asterisks in the peptide sequences indicate important amino acids for binding of AGXN (see text) as well as analogous CTX residues.

9 of bound CTX are in close proximity to residue 425 (equivalent to position 529 in rSK3) in Shaker (Goldstein et al., 1994). This arrangement places the positively charged toxin residues away from the putative rSK3 turret, but close to the floor of the vestibule where the anionic aspartic acid residues at position 535 in rSK3 are located, as shown in Figure 4.11 on the next page.

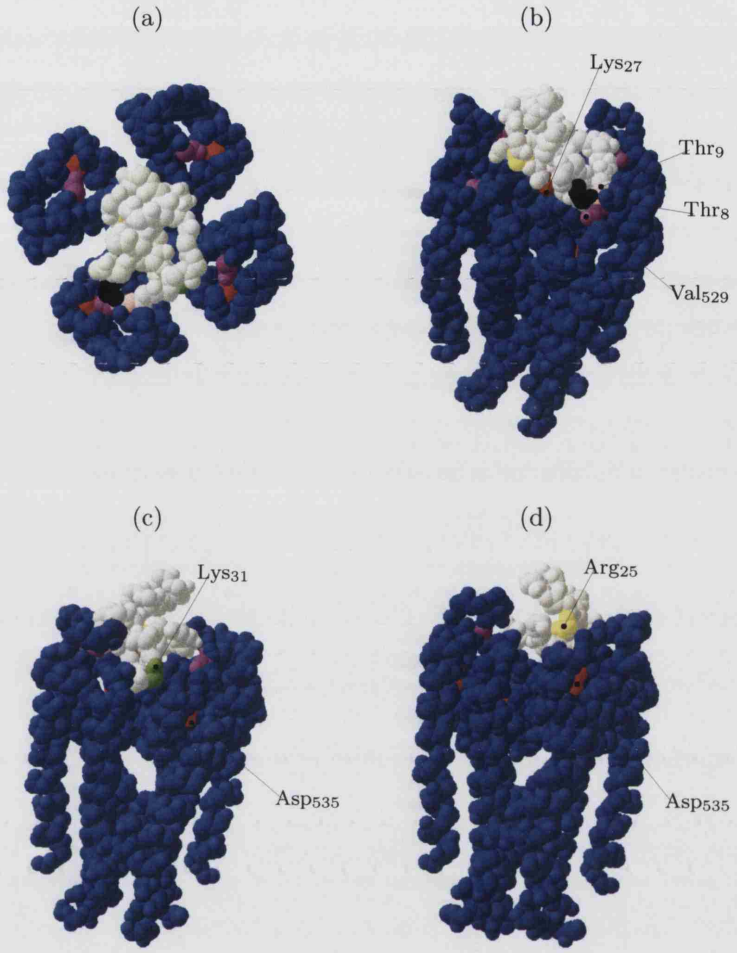


**Figure 4.11:** A model of CTX binding to a putative G535D-rSK3 pore. The G535D-rSK3 pore is represented by the crystal structure of the KcsA channel with analogous G535D-rSK3 pore residues labelled. The orientation of the CTX molecule is based on observations in the present study and those in Shaker. The red channel amino acid is residue 535-rSK3 and the purple channel amino acid is residue 529. (a) shows an aerial view spacefill representation of CTX bound to the channel pore. (b) shows an oblique view of the same proteins with the threonine at position 8, $Thr_8$ (black), and position nine, $Thr_9$ (pink), of CTX labelled. These blocker residues are thought to be located next to residue 425 in Shaker (Goldstein et al., 1994). This Shaker residue aligns with residue 529 of the rSK3 channel (Figure 1.8 on page 66). Hence the above figure depicts $Thr_8$ and $Thr_9$ of CTX to be in close contact with residue 529 of the G535D-rSK3 channel. (c) shows a putative electrostatic interaction between $Lys_{31}$ (green) of CTX and $Asp_{535}$ of a subunit from the mutant channel. (d) shows another view of CTX bound to G535D-rSK3 demonstrating a possible weak electrostatic interaction between $Arg_{25}$ (yellow) of CTX and $Asp_{535}$ (red) of a different subunit of the G535D-rSK3 mutant channel. Both the channel pore and blocker are drawn to the same scale in each case, and the latter fits just inside the inner aspect of the turret (residue 529-coloured in purple). Pictures were generated using Swiss pdb viewer and Povray.

# Chapter 5

# Molecular interactions between the rSK3 pore and UCL compounds

## 5.1 Aim

- To map residues critical for SK channel interactions with UCL blockers

## 5.2 Introduction

UCL compounds block SK channels, and a few have previously been shown to displace apamin from rSK3 channels in radioligand binding assays (Garbarg and Benton, unpublished observations), suggesting that these blockers share common or overlapping binding sites. Further, based on results obtained in mutagenesis experiments, it has been suggested by Ishii et al. (1997) and C. Vergara et al. (1998), that residues responsible for differences in high affinity apamin binding are on opposite ends of the SK channel outer pore. These sites form a good starting point to investigate the important molecular interactions between UCL compounds and the rSK3

channel, particularly as apamin and UCL compounds may share the same binding site. UCL 1848 binds to hSK1, rSK2, and rSK3 with a similar order of potencies to that seen with apamin, suggesting the molecular interactions of both UCL 1848 with rSK3, and apamin with rSK3 might be similar at some level; the interactions of UCL 1848 with rSK3 provide the focus for this chapter. In addition to reporting on the channel residues which affect block by UCL 1848 and other UCL compounds, a "map" of these residues together with a model of how UCL 1848 may block the channel, are presented.

### 5.2.1 Rationale for "pharmacology" mutants considered in this chapter

In addition to the G535D-rSK3 and V553F-rSK3 mutants described in the previous chapter, further mutants were made to characterize the interaction between SK channels and UCL compounds in more detail. The rationale on which the designs of these further mutants, designated "pharmacology mutants", are based on, involve the effects of SK channel point mutations on apamin binding. A brief summary of these mutational studies is now given.

Ishii et al. (1997), comparing mutant SK1 channels expressed in oocytes with WT SK channels, suggested that high affinity apamin sensitivity is conferred primarily by two amino acid residues, residing on opposite sides of the pore (the presence of aspartic acid at position 528 and asparagine at position 555 was suggested to confer high affinity apamin binding on SK channels (see Figure 1.8 on page 66) for the numbering system used)). In their experiments, the triple mutant, E528D, H555N, K526Q–hSK1, in which the pore amino acid sequence exactly mirrors that of rSK2, produced a channel of equivalent apamin sensitivity to WT rSK2. These results form the basis for the design of the following point mutations, since apamin and UCL 1848 have similar affinities on SK1, SK2 and SK3, suggesting that these

two blockers may share a common mechanism of interaction with the SK channel.

### Mutants V529K–rSK3 and D528K–rSK3

The effect on UCL 1848 affinity of the other "primary" residue that determines apamin sensitivity (Ishii et al., 1997), residue 528, together with the neighbouring residue at position 529, was investigated with lysine substitutions at both. Lysine was chosen to substitute for the WT amino acids at either position due to its contrasting biophysical properties compared to the WT residues. Whereas valine is an uncharged, hydrophobic molecule and aspartic acid is negatively charged (but hydrophillic), lysine is positively charged, hydrophillic and larger than both valine and aspartic acid. Interestingly, Khawaled et al. (1999) have published that residue 528 is an intrinsic molecular determinant of SK current run down; the presence of an aspartic acid at residue 528 in SK channels was proposed to reduce run down (Khawaled et al., 1999). On this basis, one might expect run down to be increased in D528K-rSK3, as the aspartic acid is substituted for a lysine residue in this mutant. Therefore, run down of this mutant channel has also been investigated in conjunction with the effect of the lysine substitution on block by UCL 1848.

### Mutant H555K-rSK3

The importance of this residue for scyllatoxin and apamin binding to SK channels has been demonstrated in mutational studies (Shakkottai et al., 2001; Ishii et al., 1997). It is one of the two critical residues identified by Ishii et al. (1997) that confers high affinity apamin sensitivity, and in addition affects scyllatoxin binding affinity to SK channels (Shakkottai et al., 2001). Since UCL 1848 (Hosseini et al., 2001; Monaghan et al., 2004) shows a similar selectivity to apamin (Strobaek et al., 2000; Ishii et al., 1997; Shah & Haylett, 2000; Grunnet, Jensen, et al., 2001) as well as scyllatoxin (Strobaek et al., 2000; Shakkottai et al., 2001) amongst SK channel subtypes (most potent on SK2, least potent on SK1), a possible UCL 1848

binding site role for this residue was examined. Although both histidine and lysine are considered to be basic amino acids, the side group of histidine is predominantly neutral at physiological pH; the acid dissociation equilibrium constant ($pK_a$) for the protonated imidazole group in histidine is 6.04 which is just below that of the external solution (pH 7.4) to which it is probably exposed (based on the crystal structure of KcsA). Calculation of the proportion of histidine residues that are basic under physiological conditions according to a rearranged Henderson-Hasselbach equation (proportion = $\frac{10^{(pK_a-pH)}}{1+10^{(pK_a-pH)}}$) yields a value of approximately 4.2%. Charged residues which are in close proximity to the imidazole group of histidine at position 555 in rSK3, will exert an electric potential that may be a factor in determining this side group's physiological $pK_d$ ($pK_{dphysiol}$). The closest charged amino acid to residue 555, based on the primary sequence of rSK3, is the anionic D551-rSK3 residue. The effect of the negative potential originating from this residue on the $pK_{dphysiol}$ of the side group of H555-rSK3, would be to increase the proportion of neutral histidine side chains, according to Equation 5.1 (derived from the classical free energy equation, $\Delta G = RT.\ln K_d$ ($\Delta G_0$ = standard Gibb's free energy change, R = Gas constant, T = temperature, $K_d$ = dissociation equilibrium constant). Therefore, the lysine side group, being longer (more linear) than the histidine side group and having a much greater estimated proportion of positively charged side groups under physiological conditions ( $\approx$ 99.9%), would be likely to reduce the affinity of UCL 1848 binding, if this residue forms part of the high affinity binding site for this blocker.

$$pK_{\mathrm{dphysiol}} = pK_{\mathrm{dintrinsic}} - \left(0.434\frac{e\Psi}{k_B T}\right) \tag{5.1}$$

where $pK_{dintrinsic}$ = intrinsic $pK_d$ ($pK_d$ in the absence of any potential

$k_B$ = Boltzmann constant

$\Psi$ = electrical potential at point of interest (H555-rSK3)

T = Temperature (K)

e = Coulomb charge

$pK_{dphysiol}$ = Physiological $pK_d$

## 5.3 Results

### 5.3.1 Characterization of the "pharmacology" mutants

Sequencing chromatograms show that all these mutants have been made successfully (Table 5.1 on page 176). These mutants were initially transiently transfected into CHO cells since, in the event that any atypical (not square) or small mutant SK currents arise, these might not be clearly separated from endogenous currents (once the mutant channels had been characterized in CHO cells, HEK 293 cells were used for subsequent experiments in this chapter which required the transient expression of SK channels, due to their increased SK current stability during the post-run down phase compared to other cell lines). All the transfected CHO cells that were selected for analysis were representative (in size and shape) of the majority of other CHO cells that were plated down. As shown in Table 5.1 on page 176, all expressed mutants produced typical nanoampere, "square" SK currents in response to voltage pulses. Recordings that were made immediately (<20-30 seconds) after going whole-cell in the presence of 1μM intracellular calcium displayed an average whole-cell current of 1.8±0.4 nA (mean±SEM) at -40 mV from CHO cells expressing V529K-rSK3 channels under voltage-clamp conditions (n=5 recordings), compared to 2.4±0.5 nA (mean±SEM) at -40 mV from CHO cells transfected with WT rSK3 and recorded under the same conditions (n=4 recordings). Recordings made immediately (<20-30 seconds) after going whole-cell in the presence of 1μM

intracellular calcium displayed an average current of 2.2±0.5 nA (mean±SEM) at -40 mV (n=5 recordings) from CHO cells expressing D528K-rSK3 channels, whilst an average current of 1.7±0.6 nA (mean±SEM) was produced under the same conditions from CHO cells expressing H555K-rSK3 channels (n=3 recordings). These currents are not significantly different ($P>0.05$) from those obtained immediately (<20-30 seconds) after going whole-cell at -40 mV from CHO cells transiently expressing WT rSK3 currents (2.4±0.5 nA at -40 mV, n=4 recordings). There was no evidence of time-dependent currents in any of these recordings, as seen in whole-cell traces from V553F-rSK3 (Figure 4.1 on page 153).

Run down of D528K-rSK3 currents was quantified next, as this residue was proposed to be one of the intrinsic determinants of SK channel run down seen in a separate study (Khawaled et al., 1999). By the end of the run down phase, whole-cell D528K-rSK3 currents that were transiently expressed in HEK 293 cells fell to 64.2±7.2% (mean±SEM) of their original value in the absence of 1 mM intracellular MgATP (n=3 recordings, data not shown), which suggests that run down is actually less in D528K-rSK3 compared to WT rSK3 channels (whole-cell currents from HEK 293 cells expressing WT rSK3 channels ran down to 39.2±10.6% (mean±SEM) under the same conditions, Figure 3.4 on page 114), although the difference between the values for D528K-rSK3 and WT rSK3 channels is not significant ($P>0.05$).

Having successfully made three new mutants, all of which express, the five mutant channels constructed to date (V529K-rSK3, D528K-rSK3, H555K-rSK3 as well as G535D-rSK3 and V553F-rSK3), were tested for their effects on UCL compound block, and compared to the WT channel.

In order to produce a channel "map" of residues thought to interact with UCL compounds, it is desirable to obtain as many interacting and non-interacting sites as possible, as this would help to ascertain any patterns that might outline a binding site. For this purpose, the effect of a point mutation on a single dose of the UCL compound being tested was usually sufficient to determine the importance of par-

| Mutation | Chromatogram | Current trace |
|---|---|---|
| V529K–rSK3 | 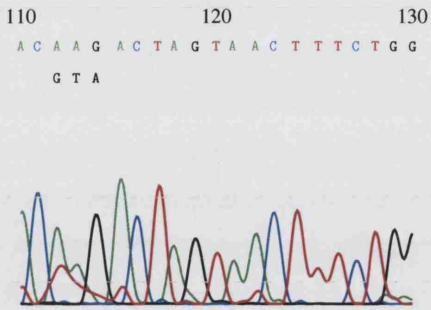  | 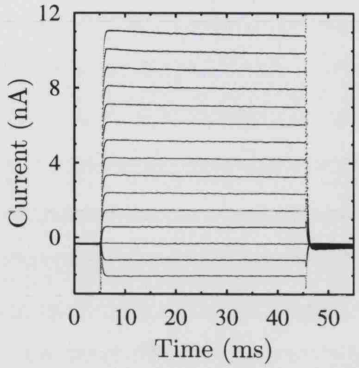  |
| D528K–rSK3 | 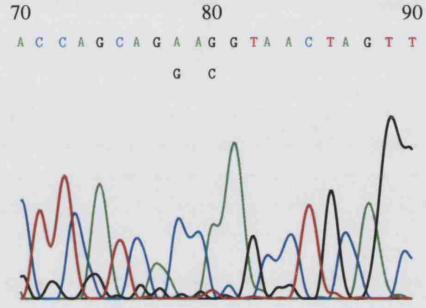  | 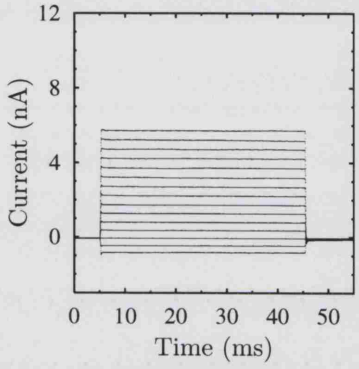  |
| H555K–rSK3 | 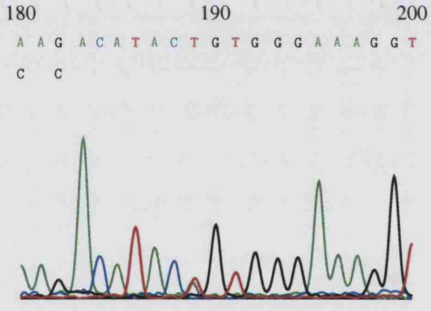  | 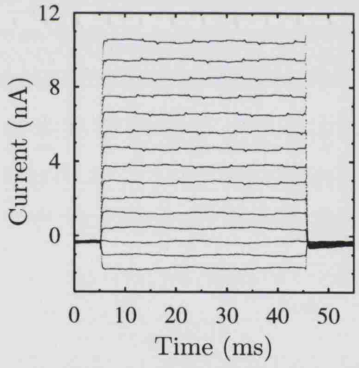  |

**Table 5.1:** Table showing sections of the sequencing chromatograms spanning the mutated bases of the "pharmacology" mutants and the representative current traces produced after their cellular expression. CHO cells, from which current traces were generated had been transiently transfected with mutant DNA in each case and the whole-cell currents that were generated immediately (<20-30 seconds) after going whole-cell, are shown. Each cell was voltage-clamped in the whole-cell configuration and held at −80 mV, before being stepped to voltages between −100 mV and +40 mV (in 10 mV increments). After 40 ms at the appropriate step, the cells were returned to −80 mV. Pipette solutions contained 1 μM free calcium and 1 mM MgATP. Bases below the main sequence in the chromatograms are the WT rSK3 bases at the equivalent positions to the mutated bases directly above them. Numbers above bases begin from the start of the read in each case, and do not relate to the entire sequence for rSK3.

ticular channel pore residue for UCL compound binding, and so full dose-response curves were not obtained in most experiments.

### 5.3.2 UCL 1848 binding to the WT rSK3 channel

The control for most of the experiments in this chapter is the effect of UCL 1848 on WT rSK3 channels. Clearly, it was important to obtain a dose-response curve for this drug on these channels. This is shown in Figure 5.1 on the following page using transiently transfected HEK 293 cells. The $IC_{50}$ for block by UCL 1848 is 2.11±0.19 nM (mean±SD), which is similar to that seen in CHO cells (Hosseini et al., 2001).

### 5.3.3 Effect of the G535D–rSK3 mutation on UCL compound binding

The G535D-rSK3 channel was chosen as a starting point to investigate the residues which interact with UCL compounds, since it has previously been shown that SK4, which contains an aspartic acid at the position equivalent to residue 535 of rSK3, is insensitive to UCL 1848, UCL 1530 (personal communication with Dr Benton), and UCL 1684 (Malik-Hall et al., 2000), suggesting a crucial role for this residue in SK channel binding. Firstly, the effect of UCL 1684 on the mutant channel was tested and the result is shown in Figure 5.2 on page 180. 5 nM UCL 1684 has been shown to cause approximately 50% block of WT rSK3 current (Hosseini et al., 2001). This dose produced only 11.5±1.8% (mean±SEM) current block at -40 mV (n=3 recordings). This finding demonstrates that position 535 is important for the interaction between rSK3 channels and UCL 1684. Next, to examine the generality of the effect amongst the UCL compounds, a 10 nM dose of UCL 1848 was tested. A 10 nM UCL 1848 dose is five times its $IC_{50}$ value on the WT channel (Hosseini et al., 2001). This dose was selected since a low dose of UCL 1684 (equivalent to its $IC_{50}$ on WT rSK3) did not produce much blocking effect on the mutant channel. A block

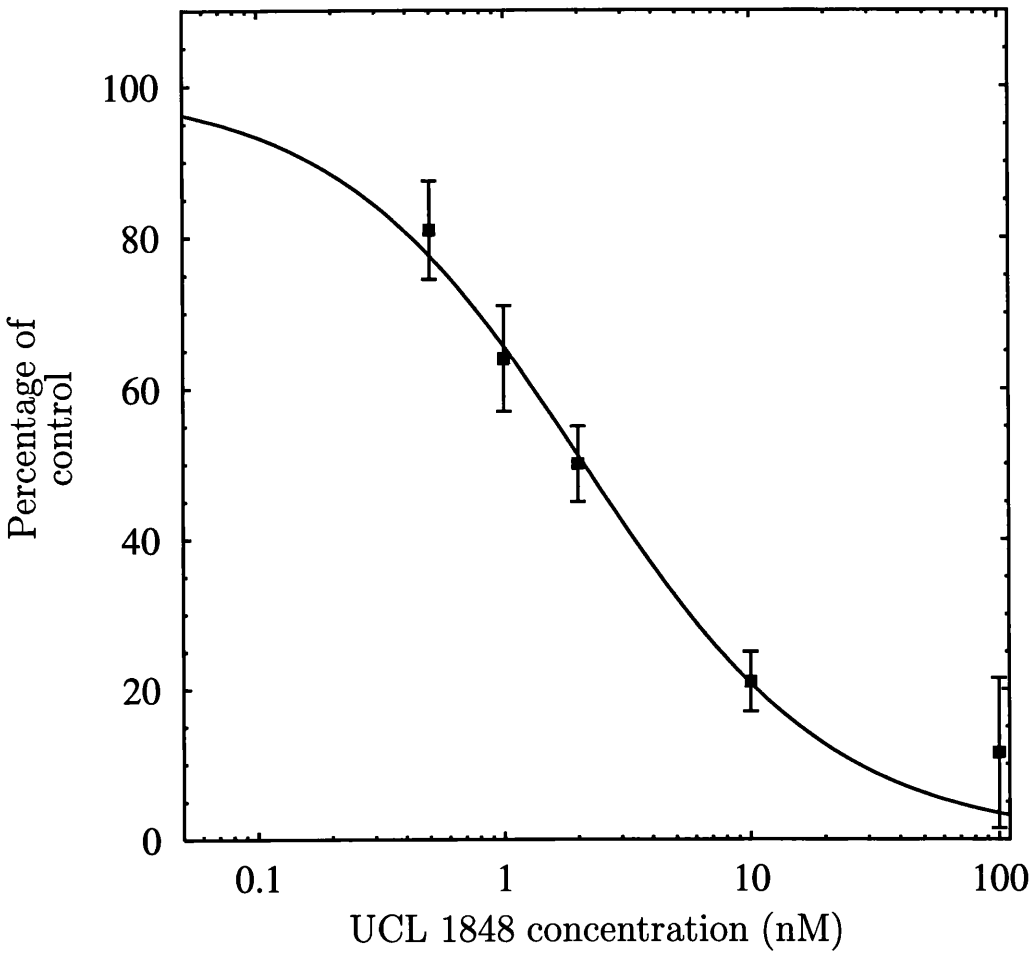


**Figure 5.1:** The dose-response curve for UCL 1848 block of WT rSK3 currents. The UCL 1848 concentration has been plotted on a log scale. The data are fitted to the Hill equation with an estimated $IC_{50}$ of 2.11±0.19 nM (mean±SD) and Hill coefficient of 0.86±0.07 (mean±SD). $B_{max}$ was constrained to 100% as described in the Methods. Cells were held at -80 mV and average currents, used to calculate the percentage current remaining in whole-cells, were recorded at -40 mV. Each data point is the average of three observations and the vertical bars indicate the SEM. All the recordings used in these experiments were made from HEK 293 cells that had been transiently transfected with WT rSK3.

of only 21.9%±5.3% (mean±SEM) (n=3 recordings) was observed (Figure 5.3 on page 181). This shows that the binding affinity of UCL 1848 substantially decreases (>5-fold) when the glycine residue at position 535 in WT rSK3 is substituted for an aspartic acid residue. This result was pursued further and sufficient applications of UCL 1848 were made to allow some crude dose-response data to be obtained for this mutant as shown in Figure 5.4 on page 182. Finally, a 500 nM dose of UCL 1530 was tested on the G535D-rSK3 mutant. This is approximately two and a half times the $IC_{50}$ value observed in the WT channel (Dr David Benton, personal communication). As shown in Figure 5.5 on page 183, the G535D-rSK3 mutant showed no sensitivity to this concentration of UCL compound. In three voltage-clamp experiments, the mean normalized current following application of 500 nM UCL 1530 was 0.95±0.02 (mean±SEM) at -40 mV, and the mean normalized current after washout of the drug was 0.96±0.03 (mean±SEM) at -40 mV (currents have been normalized to the control currents and then averaged). These results show that the glycine for aspartic acid substitution at residue 535 of the rSK3 channel decreases the binding affinities of UCL 1848, UCL 1684, UCL 1530.

### 5.3.4 Effect of the V553F–rSK3 mutation on UCL compound binding

The effects on UCL compound pharmacology caused by the V553F–rSK3 mutation were initially investigated by applying 5 nM UCL 1684 to the bath medium. This concentration of UCL 1684 is approximately equivalent to its $IC_{50}$ for the WT channel (5.8 nM, Hosseini et al. (2001)). This did not produce any block (Figure 5.6 on page 185) of the V553F-rSK3 channel. In three voltage-clamp experiments, the mean normalized current following application of 5 nM UCL 1684 was 0.99±0.02 (mean±SEM) at -40 mV, and the mean normalized current after washout of the drug was 0.97±0.04 (mean±SEM) at -40 mV (currents have been normalized to the

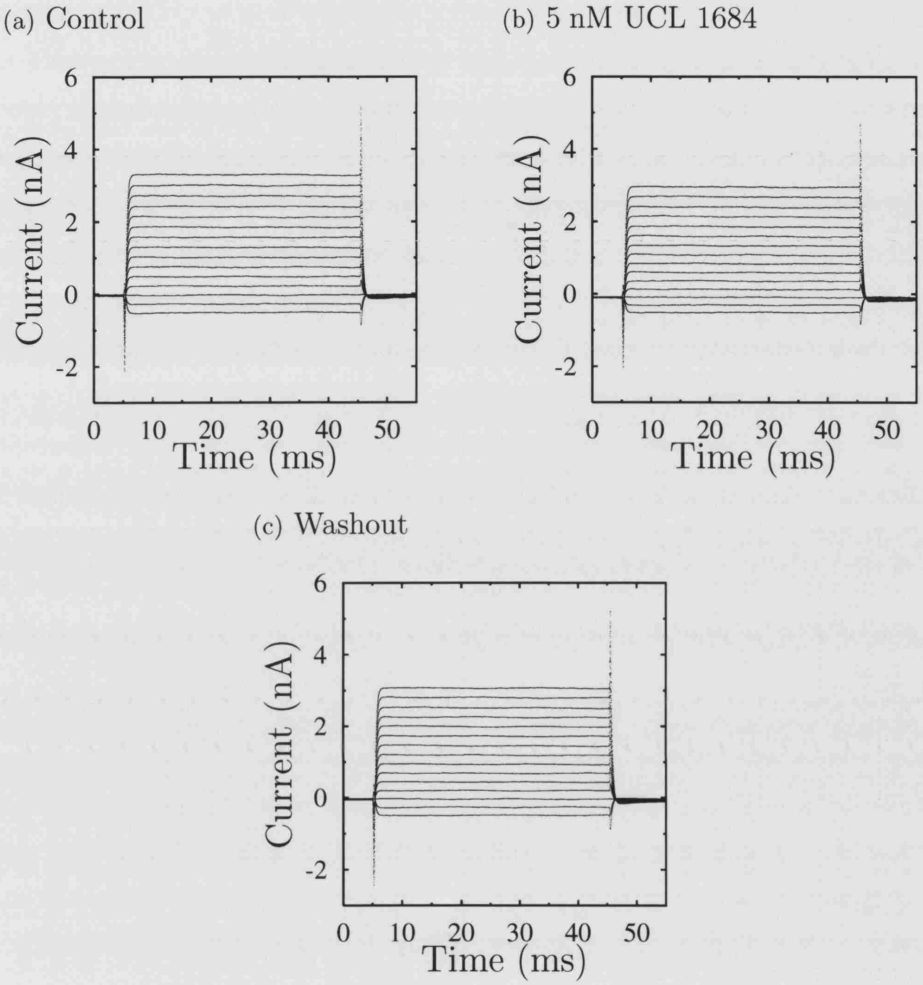


**Figure 5.2:** The effect of 5 nM UCL 1684 on G535D–rSK3 currents. Whole-cell currents from a HEK 293 cell which was transiently transfected with G535D–rSK3, are shown. In each trace, the transmembrane potential of the cell was held at −80 mV, before being stepped to voltages between −100 mV and +40 mV (in 10 mV increments). After 40 ms at the appropriate step, the potential was returned to −80 mV. Using this voltage-clamp protocol, the cell was perfused with standard bath solution (a), standard bath solution supplemented with 5 nM UCL 1684 (b), and again perfused with standard bath solution only (washout) (c). In three such recordings, 5 nM UCL 1684 produced 11.5±1.8% (mean±SEM) block at a step potential of -40 mV. The intracellular solutions all contained 1 mM Mg–ATP, 130 mM KCl, and 1 μM free calcium. A standard bath solution (containing 5 mM $K^+$) was used for each recording.

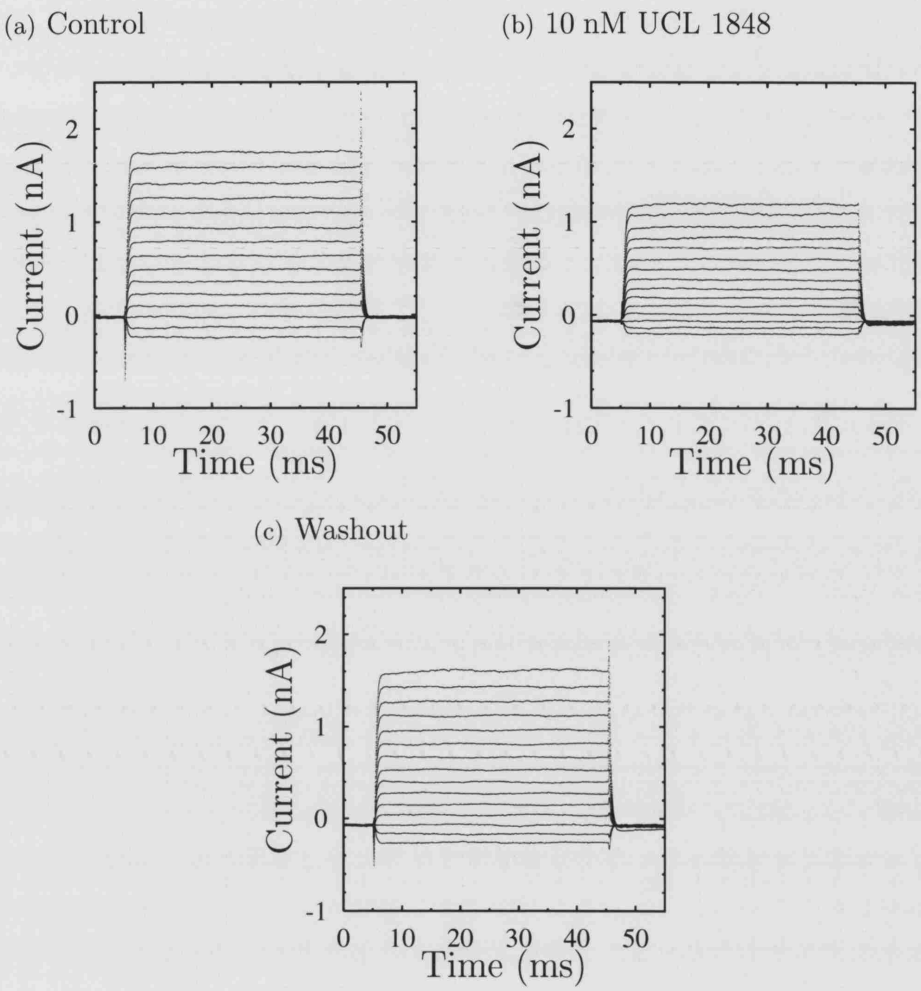


**Figure 5.3:** The effect of 10 nM UCL 1848 on G535D–rSK3 currents. Whole-cell currents from a HEK 293 cell which was transiently transfected with G535D–rSK3, are shown. In each trace, the transmembrane potential of the cell was held at −80 mV, before being stepped to voltages between −100 mV and +40 mV (in 10 mV increments). After 40 ms at the appropriate step, the potential was returned to −80 mV. Using this voltage-clamp protocol, the cell was perfused with standard bath solution (a), standard bath solution supplemented with 10 nM UCL 1848 (b), and again perfused with standard bath solution only (washout) (c). In three such recordings, 10 nM UCL 1848 produced 21.9±5.3% (mean±SEM) block at a step potential of -40 mV. The intracellular solutions all contained 1 mM Mg–ATP, 130 mM KCl, and 1 μM free calcium. A standard bath solution (containing 5 mM $K^+$) was used for each recording.

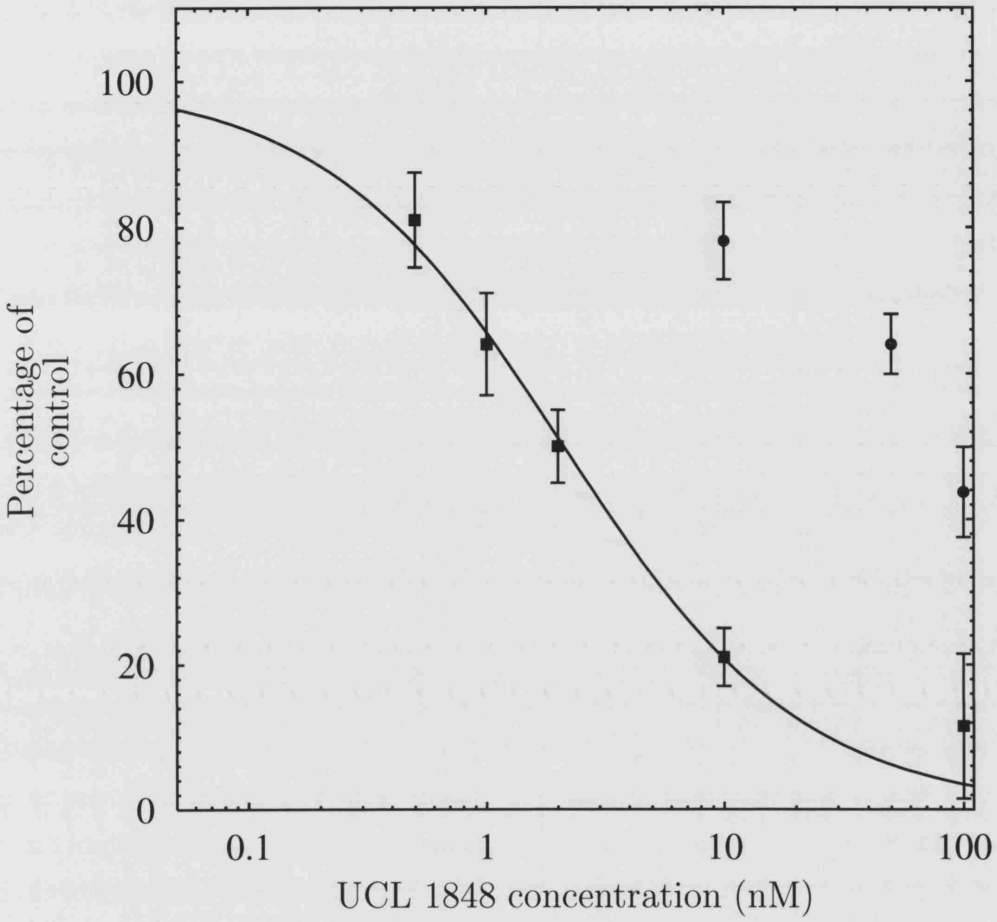


**Figure 5.4:** Dose-response relationship for UCL 1848 block of G535D–rSK3 currents. The dose-response curve for UCL 1848 on WT rSK3 channels has been plotted (*squares*) along with this blocker's dose-response relationship on G535D-rSK3 (*circles*). Data for block of G535D-rSK3 channels by UCL 1848 has not been fitted to the Hill equation due to the lack of concentration points. The data for UCL 1848 block of WT rSK3 channels have been fitted to the Hill equation with an estimated $IC_{50}$ of 2.11±0.19 nM (mean±SD) and Hill coefficient of 0.86±0.07 (mean±SD). UCL 1848 concentration has been plotted on a log scale. Data points are the average of three experiments each and the vertical bars indicate the SEM. All experiments were carried out using HEK 293 cells that had been transiently transfected with the relevant DNA. Cells were held at a potential of -80 mV and percentage current remaining was analyzed at -40 mV for each experiment.

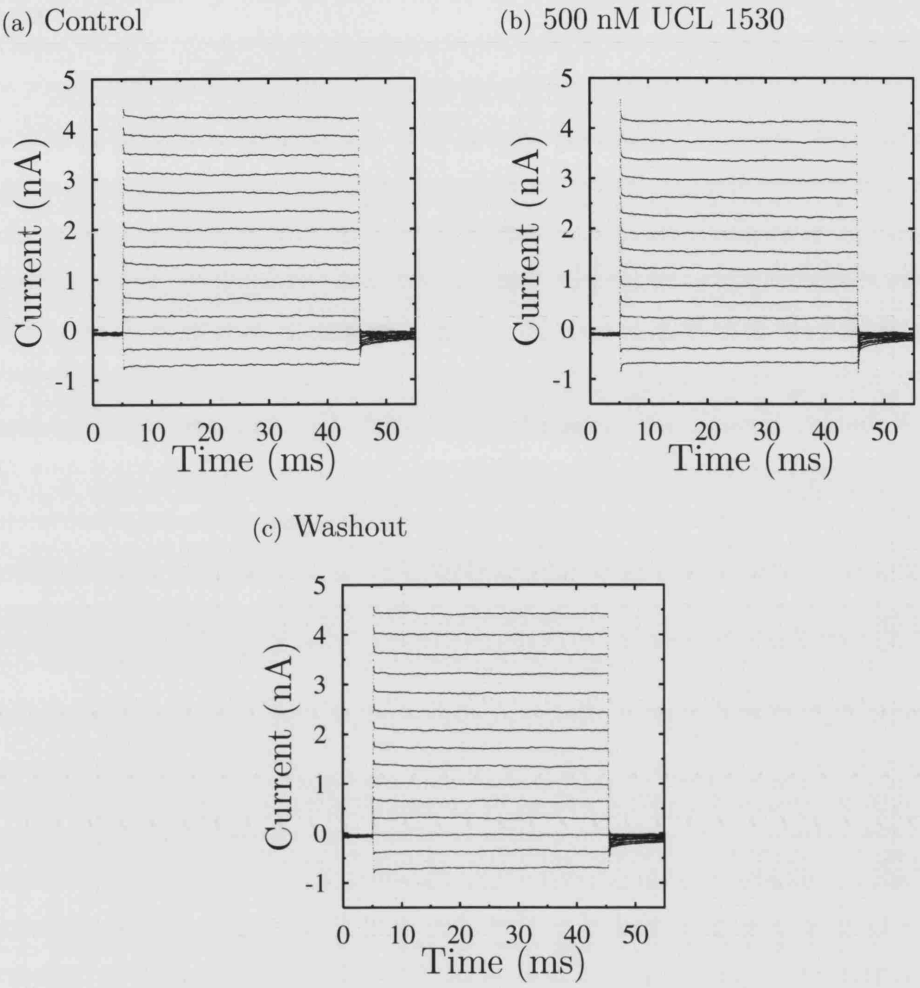


**Figure 5.5:** The effect of 500 nM UCL 1530 on G535D–rSK3 currents. Representative whole-cell currents from a HEK 293 cell which was transiently transfected with G535D–rSK3, are shown. In each trace, the transmembrane potential of the cell was held at −80 mV, before being stepped to voltages between −100 mV and +40 mV (in 10 mV increments). After 40 ms at the appropriate step, the potential was returned to −80 mV. Using this voltage-clamp protocol, the cell was perfused with standard bath solution (a), standard bath solution supplemented with 500 nM UCL 1530 (b), and again perfused with standard bath solution only (washout) (c). In three such recordings, 500 nM UCL 1530 produced no block of G535D–rSK3 currents: the mean normalized current following application of 500 nM UCL 1530 was 0.95±0.02 (mean±SEM) at -40 mV, and the mean normalized current after washout of the drug was 0.96±0.03 (mean±SEM) at -40 mV (currents have been normalized to the control currents and then averaged). The intracellular solutions all contained 1 mM Mg–ATP, 130 mM KCl, and 1 μM free calcium. A standard bath solution (containing 5 mM $K^+$) was used for each recording.

control currents and then averaged). Next, the effect of the V553F-rSK3 mutation on UCL 1848 was examined. Since a concentration of UCL 1684 equal to its $IC_{50}$ on the WT channel had no effect, UCL 1848 was tested at a higher effective concentration. A 10 nM dose of UCL 1848 was applied to the mutant channel (Figure 5.7 on page 186). This concentration of UCL 1848 is five times its $IC_{50}$ for the WT channel (Hosseini et al., 2001). However, it did not produce any block of the V553F–rSK3 current on the three occasions that the experiment was performed using different voltage-clamped whole-cells: the mean normalized current following application of 10 nM UCL 1848 was 0.95±0.03 (mean±SEM) at -40 mV, and the mean normalized current after washout of the drug was 0.95±0.04 (mean±SEM) at -40 mV (currents have been normalized to the control currents and then averaged). These results show that the binding affinities of UCL 1684 and UCL 1848 substantially decrease when the valine residue at position 553 in WT rSK3 is substituted for a phenylalanine residue.

### 5.3.5 Effect of the H555K-rSK3 mutation on UCL 1848 binding

Substitution of histidine by lysine at position 555 in rSK3 resulted in a channel (H555K-rSK3) that was completely insensitive to UCL 1848 up till 100 nM (Figure 5.8 on page 187). In three experiments that were performed using a standard voltage clamp protocol, the mean normalized current following application of 100 nM UCL 1848 was 0.98±0.02 (mean±SEM) at -40 mV, and the mean normalized current after washout of the drug was 1.02±0.04 (mean±SEM) at -40 mV (currents have been normalized to the control currents and then averaged). This concentration of drug is approximately 50 times its $IC_{50}$ on the WT channel and therefore would be expected to block most of the WT current, showing that the lysine for histidine substitution at position 553 in rSK3 reduces the affinity of UCL 1848 binding.

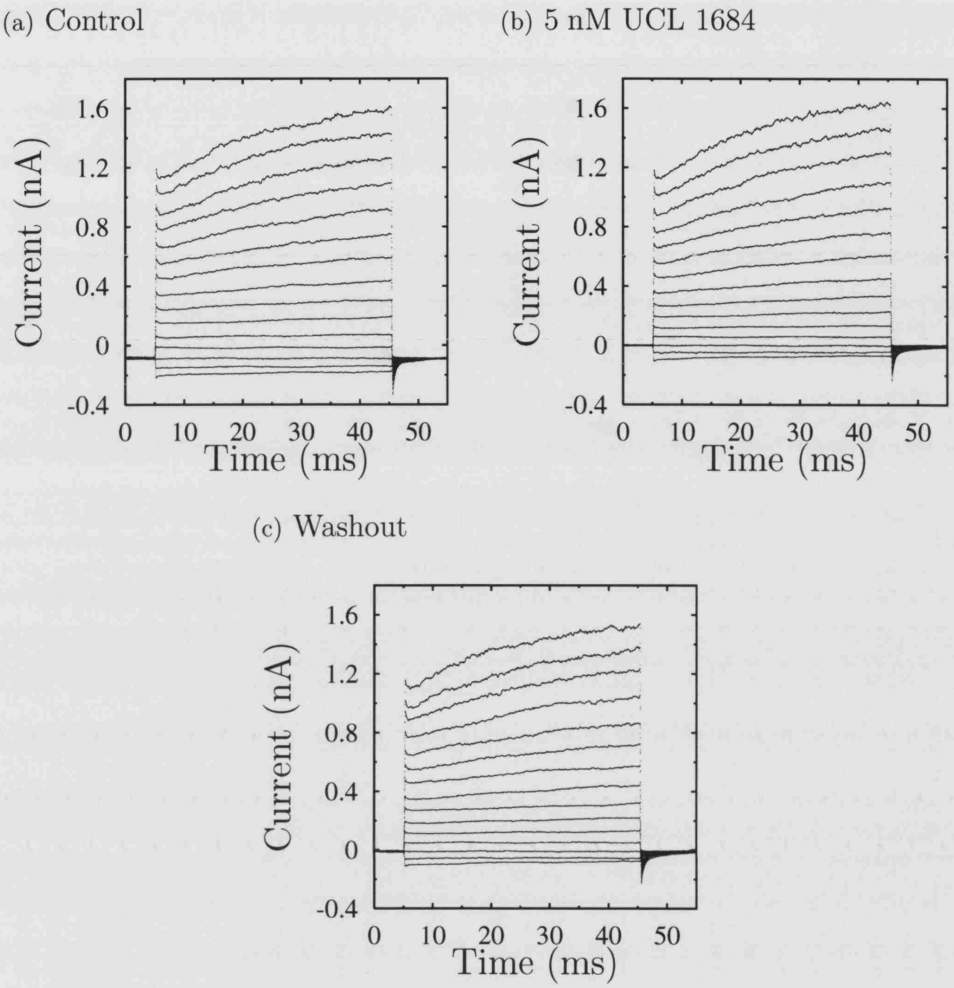


**Figure 5.6:** The effect of 5 nM UCL 1684 on V553F–rSK3 currents. Representative whole-cell currents from a HEK 293 cell which was transiently transfected with V555F–rSK3, are shown. In each trace, the transmembrane potential of the cell was held at −80 mV, before being stepped to voltages between −100 mV and +40 mV (in 10 mV increments). After 40 ms at the appropriate step, the potential was returned to −80 mV. Using this voltage-clamp protocol, the cell was perfused with standard bath solution (a), with standard bath solution supplemented with 5 nM UCL 1684 (b), and again perfused with standard bath solution (washout) (c). In three such recordings, 5 nM UCL 1684 produced no block of V555F–rSK3 currents: the mean normalized current following application of 5 nM UCL 1684 was 0.99±0.02 (mean±SEM) at -40 mV, and the mean normalized current after washout of the drug was 0.97±0.04 (mean±SEM) at -40 mV (currents have been normalized to the control currents and then averaged). Currents were averaged over the whole of the -40 mV step interval in each recording. Intracellular solutions used for each cell contained 1 mM Mg–ATP, 130 mM KCl, and 1 μM free calcium. A standard bath solution (containing 5 mM $K^+$) was used for cell recordings.

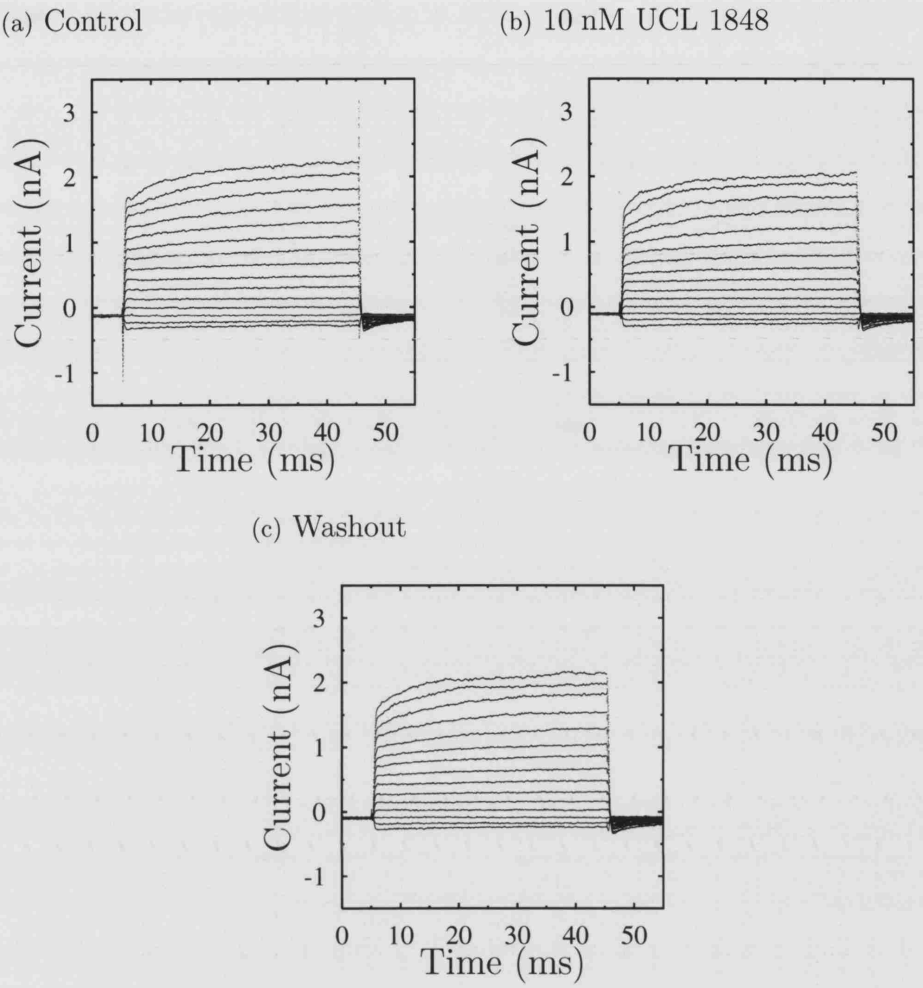


**Figure 5.7:** The effect of 10 nM UCL 1848 on V553F–rSK3 currents. Representative whole-cell currents from a HEK 293 cell which was transiently transfected with V553F–rSK3, are shown. In each trace, the transmembrane potential of the cell was held at −80 mV, before being stepped to voltages between −100 mV and +40 mV (in 10 mV increments). After 40 ms at the appropriate step, the potential was returned to −80 mV. Using this voltage-clamp protocol, the cell was perfused with standard bath solution (a), with standard bath solution supplemented with 10 nM UCL 1848 (b), and again perfused with standard bath solution (washout) (c). In three such recordings, 10 nM UCL 1848 did not produce a significant block of V553F–rSK3 current: the mean normalized current following application of 10 nM UCL 1848 was 0.95±0.03 (mean±SEM) at -40 mV, and the mean normalized current after washout of the drug was 0.95±0.04 (mean±SEM) at -40 mV (currents have been normalized to the control currents and then averaged). Currents were averaged over the whole of the -40 mV step interval in each recording. The intracellular solutions all contained 1 mM Mg–ATP, 130 mM KCl, and 1 μM free calcium. A standard bath solution (containing 5 mM $K^+$) was used for cell recordings.

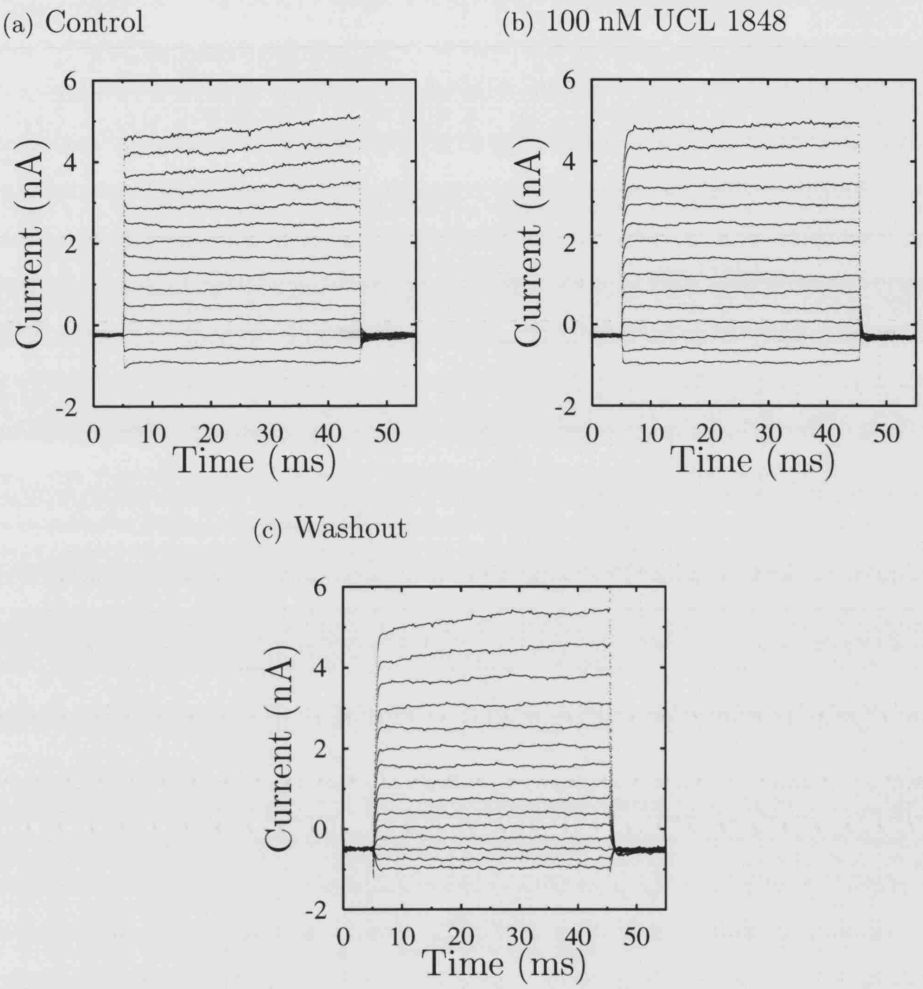


**Figure 5.8:** The effect of 100 nM UCL 1848 on H555K–rSK3 currents. Representative whole-cell currents from a HEK 293 cell which was transiently transfected with H555K–rSK3, are shown. In each trace, the transmembrane potential of the cell was held at −80 mV, before being stepped to voltages between −100 mV and +40 mV (in 10 mV increments). After 40 ms at the appropriate step, the potential was returned to −80 mV. Using this voltage-clamp protocol, the cell was perfused with standard bath solution (a), standard bath solution containing 100 nM UCL 1848 (b), and again perfused with standard bath solution only (c). In three such recordings, 100 nM UCL 1848 produced no block of H555K–rSK3 currents: the mean normalized current following application of 100 nM UCL 1848 was 0.98±0.02 (mean±SEM) at -40 mV, and the mean normalized current after washout of the drug was 1.02±0.04 (mean±SEM) at -40 mV (currents have been normalized to the control currents and then averaged). The intracellular solutions all contained 1 mM Mg–ATP, 130 mM KCl, and 1 μM free calcium. A standard bath solution (containing 5 mM $K^+$) was used for cell recordings.

### 5.3.6 Effect of the V529K-rSK3 mutation on UCL 1530 and UCL 1848 binding

Next, the valine residue at position 529 was replaced by a bulkier cationic lysine amino acid. The effect of this mutation on UCL compound binding was then investigated. Initially, a series of UCL 1530 concentrations up till 500 nM were applied extracellularly to V529K-rSK3 channels (Figure 5.9 on page 190). This dose is approximately two and a half times its $IC_{50}$ on WT rSK3 (Dr David Benton, personal communication). Whole-cells were voltage-clamped and subjected to a typical "step" protocol as outlined in the Methods chapter. No effect of the drug at a concentration equal to its $IC_{50}$ on the WT rSK3 channel (200 nM) could be seen on the three occasions that the experiment was performed: the mean normalized current following application of 200 nM UCL 1530 was 0.98±0.03 (mean±SEM) at -40 mV (currents have been normalized to the control currents and then averaged). Washout was not achieved for all experiments, but the currents had stabilized by the time control recordings were made. As a 200 nM dose of UCL 1530 was ineffective, it was decided to test a higher dose of UCL 1848 relative to its $IC_{50}$ (2.1 nM, Hosseini et al., 2001). 100 nM UCL 1848 was applied extracellularly to V529K-SK3 mutant channels which were expressed in a HEK 293 cell that was voltage-clamped (Figure 5.10 on page 191). This dose is 50 times the $IC_{50}$ value of the drug on WT rSK3. However, no effect of the drug could be seen when it was applied to three different whole-cells held under voltage-clamp which were expressing V529K-rSK3 channels: the mean normalized current following application of 100 nM UCL 1848 was 0.97±0.03 (mean±SEM) at -40 mV (currents have been normalized to the control currents and then averaged). Again, washout was not achieved for all experiments, but the currents had stabilized by the time control recordings were made. These results show that the binding affinities of UCL 1530 and UCL 1848 substantially decrease when the valine residue at position 529 in WT rSK3 is substituted

by a lysine residue.

### 5.3.7 Effect of the D528K-rSK3 mutation on UCL 1848 and UCL 1684 binding

Finally, the residue adjacent to V529-rSK3, aspartic acid at position 528, was replaced by a lysine amino acid. 100 nM UCL 1848 was applied to the extracellular side of the D528K-rSK3 channel. This concentration was chosen since this residue, and not V529K-rSK3, was believed to be critical for UCL 1848 binding (from mutational studies involving apamin), and therefore one would expect D528K-rSK3, adjacent to V529K-rSK3 which is not blocked by 100 nM UCL 1848, to be at least as insensitive to this concentration of UCL 1848. A step protocol was applied to voltage-clamped whole-cells and 70.1±6.7% (mean±SEM) (n=3 recordings) block of the mean current at -40 mV was obtained (Figure 5.11 on page 192). As a consequence of this surprising result, a much smaller dose of UCL 1684, relative to its $IC_{50}$ on WT rSK3 channels, was used as the next test concentration on the D528K-rSK3 channel. A 10 nM dose of UCL 1684 was selected, which is approximately double the $IC_{50}$ of the drug on the WT channel. A step protocol was applied to voltage-clamped whole-cells expressing D528K-rSK3 and 51.2±4.1% (mean±SEM) (n=3 recordings) of the current was blocked at -40 mV upon application of this dose of drug (Figure 5.12 on page 193). Both these results were pursued further and sufficient applications of UCL 1848 and UCL 1684 were made to allow some crude dose-response data to be obtained for this mutant as shown in Figure 5.13 on page 194 and 5.14 on page 195. These results show that residue 528 is not as important a binding site as residue 529 for determining either UCL 1684 or UCL 1848 affinity for the rSK3 channel.

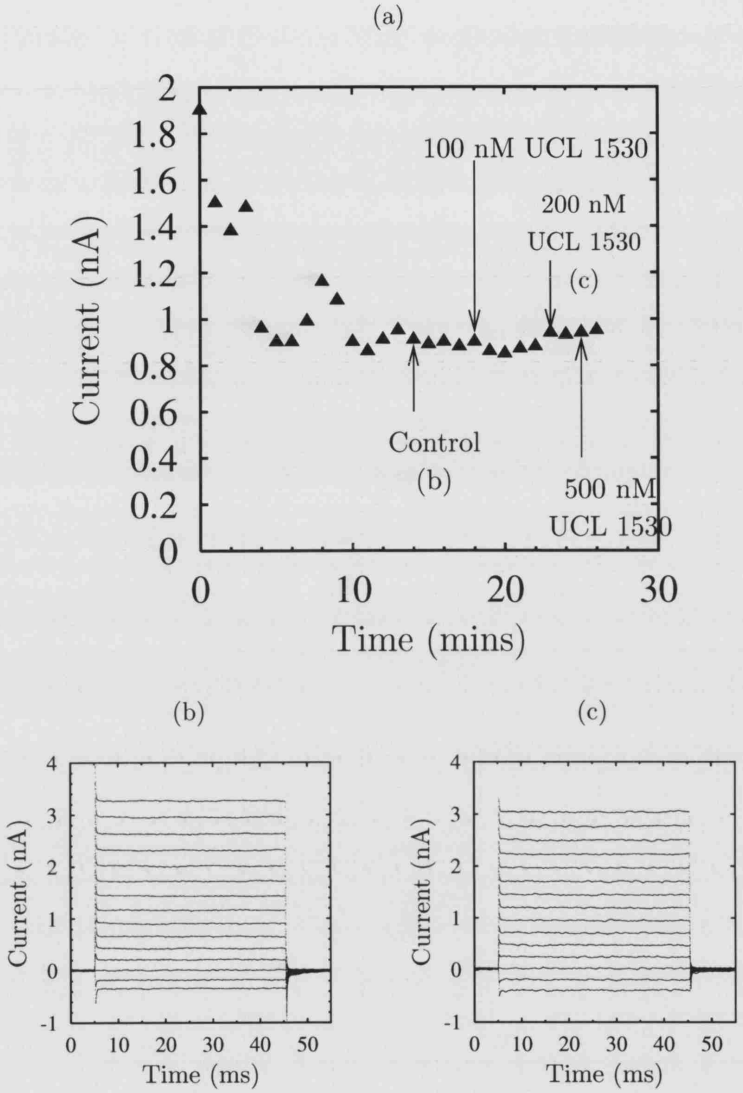


**Figure 5.9:** The effect of UCL 1530 on V529K–rSK3 currents. (a) Time-dependency of whole-cell V529K-rSK3 currents during which several different applications of UCL 1530 were made. A HEK 293 cell which was transiently transfected with V529K-rSK3 was voltage-clamped and held at −80 mV, before being stepped to voltages between −100 mV and +40 mV (in 10 mV increments). After 40 ms at the appropriate step, the cell was returned to −80 mV. The current at -40 mV was plotted every minute. Following stabilization of the current, a control recording was made (b), and then 100 nM UCL 1530 was immediately perfused extracellularly. After 4 minutes of perfusion, no block had occurred and 200 nM UCL 1530 was perfused over the next 5 minutes, but again no block was produced (c). Finally 500 nM UCL 1530 was perfused over the following 2 minutes of the recording, without effect. In three recordings made in this way, the mean normalized current following application of 200 nM UCL 1530 was 0.98±0.03 (mean±SEM) at -40 mV (currents have been normalized to the control currents and then averaged). The intracellular solutions all contained 1 mM Mg–ATP, 130 mM $K^+$, and 1 μM free calcium. A standard bath solution (containing 5 mM $K^+$) was used for cell recordings.

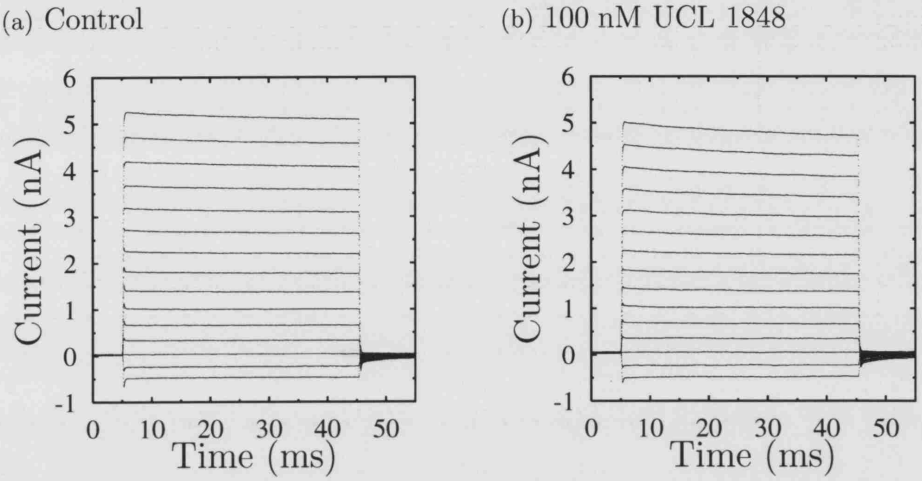


**Figure 5.10:** The effect of 100 nM UCL 1848 on V529K–rSK3 currents. Representative whole-cell currents from a HEK 293 cell which was transiently transfected with V529K–rSK3, are shown. In each trace, the transmembrane potential of the cell was held at −80 mV, before being stepped to voltages between −100 mV and +40 mV (in 10 mV increments). After 40 ms at the appropriate voltage, the potential was returned to −80 mV. Using this voltage-clamp protocol, the cell was perfused with standard bath solution until the currents had stabilized (a), and then with bath solution containing 100 nM UCL 1848 (b). In three such recordings, 100 nM UCL 1848 produced no block of V529K–rSK3 currents: the mean normalized current following application of 100 nM UCL 1848 was 0.97±0.03 (mean±SEM) at -40 mV (currents have been normalized to the control currents and then averaged). The intracellular solutions all contained 1 mM Mg–ATP, 130 mM $K^+$, and 1 μM free calcium. A standard bath solution (containing 5 mM $K^+$) was used for cell recordings.

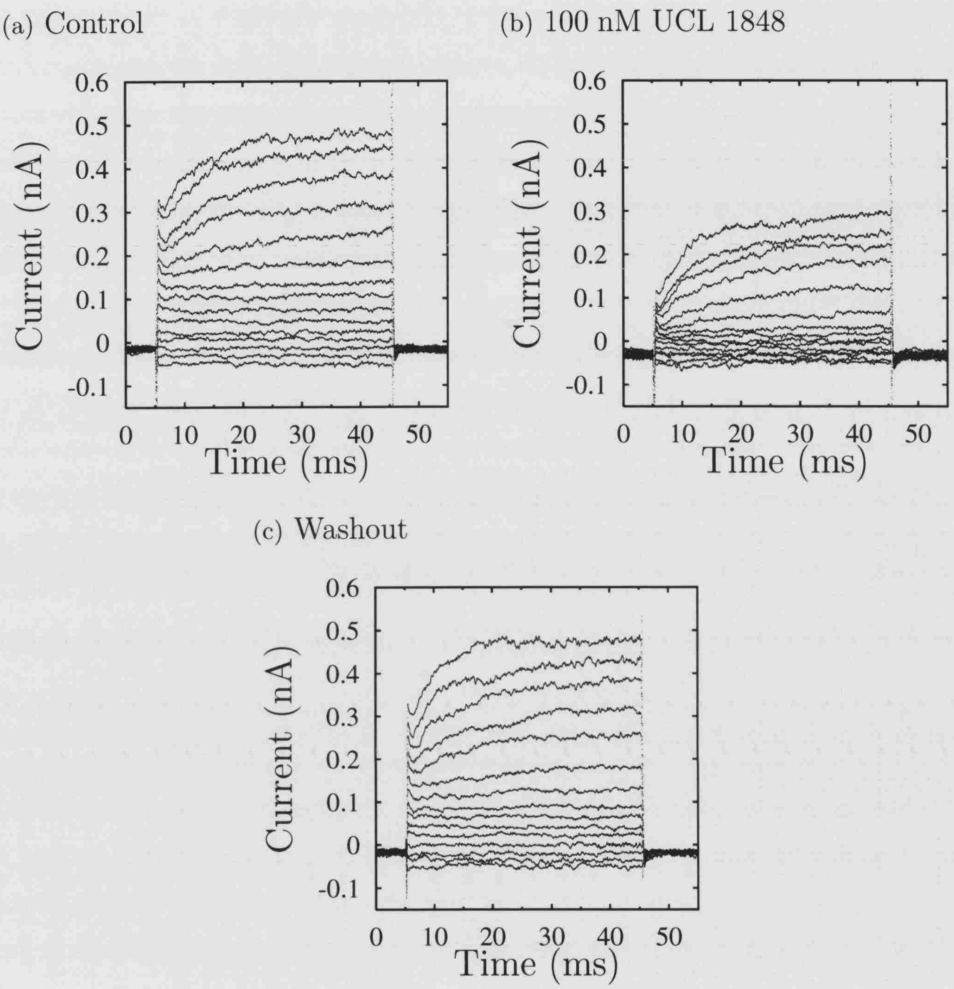


**Figure 5.11:** The effect of 100 nM UCL 1848 on D528K–rSK3. Whole-cell currents from a HEK 293 cell which was transiently transfected with D528K–rSK3, are shown. In each trace, the transmembrane potential of the cell was held at −80 mV, before being stepped to voltages between −100 mV and +40 mV (in 10 mV increments). After 40 ms at the appropriate step, the potential was returned to −80 mV. Using this voltage-clamp protocol, the cell was perfused with standard bath solution (a), standard bath solution supplemented with 100 nM UCL 1848 (b), and again perfused with standard bath solution (c). In three such recordings, 70.1±6.7% block was seen at a step potential of -40 mV. The intracellular solutions all contained 1 mM Mg–ATP, 130 mM KCl, and 1 μM free calcium. A standard bath solution (containing 5 mM $K^+$) was used for cell recordings.

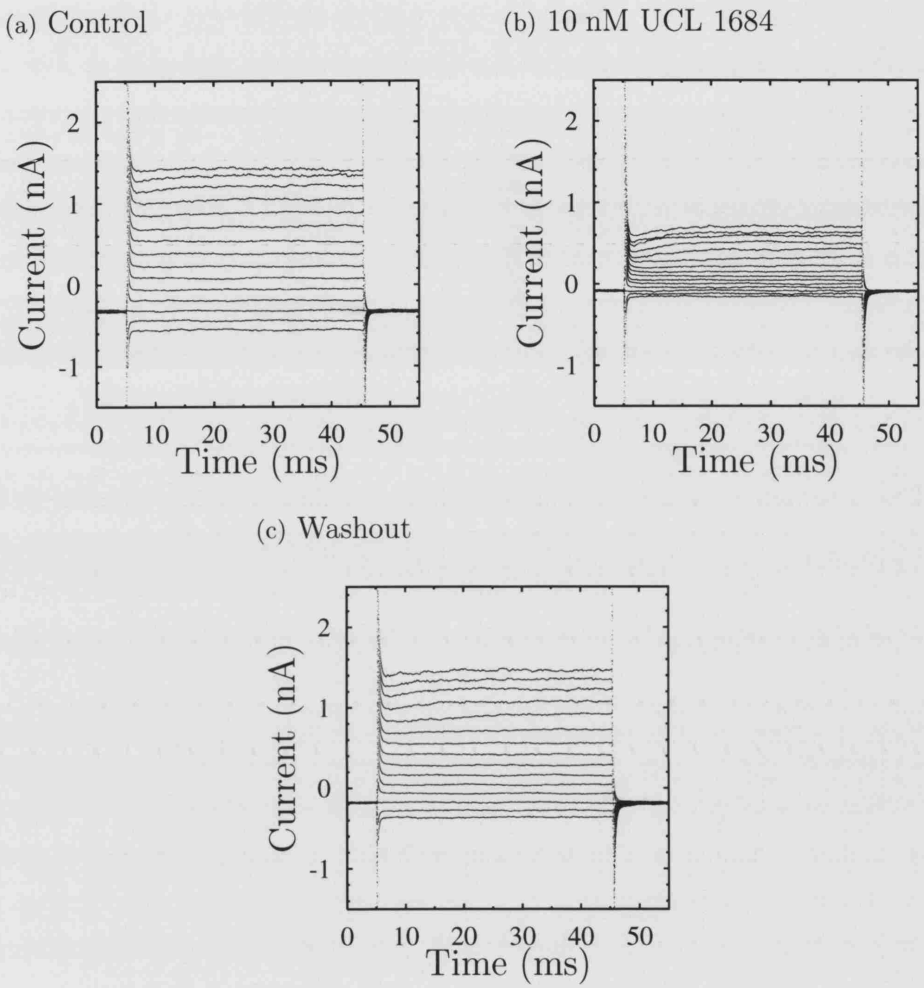


**Figure 5.12:** The effect of 10 nM UCL 1684 on D528K–rSK3 currents. Whole-cell currents from a HEK 293 cell which was transiently transfected with D528K–rSK3, are shown. In each trace, the transmembrane potential of the cell was held at −80 mV, before being stepped to voltages between −100 mV and +40 mV (in 10 mV increments). After 40 ms at the appropriate step, the potential was returned to −80 mV. Using this voltage-clamp protocol, the cell was perfused with standard bath solution (a), standard bath solution supplemented with 10 nM UCL 1684 (b), and again perfused with standard bath solution (c). In three such recordings, 51.2±4.1% block was seen at a step potential of -40 mV. The intracellular solutions all contained 1 mM Mg–ATP, 130 mM KCl, and 1 μM free calcium. A standard bath solution (containing 5 mM $K^+$) was used for cell recordings.

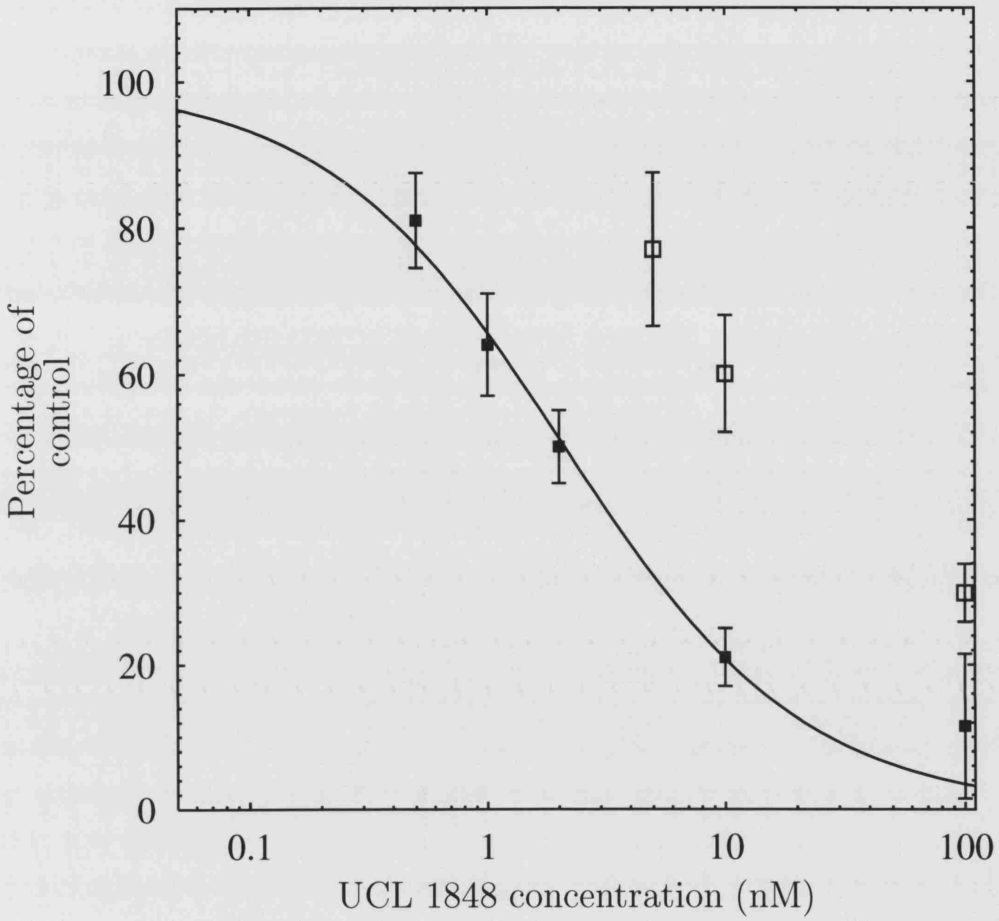


**Figure 5.13:** Dose-response relationship for UCL 1848 block of D528K–rSK3 currents. The dose-response curve for UCL 1848 on WT rSK3 (*Filled squares*) has been plotted along with this blocker's dose-response relationship on D528K-rSK3 (*Open squares*). Data for block of the D528K-rSK3 channel by UCL 1848 has not been fitted to the Hill equation due to the lack of concentration points. The data for UCL 1848 block of WT rSK3 channels have been fitted to the Hill equation with an estimated $IC_{50}$ of 2.11±0.19 nM (mean±SD) and Hill coefficient of 0.86±0.07 (mean±SD). UCL 1848 concentration has been plotted on a log scale. Data points are the average of three experiments. The vertical bars indicate the SEM. All experiments were carried out using HEK 293 cells that had been transiently transfected with the relevant DNA. Cells were held at a potential of -80 mV and percentage current remaining was analyzed at -40 mV for each experiment.

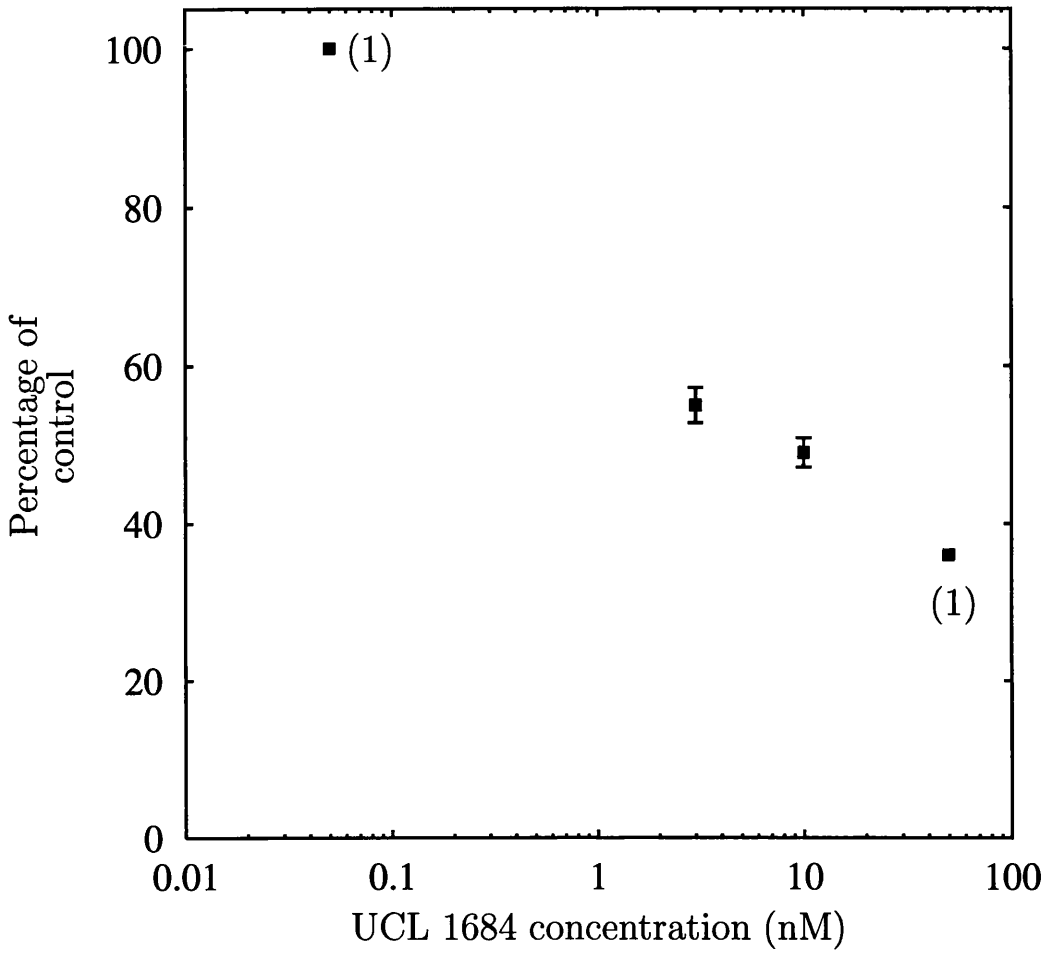


**Figure 5.14:** Dose-response relationship for UCL 1684 block of D528K–rSK3 currents. Data for block of D528K-rSK3 by UCL 1684 has not been fitted to the Hill equation due to the lack of concentration points. UCL 1684 concentration has been plotted on a log scale. Data points are the average of three experiments except the data points which have parentheses next to them. These latter points show the result of one experiment. The vertical bars indicate the SEM. All experiments were carried out using HEK 293 cells that had been transiently transfected with D528K–rSK3 DNA. Cells were held at a potential of -80 mV, and the percentage current remaining in whole cells was analyzed at -40 mV in each experiment.

### 5.3.8 The mechanism of inhibition of UCL 1848 by the V529K-rSK3 mutation

In the V529K–rSK3 mutant channel, position 528 would be negatively charged and 529 positively charged whereas in the D528K–rSK3 channel, 528 would be positively charged and 529 uncharged. If the loss of UCL compound affinity observed in V529K-rSK3 were purely electrostatic in origin, one would expect that this mutant would have a greater affinity for positively charged UCL compounds compared to D528K-rSK3, since the former contains an extra negatively charged pore amino acid. On the contrary, UCL compounds were more potent on the D528K-rSK3 channel which led to the possibility that the V529K–rSK3 mutation sterically inhibits UCL 1848 more so than the D528K–rSK3 mutation. It was therefore decided to create another channel mutant, V529L–rSK3, to determine whether the reduced UCL 1848 affinity of the V529K–rSK3 channel could be accounted by a through-space (electrostatic) mechanism or a model involving physical interactions.

Sequencing chromatograms showed that this mutant was made successfully. The mutant was subsequently expressed in CHO cells to examine the currents flowing through it. All the transfected CHO cells that were selected for analysis were representative (in size and shape) of the majority of other CHO cells that were plated down. Expression of V529L-rSK3 channels in CHO cells produced nanoampere currents under voltage-clamp that were typical of SK channels (Table 5.2 on page 198). Immediately after going whole-cell, an average current of 1.9±0.5 nA (mean±SEM) at -40 mV was obtained from CHO cells transiently expressing V529L-rSK3 channels under voltage-clamp conditions (n=3 recordings). This compared to an average current recorded immediately after going whole-cell of 2.4±0.5 nA (mean±SEM) at -40 mV from CHO cells transiently expressing WT rSK3 channels under the same conditions (n=4 recordings). These currents are not significantly different from one another ($P>0.05$).

### Effect of the V529L–rSK3 mutation on UCL 1848 binding

To compare the UCL compound sensitivity of this channel to that of V529K-rSK3, a 100 nM dose of UCL 1848 was perfused with the extracellular solution onto a voltage-clamped whole-cell that was expressing the V529L-rSK3 channel. Figure 5.15 on page 199 shows traces from such an experiment. The V529L-rSK3 point mutant was completely insensitive to this concentration of UCL 1848 on this occasion and another two occasions when the experiment was repeated: the mean normalized current following application of 100 nM UCL 1848 was 0.98±0.01 (mean±SEM) at -40 mV, and the mean normalized current after washout of the drug was 0.92±0.01 (mean±SEM) at -40 mV (currents have been normalized to the control currents and then averaged). Therefore point mutations at position 529 in the rSK3 channel appear to produce the same effect on UCL 1848 binding, irrespective of the charge on the substituted amino acid, which supports a model in which bulkier residues at position 529 in rSK3 can sterically hinder the binding of UCL 1848.

## 5.3.9 The subunit stoichiometry of UCL 1848 binding to rSK3 channels

When a mutation is made in the rSK3 channel, the resulting tetrameric channel has four residues that differ from the WT, one in each subunit. These residues can potentially make as many as four interactions with the blocking molecule or as few as one. Mutant and WT subunits were co-expressed in a 1:1 ratio, and the pharmacology of co-assembled channels was examined in order to partially determine the mechanism of UCL 1848 interaction with the rSK3 channel. When co-expressing two non-identical DNAs, a heterogenous pool of channels will form. Each type of channel is known as a species, and it is possible to predict the spread of channel species assuming purely stochastic associations (Figure 5.17 on page 203). In such cases, the first channel species to be blocked would be predicted to be the four WT

| Mutation | Chromatogram | Current trace |
|---|---|---|
| V529L–rSK3 | 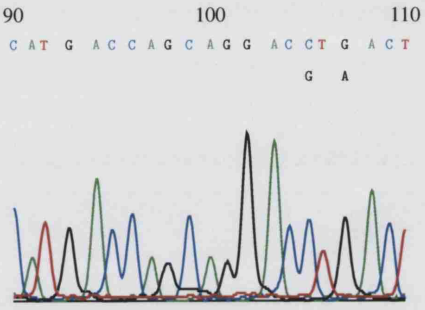 | 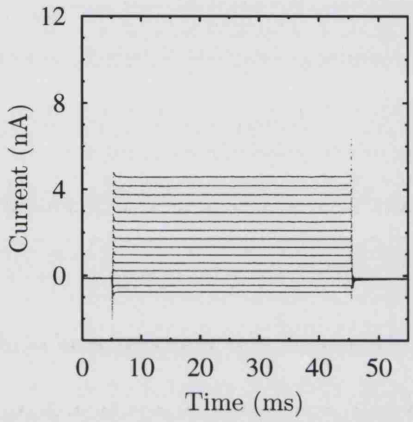 |



**Table 5.2:** Table showing sections of the sequencing chromatograms spanning the mutated bases of the V529L-rSK3 mutant and the representative current trace produced after its cellular expression. The whole-cell current trace has been generated immediately (<20-30 seconds) after going whole-cell, and is from a CHO cell that had been transiently transfected with V529L-rSK3. This cell was held at −80 mV, before being stepped to voltages between −100 mV and +40 mV (in 10 mV increments). After 40 ms at the appropriate step, the cell was returned to −80 mV. Intracellular solution used contained 1 mM Mg–ATP, 130 mM KCl, and 1 μM free calcium. A standard bath solution (containing 5 mM $K^+$) was used. Bases below the main sequence in the chromatogram are the WT rSK3 bases at the equivalent positions to the mutated bases directly above them. Numbers above bases begin from the start of the read, and do not relate to the entire sequence for rSK3.

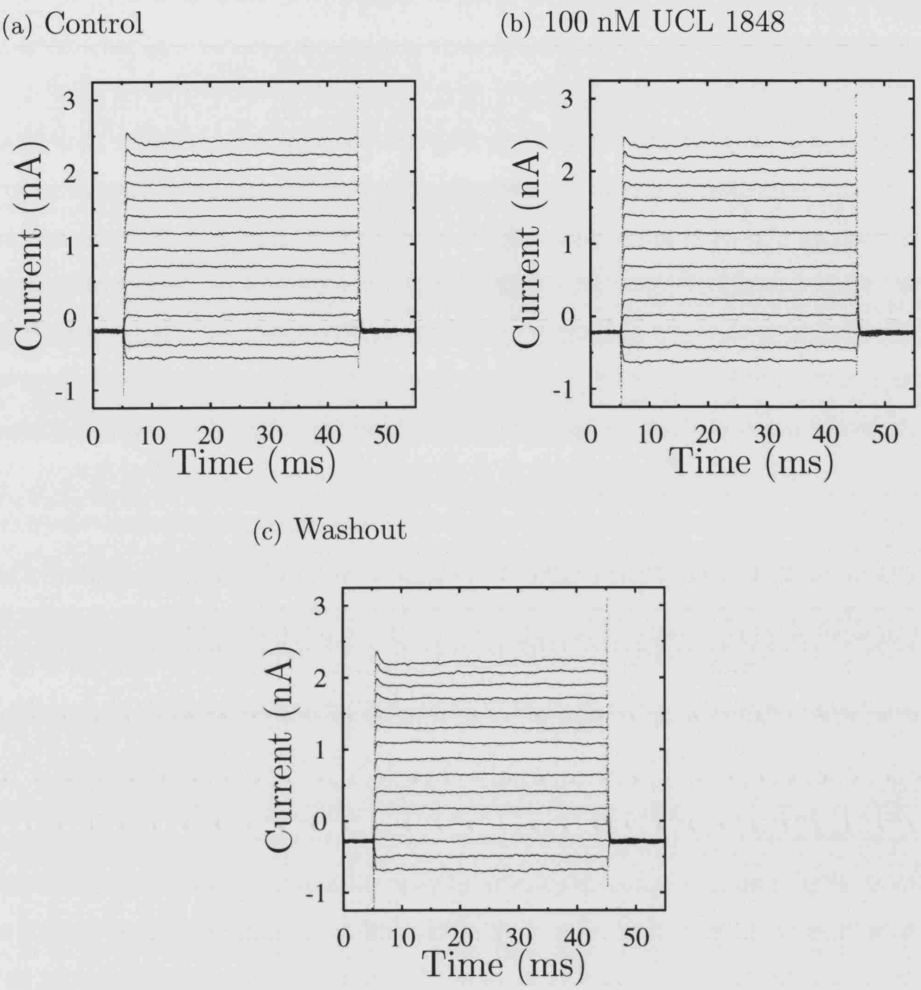


**Figure 5.15:** V529L–rSK3 currents are unaffected by 100 nM UCL 1848. Representative whole-cell currents from a HEK 293 cell which was transiently transfected with V529L–rSK3, are shown. In each trace, the transmembrane potential of the cell was held at −80 mV, before being stepped to voltages between −100 mV and +40 mV (in 10 mV increments). After 40 ms at the appropriate step, the potential was returned to −80 mV. Using this voltage-clamp protocol, the cell was perfused with standard bath solution (a), standard bath solution supplemented with 100 nM UCL 1848 (b), and again perfused with standard bath solution (c). In three such recordings, 100 nM UCL 1848 produced no block of V529L–rSK3 currents: the mean normalized current following application of 100 nM UCL 184 was 0.98±0.01 (mean±SEM) at -40 mV, and the mean normalized current after washout of the drug was 0.92±0.01 (mean±SEM) at -40 mV (currents have been normalized to the control currents and then averaged). Intracellular solutions used for each cell contained 1 mM Mg–ATP, 130 mM KCl, and 1 μM free calcium. A standard bath solution (containing 5 mM $K^+$) was used for all the cell recordings.

rSK3 subunit species, followed by channels containing mutant (insensitive) and WT (sensitive) subunits. The binding affinity of UCL 1848 for these channel species will decrease as the number of mutant subunits increase, resulting in an overall dose-response curve that is, in essence, a composite of numerous smaller dose-response curve, each representing the $IC_{50}$ of the different channel species formed. These composite dose-response curves would not be able to be seen unless large numbers of concentration-inhibition data points are obtained, but the loss of a binding site for UCL 1848 as a result of the incorporation of a further mutant subunit should cause a much larger increase in the $IC_{50}$ that can clearly be seen.

To investigate the number of interactions that UCL 1848 makes with a particular residue in the tetrameric channel, the overall dose-response curves were obtained from a 1:1 co-transfection of V529K-rSK3 and WT rSK3 DNAs and also from a 1:1 co-transfection of H555K-rSK3 and WT rSK3 DNAs. The residues from these mutant channels would provide an 8-point map of the residues that interact with UCL 1848 on the rSK3 channel surface, generating a more accurate model of its binding to the outer pore region.

The dose-response curve for UCL 1848 on the channels arising from the co-transfection of V529K-rSK3 and WT rSK3 DNAs, can be seen in Figure 5.16 on page 202. The analysis shows a right-shift in the curve from an $IC_{50}$ of 2.11±0.19 nM (mean±SEM) and Hill coefficient of 0.86±0.07 (mean±SD) for the WT channels (Figure 5.1 on page 178) to an $IC_{50}$ of 14.9±4.0 nM (mean±SD) and Hill coefficient of 0.63±0.1 (mean±SD) for the co-expressed channels (Figure 5.16 on page 202). Assuming equivalent levels of protein expression and random assemblies of ion channel subunits, as outlined above, one would expect to see UCL 1848 block plateau at the point where binding affinity begins to be lost, as a result of the incorporation of a further V529K-rSK3 mutant subunit, and then continue to block co-expressed channels when the blocker concentration increases. The subsequent incorporation of yet another V529K-rSK3 mutant subunit would produce a further

plateau in the dose-response curve and so on until UCL 1848 insensitive homomeric mutant channels remain. Since only four or five data points have been obtained per dose-response curve, the overall curve would appear steeper at the lower drug concentrations where binding sites are not lost, than at the higher concentrations where these plateau regions would occur. However, the dose-response curve for the co-expressed channel does not appear to be multi-phasic since a single component Hill-Langmuir isotherm fits the data well, suggesting that the number of subunits interacting with UCL 1848 for each co-expressed channel at 100 nM, is the same as the number of subunits interacting with UCL 1848 for each co-expressed channel at 1 nM. Since a single component Hill isotherm appears to fit the data best and a 72.6±4.2% (mean±SEM) current block was observed at 100 nM (n=3 recordings), which should include those channels containing four, three, two and one WT rSK3 subunits, UCL 1848 is probably interacting with the same number of subunits in each of these channel species. Therefore UCL 1848 probably interacts with only one of the four residues at position 529 in the tetrameric channel.

Next, the same issue was investigated using the H555K-rSK3 mutant. H555K-rSK3 and WT rSK3 DNAs were co-transfected in a 1:1 ratio and current block by UCL 1848 was examined. The block was sufficiently potent to allow a full dose-response curve to be obtained for the co-assembled channels (Figure 5.18 on page 204). The data again fitted well to a single component Hill-Langmuir isotherm with a Hill coefficient of 0.75±0.08 (mean±SD) and an $IC_{50}$ of 11.0±2.1 nM (mean±SD). Assuming random subunit associations and equal expression of each protein (Figure 5.17 on page 203), channels containing zero, one, two, or three mutant subunits are probably being blocked when more than 69% current block is observed. Since a single component Hill isotherm appears to fit the data best and an 84.0±3.6% (mean±SEM) block was obtained at 100 nM (a concentration of UCL 1848 that does not block homomeric H555K-rSK3 channels), UCL 1848 probably interacts with only one of the four residues at position 555 in the tetrameric channel.

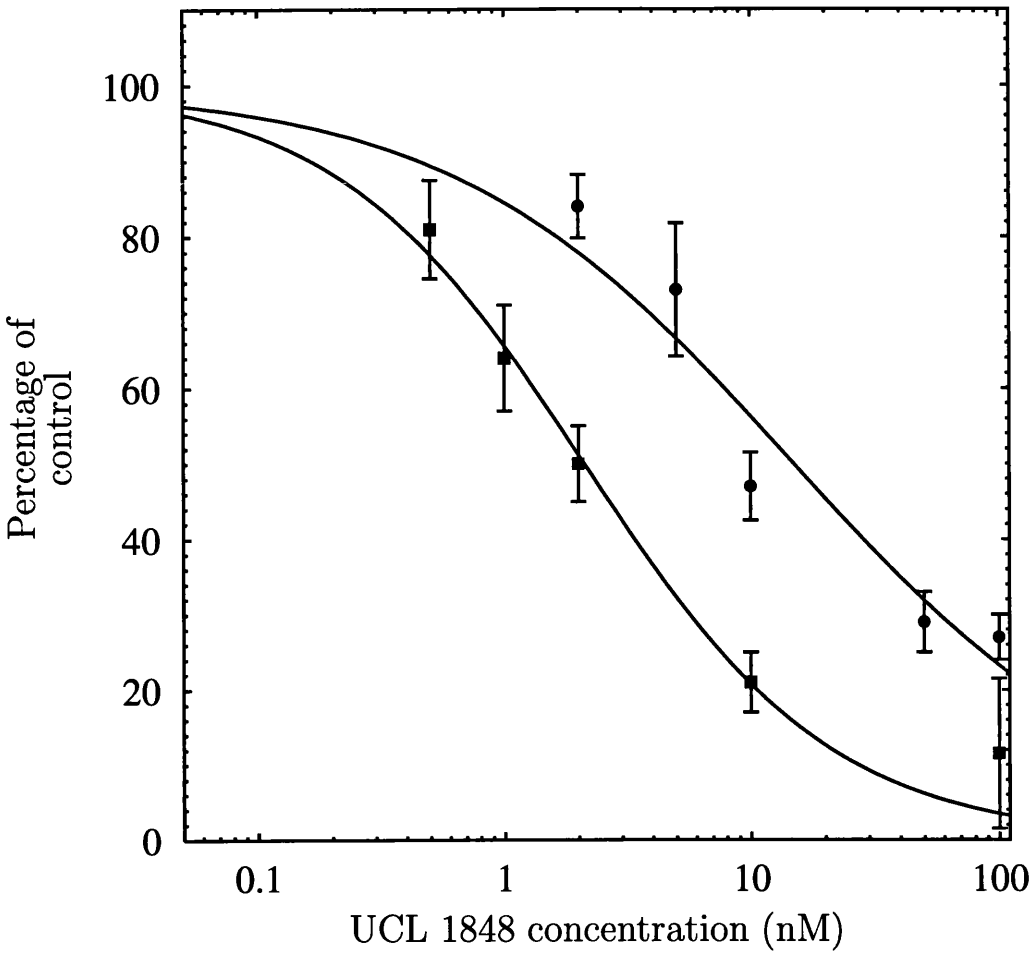


**Figure 5.16:** The dose-response curve for UCL 1848 block of current in cells where WT rSK3 DNA and V529K–rSK3 DNA had been co-transfected in a 1:1 ratio. The dose-response curve for UCL 1848 on WT rSK3 (*squares*) has been plotted along with the dose-response curve for this blocker on the co-expressed channel (*circles*). Both sets of data have been fitted to the Hill equation with their respective $IC_{50}$ and Hill coefficient parameters allowed to vary. From the fit, the estimated $IC_{50}$ for block of the co-expressed channel is 14.9 ± 4.0 nM (mean±SD) with a Hill coefficient of 0.63±0.1 (mean±SD). The data for UCL 1848 block of WT rSK3 channels has been fitted to the Hill equation with an estimated $IC_{50}$ of 2.11±0.19 nM (mean±SD) and Hill coefficient of 0.86±0.07 (mean±SD). UCL 1848 concentration has been plotted on a log scale. Each data point is the mean of three observations and the vertical bars indicate the SEM. All experiments were carried out using HEK 293 cells that had been transiently transfected either with both WT rSK3 DNA and V529K–rSK3 DNA or with WT rSK3 DNA alone. All cells were held at a potential of -80 mV between recordings, and and percentage current remaining was analyzed at -40 mV for each experiment.

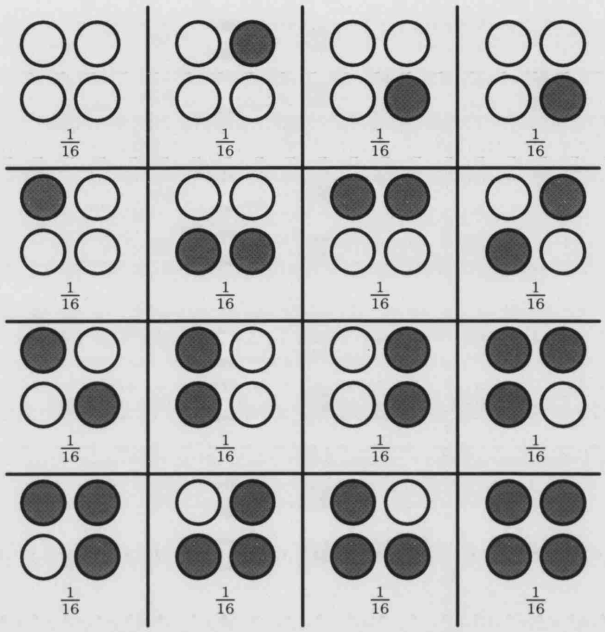

WT ○ subunits have 50% chance of incorporation (1:1 co-transfection)

MUTANT ● subunits have 50% chance of incorporation (1:1 co-transfection)

For a 1:1 co-assembly ratio, the proportion of channels containing

| | |
|---|---|
| 0 mutant subunits $\frac{1}{2} \times \frac{1}{2} \times \frac{1}{2} \times \frac{1}{2} = \frac{1}{16}$. | For 1 channel $= \frac{1}{16} \times 1 = \frac{1}{16}$. |
| 1 mutant subunit $\frac{1}{2} \times \frac{1}{2} \times \frac{1}{2} \times \frac{1}{2} = \frac{1}{16}$. | For 4 channels $= \frac{1}{16} \times 4 = \frac{4}{16} = \frac{1}{4}$. |
| 2 mutant subunits $\frac{1}{2} \times \frac{1}{2} \times \frac{1}{2} \times \frac{1}{2} = \frac{1}{16}$. | For 6 channels $= \frac{1}{16} \times 6 = \frac{6}{16} = \frac{3}{8}$. |
| 3 mutant subunits $\frac{1}{2} \times \frac{1}{2} \times \frac{1}{2} \times \frac{1}{2} = \frac{1}{16}$. | For 4 channels $= \frac{1}{16} \times 4 = \frac{4}{16} = \frac{1}{4}$. |
| 4 mutant subunits $\frac{1}{2} \times \frac{1}{2} \times \frac{1}{2} \times \frac{1}{2} = \frac{1}{16}$. | For 1 channel $= \frac{1}{16} \times 1 = \frac{1}{16}$. |

**Figure 5.17:** Quantitative prediction of the channel species profile for a 1:1 co-transfection ratio assuming random subunit aggregation and equal expression of each protein. The grid shows the possible permutations for channel assembly following such a co-transfection. The calculations under the grid, on the left hand side, show the expected channel fractions that are formed by each hybrid when the subunits are co-expressed in a 1:1 ratio. Each channel shown in the grid would be expected to form $\frac{1}{16}$ of the total number of fully assembled channels. The other calculations (right hand side) show the expected fractions of channel species containing different numbers of mutant subunits.

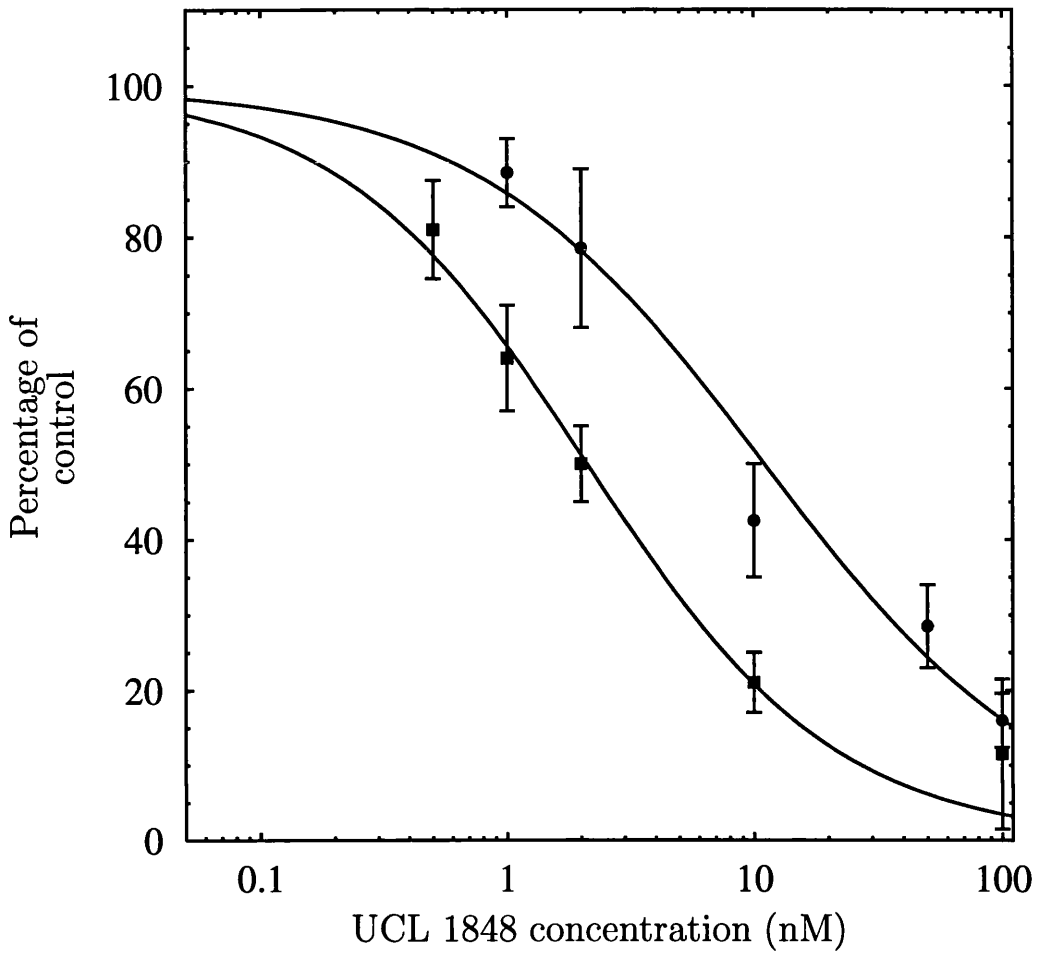


**Figure 5.18:** The dose-response curve for UCL 1848 block of current in cells where WT rSK3 DNA had been co-transfected with H555K–rSK3 DNA in a 1:1 ratio. The dose-response curve for UCL 1848 on WT rSK3 (*squares*) has been plotted along with this blocker's dose-response relationship on the co-expressed channel (*circles*). Both sets of data have been fitted to Hill equations with the $IC_{50}$s and Hill coefficients allowed to vary. From the fit, the estimated $IC_{50}$ of co-transfected cells is 11.0±2.1 nM (mean±SD) with a Hill coefficient of 0.75±0.08 (mean±SD). The data for UCL 1848 block of WT rSK3 channels has been fitted to the Hill equation with an estimated $IC_{50}$ of 2.11±0.19 nM (mean±SD) and Hill coefficient of 0.86±0.07 (mean±SD). UCL 1848 concentration has been plotted on a log scale. Each data point is the mean of three observations and the vertical bars indicate the SEM. All experiments were carried out using HEK 293 cells that had been transiently co-transfected with WT rSK3 DNA and H555K–rSK3 DNA or with WT rSK3 DNA alone. All cells were held at a potential of -80 mV between recordings, and percentage current remaining was analyzed at -40 mV for each experiment.

### 5.3.10 Follow-up work to investigate the molecular mechanisms of differential UCL 1848 sensitivity amongst SK subtypes

Since the aspartic acid residue at position 528 in rSK3 appears to be unimportant in determining UCL 1848 block, the molecular determinants of disparate subtype sensitivities with respect to this blocker were investigated further by creating more mutants of the rSK3 sequence. Several mutants based on differences in the pore region of the SK channel subtypes were designed and created (Table 5.3 on the following page) but remain to be tested. The V519A, H555N-rSK3 mutant has also been created, but remains to be tested.

## 5.4 Discussion

### 5.4.1 The molecular determinants of apamin and UCL 1848 binding to SK channels are probably different

Even though UCL 1848 and apamin have similar binding affinities to the SK channel subtypes, the observation that the D528K–rSK3 channel is nearly as sensitive to UCL 1848 as WT rSK3 channels suggests that the molecular mechanisms which determine its binding to SK channels are distinct from those involved for apamin (Ishii et al., 1997). D528K-rSK3 has neither of the two high affinity binding sites that have been proposed to be responsible for apamin block of SK channels (Ishii et al., 1997). Hence the observation that D528K-rSK3 channels are nearly as sensitive as WT rSK3 channels to UCL 1848 block, suggests that neither of these two sites are responsible for high affinity UCL 1848 binding to rSK3 channels. Therefore, the molecular mechanisms of UCL 1848 binding to SK channels appear to be distinct from those of apamin. A degree of caution regarding the mechanism of apamin

| Mutation | Chromatogram |
|---|---|
| V519A–rSK3 | 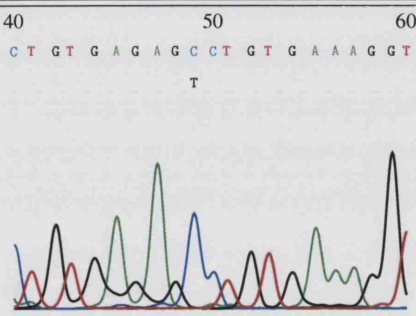 |
| H555N–rSK3 | 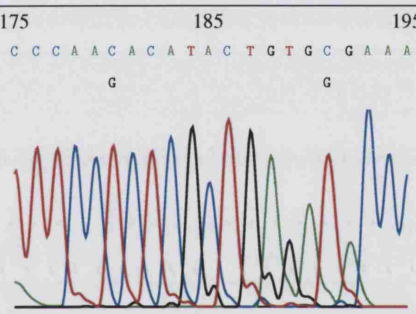 |
| Q526K–rSK3 | 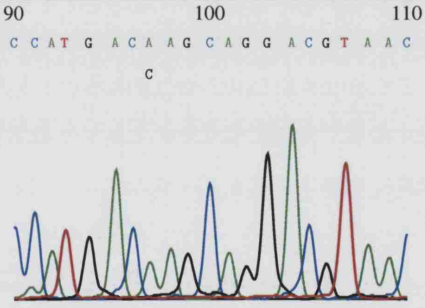 |



**Table 5.3:** Table showing sections of the sequencing chromatograms spanning the mutated bases of further "pharmacology" mutants. Bases below the main sequence in the chromatograms are the WT rSK3 bases at the equivalent positions to the mutated bases directly above them. Numbers above bases begin from the start of the read, and do not relate to the entire sequence for rSK3.

binding to SK channels should be exerted, since the WT hSK1 channel, which was used to investigate the molecular determinants of apamin binding (Ishii et al., 1997), has subsequently been reported to be highly sensitive to apamin (Shah & Haylett, 2000; Grunnet, Jensen, et al., 2001). Therefore, in these latter reports, the molecular determinants of high affinity apamin binding are unlikely to be solely mediated by residues 528 and 555, as suggested by Ishii et al. (1997).

### 5.4.2 Interactions between the rSK3 channel and UCL compounds suggest that the crystal structure of the KcsA channel is a good structural model for the rSK3 pore

#### The KcsA channel model does provide an explanation why residues 529 and 535, but not residue 528 of rSK3 would disrupt UCL 1848 binding

The crystal structure of the KcsA channel offers an answer as to why only one of the two adjacent amino acids leads to a spatially-induced reduction in blocker potency. V529-rSK3 "juts" out into the heart of the pore and would therefore be more likely to contact blockers which bind in the vestibule compared with the D528-rSK3 residue (Figure 1.9 on page 67). This suggests that the structure of this region of the turret is well conserved amongst SK and KcsA channels.

The loss in UCL compound binding affinity of the G535D-rSK3 channel mutant is more likely to be due to spatial hindrance of the blocker, since repulsion between the negatively charged aspartic acid in the G535D-rSK3 channel and positively charged blocker would not occur. Using the KcsA-based rSK3 pore model (Figure 1.9 on page 67), a mechanism for the loss of UCL compound affinity through a spatial mechanism could be feasible from the estimated position of residue 535. This KcsA-based model of the rSK3 pore has residue 535 jutting out towards the heart of the pore from a point slightly lower than residue 529, providing an ideal place for this residue to affect blocker binding substantially, as was observed. Creating a

serine-substituted G535S-rSK3 point mutant, and re-examining the UCL compound pharmacology should determine whether an electrostatic or a spatial mechanism is responsible for this loss in affinity, since serine is uncharged but of similar size to aspartic acid.

**Valine at position 529 in rSK3 probably shares a common structural location with the analogous amino acid in Shaker channels**

The previous chapter provided evidence for general similarities in structure between KcsA, Shaker and SK channels. Further, more detailed similarities have been found in the effect of point mutations upon UCL 1848 binding using the V529L–rSK3 channel. The analogous position of residue 529 in rSK3, is 425 in Shaker (Figure 1.8 on page 66), and a phenylalanine residue is present at this position in the WT Shaker channel. Substitution of progressively less bulky amino acids at residue 425 has been shown to increase the affinity of CTX block (Goldstein et al., 1994). For example, the addition of one extra methyl group at position 425 in Shaker (G425A-Shaker) produced a 6-fold loss in CTX affinity. In addition, this study clearly shows that a conservative change at the analogous position in the rSK3 channel, a valine for leucine substitution at residue 529, produces a large loss in blocker affinity. This suggests that these residues might share a common structural location in their respective outer vestibules which forms an important contact point for blockers.

### 5.4.3 "Maps" of important rSK3 channel residues involved in UCL compound binding

This section summarizes the SK channel residues that have been investigated so far, which interact with UCL 1848 (Figure 5.19 on page 211), UCL 1684, and UCL 1530 (Figure 5.20 on page 212). In each case the crystallographic structure of KcsA has been used as a template, since this appears to be a good structural model of the

rSK3 pore. The pattern of mutated residues which produce either a clear change in affinity or which produce little or no changes distinguishable from the WT channel are shown. This pattern of affinity changes are likely to delineate a blocker's binding site, since many of the point mutations that have been made are non-conservative single amino acid substitutions, designed to maximally disrupt blocker binding if they form part of the blocker's binding site. The binding site maps for each blocker are all roughly similar to a first approximation. However, G535D-rSK3 did not appear to be a major component of the binding site of UCL 1684 (Figure 5.20 on page 212) unlike UCL 1848 and UCL 1530. This might be expected since the relative affinity changes of UCL 1684 on hSK1 and rSK3 ($IC_{50}$ for UCL 1684 on hSK1: $IC_{50}$ for UCL 1684 on rSK3 = 0.14 (Hosseini et al., 2001; Shah & Haylett, 2000)) and UCL 1848 on hSK1 and rSK3 ($IC_{50}$ for UCL 1848 on hSK1: $IC_{50}$ for UCL 1848 on rSK3 = 0.52 (Hosseini et al., 2001; Shah & Haylett, 2000)) are different, indicating the molecular differences between the subtypes affect binding in different ways. Furthermore, the more central channel residue (V553-rSK3) appears to be a more important binding site compared to the peripheral residues in the rSK3 pore model for UCL 1684, but not UCL 1848 and UCL 1530, which might also be expected since UCL 1684 is physically the smallest of the three UCL compounds (Figure 1.7 on page 60). More detailed binding site maps will probably reveal further differences in the binding patterns of these UCL compounds.

The approximate position of a bound UCL 1848 molecule based on the results from this study, is shown in Figure 5.21 on page 213. This shows one possible orientation and position of the blocker, although it is by no means the only possible one based on the evidence of this study. For example, the co-expression experiments carried out suggest the UCL 1848 molecule binds to the residue at position 529 of one subunit only, and also to the residue at position 555 of one subunit only in the tetrameric channel. It is perfectly feasible that the blocker binds to one of these residues on one subunit and to the other residue on an adjacent subunit. Construc-

tion and then expression of a G535D, H555K-rSK3/WT rSK3 dimer would produce a fixed stoichiometry of channels containing alternating mutant and wildtype subunits that can be used to determine which model is likely to be correct. The mutations of this double mutant are located at neighbouring edges of adjacent subunits in the rSK3 model pore, and so UCL 1848 can only bind with high affinity to the two WT subunits if binding occurs to one subunit only, or to much lower affinity sites on the channel (due to the presence of at least one blocker disrupting mutation at every possible binding permutation), if binding is spread across two subunits. One of the premises of such an experiment would be that the KcsA channel is an accurate structural model of the rSK3 channel pore, and this does appear to be the case based on the evidences presented in the last couple of chapters.

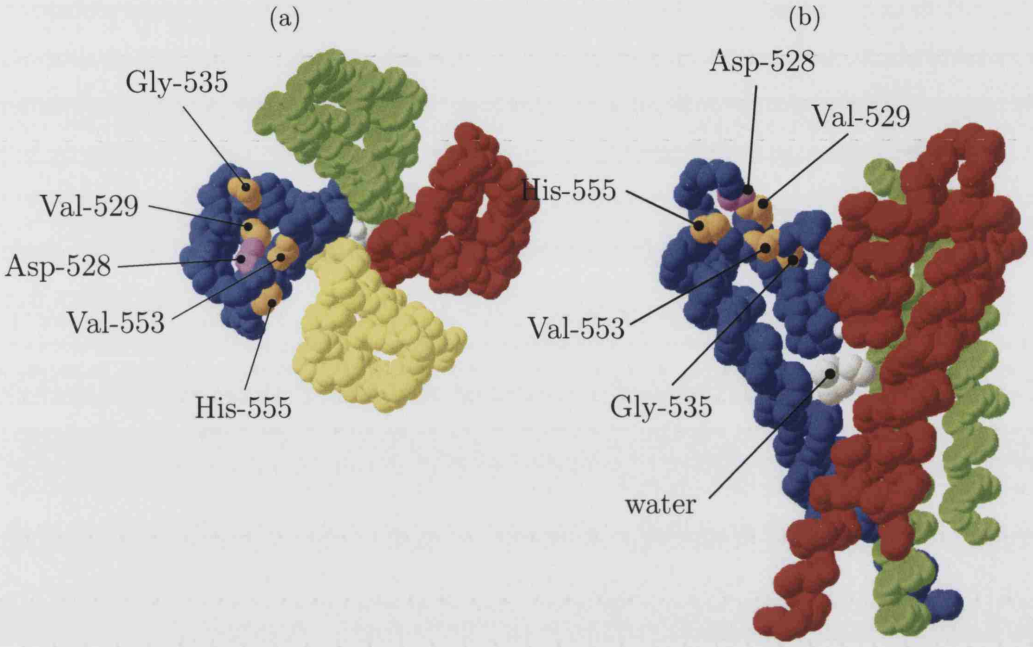


**Figure 5.19:** Channel pore maps showing the strengths of the interactions of mutated rSK3 residues with UCL 1848. The KcsA channel has been used as a model of the rSK3 pore. Channel subunits are coloured in green, red, yellow and blue. Light brown amino acids *strongly* affect UCL 1848 binding (i.e. non-conservative point mutations of these residues produce mutant channels that are insensitive to a concentration of UCL 1848 that is equal to its $IC_{50}$ for WT rSK3 channels). Magenta amino acid, *weakly* affects UCL 1848 binding (i.e. a non-conservative point mutation of this residue produces a mutant channel that is still sensitive to a concentration of UCL 1848 that is equal to its $IC_{50}$ for WT rSK3 channels). (b) has one subunit removed for clarity. It appears that the light brown (strongly interacting) amino acids are more centrally located than the magenta amino acid (weakly interacting) which is consistent with central pore binding of the blocker, and confirms a logical spatial arrangement of amino acids that is consistent with use of the KcsA channel crystal structure as a template. Graphics were generated using Swiss pdb viewer/Povray.

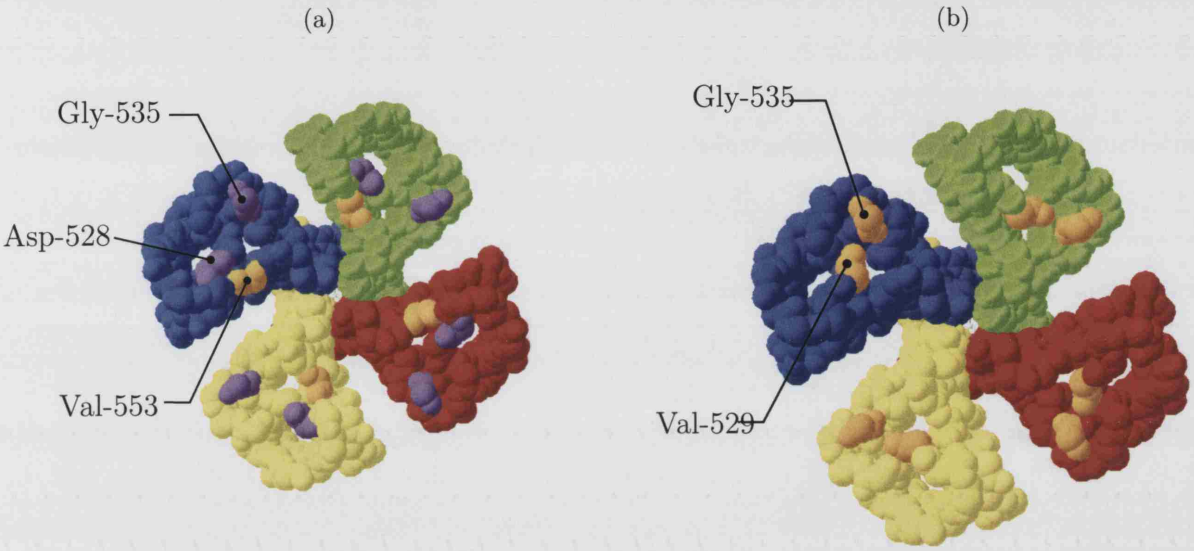


**Figure 5.20:** Channel maps showing the strengths of the interactions of mutated rSK3 residues with UCL 1684 (a) and UCL 1530 (b). The KcsA channel has been used as a model of the rSK3 pore. Channel subunits are coloured in green, red, yellow and blue. Light brown amino acids *strongly* affect UCL 1684/UCL 1530 binding (i.e. non-conservative point mutations of these residues produce mutant channels that are insensitive to a concentration of UCL 1684/UCL 1530 that is equal to its $IC_{50}$ for WT rSK3 channels). Magenta amino acids *weakly* affect UCL 1684/UCL 1530 binding (i.e. non-conservative point mutations of these residues produce a mutant channel that is still sensitive to a concentration of UCL 1684/UCL 1530 that is equal to its $IC_{50}$ for WT rSK3 channels). Graphics were generated using Swiss pdb viewer/Povray.

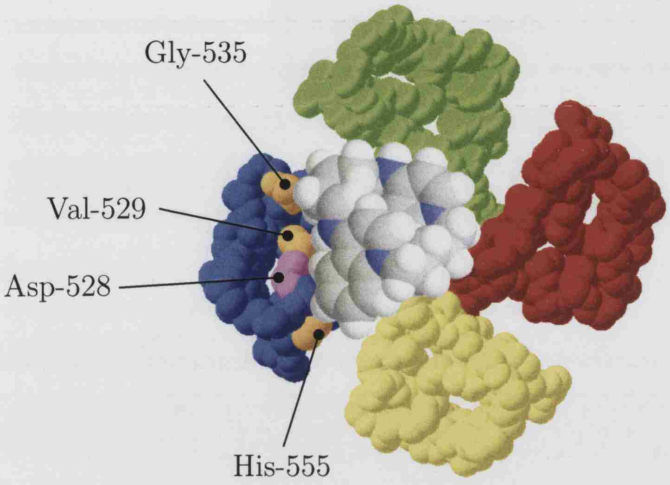


**Figure 5.21:** A model of possible UCL 1848 binding to a putative rSK3 channel pore. The KcsA channel has been used as a model of the rSK3 pore. UCL 1848 is shown in grey/white/blue. The blue residues of the UCL 1848 molecule represent the bisquinolinium amino groups. The mechanism of UCL 1848 binding to SK channels is not known. A peripheral region of UCL 1848 is likely to be located next to Val-529 as this study shows that a conservative point mutation of this residue reduces UCL 1848 sensitivity. Hence the UCL 1848 molecule has been located over one subunit just within the turret edge of the same subunit (residue 529), and covering the central pore. The orientation of the UCL 1848 molecule appears to optimally complement the pattern of interacting residues when orientated as shown. Channel subunits are coloured in green, red, yellow and blue, and important residues for the interaction with UCL 1848 are coloured in light brown (residues which strongly affect UCL 1848 binding (i.e. channels carrying a non-conservative mutation at this position are not sensitive to the blocker at a concentration equal to its $IC_{50}$ for the WT rSK3 channel))) and magenta (residue which weakly affects UCL 1848 binding (i.e. channels carrying a non-conservative mutation at this position are still sensitive to the blocker at a concentration equal to its $IC_{50}$ for the WT rSK3 channel)). Channel graphics were generated with Swiss pdb viewer/Povray.

# Chapter 6

# Non-functional point mutants of rSK3 channels

## 6.1 Aim

- To begin to understand SK channel heteromeric assembly using point mutants of the rSK3 channel.

## 6.2 Introduction

Change of function mutants are particularly useful in assessing possible heteromerization in cases where there is not much difference in the pharmacological properties of the subtypes. This situation certainly applies to the well-characterized SK channel blockers like apamin, and UCL compounds where the nanomolar to picomolar affinities make it difficult to detect intermediate components on the concentration-inhibition curve. Therefore, for the purposes of investigating the heteromerization potential of rSK3 subunits, putative dominant negative mutants were initially created since they would clearly eliminate most of the SK current in the case of heteromerization occurring.

### 6.2.1 Rationale for "dominant negative" mutants

Point mutants which, from comparison with KcsA, are assumed to form the turret and "floor" of the outer vestibule have been found to significantly affect the pharmacological profile in the previous chapters. Mutations made in the selectivity filter and pore helix regions would be expected to disrupt channel function rather than pharmacology since these regions do not directly contribute to the walls of the outer vestibule.

#### W538F–rSK3

The tryptophan at position 538 is conserved at an equivalent position in many potassium channels which suggests a degree of importance throughout evolution. Alignments that compare the rSK3 pore with the KcsA channel indicate its location is likely to be in the putative rSK3 pore helix region. A phenylalanine for tryptophan substitution at the equivalent point (434) in Shaker results in channels that do not conduct ions to an appreciable extent under physiological conditions, although the charge movements associated with the channel's voltage sensor (gating charge) remain intact (Perozo et al., 1993). This suggests that it does not cause a gross structural disruption of the channel. It thus seems like a good candidate for creating a non-conducting but otherwise functional SK channel.

#### H555N, G559A–rSK3

This mutation was made in error, whilst creating the H555N–rSK3 mutant. The glycine residue (559) of this mutant is again conserved in many potassium channels (a notable exception being hERG). This is a particularly conservative change to make but if the resulting channel is non-functional then one can assume that this amino acid must have an important structural role.

**G548R–rSK3**

This residue forms the first glycine in the selectivity filter of potassium channels. Previous work indicates that mutation of this residue to a serine results in a non-selective channel in Shaker (Heginbotham et al., 1994). As arginine is a comparatively larger amino acid, and positively charged, one might expect an even greater disruption of channel function.

## 6.3 Results

### 6.3.1 Functional characterization of the "dominant negative" mutants

Firstly, cells were transfected with these mutant constructs to see if channel function had been disrupted. Channels were expressed in CHO cells as there was the possibility that small mutant currents would be swamped by larger endogenous currents in HEK 293 cells. All the transfected CHO cells that were selected for analysis were representative (in size and shape) of the majority of other CHO cells that were plated down. As shown in Table 6.1 on page 218, expression of both W538F-rSK3 and G548R-rSK3 produced currents that were indistinguishable from the endogenous CHO cell conductance. In recordings that were made immediately (<20-30 seconds) after going whole-cell, a current of 4.2±2.6 pA (mean±SEM) was obtained at -40 mV from CHO cells transiently expressing W538F-rSK3 channels under voltage-clamp conditions (n=3 recordings), whilst 5.8±1.4 pA (mean±SEM) was obtained from CHO cells expressing G548R-rSK3 channels at the same potential (n=3 recordings). Endogenous CHO whole-cell currents that were recorded in a similar way (recorded immediately (<20-30 seconds) after going whole-cell at -40 mV) from untransfected CHO cells, amounted to 4.2 pA±1.1 pA (mean±SEM) at -40 mV with 1μM intracellular calcium (n=4 recordings, Figure 3.1 on page 107),

which is not significantly different from either mutant's whole-cell currents (P>0.05). However, the mean current produced at -40 mV immediately (<20-30 seconds) after going whole-cell from CHO cells that were transiently expressing WT rSK3 DNA (2.4±0.5 nA (mean±SEM), data summarized in Figure 6.1 on page 219, n=4 recordings), was significantly different (P<0.05) from these W538F-rSK3 and G548R-rSK3 average whole-cell currents when recorded at the same potential using identical intracellular solutions. The double mutant, H555N, G559A-rSK3, did show a picoampere $K^+$-selective conductance which appeared to rectify, when transiently expressed in CHO cells. In recordings made immediately (<20-30 seconds) after going whole-cell, a current of 164±45 pA (mean±SEM) was obtained at -40 mV (n=3 recordings), which was significantly different from both the CHO cell endogenous current recorded immediately after going whole-cell and from the transiently expressed WT rSK3 current recorded immediately after going whole-cell in CHO cells (P<0.05). Mutants W538F-rSK3 and G548R-rSK3 therefore were potential dominant negatives. H555N, G559A-rSK3 was not a dominant negative in the strictest sense. However, because the currents were relatively small, it may serve the same purpose by reducing significantly greater whole-cell currents so that co-assembly may be recognized.

### 6.3.2 The suitability of these non-functional mutants as dominant negatives

#### Co-expression experiments reveal that W538F–rSK3 and H555N, G559A–rSK3 are not dominant negatives

In order to test whether W538F–rSK3 behaves as a dominant negative when co-expressed with WT subunits, current sizes were compared between WT rSK3 transfected CHO cells, and CHO cells in which WT rSK3 and W538F–rSK3 had been co-transfected in a 1:1 ratio. CHO cells were chosen to express these channels be-

| Mutation | Chromatogram | Current trace |
|---|---|---|
| W538F-rSK3 | 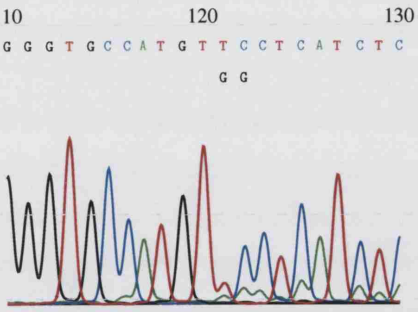  | 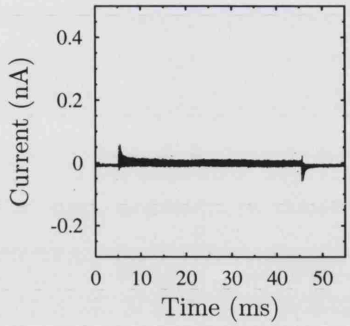  |
| H555N, G559A-rSK3 | 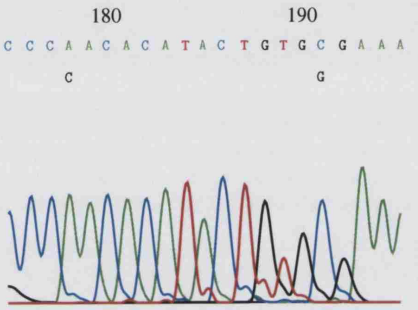  | 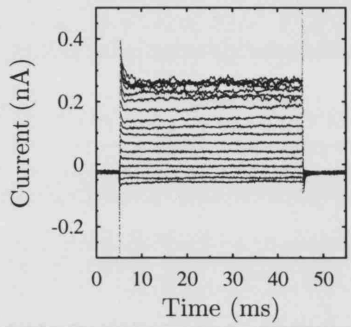  |
| G548R-rSK3 | 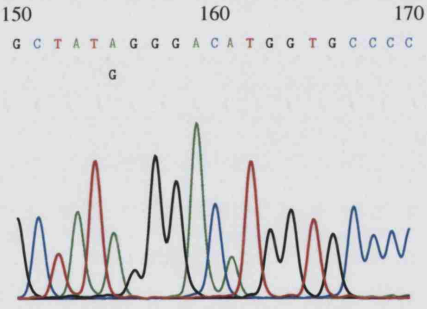  | 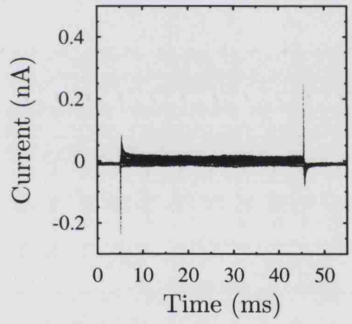  |

**Table 6.1:** Table showing sections of the sequencing chromatograms spanning the mutated bases of "dominant negative" mutants and the representative current traces produced after their cellular expression. Representative whole-cell current traces were generated immediately (<20-30 seconds) after going whole-cell from CHO cells that were transiently transfected with either W538F-rSK3 or H555N,G559A-rSK3 or G548R-rSK3. These cells were held at −80 mV, before being stepped to voltages between −100 mV and +40 mV (in 10 mV increments). After 40 ms at the appropriate voltage, the cells were returned to −80 mV. Only H555N,G559A-rSK3 exhibited a small SK current, which together with the other two mutant currents was significantly smaller than WT rSK3 ($P<0.05$). G548R-rSK3 and W538F-rSK3 did not express any SK current. The intracellular solutions all contained 1 mM Mg–ATP, 130 mM KCl, and 1 μM free calcium. A standard bath solution (5 mM $K^+$) was used for each cell. Bases below the main sequence in the chromatograms are the WT rSK3 bases at the equivalent positions to the mutated bases directly above them. Numbers above bases begin from the start of the read, and do not relate to the entire sequence for rSK3.

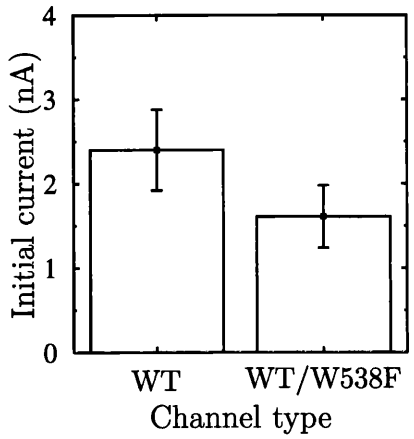


**Figure 6.1:** Bar graph showing the average current ("Initial current") present immediately (<20-30 seconds) after going whole-cell in CHO cells transiently transfected with WT rSK3 DNA (10 μg), or equal quantities of WT rSK3 DNA and W538F–rSK3 DNA (5 μg each). WT and W538F-rSK3 have been abbreviated to WT and W538F respectively. Cells were voltage-clamped and the whole-cell currents that were generated at -40 mV from four WT rSK3 transfected cells were averaged and plotted together with the standard errors in the bar chart. The average current recorded at -40 mV in these cells was 2.40±0.48 nA (mean±SEM). Four further cells that had been co-transfected with WT rSK3 and W538F-rSK3 were recorded and presented in a similar way. The average current recorded at -40 mV in these cells was 1.61±0.37 nA (mean±SEM). The intracellular solutions all contained 1 mM Mg–ATP, 130 mM KCl, and 1 μM free calcium. A standard bath solution (5 mM $K^+$) was used to bathe each cell.

cause of the small SK currents which may result from the incorporation of dominant negative subunits into channels composed of WT and mutant subunits. Figure 6.1 shows that significant SK currents (1.61±0.37 nA (at -40 mV)) could be seen in whole-cell recordings resulting from the co-expression of WT rSK3 and W538F-rSK3 subunits. This demonstrates that W538F–rSK3 is not a dominant negative.

The H555N-G559A-rSK3 mutant was also tested for its ability to function as a dominant negative. Co-expression of H555N, G559A–rSK3 with WT rSK3 in CHO cells (again using a 1:1 co-transfection ratio) revealed that a substantial current was present (Figure 6.2 on the next page). Like W538F–rSK3, the reduced $K^+$ conduction in H555N, G559A–rSK3 appears to be confined only to homomeric channels. G548R-rSK3 has been co-expressed with WT rSK3 by other members in the lab,

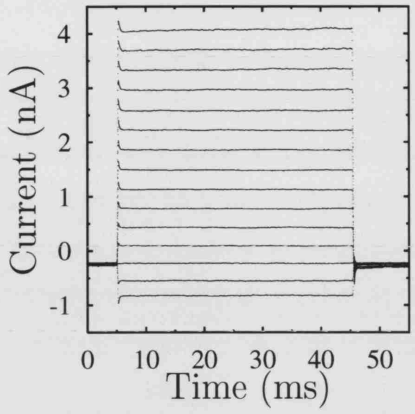


**Figure 6.2:** Current trace made immediately (<20-30 seconds) after going whole-cell showing a large SK current resulting from the transient co-transfection of 4 μg WT rSK3 DNA and 4 μg H555N, G559A–rSK3 DNA into a CHO cell. The cell was voltage-clamped and held at −80 mV, before being stepped to voltages between −100 mV and +40 mV (in 10 mV increments). After 40 ms at the appropriate step, the cell was returned to −80 mV. The average whole-cell current at -40 mV was 1.4 nA (n=2 recordings), suggesting that this mutant is not a dominant negative. The intracellular solutions all contained 1 mM Mg–ATP, 130 mM KCl, and 1 μM free calcium. A standard bath solution (5 mM $K^+$) was used for each cell recording.

but it was reported that the transfected cells appeared unhealthy. Such cells did not exhibit any currents, but it was uncertain whether this was because they were unhealthy or because this mutation was actually a dominant negative.

### Antibody staining of putative dominant negative constructs

In order to eliminate the possibility that SK protein of these constructs was not being expressed, these mutants were transiently transfected into HEK 293 cells and immunocytochemical staining was carried out (see Figures 6.3 to 6.6 on pages 222–225). Protein expression of H555N, G559A–rSK3 was also tested as, upon transfection, this double mutant produced small SK-like currents.

### Controls for anti-rSK3 staining of mutants

As an indicator of background antibody binding, negative controls were carried out that involved immunostaining of cells which had been transfected with 10 μg of GFP DNA only. Figure 6.3 on the following page shows that GFP was expressing in cells that have been transfected in this way. However, the lack of TRITC staining indicated that the rSK3 protein was not expressing endogenously in these HEK 293 cells. Positive controls were also performed which involved staining HEK 293 cells that had been co-transfected with 5 μg of GFP and 5 μg of WT rSK3 DNA. The right hand panel in Figure 6.3 on the next page shows the confocal images of these co-transfected cells. Some of those cells which have been stained for GFP also were expressing rSK3 protein.

### W538F–rSK3

Typically, W538F–rSK3 expression in CHO cells produced very little SK current (Table 6.1 on page 218) and co-expression with WT rSK3 produced whole-cell currents of the same order of magnitude as cells transfected with WT rSK3 only (Figure 6.1 on page 219). To eliminate the possibility that W538F-rSK3 was not expressing in these experiments, HEK 293 cells which had been co-transfected with 5 μg W538F-rSK3 and 5 μg GFP were stained for rSK3 protein with TRITC. Figure 6.4 on page 223 shows that many cells which expressed GFP also expressed W538F–rSK3 protein.

### G548R–rSK3

Like W538F–rSK3, these channels were non-functional (as homomers) and displayed virtually no SK current upon expression (Table 6.1 on page 218). Again, to determine whether rSK3 protein was expressing in this instance, HEK 293 cells which had been co-transfected with 5 μg G548R-rSK3 and 5 μg GFP were stained for rSK3

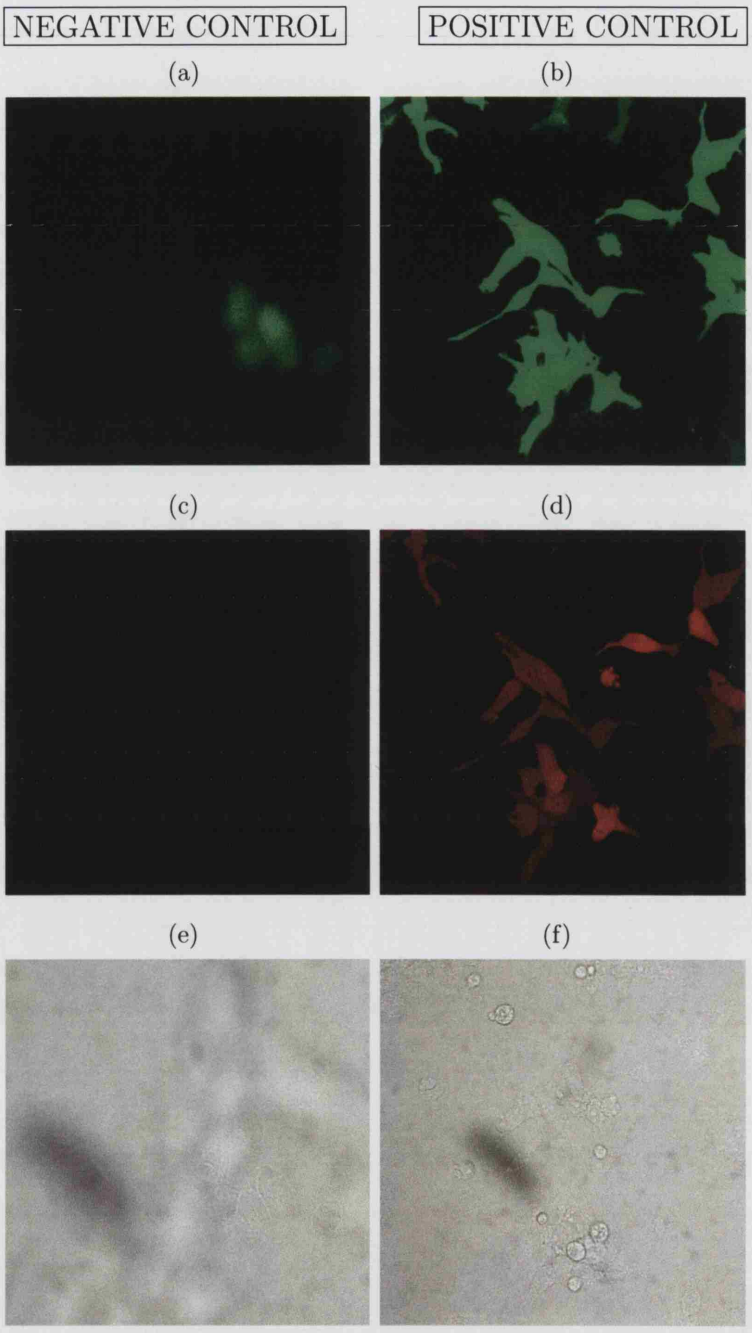


**Figure 6.3:** Positive and negative controls for antibody staining. HEK 293 cells were transiently transfected with 10 μg GFP DNA only (left) or 5 μg WT rSK3 DNA and 5 μg GFP DNA (right) *Top panel* shows the signal recorded from GFP with filter set to allow green light. *Middle panel* Filter set to allow red light through. This panel shows the antibody luminescence. Significantly more TRITC fluorescence was observed when WT rSK3 was transfected. *Lower panel* Brightfield images of the above.

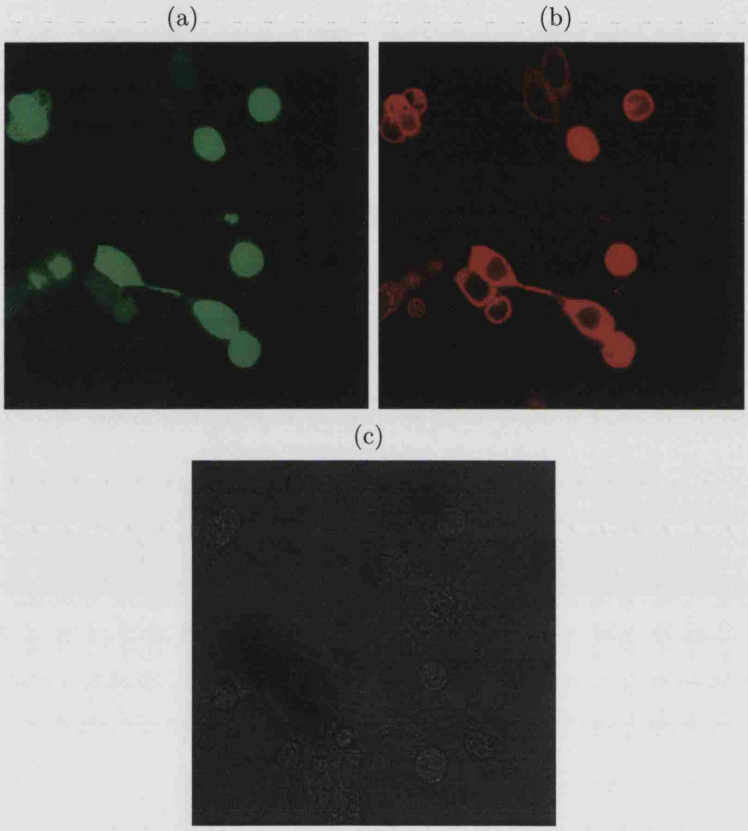


**Figure 6.4:** Images taken using different filter settings under the confocal microscope. Filters for viewing GFP(a), and TRITC (identifies cellular anti-rSK3 antibody binding) (b) in HEK 293 cells that have been transiently co-transfected with 5 µg GFP DNA and 5 µg W538F–rSK3 DNA. (c) Brightfield image of the same cells.

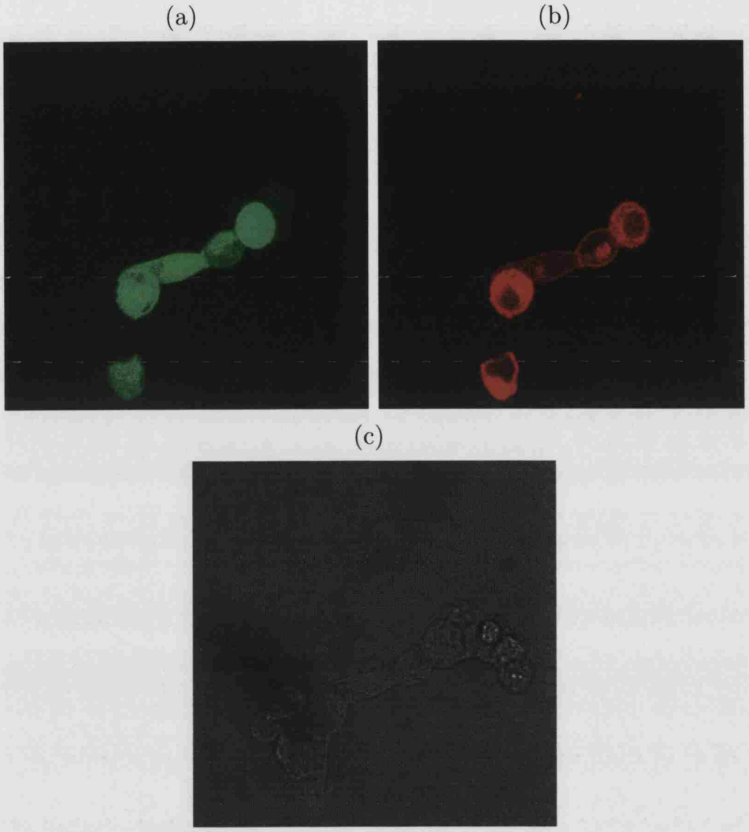


**Figure 6.5:** Images of the same field of cells with filters for viewing GFP fluorescence (a), and TRITC (identifies cellular anti-rSK3 antibody binding) (b), in HEK 293 cells that have been transiently co-transfected with 5 μg GFP DNA and 5 μg G548R–rSK3 DNA. (c) Brightfield image of the same cells.

protein with TRITC. Figure 6.5 shows that many cells which expressed GFP also expressed G548R–rSK3 protein.

### H555N, G559A–rSK3

In contrast to W538F–rSK3, this double mutant did conduct a small current that was clearly much smaller than WT currents. The current trace shown in Table 6.1 on page 218 is that of a potassium-selective current and this suggests the channel has assembled in the membrane. Mutant rSK3 protein expression was confirmed by co-transfecting HEK 293 cells with 5 μg H555N, G559A-rSK3 DNA and 5 μg GFP DNA, which were then stained for rSK3 protein with TRITC (Figure 6.6 on the following page).

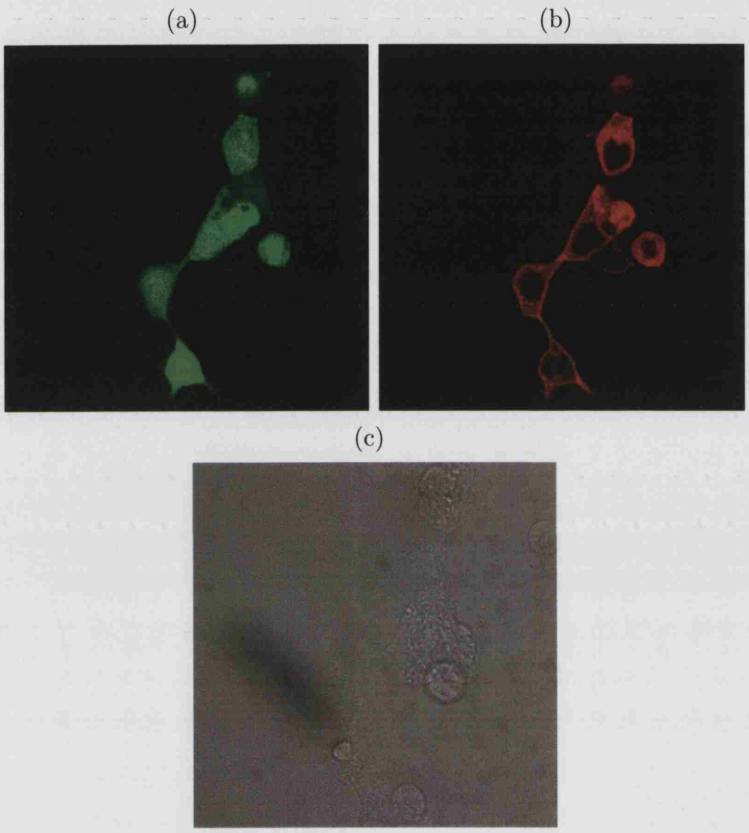


**Figure 6.6:** Confocal images from the same field of cells with filters for viewing GFP fluorescence (a), and TRITC (identifies cellular anti-rSK3 antibody binding) (b), in HEK 293 cells that have been transiently co-transfected with 5 μg GFP DNA and 5 μg H555N, G559A–rSK3 DNA. (c) Brightfield image of the same cells.

**Strategy for investigating SK subtype heteromerization**

The results clearly demonstrate that mutated SK subunit protein is expressing for each "dominant negative". However, the data in Figure 6.1 on page 219 and 6.2 on page 220 indicate that the W538F-rSK3 and H555N, G559A-rSK3 mutants cannot be used for the purposes of investigating heteromerization. Because of uncertainty surrounding the co-expression experiments with G548R-rSK3, the decision was taken to use a well-characterized mutant with altered pharmacology for the purposes of investigating heteromerization. V529K–rSK3 was used to evaluate subunit association because it is insensitive to UCL 1848, and the mechanism of its binding is now known, in part.

### 6.3.3 Co-expression of hSK1 subunits with rSK3 subunits

Since a single subunit of V529K-rSK3 is completely insensitive to UCL 1848 (up till 100 nM), one can expect that the UCL 1848 affinity of channels composed of WT hSK1 subunits and V529K-rSK3 subunits would be decreased relative to homomeric WT hSK1 channels. The $IC_{50}$ of UCL 1848 on the WT hSK1 channel is 1.1 nM (Hosseini et al., 2001). Figure 6.7 on page 228 shows representative traces demonstrating the effect of 1 nM UCL 1848 on channels resulting from the transient co-transfection of V529K-rSK3 and hSK1 DNAs into a HEK 293 cell (transiently co-transfected HEK 293 cells were used for this experiment rather than CHO cells, since the transiently-expressing SK currents generated in HEK 293 cells are more stable during the post-run down phase compared to other cell lines). A step protocol was applied to voltage-clamped whole-cells and 9.6±4.8% (mean±SEM) (n=3 recordings) block of the mean current at -40 mV was obtained (Figure 6.7 on page 228). The reduction in affinity suggests that heteromeric channels have formed upon co-expression of hSK1 and rSK3 subunits, but to show that heteromeric assemblies were functional, a substantial block of the current was required; heteromeric chan-

nels would be expected to be sensitive to UCL 1848 since it is known that only one WT SK subunit is required for its binding. Therefore, the effect of a 100 nM concentration of UCL 1848 on the co-expressed channel was investigated. This concentration of UCL 1848 was selected for two reasons. Firstly, it does not produce any block of homomeric V529K-rSK3 channels, and so any block produced at this concentration must be of either homomeric hSK1 channels or heteromeric assemblies of hSK1 and rSK3 subunits. Secondly, it might be expected to produce a substantial block of the whole-cell current (over 70%) based on previous co-expression studies using WT rSK3 and V529K-rSK3 subunits (Figure 5.16 on page 202). However, 100 nM UCL 1848 produced 26.5±4.4% (mean±SEM) block of co-expressed channels (n=3 recordings) (Figure 6.8 on page 229). A further test concentration at a higher dose (1 μM UCL 1848) did not produce much more block. 1000 nM UCL 1848 produced 32.6% (n=2 recordings) block of whole-cell currents from co-transfected cells (Figure 6.9 on page 230), suggesting that block of the co-expressed channels may have "plateaued out" at concentrations higher than 100 nM UCL 1848. This result was unexpected as it suggests a substantial component of the whole-cell currents from channels produced by a 1:1 co-transfection of V529K-rSK3 and hSK1 DNAs, is insensitive to UCL 1848 up till 1 μM.

## 6.4 Discussion

Due to substitution of the highly conserved amino acids in the non-functional mutants, it might be expected that conservative changes to one subunit may result in functionally impaired or "dominant negative" channels. However, it appears that W538F–rSK3 is not a dominant negative (Figure 6.1 on page 219). Co-expression of H555N, G559A–rSK3 and WT rSK3 shows that this mutant is not a dominant negative either (Figure 6.2 on page 220). The subunits of these mutants were being expressed in both these cases, as was shown by the TRITC fluorophore silhouettes

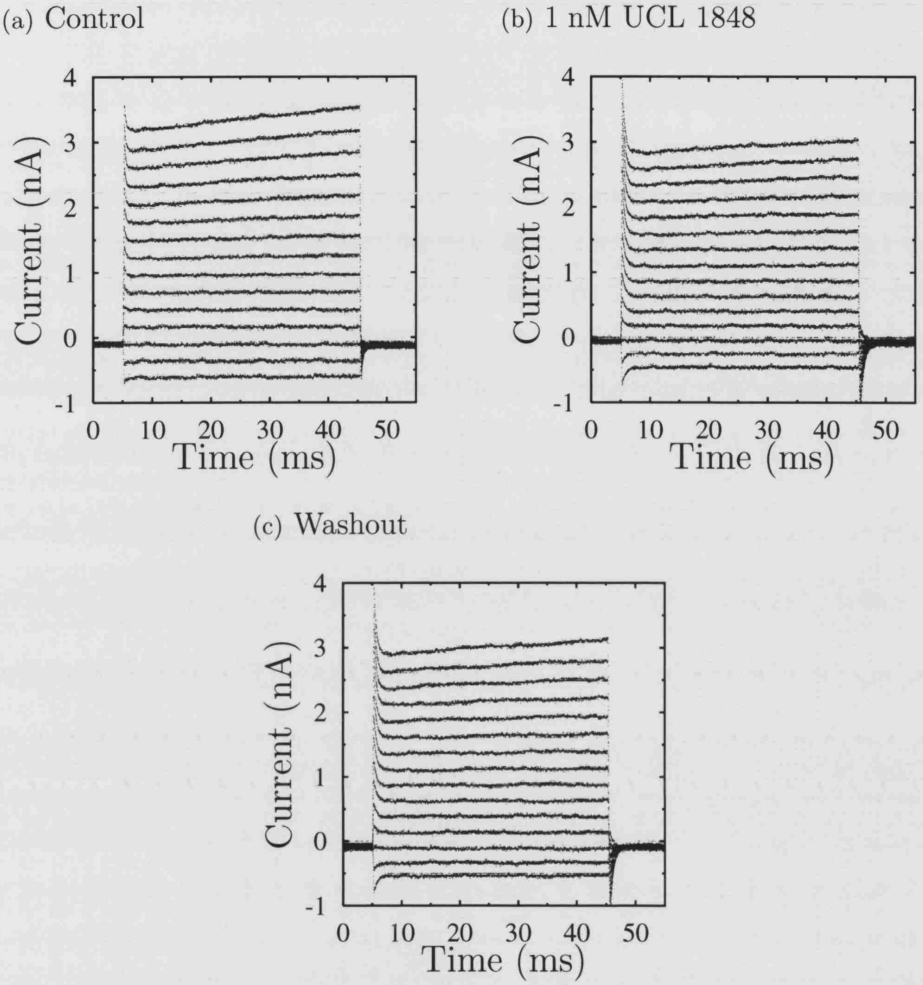


**Figure 6.7:** Effect of UCL 1848 on heteromeric channels resulting from a 1:1 co-transfection of WT hSK1 DNA and V529K–rSK3 DNA, using a drug concentration (1 nM) that would produce ≈50% block of WT hSK1 currents (Shah & Haylett, 2000). Whole-cell currents from a HEK 293 cell which had been transiently co-transfected, are shown. In each trace, the transmembrane potential of the cell was held at −80 mV, before being stepped to voltages between −100 mV and +40 mV (in 10 mV increments). After 40 ms at the appropriate step, the potential was returned to −80 mV. Using this voltage-clamp protocol, the cell was perfused with standard bath solution (a), standard bath solution supplemented with 1 nM UCL 1848 (b), and again perfused with standard bath solution (c). In three such recordings, 9.6±4.8% (mean±SEM) block was produced by 1 nM UCL 1848 at a step potential of -40 mV. The intracellular solutions all contained 1 mM Mg–ATP, 130 mM KCl, and 1 μM free calcium. A standard bath solution (5 mM $K^+$) was used for each recording.

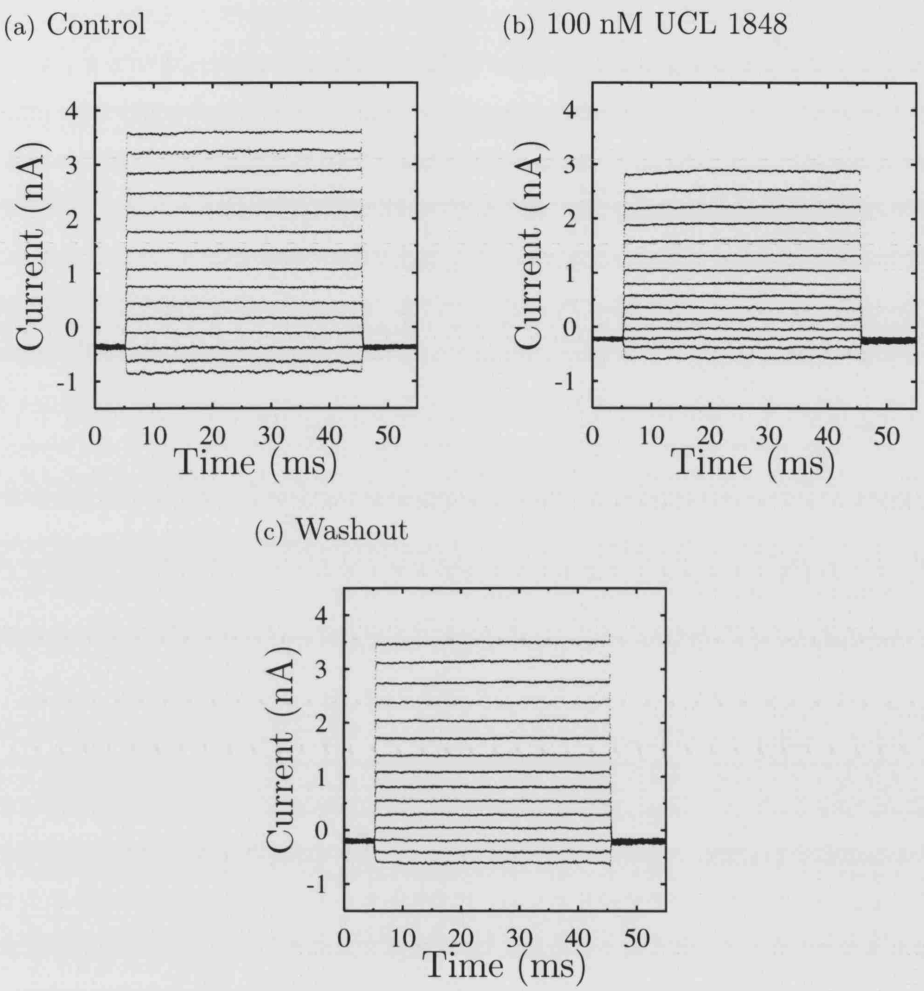


**Figure 6.8:** Three representative whole-cell traces showing the effect of 100 nM UCL 1848 on a HEK 293 cell which has been transiently co-transfected with V529K-rSK3 DNA and WT hSK1 DNA in a 1:1 ratio. In each trace, the transmembrane potential of the cell was held at −80 mV, before being stepped to voltages between −100 mV and +40 mV (in 10 mV increments). After 40 ms at the appropriate step, the potential was returned to −80 mV. Using this voltage-clamp protocol, the cell was perfused with standard bath solution (a), standard bath solution supplemented with 100 nM UCL 1848 (b), and again perfused with standard bath solution (washout) (c). In three such recordings, 26.5±4.4% (mean±SEM) block was seen at a step potential of -40 mV. The intracellular solutions all contained 1 mM Mg–ATP, 130 mM KCl, and 1 μM free calcium. A standard bath solution (5 mM $K^+$) was used for each cell.

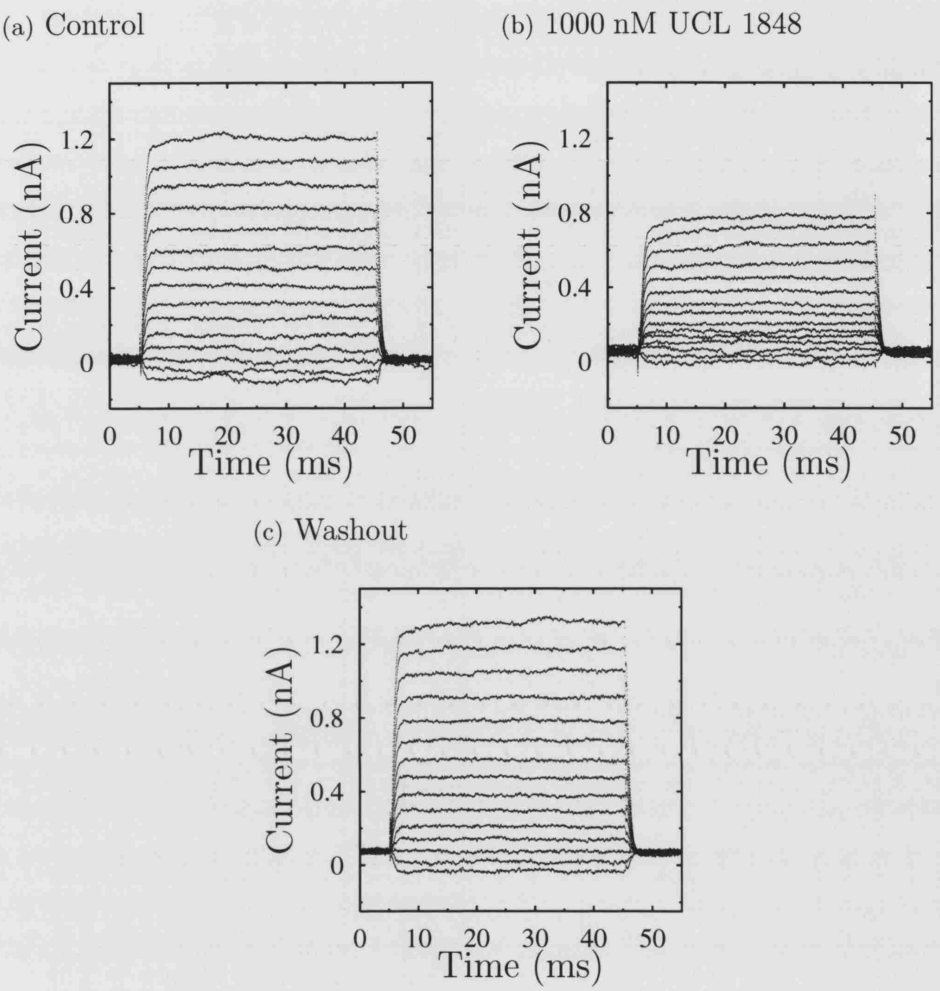


**Figure 6.9:** Three representative whole-cell traces showing the effect of 1000 nM UCL 1848 on a HEK 293 cell which has been transiently co-transfected with V529K-rSK3 DNA and WT hSK1 DNA in a 1:1 ratio. In each trace, the transmembrane potential of the cell was held at −80 mV, before being stepped to voltages between −100 mV and +40 mV (in 10 mV increments). After 40 ms at the appropriate step, the potential was returned to −80 mV. Using this voltage-clamp protocol, the cell was perfused with standard bath solution (a), standard bath solution supplemented with 1000 nM UCL 1848 (b), and again perfused with standard bath solution (washout) (c). In two such recordings, 32.6% block was seen at a step potential of -40 mV. The intracellular solutions all contained 1 mM Mg–ATP, 130 mM KCl, and 1 μM free calcium. A standard bath solution (5 mM $K^+$) was used for each cell.

on transfected cells. Furthermore, the production of functional H555N, G559A–rSK3 channels suggests that subunit assembly is not affected in this mutant. The following section considers possible causes for the loss of function in fully-assembled channels bearing these point mutations.

### 6.4.1 The dysfunctional homomers

**Possible mechanisms for the loss SK function as a result of a phenylalanine for tryptophan substitution at residue 538 in rSK3**

**1) C-type inactivation** Yang et al. (1997) have investigated the properties of W434F–Shaker (residue 434 in Shaker is equivalent to residue 538 in rSK3 (see alignment in Figure 1.8 on page 66)) by creating tetramer constructs, joined through inert linker regions, with either one or two mutant subunits. A number of their observations may be relevant to the W538F-rSK3 mutant and will briefly be described. ShΔ (a Shaker channel mutant lacking the $NH_2$-terminal "inactivation" particle) current decays over the course of several seconds (Hoshi et al., 1991). This inactivation cannot therefore be N-type. Extracellular $K^+$ ions are known to alter the rate of C-type inactivation as well as the magnitude of peak currents (Lopez-Barneo et al., 1993; Pardo et al., 1992; Heginbotham et al., 1994) although both remained unaffected in ShΔ in response to a change in extracellular ion concentration (Yang et al., 1997). In contrast, when W434F subunits were introduced into tetramers containing ShΔ subunits, current decay was reduced by increasing extracellular $K^+$ (Yang et al., 1997). This suggests that the phenylalanine substitution at the corresponding position in rSK3 could induce C-type inactivation i.e it may stabilize a closed state of the channel.

**2) Loss of "restoring" forces on the selectivity filter** The signature sequence of most $K^+$ channels is a highly conserved GYG motif involved in ion selectivity (Slesinger et al., 1996; Navarro et al., 1996; Heginbotham et al., 1994).

Splitt et al. (2000) have found that Y78A (the tyrosine in the signature sequence, GYG) halts tetrameric assembly while Y78F leads to tetramers of reduced stability in KcsA. Although the side groups of Y78 are not pointing inwards to the pore, they do interact with W67 (equivalent to W538F–rSK3) and W68 through hydrogen bonds and Van der Waal's contacts, forming a cuff of aromatic amino acids that behave as "molecular springs" (Doyle et al., 1998). This structure provides restoring forces to the selectivity filter (Figure 6.10 on the next page). Substitution of Y78 for another aromatic side group may maintain the aromatic cuff, albeit at reduced affinity. A loss of function in W538F–rSK3 may therefore be due to a loss in the efficacy of the molecular springs, similar to the effect described with Y78F-KcsA above.

**3) Loss of an open-state stabilizing binding site** Recent experiments in Shaker channels demonstrate that the network of amino acids forming the stabilizing molecular springs may not be a permanent part of this channel (Avdonin & Hoshi, 2001). Application of free form indole, intended to mimic the indole side group of tryptophan, slowed voltage-dependent activation in a concentration-dependent manner. This was believed to be due to competition for a steric tryptophan binding site that stabilized the channel, the molecular springs, and ultimately the selectivity filter. However, the binding site must be evacuated at negative potentials in order for competition to occur upon activation; hence the suggestion of a dynamic structural rearrangement of the channel upon activation. The same process may be occurring in WT rSK3 when the channel activates through exposure to intracellular calcium. The phenylalanine at position 538 in W538F–rSK3 may not be able to bind to the tryptophan binding site resulting in a dysfunctional molecular spring and a collapsed or unstable selectivity filter.

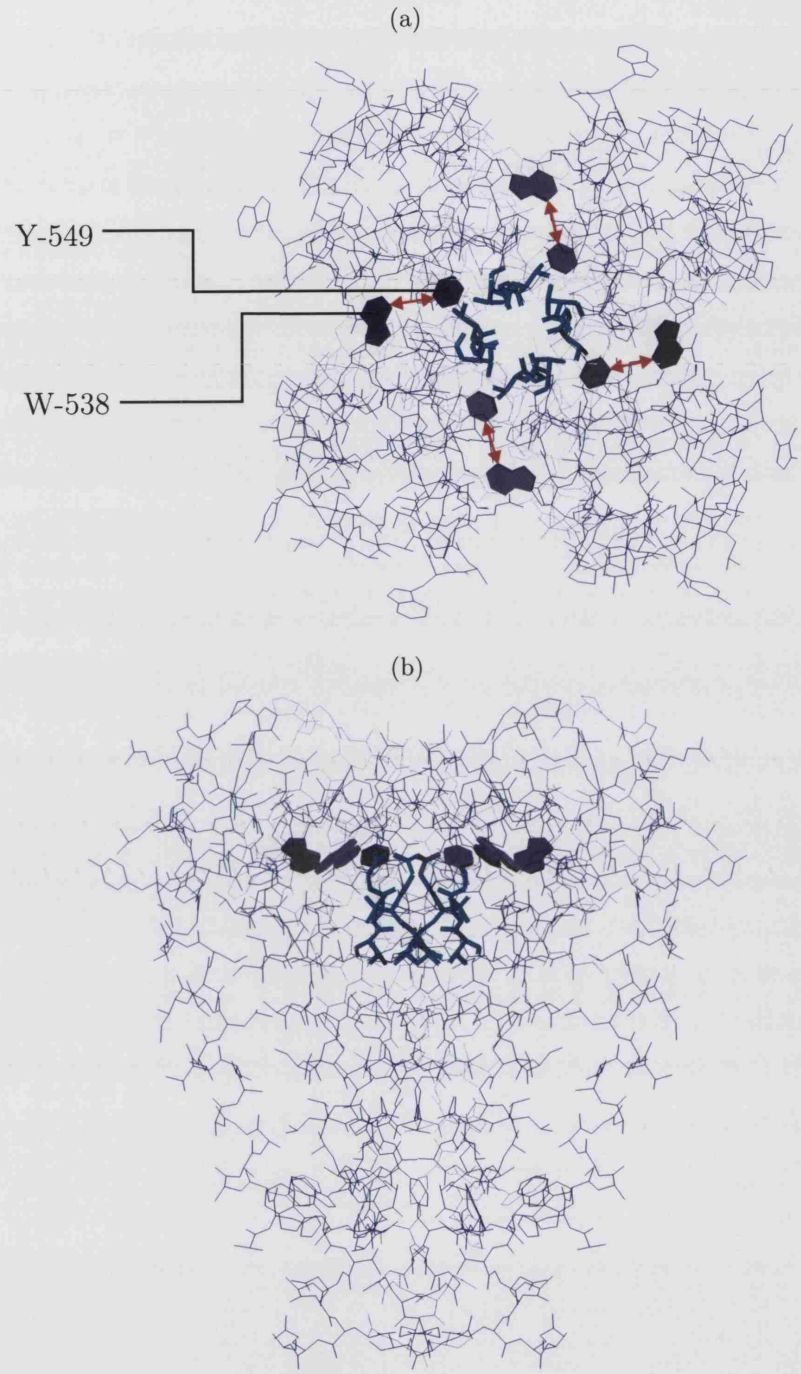


**Figure 6.10:** Wireframe diagrams depicting the hypothetical interaction between trytophan-538 (W-538) and tyrosine-549 (Y-549) in a model of the rSK3 pore based on the crystal structure of the KcsA. This interaction serves to hold the selectivity filter open. Arrowheaded line (red) indicates an attractive force (hydrogen bonds and van der Waals interactions) between the two aromatic groups of each residue. (a) is a view of the channel pore from above and (b) is a side view. The selectivity filter region (residues 547 and 548) is shown in thick, blue wireframe. Aromatic groups of residues 549 and 538 are shaded. Pictures were in Swiss pdb viewer/Povray.

### Loss of tetramerization may account for the lack of SK current expression resulting from the glycine for arginine substitution at residue 548 in rSK3

Point mutations of sites equivalent to residue 548 in the rSK3 channel have previously been made in both KcsA (residue 77) and Shaker (residue 444) channels (see Figure 1.8 on page 66 for the numbering system used). G444A–Shaker resulted in a functional but non-selective channel (Heginbotham et al., 1994). Gating current analysis of an anionically-substituted point mutant, G444E–Shaker, shows that no gating currents are present upon expression of the subunits. G77A-KcsA assembles as a non-functional tetramer and it has been suggested that the ion permeation pathway is blocked by the slightly more bulky alanine (Splitt et al., 2000). Furthermore, the non-conservative change, G77E-KcsA, leads to loss of tetramerization (Splitt et al., 2000). As the selectivity filter region of $K^+$ channels is a conserved signature sequence, G548R–rSK3 may also lose the ability to tetramerize. However, it would seem unlikely that the ion conduction pathway is disrupted by the presence of the positive charge on arginine, since its cationic side group would be predicted to point away from the selectivity filter, based on the crystal structure of KcsA. It is possible that the arginine residues at position 548 of neighbouring subunits get impinged upon by each other in the mutant channel, which could lead to a loss of quaternary structure.

### A possible molecular basis for the reduced $K^+$ conduction in the H555N, G559A–rSK3 channel

**Disruption of the selectivity filter** The SCAM-based chemo-mechanical model of SK channel gating (Figure 1.6 on page 44) predicts the transmission of mechanical energy from the open-state C-terminal CaMBD dimers, to the selectivity filter. The force transmitted should be perfectly honed to open the selectivity filter to the diameter required in order to perfectly coordinate a $K^+$ ion. Altering the degree

to which the selectivity filter is opened would result in a loss of $K^+$ conduction, as $K^+$ coordination is lost. The open-state selectivity filter diameter is likely to be dependent on the closed-state selectivity filter diameter, since the mechanical force generated by dimerization of the CaMBDs, upon opening of the rSK3 channel, is probably of constant value in order to open the selectivity filter to the correct diameter each time. Therefore if the closed selectivity filter diameter is not appropriate, the open selectivity filter diameter will not be either. The alanine substitution in the H555N, G559A-rSK3 channel may be causing a displacement of the external vestibule floor region, which might increase the closed diameter of the selectivity filter slightly, compared to the WT channel. This displacement would arise because residue 559 is buried below and in close apposition with external vestibule floor residues (e.g. T556-rSK3) that link to the selectivity filter (Figure 6.11 on the following page). A subsequent "tug" on the selectivity filter, as a result of dimer formation at the C-termini CaMBDs following calcium binding, may now expand the selectivity filter diameter too much for perfect $K^+$ coordination. It is possible that some but not all the four $K^+$ binding sites in the selectivity filter are lost as a result of the change in dimensions, since some SK current was found to be generated when H555N, G559A-rSK3 channels were expressed in CHO cells (Table 6.1 on page 218). A reduction in current would be expected from the loss of $K^+$ ion binding sites, since high $K^+$ ion flux is partly a result of repulsion between ions at binding sites in the multi-ion pore of the selectivity filter of $K^+$ channels (Doyle et al., 1998). It is possible, for example, that the first three extracellular coordination sites are lost as a result of the "tug" on the selectivity filter. This would leave one $K^+$ binding site at the intracellular side of the selectivity filter that would conduct ions at a much slower rate due to the loss of repulsion between $K^+$ ions in the pore. In fact, the intracellular side of the selectivity filter is probably intact since H555N, G559A-rSK3 channels appear to rectify, which would be consistent with the "unmasking" of $Mg^{2+}$-based inward rectification when small currents are expressed, as

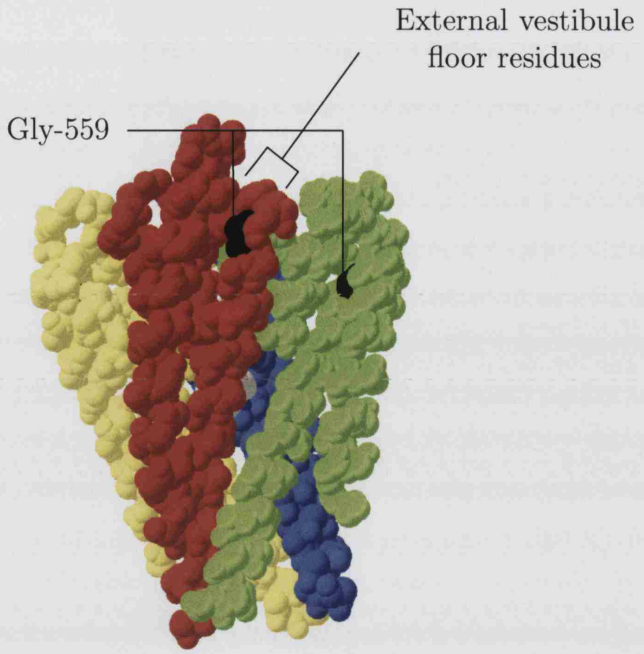


**Figure 6.11:** Spacefill diagram showing the location of G559-rSK3 (Gly-559) on a homology model of the rSK3 pore based on the crystal structure of KcsA. This glycine residue is in close contact with several residues of the external vestibule floor which form a chain of amino acids that link the inner helix with the selectivity filter. Picture generated in Swiss pdb/Povray.

seen in inside-out patches earlier in this study. This corroborates with the theory that the high currents, and therefore high series resistances, at positive pipette potentials in whole-cell recordings from WT rSK3 channels, "mask" the rectification of rSK3 currents as seen in patches due to the transmembrane voltages not being positive enough to observe this rectification. Removal of intracellular $Mg^{2+}$ ions and a re-examination of the whole-cell currents from H555N, G559A-rSK3 channels would establish that the source of the observed whole-cell rectification from this channel is $Mg^{2+}$-based.

### 6.4.2 The importance of the properties of residue 559 for normal SK channel function - Possible implications for structural diversity of $K^+$ channels

The exceptional degree of conservation of this glycine residue (G559-rSK3) amongst other $K^+$ channels, suggests that proper functionality of these $K^+$ channels is dependent on the presence of a glycine amino acid at this position. The effect of mutation of this residue on normal SK channel function bears out this hypothesis, as shown in this study. Since hERG channels contain a much larger aspartic acid residue at the equivalent position (position 637 of hERG, accession number; U04270), hence forming one of the few $K^+$ channel families that do not contain a glycine residue at this position, they may have a radically different structure to those $K^+$ channels in which glycine is conserved at this position. In evolutionary terms, it would be logical to assume an early divergence between hERG channels and the majority of other $K^+$ channels in which this residue is conserved, if the architecture of the hERG channel is radically different to the majority of other $K^+$ channels. Alignment of the rSK3 pore sequence with the corresponding region of hERG suggests further structural differences, in addition to the aforementioned one; the hERG counterparts to M537–rSK3 (Y67-KcsA), W538–rSK3 (Y68-KcsA), and Y549–rSK3 (Y78-KcsA) are a tyrosine, phenylalanine, and a phenylalanine respectively. In hERG, no hydrogen bonds are possible between these aromatic amino acids which suggests "molecular springs" are probably not present or are relatively weak in this channel. Furthermore, cysteine point mutagenesis studies of hERG channels have shown that it is likely its pore entryway is narrower than that of Shaker (Fan et al., 1999). These evidences suggest that hERG channels have a pore architecture distinct from other $K^+$ channels. One further difference between hERG and other $K^+$ channels, including SK channels, is that the rectification is not of the same ilk as rSK3 or inward rectifiers since it is intrinsically generated, possibly through C-type inactivation (Smith et al., 1996).

### 6.4.3 Heteromerization amongst SK channels

The surprising result from this study was the presence of a substantial unblockable component of the whole-cell current produced from cells co-transfected with WT hSK1 and V529K-rSK3 DNAs. One would expect that, following a slight block of homomeric hSK1 channels by 1 nM UCL 1848, a much higher concentration of UCL 1848 applied to the co-expressed channels would block heteromeric channels made up of WT hSK1 and V529K-rSK3 subunits. Clearly, this did not happen when WT hSK1 was co-transfected with V529K-rSK3, since only a further 16.9% current block was observed at 100 nM compared with 1 nM UCL 1848. Furthermore, block of the co-expressed channels by UCL 1848 appeared to plateau by 100 nM. The presence of a large unblockable component at 100 nM UCL 1848 cannot be due to homomeric WT hSK1 channels as these would be completely blocked at this dose. Likewise, the unblockable component seems unlikely to be heteromeric assemblies since channels comprising of WT hSK1 and V529K-rSK3 subunits might be expected to be blocked by UCL 1848 in a similar manner to heteromers of WT rSK3 and V529K-rSK3 (both WT hSK1 and WT rSK3 have similar $IC_{50}$ values (Hosseini et al., 2001)), as seen before (Figure 5.16 on page 202)). This leaves V529K-rSK3 channels to account for over 70% of the whole-cell current. Over-expression of the V529K-rSK3 subunit might account for this unblocked current.

Further experiments performed in this lab have provided an answer to the question of why over-expression of one subtype might be occurring. Heteromeric channels consisting of hSK1 and rSK3 subunits may not be reaching the membrane surface, and instead may be getting trapped intracellularly (Monaghan et al., 2004). If this occurs, the dose-response relationship of the co-expressed channels will be a composite of the homomeric ones, as these would only express in such a situation. Accordingly, following the application of 100 nM UCL 1848 to the co-expressed channels, the unblockable component must be V529K-rSK3 homomers (not blocked

by 100 nM UCL 1848 (Figure 5.10 on page 191)), and the blocked component must be homomeric hSK1 channels. In this case, the block at 1 nM would be expected to be entirely of homomeric hSK1 channels, and would be predicted to be approximately half the maximal current block at the plateau region (i.e. at 100 nM); $\frac{26}{2} \approx$ 13% block, which is not much different to what was observed.

The ability of SK subunits to form heteromers would allow considerably more structural and functional channel diversity. Fanger et al. (2001) demonstrated that SK2 could not assemble with SK4. This may be expected since SK4 is considerably more diverse sequentially from the other SK channels and is sometimes considered to be an intermediate conductance channel. According to Ishii et al. (1997), SK1 and SK2 channels are capable of heteromerizing. M. Miller et al. (2001) have shown that SK3 dominant negatives can combine with endogenous SK2 channels in human Jurkat cells, and Monaghan et al. (2004) have confirmed that clonal rSK3 and rSK2 channels can heteromerize in heterologous expression systems. The results from this lab now suggest that although SK1 and SK3 may form heteromeric channels, these assemblies are probably getting trapped intracellularly (Monaghan et al., 2004), adding to the complexity of SK channel function in tissues where these subtypes may be co-expressed.

# Chapter 7

# Summary and future directions

Solving the crystal structure of the KcsA channel (Doyle et al., 1998) was arguably the most significant advance in the potassium channel field in recent times, for two reasons. Firstly, it gave an insight into the mechanisms involved in potassium ion conduction and selectivity, and secondly it suggested that there is a high degree of structural similarity between the different classes of potassium channels. Various structures, that were hypothesized based on indirect evidence from functional studies in eukaryotic potassium channels were also found in the crystal structure of the KcsA channel. For example, thermodynamic mutant cycle analyses applied between Shaker and AGXN, indicated that the Shaker channel vestibule was a "shallow cone" (Ranganathan et al., 1996) and a similar outer vestibule structure was observed later in the crystal structure of the KcsA channel (Doyle et al., 1998). There are numerous other examples of such indirectly generated channel configurations (MacKinnon & Miller, 1989; MacKinnon, 1991), which suggest a common gross structure between the pore regions of many known potassium channels. The structural similarities that are thought to exist between the pore regions of different eukaryotic and prokaryotic potassium channels suggest that archaic potassium channels developed from early on in evolution giving rise to the vast numbers of different channels that have been cloned. Certain mutations, which probably were favoured through natural selection,

might have given rise to the different types of potassium channels, some of which have been cloned in recent years. Amino acid differences between the majority of potassium channels and hERG channels, such as in the signature sequence and the extremely conserved glycine residue usually found just after the selectivity filter (position 559 in rSK3 and position 88 in KcsA), suggest that hERG channels may have a radically different structure, possibly with a distinct evolution. On the other hand, the SK channel pore contains many of the conserved residues found in other potassium channel pores, suggesting that a common underlying architecture may be shared between such structures.

The empirical evidence, based on the mutational studies presented in this thesis, favours the view that the SK, KcsA and Shaker channel pores share a similar overall architecture. The most notable of this evidence included the successful prediction of pore mutations that endow TEA and CTX sensitivities on the rSK3 channel, and the discovery that the very conserved glycine residue towards the carboxy end of the pore (residue 559 in rSK3) is essential for normal channel functioning. Knowledge of such architectural similarities is useful since they can be used in the design of novel, more selective blockers. For example, CTX has previously been mutated to distinguish between IK and $K_v$ channels of T-lymphocytes (Rauer et al., 2000). CTX analogs targeting the negatively charged residues of the putative turret in $K_v$ channels were created by substituting negatively charged residues into the peptidyl inhibitor, thus creating a compound which was several fold more potent on IK channels. Once the mechanisms for binding of SK channel blockers are better known, similar rationale may be applied to improve the potency of drug binding, having established structural commonality with the known crystal structure of the KcsA channel in this study.

The mechanisms of inhibition for three of these SK channel blockers, UCL 1848, UCL 1684 and UCL 1530 were partially elucidated in this study using point mutants containing non-conservative single amino acid substitutions that were designed to maximally disrupt blocker binding. From the effects of such point mutations on

blocker affinities, "maps" of the important binding site residues were generated at the molecular level (Figure 5.19 on page 211 and 5.20 on page 212). It was interesting to note that the G535D-rSK3 mutant channel was several fold less sensitive to all the UCL compounds tested on it, since the WT SK4 channel, which also has an aspartic acid residue at the equivalent position (residue 240 of WT SK4 as shown in Figure 1.8 on page 66), is insensitive to UCL 1848, UCL 1530 and UCL 1684 (personal communication with Dr Benton and Malik-Hall et al. (2000)). This raises the possibility that a D240G-SK4 mutant channel may show UCL compound sensitivity, since the presence of a glycine amino acid at the equivalent position in the rSK3 channel (position 535) appeared to be an important determinant of its UCL compound sensitivity (Figure 5.2 on page 180 and 5.3 on page 181 and 5.5 on page 183); the D240G-SK4 point mutant would be expected to lose CTX sensitivity but to gain UCL compound sensitivity. It would also be interesting to determine whether UCL compound binding is entirely a pore phenomenon or if there is a contribution from residues outside the pore. For example, it has recently been shown using chimeric channels, that apamin binding to SK1 is not solely determined by pore residues (D'hoedt et al., 2004). A chimeric channel in which the core region of rSK1 (S1-S6) has been substituted for the analogous region of hSK1, could be used to examine whether the binding of UCL 1848 is determined by residues outside of the pore, by comparing the $IC_{50}$ of its block on this chimer with that of WT hSK1. If these affinities differ, then UCL 1848 binding is not exclusively a pore phenomenon since the pore sequences of both these channels would be exactly the same. The V519A,H555N-rSK3 mutant which has been created in this study could also be used for the same purpose, as it has a P-loop sequence which exactly resembles that of the rSK2 channel. Further work to determine the mechanism of binding of UCL 1848 to the SK pore would facilitate a more accurate structural representation of this interaction and would give a rough indication of the size of the SK channel outer vestibule. Knowledge of the approximate outer vestibule dimensions would be

useful for the synthesis of more potent drugs, and a method of its measurement is described next.

A quantitative estimate of the outer vestibule dimensions of SK channels could be carried out by examining pH-dependency of TEA block in the outer vestibule, similar to the way that TEA has been used in the past for this purpose (Bretschneider et al., 1999). The algorithm involved uses the Gouy-Chapman equation and assumes that a pH-dependent histidine repels the blocker when protonated (for calculation see Bretschneider et al. (1999)). H555-rSK3 may fulfill this role so long as the other rSK3 pore histidine (residue 524) does not affect TEA affinity in a pH-dependent manner. It is unlikely that it will since it is located at the edge of the pore, but mutations of this residue (H524K-rSK3 and H524N-rSK3 (positive and uncharged controls, respectively) could determine its contribution to TEA affinity (alternatively, a P554H-rSK3 mutant should be able to repel TEA in a pH-dependent manner, if H555-rSK3 is ineffective).

Residue 555 warrants further study on the basis that it has been found to be an important binding site for UCL 1848 in this study, and it might also be responsible for differential UCL 1848 affinity on the SK channel subtypes as it is one of three pore residues that differ between SK1, SK2, and SK3. Therefore, it is important to thoroughly understand its contribution to UCL 1848 binding. By decreasing the pH of the extracellular solution, in order to increase protonation of residue 555 in WT rSK3, it should be possible to decrease the UCL 1848 affinity for the WT rSK3 channel, if the loss in affinity for the H555K-rSK3 mutant channel is caused by the presence of a positive charge. This would indicate whether the reduction in UCL 1848 affinity for the H555K-rSK3 channel could be occurring due to an electrostatic repulsive force between the mutant channel and blocker (both are positively charged), or possibly due to the presence of the more bulky lysine group hindering UCL 1848 binding. The results from this study do not shed any light as to the mechanism by which the lysine substitution eliminates UCL 1848

sensitivity in the H555K-rSK3 channel. Determining the contribution by which the polarity of this residue affects UCL 1848 binding would be useful to know since an electrostatic effect may account for the greater sensitivity of WT rSK2 channels for UCL 1848. WT rSK2 channels have a neutral asparagine residue at position 555, but spontaneous degradation of some asparagine-containing peptides (via succinimide intermediates) has been observed with the production of negatively charged species (Stephenson & Clarke, 1989). If the positive charge of UCL 1848 is able to interact with a charge at residue 555, then this would facilitate a more accurate, empirically-based representation of UCL 1848 binding to SK channels. The effect of the H555N-rSK3 point mutation on UCL 1848 affinity can be tested using the H555N-rSK3 mutant produced in this study and would be expected to show an increased sensitivity compared to the WT rSK3 channel.

SK channels contain several charged residues, some of which have been proposed to be important sites for differential apamin sensitivity amongst SK channel subtypes (Ishii et al., 1997). One of these is H555-rSK3, which has just been discussed. However, the mutagenesis study carried out here demonstrates that the sensitivities of UCL 1848, a drug with similar affinities for the SK subtypes as apamin (Hosseini et al., 2001), to various point mutants of the rSK3 channel, does not reflect all these apamin binding sites, though clearly the UCL compounds tested here bind in the pore of the rSK3 channel. In particular, D528-rSK3, proposed to be an important residue of the apamin binding site, does not interact with UCL 1848 significantly. By aligning the pore residues of the various SK subtypes (Figure 1.8 on page 66), it can be demonstrated that there are only three other pore residues which could account for differential UCL 1848 blockade between the SK subtypes. Amongst the rSK3 pore amino acids, it is possible that valine (V) at position 519, glutamine (Q) at position 526, and histidine (H) at position 555 all contribute to the differential sensitivity. Mutations of these amino acids have been successfully made (Table 5.3 on page 206) and prepped so that their effects, if any, on UCL 1848 binding can be

evaluated. Based on the positions of these residues in the P-loop, it is not very likely that residue 519 contributes significantly to this blocker's affinity, as it is located at the edge of this amino acid sequence. The only remaining pore residue which could account for differential UCL 1848 affinities among the SK subtypes is Q526-rSK3. The presence of a lysine in the WT hSK1 channel at the residue equivalent to 526-rSK3 may partially account for the differential UCL 1848 affinities between SK subtypes, as is the case for apamin (Ishii et al., 1997), and a mutant channel (Q526K-rSK3) has been generated and purified, which could be used to test this hypothesis.

Although the SK1, SK2 and SK3 subtypes have been shown to co-assemble *in vitro* (M. Miller et al., 2001; Ishii et al., 1997; Monaghan et al., 2004), their abilities to heteromerize with each other have not been demonstrated *in vivo*. The current evidence suggests that heteromerization between the SK subtypes does not occur extensively in the CNS (Sailer et al., 2002). However, in the cells of tissues where SK channel heteromerization does occur, slight alterations in the electrical responses of cells, caused by such associations, could provide additional functional diversity. It might be possible to utilize the fact that co-expression of SK1 and SK3 causes internalization of heteromers, to investigate whether SK1 channels underlie the $sI_{AHP}$ in certain cells. Although SK1 has been shown to be sensitive to apamin in heterologous expression systems (Shah & Haylett, 2000), it might be that a $\beta$-subunit is causing a loss of apamin sensitivity *in vivo*. Over-expression of transfected SK3 subunits might be able to internalize any SK1 subunits that may, if SK1 channels underlie such currents, result in a loss of the apamin-insensitive $sI_{AHP}$. This might shed some light on the identity of the channels underlying the $sI_{AHP}$.

To conclude, this thesis has demonstrated important interactions between SK channel residues and highly potent UCL compound blockers. It is important to determine such blocker and channel interactions at the molecular level, so that these can be used to create more potent inhibitors. By establishing the strongly interactive

regions of an inhibitor with the pore region of SK channels, one can mutate the same inhibitor to create an even more potent blocker. This has the potential to create subnanomolar inhibitors of the rSK3 channel, and other SK channels. A knowledge of the contact points between an inhibitor and the channel also can be important in designing better fitting blockers. For example, switching the *para*-Benzene and *meta*-Benzene linkers of UCL 1684 round, produces a substantial loss of binding affinity to the rSK3 channel, presumably as a result of more spatial hindrance to binding (Campos-Rosa et al., 1998). The precise configuration with which UCL compounds bind to SK channels, in combination with detailed knowledge of SK channel structure, will provide further ideas for designing drugs of greater affinity and selectivity. Ultimately, understanding the interactions between SK channels and blockers should lead to the large scale production of cheap, highly selective and potent blockers of SK channels, which could be used to alleviate certain conditions related to SK channel dysfunction.

# Appendix A

# Effective dissociation equilibrium constants of HEDTA and ATP (at 25 °C, in 0.1 M solutions)

HEDTA has a valency of 4. In solution, therefore, it may bind up to 4 $H^+$ ions;

$$[\text{MHEDTA}] \rightleftharpoons [\text{M}] + [\text{HEDTA}]$$

$$\text{Effective } K_d \text{ of HEDTA} = \frac{[\text{M}][\text{all forms of HEDTA not bound to M}]}{[\text{MHEDTA}]}$$

where [M] = Metal cation

At pH $\geq$ 4.0, the following equilibria exist:

$$H + HEDTA^{4-} \overset{pK_1}{\rightleftharpoons} H.HEDTA^{3-} \quad \text{(Singly-protonated species)}$$

$$H + H.HEDTA^{3-} \overset{pK_2}{\rightleftharpoons} H_2HEDTA^{2-} \quad \text{(Doubly-protonated species)}$$

The association constants ($pK_a$'s) for each reaction may be related by using the

Henderson-Hasselbach equation;

$$
\begin{aligned}
[\mathrm{H.HEDTA^{3-}}] &= [\mathrm{HEDTA^{4-}}]10^{(\mathrm{pK_1-pH})} \\
[\mathrm{H_2HEDTA^{2-}}] &= [\mathrm{H.HEDTA^{3-}}]10^{(\mathrm{pK_2-pH})} \\
[\text{All forms of unbound HEDTA}] &= \mathrm{L + HL + H_2L} \\
\text{where } [\mathrm{HL^{3-}}] &= [\mathrm{L^{4-}}].10^{(\mathrm{pK_1-pH})} \\
[\mathrm{H_2L^{2-}}] &= [\mathrm{L^{3-}}].10^{(\mathrm{pK_2-pH})} \\
\begin{bmatrix}\text{all forms of HEDTA} \\ \text{not bound to M}\end{bmatrix} &= \mathrm{L^{4-} + (L^{4-}.10^{(pK_1-pH)}) + (HL^{3-}.10^{(pK_1-pH)})}
\end{aligned}
$$

But,

$$
\begin{aligned}
[\mathrm{HL^{3-}}] &= [\mathrm{L^{4-}}].10^{(\mathrm{pK_1-pH})} \\
\Rightarrow \begin{bmatrix}\text{all forms of HEDTA} \\ \text{not bound to M}\end{bmatrix} &= \mathrm{L^{4-} + (L^{4-}.10^{(pK_1-pH)}) + (L^{4-}.10^{(pK_1+pK_2+2pH)})}
\end{aligned}
$$

Factorizing gives,

$$
\begin{aligned}
\begin{bmatrix}\text{all forms of HEDTA} \\ \text{not bound to M}\end{bmatrix} &= \mathrm{L^{4-}[1 + 10^{(pK_1-pH)} + 10^{(pK_1+pK_2-pH)}]} \\
\Rightarrow \text{Effective } \mathrm{K_d} &= \frac{\mathrm{[M].[L].[1 + 10^{(pK_1-pH)} + 10^{(pK_1+pK_2-2pH)}]}}{\mathrm{[ML]}}
\end{aligned}
$$

Also, three ion species of ATP exist in solution at pH 4. Working in a similar way to the above, the effective dissociation equilibrium constant of ATP ($K_{ATP}$) for a metal ion, M, is,

$$
\mathrm{K_{ATP}} = \frac{\mathrm{[M^{2+}][ATP^{3-}][1 + 10^{(pK_1-pH)} + 10^{(pK_1+pK_2-2pH)}]}}{\mathrm{[MATP]}}
$$

## A.1 Effective dissociation equilibrium constant of HEDTA for calcium ($K^{Ca}_{HEDTA}$) (at 25 °C, in a 0.1 M solution)

$$K^{Ca}_{HEDTA} = \frac{1}{K_{Ca^{HEDTA}}} \times [1 + 10^{(pK_1 - pH)} + 10^{(pK_1 + pK_2 - 2pH)}]$$

where $K_{Ca^{HEDTA}}$ = Dissociation equilibrium constant of Ca in the equilibrium;

$[CaHEDTA] \rightleftharpoons [Ca][HEDTA]$

However, $pK_d \neq -[\log H^+]$ according to the National Bureau of Standards Convention. It is physiologically more accurate to say that $pK_d = -[\log H^+ \text{activity}] = -\log(0.78[H^+])$. This correction factor increases uncorrected pH/pK values by 0.11 units;

$$\begin{aligned}
-\log K_{Ca^{HEDTA}} &= 8.31 \quad \text{(with correction factor)} \\
-\log K_1 &= 9.92 \quad \text{(with correction factor)} \\
-\log K_2 &= 5.48 \quad \text{(with correction factor)} \\
\text{pH of pipette solution used} &= 7.31 \quad \text{(with correction factor)} \\
\Rightarrow K^{Ca}_{HEDTA} &= \frac{1}{10^{8.31}} \times [1 + 10^{2.61} + 10^{0.78}] \\
&= \frac{1}{10^{8.31}} \times [414.41] \\
&= 2.03\ \mu M
\end{aligned}$$

## A.2 Effective dissociation equilibrium constant of HEDTA for magnesium ($K^{Mg}_{HEDTA}$) (at 25 °C, in a 0.1 M solution)

$$K^{Mg}_{HEDTA} = \frac{1}{K_{Mg^{HEDTA}}} \times [1 + 10^{(pK_1 - pH)} + 10^{(pK_1 + pK_2 - 2pH)}]$$

where $K_{Mg^{HEDTA}}$ = Dissociation equilibrium constant of Mg in the equilibrium:

$$[MgHEDTA] \rightleftharpoons [Mg][HEDTA]$$

$$-\log K_{Mg^{HEDTA}} = 7.11 \quad \text{(with correction factor)}$$

$$-\log K_1 = 9.92 \quad \text{(with correction factor)}$$

$$-\log K_2 = 5.48 \quad \text{(with correction factor)}$$

$$\text{pH of pipette solution used} = 7.31 \quad \text{(with correction factor)}$$

$$\Rightarrow K_{Mg^{HEDTA}} = \frac{1}{10^{7.11}} \times [1 + 10^{2.61} + 10^{0.78}]$$

$$= \frac{1}{10^{7.11}} \times [414.41]$$

$$= 32.17\ \mu M$$

## A.3 Effective dissociation equilibrium constant of ATP for calcium ($K^{Ca}_{ATP}$) (at 25 °C, in a 0.1 M solution)

$$K^{Ca}_{ATP} = \frac{1}{K_{Ca^{ATP}}} \times [1 + 10^{(pK_1 - pH)} + 10^{(pK_1 + pK_2 - 2pH)}]$$

where $K_{Ca^{ATP}}$ = Dissociation equilibrium constant of Ca in the equilibrium;

$$
\begin{aligned}
[\mathrm{CaATP}] &\rightleftharpoons [\mathrm{Ca}][\mathrm{ATP}] \\
-\log \mathrm{K}_{\mathrm{Ca^{ATP}}} &= 3.88 \quad \text{(with correction factor)} \\
-\log \mathrm{K}_1 &= 6.62 \quad \text{(with correction factor)} \\
-\log \mathrm{K}_2 &= 4.17 \quad \text{(with correction factor)} \\
\text{pH of pipette solution used} &= 7.31 \quad \text{(with correction factor)} \\
\Rightarrow \mathrm{K}_{\mathrm{Ca^{ATP}}} &= \frac{1}{10^{3.88}} \times [1 + 10^{-0.67} + 10^{-3.83}] \\
&= \frac{1}{10^{3.88}} \times [1.20415] \\
&= 158.9\ \mu\mathrm{M}
\end{aligned}
$$

## A.4 Effective dissociation equilibrium constant of ATP for magnesium ($K_{ATP}^{Mg}$) (at 25 °C, in a 0.1 M solution)

$$
\begin{aligned}
\mathrm{K}_{\mathrm{ATP}}^{\mathrm{Mg}} &= \frac{1}{\mathrm{K}_{\mathrm{Mg^{ATP}}}} \times [1 + 10^{(\mathrm{pK_1}-\mathrm{pH})} + 10^{(\mathrm{pK_1}+\mathrm{pK_2}-2\mathrm{pH})}] \\
\text{where } \mathrm{K}_{\mathrm{Mg^{ATP}}} &= \text{Dissociation equilibrium constant of Mg in the equilibrium:} \\
[\mathrm{MgATP}] &\rightleftharpoons [\mathrm{Mg}][\mathrm{ATP}] \\
-\log \mathrm{K}_{\mathrm{Mg^{ATP}}} &= 4.17 \quad \text{(with correction factor)} \\
-\log \mathrm{K}_1 &= 6.62 \quad \text{(with correction factor)} \\
-\log \mathrm{K}_2 &= 4.17 \quad \text{(with correction factor)} \\
\text{pH of pipette solution used} &= 7.31 \quad \text{(with correction factor)} \\
\Rightarrow \mathrm{K}_{\mathrm{Mg^{ATP}}} &= \frac{1}{10^{4.17}} \times [1 + 10^{-0.67} + 10^{-3.83}] \\
&= \frac{1}{10^{4.17}} \times [1.20415] \\
&= 81.4\ \mu\mathrm{M}
\end{aligned}
$$

| Dissociation equilibrium constant | Value at 18 °C |
|---|---|
| $K_{HEDTA}^{Ca}$ | 2.63 μM |
| $K_{HEDTA}^{Mg}$ | 36.82 μM |
| $K_{ATP}^{Ca}$ | 97.3 μM |
| $K_{ATP}^{Mg}$ | 165.3 μM |

**Table A.1:** Table showing calculated values of the dissociation equilibrium constants for calcium and magnesium-buffering molecules in the pipette solution at 18 °C. The method of Tsien (1989) has been used in all calculations. $K_{HEDTA}^{Ca}$ is the dissociation equilibrium constant of CaHEDTA. $K_{HEDTA}^{Mg}$ is the dissociation equilibrium constant of MgHEDTA. $K_{ATP}^{Ca}$ is the dissociation equilibrium constant of CaATP. $K_{ATP}^{Mg}$ is the dissociation equilibrium constant of MgATP.

The above $K_d$ values need to be converted to ones that accurately represent the conditions. All pipette solutions were approximately 0.1 M but the temperatures of the solutions used were about 18–19 °C (measured using a standard mercury glass thermometer). To estimate the associated $K_d$ changes, standard enthalpy of complexation values ($\Delta H$) may be employed using the following relationship:

$$\frac{\Delta H}{2.303RT^2} = \frac{\delta \log K}{\delta T}$$

Temperature used for measuring ΔH is 298 K

$$\log {K_d}^{25} = \log {K_d}^{18} + \frac{\Delta H(T^{25} - T^{18})}{1699524.7}$$

where ${K_d}^{25}$ = Dissociation equilibrium constant at 25°C

${K_d}^{18}$ = Dissociation equilibrium constant at 18°C

$T^{25}$ = 298 K

$T^{18}$ = 291 K

The $\Delta H$ values given in the Martell and Smith compendium need to be multiplied by 4.184 to be converted into SI units of kJ/mol. The resulting ${K_d}^{18}$ values given by this method are shown in table Table A.1.

# Appendix B

# Loss of slow current transient

The fast transient current arises from the capacitive currents which charge the pipette, whereas the slow transient arises from the current which charges the cell membrane in the whole-cell configuration. The current at any time, $t$, may be derived theoretically, as described by Equation B.1. Drastic changes in series resistance and cell capacitance using the auto function of the EPC-9 were occasionally observed; delayed rectifier currents appeared to be compensated for correctly, but SK currents would not be a lot of the time. The auto-compensation circuit of the EPC-9 is based on the equation below (Equation B.1). By deriving the ratio of the current at time zero and infinity, it can be seen that the slow transients do disappear when the membrane resistance drops well below the series resistance. This algebraic derivation suggests that the incorrectly compensated values are not a problem with the EPC-9 auto-compensation itself but an artifact produced by such a small transient integral. Furthermore, this process was occasionally observed, when, immediately after going whole-cell the slow current transients would quickly disappear within one or two seconds.

$$I_{(t)} = V_0[G_s e^{\frac{-t}{\tau}} + G_{\text{inf}}(0.5 - e^{\frac{-t}{\tau}}] \qquad \text{(B.1)}$$

where $\tau = \frac{C_m}{G_m+G_s}$
$G_{\text{inf}} = \frac{G_m \times G_s}{G_m+G_S}$

When I $\rightarrow \infty$,

$$I_{\text{inf}} = \frac{V_0 G_{\text{inf}}}{2}$$

When I $\rightarrow 0$,

$$\begin{aligned} &= \frac{V_0(2G_s - G_{\text{inf}})}{2} \\ \frac{I_0}{I_{\text{inf}}} &= \frac{(2G_s - G_{\text{inf}})}{G_{\text{inf}}} \\ &= \frac{2G_s}{G_{\text{inf}}} - 1 \\ &= 2G_s \frac{(G_m + G_s)}{G_m G_s} - 1 \\ &= 2 + \frac{2G_s}{G_m} - 1 \\ \frac{I_0}{I_{\text{inf}}} &= 1 + \frac{2G_s}{G_m} \end{aligned}$$

where $I_{(t)}$ = Current at time, $t$
$V_0$ = voltage step
$G_{\text{inf}}$ = Infinity conductance
$G_m$ = Membrane conductance
$C_m$ = Membrane capacitance
$I_{\text{inf}}$ = Current at time equal to infinity

when $R_m$ gets very small (a hundredth of $R_s$), then the transient will be very small = 1.02; this is too small a value to compensate. This will occur whenever the SK current in the cell is very large.

# Appendix C

# Reference table of amino acid codes

| Amino acid name | One letter code | Three letter code |
|---|---|---|
| Alanine | A | Ala |
| Arginine | R | Arg |
| Asparagine | N | Asn |
| Aspartic acid | D | Asp |
| Cysteine | C | Cys |
| Glutamine | Q | Gln |
| Glycine | G | Gly |
| Histidine | H | His |
| Isoleucine | I | Iso |
| Leucine | L | Leu |
| Lysine | K | Lys |
| Methionine | M | Met |
| Phenylalanine | F | Phe |
| Proline | P | Pro |
| Serine | S | Ser |
| Threonine | T | Thr |
| Tryptophan | W | Try |
| Tyrosine | Y | Tyr |
| Valine | V | Val |

**Table C.1:** Table showing the one-letter codes and three letter codes of the amino acids which form proteins.

# Acknowledgements

I would like to thank Dr Guy Moss for his academic help and guidance throughout the last four years. In addition, I would like to thank the following people for their individual contributions:

Dr Ramine Hosseini for guiding me through the immunostaining procedure

Dr Stuart Lansdale for running some of my sequencing reactions on his gels

Dr Dennis Haylett for helpful discussions and supplying the structure of UCL 1848.

# References


Abrams, C., Davies, N., Shelton, P., & Stanfield, P. (1996). The role of a single aspartate residue in ionic selectivity and block of a murine inward rectifier $K^+$ channel, Kir2.1. *J Physiol, 493 (Pt 3)*, 643-649.

Aguilar-Bryan, L., Nichols, C., Wechsler, S., Clement, J., & Boyd, A. (1995). Cloning of the $\beta$-cell high affinity sulfonylurea receptor : A regulator of insulin secretion. *Science, 268*, 423-426.

Ahn, J., Aoki, N., Adachi, T., Mizuno, Y., Nakamura, R., & Matsuda, T. (1995). Isolation and culture of bovine mammary epithelial cells and establishment of gene transfection conditions in the cells. *Biosci Biotechnol Biochem, 59 (1)*, 59-64.

Allen, T., Bliznyuk, A., Rendell, A., Kuyucak, S., & Chung, S.-H. (2000). The potassium channel: Structure, selectivity, and diffusion. *Journal of Chemical Physics, 112*(18), 8191–8204.

Ammala, C., Bokvist, K., Larsson, O., Berggren, P., & Rorsman, P. (1993). Demonstration of a novel apamin-insensitive calcium-activated $K^+$ channel in mouse pancreatic $\beta$-cells. *Pflugers Archives, 422*, 443-8.

Armstrong, C., & Bezanilla, F. (1973). Currents related to the movement of the gating particles of the sodium channels. *Nature, 242*, 459-461.

Artalejo, A., Garcia, A., & Neher, E. (1993). Small conductance $Ca^{2+}$-activated $K^+$ channels in bovine chromaffin cells. *Pflugers Archives, 423 (1-2)*, 97-103.

Austin, C., Holder, D., Ma, L., Mixson, L., & Caskey, C. (1999). Mapping of hKCa3 to chromosome 1q21 and investigation of linkage of CAG repeat polymorphism to schizophrenia. *Mol Psychiatry, 4 (3)*, 261-266.

Avdonin, V., & Hoshi, T. (2001). Modification of voltage-dependent gating of potassium channels by free form of tryptophan side chain. *Biophysical J, 81*, 97-106.

Baba, Y., Hirukawa, N., Tanohira, N., & Sodeoka, M. (2003). Structure-based design of a highly selective catalytic site-directed inhibitor of Ser/Thr protein phosphatase 2B (calcineurin). *Journal Am Chem Soc, 125 (32)*, 9740-9749.

Ballantyne, D., & Schneid, P. (2000). Mammalian brainstem chemosensitive neurones: Linking them to respiration *in vitro*. *J Physiol (London), 525*, 567-577.

Bang, H., Kim, Y., & Kim, D. (2000). TREK-2, a new member of the mechanosensitive tandem pore $K^+$ channel family. *Journal of Biological Chemistry, 275*, 17412-17419.

Banks, B., Brown, C., Burgess, G., Burnstock, G., Claret, M., Cocks, T., et al. (1979). Apamin blocks certain neurotransmitter-induced increases in potas-

sium permeability. *Nature, 282*, 415-7.

Bayguinov, O., Vogalis, F., Morris, B., & Sanders, K. (1992). Patterns of electrical activity and neural responses in canine proximal duodenum. *American Journal of Physiology, 263 (6 Pt 1)*, G887-894.

Behnisch, T., & Reymann, K. (1998). Inhibition of apamin-sensitive calcium-dependent potassium channels facilitate the induction of long-term potentiation in the CA1 region of rat hippocampus *in vitro*. *Neuroscience Letters, 253*(2), 91–94.

Behrens, M., Serani, A., Vergara, F., & Alvarez, O. (1994). Possible role of apamin-sensitive $K^+$ channels in myotonic dystrophy. *Muscle Nerve, 17 (11)*, 1264-1270.

Benington, J., Wondenberg, M., & Heller, H. (1995). Apamin, a selective SK potassium channel blocker suppresses REM sleep without a compensatory rebound. *Brain Research, 692/1-2*, 86-92.

Bennett, M., Garcia-Arraras, J., Elferink, L., Peterson, K., Fleming, A., & Hazuka, C. (1993). The syntaxin family of vesicular transport receptors. *Cell, 74*, 863-873.

Berdiev, B., Prat, A., Cantiello, H., Ausiello, D., Fuller, C., Jovov, B., et al. (1996). Regulation of epithelial sodium channels by short actin filaments. *Journal of Biological Chemistry, 271 (30)*, 17704-17710.

Bergman, H., Wichmann, T., Kamon, B., & DeLong, M. (1994). The primate subthalamic nucleus. II. Neuronal activity in the MPTP model of Parkinsonism. *Journal of Neurophysiology, 72 (2)*, 507-520.

Berjukow, S., Doring, F., Froschmayr, M., Grabner, M., Glossmann, H., & Hering, S. (1996). Endogenous calcium channels in human embryonic kidney (HEK 293) cells. *British Journal of Pharmacology, 118*, 748-754.

Biervert, C., Schroeder, B., Kubisch, C., Berkovic, S., Propping, P., Jentsch, T., et al. (1998). A potassium channel mutation in neonatal human epilepsy. *Science, 279 (5349)*, 403-6.

Blank, T., Nijholt, I., Kye, M., Radulovic, J., & Speiss, J. (2003). Small conductance, $Ca^{2+}$-activated $K^+$ channel SK3 generates age-related memory and LTP. *Nature Neuroscience, 6.(9)*, 911-912.

Blatz, A., & Magleby, K. (1986). Single apamin blocked $Ca^{2+}$-activated $K^+$ channels of small conductance in cultured rat skeletal muscle. *Nature, 323*, 718-720.

Bond, C., Maylie, J., & Adelman, J. (1999). Small conductance calcium-activated potassium channels. *Annals of NY Academy of Sciences*, 371-378.

Bond, C., Pessia, M., Xia, X., Lagrutta, A., Kavanough, M., & Adelman, J. (1994). Cloning and functional expression of a family of inward rectifier potassium channels. *Receptors and Ion Channels, 2*, 183–91.

Brading, A. (1992). Ion channels and control of contractile activity in urinary bladder smooth muscle. *Japanese Journal of Pharamcology, 58*, 120-127P.

Braun, A., & Sy, L. (2001). Contribution of potential EF hand motifs to the calcium-dependent gating of a mouse brain large conductance, calcium-sensitive $K^+$ channel. *Journal of Physiology, 533 (Pt 3)*, 681-695.

Brenner, R., Perez, G., Bonev, A., Eckman, D., Kosek, J., Wiler, S., et al. (2000). Vasoregulation by the $\beta 1$ subunit of the calcium-activated potassium channel.

*Nature, 407 (6806)*, 847-848.

Bretschneider, F., Wrisch, A., Lehmann-Horn, F., & Grissmer, S. (1999). External tetraethylammonium as a molecular caliper for sensing the shape of the outer vestibule of potassium channels. *Biophysical Journal, 76*, 2351-2360.

Browne, D., Gancher, S., Nutt, J., Brunt, E., Smith, E., Kramer, P., et al. (1994). Episodic ataxia/myokymia syndrome is associated with point mutations in the human potassium channel gene, KCNA1. *Nature Genetics, 8 (2)*, 136-140.

Bruening-Wright, A., Schumacher, M., Adelman, J., & Maylie, J. (2002). Localization of the activation gate for small conductance $Ca^{2+}$-activated $K^+$ channels. *Journal of Neuroscience, 22 (15)*, 6499-6506.

Buckler, K. (1997). A novel oxygen-sensitive potassium current in rat carotid body type I cells. *J Physiol (London), 498*, 649-662.

Burgess, G., Claret, M., & Jenkinson, D. (1981). Effects of quinine and apamin on the calcium-dependent potassium permeability of mammalian hepatocytes and red cells. *Journal of Physiology, 317*, 67–90.

Busch, A., & Suessbrich, H. (1999). The IKs channel: Coassembly of IsK (minK) and KvLQT1 proteins. *Reviews of Physiol Biochem Parmacol, 137*, 191-226.

Calabro, V., Sabatier, J., Blanc, E., Lecomte, C., Van Rietschoten, V., & Darbon, H. (1997). Differential involvement of disulfide bridges on the folding of a scorpion toxin. *Journal of Peptide Research, 50 (1)*, 39-47.

Campos-Rosa, J., Galanakis, D., Ganellin, R., Dunn, P., & Jenkinson, D. (1998). Bis-quinolinium cyclophanes: UCL 1684, the first naomolar, non-peptidic blocker of apamin-sensitive calcium-activated potassium channels. *Journal of Med Chemistry, 41*, 2-5.

Campos-Rosa, J., Galanakis, D., Piergentili, A., Bhandari, K., Ganellin, C., Dunn, P., et al. (2000). Synthesis, molecular modelling, and pharmacological testing of bisquinolinium cyclophanes: Potent, non-peptidic blockers of the apamin-sensitive $Ca^{2+}$-activated $K^+$ channel. *Journal of Medicinal Chemistry, 43 (3)*, 420-431.

Caretta, B. (1994). Calcium-activated hyperpolarizations in neurones of the medio-lateral part of the lateral septum : Intracellular studies from guinea-pig brain slices. *Experimental Brain Research, 102*, 297-304.

Carignani, C., Roncarati, R., Rimini, R., & Terstappen, G. (2002). Pharmacological and molecular characterisation of SK3 channels in the TE671 human medulloblastoma cell line. *Brain Research, 939 (1-2)*, 11-18.

Cartier, E., Conti, L., Vandenberg, C., & Shyng, S. (2001). Defective trafficking and function of $K_{ATP}$ channels caused by a sulfonylurea receptor 1 mutation associated with persistent hyperinsulinemic hypoglycemia of infancy. *Proc Natl Acad Sci USA, 98 (5)*, 2882-2887.

Castle, N. (1999). Recent advances in the biology of small conductance calcium-activated potassium channels. *Perspectives in Drug Discovery and Design, 15-16*, 131-154.

Chandy, K., Fantio, E., Wittenkindt, O., Kalman, K., Tong, L., Ho, T., et al. (1998). Isolation of a novel potassium channel gene hSKCa3 containing a polymorphic CAG repeat: A candidate for schizophrenia and bipolar disorder? *Molecular Psychology, 3/1*, 32-37.

Chen, J., Galankis, D., Ganellin, C., Dunn, P., & Jenkinson, D. (2000). Bisquinolinium cyclophanes: UCL 1848, a highly potent and selective, nonpeptidic blocker of the apamin-sensitive $Ca^{2+}$-activated $K^+$ channel. *J Medicinal Chemistry, 43*, 3478-3481.

Cingolani, L., Gymnopoulos, M., Boccaccio, A., Stocker, M., & Pedarzani, P. (2002). Developmental regulation of small conductance $Ca^{2+}$-activated $K^+$ channel expression and function in rat Purkinje neurones. *Journal of Neuroscience, 22 (11)*, 4456-4467.

Coetzee, W., Amarillo, Y., Chiu, J., Chow, A., Lau, D., McCormack, T., et al. (1999). Molecular diversity of $K^+$ channels. *Annals NY Acad Sci, 868*, 223-285.

Cook, N., & Haylett, D. (1985). Effects of apamin, quinine and neuromuscular blockers on calcium-activated potassium channels in guinea-pig hepatocytes. *Journal of Physiology, 358*, 373–394.

Coucke, P., Van Hauwe, P., Kelley, P., Kunst, H., Schatteman, I., Van Velzen, D., et al. (1999). Mutations in the KCNQ4 gene are responsible for autosomal dominant deafness in DFNA2 families. *Human Mol Genetics, 8 (7)*, 1321-8.

Crouzy, S., Berneche, S., & Roux, B. (2001). Extracellular blockade of $K^+$ channels by TEA: Results from molecular dynamics simulations of the KcsA channel. *J General Physiology, 118*, 207-17.

Curran, M., Splawski, I., Timothy, K., Vincent, G., Green, E., & Keating, M. (1995). A molecular basis for cardiac arrhythmia: hERG mutations cause long QT syndrome. *Cell, 80 (5)*, 299-307.

Cushman, S., Nanao, M., Jahng, A., DeRubeis, D., Chloe, S., & Pfaffinger, P. (2000). Voltage-dependent activation of potassium channels is coupled to T1 domain structure. *Nat. Struc.Biol., 7*, 403-407.

Dale, T., Cryan, J., Chen, M., & Tresize, D. (2002). Partial apamin sensitivity of human small conductance $Ca^{2+}$-activated $K^+$ channel stably expressed in Chinese hamster ovary cells. *Naunyn Schmiedebergs Arch Pharmacol, 366 (5)*, 470-477.

Degtiar, V., Scheller, R., & Tsien, R. (2000). Syntaxin modulation of slow inactivation of N-type calcium channels. *Journal of Neuroscience, 20*, 4355-4367.

Demonchaux, P., Ganellin, C., Dunn, P., Haylett, D., & Jenkinson, D. (1991). Search for the pharmacophore of the $K^+$ channel blocker, apamin. *Eur J of Medicinal Chem, 26*, 915-20.

Derst, C., Konrad, M., Kockerling, A., Karolyi, L., Deschenes, G., Daut, J., et al. (1997). Mutations in the ROMK gene in antenatal Bartter's syndrome are associated with impaired $K^+$ channel function. *Biochem Biophys Res Commun, 230 (3)*, 641-645.

Devor, D., & Frizzell, R. (1998). Modulation of $K^+$ channels by arachidonic acid in T84 cells. I. Inhibition of the $Ca^{2+}$-activated $K^+$ channel. *Am J Physiology, 274 (Pt 1)*, C138-C148.

D'hoedt, D., Hirzel, K., Pedarzani, P., & Stocker, M. (2004). Domain analysis of the calcium-activated potassium channel SK1 from rat brain: Functional expression and toxin sensitivity. *Journal of Biological Chemistry, 279 (13)*, 12088-12092.

Doyle, D., Cabral, J., Pfuetzner, R., Kuo, A., Gulbis, J., Cohen, S., et al. (1998). The structure of the potassium channel: Molecular basis of $K^+$ conduction and selectivity. *Science, 280*, 69-77.

Dunn, P., Benton, D., Campos Rosa, J., Ganellin, C., & Jenkinson, D. (1996). Discrimination between subtypes of apamin-sensitive $Ca^{2+}$-activated potassium channels by gallamine and a novel bis-quaternary quinolinium cyclophane, UCL 1530. *British Journal of Pharmacology, 117*, 35-42.

Dunne, M., Kane, C., Shepherd, R., Sanchez, J., James, R., Johnson, P., et al. (1997). Familial persistent hyperinsulinemic hypoglycemia of infancy and mutations in the sulfonylurea receptor. *The New England Journal of Medicine, 336*, 703-706.

Faber, E., & Sah, P. (2002). Physiological role of calcium-activated potassium currents in the rat lateral amygdala. *Journal of Neuroscience, 22 (5)*, 1618-1628.

Fan, J.-S., Jiang, M., Dun, W., McDonald, T., & Tseng, G.-N. (1999). Effects of outer mouth mutations on hERG channel function: A comparison with similar mutations in the Shaker channel. *Biophysical J, 76*, 3128-40.

Fanger, C., Rauer, H., Neben, A., Miller, M., Rauer, H., Wulff, H., et al. (2001). Calcium-activated potassium channels sustain calcium signalling in T lymphocytes. Selective blockers and manipulated channel expression levels. *J Biological Chem, 276*, 12249-12256.

Fili, O., Michaelevski, I., Bledi, Y., Chikvashvili, D., Singer-Lahat, D., Boshwitz, H., et al. (2001). Direct interaction of a brain voltage-gated $K^+$ channel with syntaxin 1A: Functional impact on channel gating. *Journal of Neuroscience, 21 (6)*, 1964-1974.

Fletcher, S., Bowden, S., & Marrion, N. (2003). False interaction of syntaxin 1A with a $Ca^{2+}$-activated $K^+$ channel revealed by co-immunoprecipitation and pull-down assays: Implications of protein-protein interactions. *Neurpharmacology, 44 (6)*, 817-827.

Frebourg, T., Bonnet-Brihault, F., Laurent, C., Campion, D., Thibaut, F., Deleuze, J., et al. (1998). No evidence for the involvement of the hSKCa3 potassium channel gene in familial and sporadic cases of schizophrenia. *American Journal of Human Genetics, 63 (supp)*, A326.

Frech, G., VanDonger, A., Schuster, G., Brown, A., & Joho, R. (1989). A novel potassium channel with delayed rectifier properties isolated from rat brain by expression cloning. *Nature, 340 (6235)*, 642-5.

Galanakis, D., Davis, C., Ganellin, R., & Dunn, P. (1996). Synthesis and quantitaive structure-activity relationship of a novel series of small conductance $Ca^{2+}$-activated $K^+$ channel blockers related to dequalinium. *J Med Chemistry, 39*, 359-70.

Galanakis, D., Davis, C., Herrero, B., Ganellin, C., Dunn, P., & Jenkinson, D. (1995). Synthesis and QSAR of dequalinium analogues as $K^+$ channel blockers. Investigations on the role of the 4-amino group. *Bioorganic & Medicinal Chem Letters, 5*, 559-62.

Galanakis, D., Davis, C., Herrero, B., Ganellin, C., Dunn, P., & Jenkinson, D. (1995). Synthesis and structure-activity relationships of dequalinium ana-

logues as $K^+$ channel blockers. Investigations on the role of the charged heterocycle. *J Med Chemistry, 38*, 595-606.

Galanakis, D., Ganellin, R., Malik, S., & Dunn, P. (1995). Synthesis and pharmacological testing of dequalinium analogues as blockers of the apamin-sensitive $Ca^{2+}$-activated $K^+$ channel: Variation of the length of the alkylene chain. *Journal of Medicinal Chemistry, 39*, 3592-3595.

Galvez, A., Gimenez-Gallego, G., Reuben, J., Roy-Contancin, L., Feigenbaum, P., Kaczorowski, G., et al. (1990). Purification and characterization of a unique, potent, peptidyl probe for the high conductance calcium-activated potassium channel from venom of the scorpion *Buthus tamulus*. *Journal of Biological Chemistry, 265 (19)*, 11083-11090.

Gandolfo, G., Shweitz, H., Lazdunski, M., & Gotherman, C. (1996). Sleep-cycle disturbances induced by apamin, a selective blocker of $Ca^{2+}$-activated $K^+$ channels. *Brain Research, 736/1-2*, 344-347.

Garcia, M., Ying-Duo, G., McManus, O., & Kaczorowski, G. (2001). Potassium channels: From scorpion venoms to high-resolution structure. *Toxicon, 39*, 739-48.

Gehlart, D., & Gackenheimer, S. (1993). Comparison of the distribution of binding sites for the potassium channel ligands [$^{(125)}$I] charybdotoxin and [$^{(125)}$I] iodoglyburide in the rat brain. *Neuroscience, 52/1*, 191-206.

Gerlach, A., Gangopadhyay, N., & Devor, C. (2000). Kinase-dependent regulation of the intermediate conductance calcium-activated potassium channel, hIK1. *J Biol Chem, 275 (1)*, 585-598.

Gerlach, A., Syme, C., Giltinan, L., Adelman, J., & Devor, D. (2001). ATP-dependent activation of the intermediate conductance $Ca^{2+}$-activated $K^+$ channel, hIK1, is conferred by a C-terminal domain. *J Biol Chem, 276*, 10963-70.

Giangiacomo, K., Garcia, M., & McManus, O. (1992). Mechanism of iberiotoxin block of the large conductance calcium-activated potassium channel from bovine aortic smooth muscle. *Biochemistry, 31*, 6719.

Goldstein, S., & Miller, C. (1993). Mechanism of charybdotoxin block of a voltage-gated $K^+$ channel. *Biophysical J, 65*, 1613-19.

Goldstein, S., Pheasant, D., & Miller, C. (1994). The charybdotoxin receptor of a Shaker $K^+$ channel: Peptide and channel residues mediating molecular recognition. *Neuron, 12*, 1377-88.

Granier, C., Pedroso Muller, E., & Van Rietschoten, J. (1978). Use of synthetic analogs for a study on the structure-activity relationship of apamin. *European Journal of Biochemistry, 82 (1)*, 293-299.

Gray, A., Zhao, B., Kindler, C., Winegar, B., Mazurek, M., Xu, J., et al. (2000). Volatile anesthetics activate the human tandem pore domain baseline $K^+$ channel KCNK5. *Anesthesiology, 92 (6)*, 1722-30.

Grissmer, S., Lewis, R., & Cahalan, M. (1992). $Ca^{2+}$-activated $K^+$ channels in human leukemic T cells. *Journal of General Physiology, 99*, 63-84.

Grissmer, S., Nguyen, A., & Cahalan, M. (1993). Calcium-activated potassium channels in resting and activated human T lymphocytes. Expression levels, calcium dependence, ion selectivity, and pharmacology. *Journal of General*

*Physiology, 102 (4)*, 601-630.

Grunnet, M., Jensen, B., Olesen, S., & Klaerke, D. (2001). Apamin interacts with all subtypes of cloned small conductance $Ca^{2+}$-activated $K^+$ channels. *Pflu Arch - European J of Physiology, 441*, 544-50.

Grunnet, M., Jespersen, T., Angelo, K., Frokjaer-Jensen, C., Klaerke, D., Olesen, S.-P., et al. (2001). Pharmacological modulation of SK3 channels. *Neuropharmacology, 40*, 879-887.

Habermann, E. (1984). Apamin. *Pharmacol Thearap, 25 (2)*, 255-70.

Hadley, R., & Lederer, W. (1991). Properties of L-type calcium channel gating current in isolated guinea pig ventricular myocytes. *Journal of General Physiology, 98 (2)*, 265-285.

Hallworth, N., Wilson, C., & Bevan, M. (2003). Apamin-sensitive small conductance calcium-activated potassium channels, through their selective coupling to voltage-gated calcium channels, are critical determinants of the precision, pace, and pattern of action potential generation in rat subthalamic neurones *in vitro*. *Journal of Neuroscience, 23 (20)*, 7525-7542.

Han, J., Kang, T., & Kim, D. (2003). Functional properties of four splice variants of a human pancreatic tandem-pore $K^+$ channel, TALK-1. *Am J Physiol Cell Physiology, 285 (3)*, C529-38.

Hanselmann, C., & Grissmer, S. (1996). Characterization of apamin-sensitive $Ca^{2+}$-activated potassium channels in human leukaemic T-lymphocytes. *Journal of Physiology, 496 (Pt 3)*, 627-637.

Hattori, S., Murakami, F., & Song, W. (2003). Rundown of a transient potassium current is attributable to changes in channel voltage dependence. *Synapse, 48 (2)*, 57-65.

Haylett, D., & Jenkinson, D. (1990). *Potassium channels : Structure, classification, function and therapeutic potential. (In chapter) Calcium-activated potassium channels* (Cook, NA ed.). John WIley and sons, London.

Heginbotham, L., Lu, Z., Abramson, T., & MacKinnon, R. (1994). Mutations in the $K^+$ channel signature sequence. *Biophysical Journal, 66*, 1061-67.

Heginbotham, L., & MacKinnon, R. (1992). The aromatic binding site for tetraethylammonium on potassium channels. *Neuron, 8 (3)*, 483-491.

Henry, P., Lopatin, A., Makhina, E., & Nichols, C. (1995). A negative charge in M2 regulates sensitivity of inward rectifier $K^+$ channels to external cation block. *Biophysics J, 68*, A264.

Heppner, T., Boney, A., & Nelson, M. (1997). $Ca^{2+}$-activated $K^+$ channels regulate action potential repolarization in urinary bladder smooth muscle. *American Journal of Physiology, 273 (1 Pt 1)*, C110-C117.

Herrera, G., & Nelson, M. (2002). Differential regulation of SK and BK channels by $Ca^{2+}$ signals from $Ca^{2+}$ channels and ryanodine receptors in guinea-pig urinary bladder myocytes. *Journal of Physiology, 541 (Pt 2)*, 483-492.

Herzig, S., & Neumann, J. (2000). Effects of serine/threonine protein phosphatases on ion channels in excitable membranes. *Physiological Reviews, 80 (1)*, 173-210.

Hirschberg, B., Maylie, J., Adelman, J., & Marrion, N. (1998). Gating of recombinant small conductance $Ca^{2+}$-activated $K^+$ channels by calcium. *Journal of*

*General Physiology, 111*, 565-581.

Hirst, G., Johnson, S., & Van Helden, D. (1985). The slow calcium-dependent potassium current in a myenteric neurone of the guinea-pig ileum. *Journal of Physiology, 361*, 315-37.

Ho, K., Nichols, C., Lederer, W., Lytton, J., & Vassilev, P. (1993). Cloning and expression of an inwardly rectifying ATP-regulated potassium channel. *Nature, 362*, 31-8.

Hoffman, J., Joiner, W., Nehrke, K., Potapova, O., Foye, K., & Wickrema, A. (2003). The hSK4 (KCNN) isoform is the $Ca^{2+}$-activated $K^+$ channel (Gardos channel) in human red blood cells. *Proc Natl Acad Sci USA, 100 (12)*, 7366-7371.

Hoshi, T. (1995). Regulation of voltage dependence of the KAT1 channel by intracellular factors. *Journal of General Physiology, 105 (3)*, 309-328.

Hoshi, T., Zagotta, W., & Aldrich, R. (1991). Two types of inactivation in Shaker $K^+$ channels: Effects of alterations in the carboxy-terminal region. *Neuron, 7*, 547-556.

Hosseini, R., Benton, D., Dunn, P., Jenkinson, D., & Moss, G. (2001). SK3 is an important component of $K^+$ channels mediating the afterhyperpolarization in cultured rat SCG neurones. *Journal of Physiol., 535*(2), 323–334.

Hotson, J., & Prince, D. (1980). A calcium-activated hyperpolarization follows repetitive firing in hippocampal neurones. *Journal of Neurophysiology, 43*, 409-419.

Hugues, M., Romey, G., Duval, D., Vincent, J., & Lazdunski, M. (1982). Apamin as a selective blocker of the calcium-dependent potassium channel in neuroblastoma cells: Voltage-clamp and biochemical characterization of the toxin receptor. *Proc Nationl Academy Sci USA, 79 (4)*, 1308-12.

Ishii, T., Maylie, J., & Adelman, J. (1997). Determinants of apamin and d-tubocurarine block in SK potassium channels. *J of Biol.Chemistry, 272*, 239-249.

Jan, L., Barbel, S., Timpe, L., Laffer, C., Salkoff, L., O'Farrell, P., et al. (1983). Mutating a gene for a potassium channel by hybrid dysgenesis: An approach to the cloning of the Shaker locus in Drosophila. *Cold Spring Harbour Symposium Quant Biol, 48 pt 1*, 233-245.

Jan, L., & Jan, Y. (1989). Voltage-sensitive ion channels. *Cell, 56*, 13-25.

Jarvis, S., Magga, J., Beedle, A., Braun, J., & Zamponi, G. (2000). G-protein modulation of N-type calcium channels is facilitated by physical interactions between syntaxin 1A and $G\beta\gamma$. *J Biol Chem, 275 (9)*, 6388-6394.

Jenkinson, D., Haylett, D., & Cook, N. (1983). $Ca^{2+}$-activated $K^+$ channels in liver cells. *Cell calcium, 4*, 429-437.

Jensen, B., Strobaek, D., Christophersen, P., Jorgensen, T., Hansen, C., Silahtaroglu, A., et al. (1998). Characterization of the cloned intermediate-conductance $Ca^{2+}$-activated $K^+$ channel. *Am J Physiology, 275*, C848-C856.

Jensen, B., Strobaek, D., Olesen, S., & Christophersen, P. (2001). The $Ca^{2+}$-activated $K^+$ channel of intermediate conductance: A molecular target for novel treatments? *Current Drug Targets, 2(4)*, 401-422.

Jiang, Y., Lee, A., Chen, J., Cadene, M., Chait, B., & MacKinnon, R. (2002). Crys-

tal structure and mechanism of a calcium-gated potassium channel. *Nature, 417*, 515.

Jiang, Y., Lee, A., Chen, J., Cadene, M., Chait, B., & MacKinnon, R. (2002). The open pore conformation of potassium channels. *Nature, 417 (6888)*, 523-526.

Jiang, Y., & MacKinnon, R. (2000). The barium site in a potassium channel by X-ray crystallography. *J General Physiology, 115*, 269-272.

Joiner, W., Tang, M., Wang, L.-Y., Dworetzky, S., Boissard, C., Gan, L., et al. (1998). Formation of intermediate-conductance calcium-activated potassium channels by interaction of Slack and Slo subunits. *Nature, 1 (6)*, 462-469.

Joiner, W., Wang, L., Tang, M., & Kaczmarek, L. (1997). hSK4, a member of a novel subfamily of calcium-activated potassium channels. *Proc Natl Acad Scien USA, 110 (Pt 17)*, 2117-2128.

Jubelin, B., & Kannan, M. (1990). Neurons from neonatal hypertensive rats exhibit abnormal membrane properties *in vitro*. *American Journal of Physiology, 259 (3 Pt 1)*, C389-C396.

Kane, C., Shepherd, R., Squires, P., Johnson, P., James, R., Milla, P., et al. (1996). Loss of functional $K_{ATP}$ channels in pancreatic $\beta$-cells causes persistent hyperinsulinemic hypoglycemia of infancy. *Nature Med, 2 (12)*, 1344-1347.

Kang, J., Huguenard, J., & Prince, D. (1996). Development of BK channels in neocortical pyramidal neurons. *Journal of Neurophysiology, 76 (1)*, 188-198.

Karolyi, L., Koch, M., Grzeschik, K., & Seyberth, H. (1998). The molecular genetic approach to "Bartter's syndrome". *Journal of Molecular Medicine, 76 (5)*, 317-325.

Katz, B. (1949). Les constantes électriques de la membrane du muscle. *Arch Sci Physiol, 2*, 285-299.

Kavanaugh, M., Varnum, M., Osborne, P., Christie, M., Busch, A., Adelman, J., et al. (1991). Interaction between tetraethylammonium and amino acid residues in the pore of cloned voltage-dependent potassium channels. *Journal of Biological Chemistry, 266 (12)*, 7583-87.

Khanna, R., Chang, M., Joiner, W., Kaczmarek, L., & Schlicter, L. (1999). hSK4/IK1, a calmodulin-binding KCa channel in human T lymphocytes. Roles in proliferation and volume regulation. *J Biol Chem, 274 (21)*, 14838-14849.

Khawaled, R., Bruening-Wright, A., Adelman, J., & Maylie, R. (1999). Bicuculline block of small conductance calcium-activated potassium channels. *Pflugers-Archives-European Journal of Physiology, 438*, 314-321.

Kim, D. (2003). Fatty acid-sensitive two-pore domain $K^+$ channels. *Trends Pharmacol Sci, 24 (12)*, 648-54.

Kimura, T., Takahashi, M., Fujimura, H., & Sakoda, S. (2003). Expression and distribution of a small conductance calcium-activated potassium channel (SK3) protein in skeletal muscle from myotonic muscular dystrophy patients and congenital myotonic mice. *Neuroscience Letters, 347 (3)*, 191-195.

Kitamura, K., Lian, O., Carl, A., & Kuriyama, H. (1993). S-nitrocysteine, but not nitroprusside, produces an apamin-sensitive hyperpolarization in rat gastric fundus. *British Journal of Pharmacology, 109 (2)*, 415-423.

Klemm, M., & Rang, R. (2002). Distribution of $Ca^{2+}$-activated $K^+$ channel (SK2 and SK3) immunoreactivity in intestinal smooth muscles of the guinea-pig.

*Clin Exp Pharmcaol Physiol, 29 (1-2)*, 18-25.

Koh, S., Monaghan, K., Sergeant, G., Ro, S., Walker, R., Sanders, K., et al. (2001). TREK-1 regulation by nitric oxide and cGMP-dependent protein kinase. An essential role in smooth muscle inhibitory neurotransmission. *Journal of Biological Chemistry, 276*, 44338-44346.

Kohler, M., Hirschberg, B., Bond, C., Kinzie, J., Marrion, N., Maylie, J., et al. (1996). Small conductance, calcium-activated potassium channels from mammalian brain. *Science, 273*, 1709-14.

Kubisch, C., Schroeder, B., Friedrich, T., Lutjohann, B., El-Amraouui, A., Marlin, S., et al. (1999). KCNQ4, a novel potassium channel expressed in sensory outer hair cells, is mutated in dominant deafness. *Cell, 96 (3)*, 437-446.

Kubo, Y., Baldwin, T., Jan, Y., & Jan, L. (1993). Primary structure and functional expression of a mouse inward rectifier potassium channel. *Nature, 362*, 127-33.

Kubokawa, M., McNicholas, C., Higgins, M., Wang, W., & Giebisch, G. (1995). Regulation of ATP-sensitive $K^+$ channels by membrane-bound protein phosphatases in rat principal tubule cells. *American Journal of Physiology, 269 (3 Pt 2)*, F355-F362.

Lalik, P., Krafte, D., Volberg, W., & Cicarelli, R. (1993). Characterization of an endogenous sodium channel gene expressed in Chinese hamster ovary cells. *American Journal of Physiology, 264 (4 Pt1)*, 803-809.

Lancaster, B., & Adams, P. (1986). Calcium-dependent current generating the afterhyperpolarization of hippocampal neurones. *Journal of Neurophysiology, 55*, 1268-82.

Lancaster, B., Nicoll, R., & Perkel, D. (1991). Calcium activates two types of potassium channels in rat hippocampal neurones in culture. *The Journal of Neuroscience, 11(1)*, 23-30.

Latorre, R., Oberhauser, A., Labarca, P., & Alvarez, O. (1989). Varieties of calcium-activated potassium channels. *Annual Reviews of Physiology, 51*, 385-399.

LeDoux, J. (2003). The emotional brain, fear, and the amygdala. *Cell Mol Neurobiol, 23 (4-5)*, 727-738.

Lee, W., Ngo-Anh, T., Bruening-Wright, A., Maylie, J., & Adelman, J. (2003). Small conductance $Ca^{2+}$-activated $K^+$ channels and calmodulin: Cell surface expression and gating. *Journal of Biological Chemistry, 278 (28)*, 25940-25946.

Lesage, F., Guillemare, E., Fink, M., Duprat, F., Lazdunski, M., & Romey, B. J., G. (1996). TWIK-1, a ubiquitous human weakly inward rectifying $K^+$ channel with a novel structure. *EMBO journal, 15*, 1004-1011.

Leveque, C., El Far, O., Martin-Moutot, N., Sato, K., Kato, R., Takahashi, M., et al. (1994). Purification of the N-type calcium channel associated with syntaxin and synaptotagmin. A complex implicated in synaptic vesicle exocytosis. *Journal of Biological Chemistry, 269 (9)*, 6306-6312.

Leveque, C., Marqueze, B., Couraud, F., & Seagar, M. (1990). Polypeptide components of the apamin receptor associated with a calcium-activated potassium channel. *FEBS Letters, 275*, 185-189.

Levy, R., Dostrovsky, J., Lang, A., Sime, E., Hutchison, W., & Lozano, A. (2001). Effects of apomorphine on subthalamic nucleus and globus pallidus internus neurones in patients with Parkinson's disease. *Journal of Neurophysiology, 86*

*(1)*, 249-260.

Levy, R., Hutchison, W., Lozano, A., & Dostrovsky, J. (2000). High-frequency synchronization of neuronal activity in the subthalamic nucleus of Parkinsonian patients with limb tremor. *Journal of Neuroscience, 20 (20)*, 7766-7775.

Lewis, R., & Cahalan, M. (1995). Potassium and calcium channels in lymphocytes. *Annu Rev Immunology, 13*, 623-653.

Li-Smerin, Y., Hackos, D., & Swatz, K. (2000). A localized interaction surface for voltage-sensing domains on the pore domain of a $K^+$ channel. *Neuron, 25*, 411-423.

Liu, C., Au, J., Zou, H., Cotton, J., & Yost, C. (2004). Potent activation of the human tandem pore domain $K^+$ channel TRESK with clinical concentrations of volatile anesthetics. *Anesth Analg, 99 (6)*, 1715-1722.

Liu, Y., Jurman, M., & Yellen, G. (1996). Dynamic rearrangement of the outer mouth of a $K^+$ channel during gating. *Neuron, 16 (4)*, 859-867.

Logsdon, N., Kang, J., Togo, J., Christian, E., & Aiyar, J. (1997). A novel gene, hKCa4, encodes the calcium-activated potassium channel in human T lymphocytes. *J Biol Chem, 272 (52)*, 32723-32726.

Lopez-Barneo, J., Hoshi, T., Heineman, S., & Aldrich, B. (1993). Effects of external cations and mutations in the pore region on C-type inactivation of Shaker potassium channels. *Receptor Channels, 1 (1)*, 61-71.

Lu, Z., & MacKinnon, R. (1994). Electrostatic tuning of $Mg^{2+}$ affinity in an inward-rectfier $K^+$ channel. *Nature, 371*, 243-245.

Lukyanetz, E., Shkryl, V., & Kostyuk, P. (2002). Selective blockade of N-type calcium channels by levetiracetam. *Epilepsia, 43 (1)*, 9-18.

Luzhkov, V., & Aqvist, J. (2001). Mechanisms of tetraethylammonium ion block in the KcsA potassium channel. *FEBS Letters, 495*, 191-6.

MacKinnon, R. (1991). Determination of the subunit stoichiometry of a voltage-activated potassium channel. *Nature, 350*, 232-235.

MacKinnon, R. (2003). Potassium channels. *FEBS Lettters, 555 (1)*, 62-65.

MacKinnon, R., & Miller, C. (1988). Mechanism of charybdotoxin block of the high conductance $Ca^{2+}$-activated $K^+$ channel. *J General Physiology, 91*, 335-49.

MacKinnon, R., & Miller, C. (1989). Mutant potassium channels with altered binding of charybdotoxin, a pore-blocking peptide inhibitor. *Science, 245 (4924)*, 1382-1385.

MacKinnon, R., & Yellen, G. (1990). Mutations affecting TEA blockade and ion permeation in voltage-activated $K^+$ channels. *Science, 250 (4978)*, 276-279.

Maingret, F., Patel, A., Lesage, F., Lazdunski, M., & Honore, E. (2000). Lysophospholipids open the two-pore domain mechano-gated $K^+$ channels TREK-1 and TRAAK. *Journal of Biological Chemistry, 275 (14)*, 10128-10133.

Malik-Hall, M., Ganellin, R., Galanakis, D., & Jenkinson, D. (2000). Compounds that block both intermediate-conductance (IK(Ca)) and small conductance (SK(Ca)) calcium-activated potassium channels. *British Journal of Pharmacology, 129 (7)*, 1431-1438.

Manabe, I., Tsuboi, M., Ahmmed, G., Sasaki, N., Ohtahara, A., Yamamoto, Y., et al. (1998). Expression of Shaker-type voltage-gated potassium channel genes in the guinea-pig. *Res Commun Mol Pathol Pharmacol, 99 (1)*, 33-40.

Manor, D., & Moran, N. (1994). Modulation of small conductance calcium-activated potassium channels in C6 glioma cells. *Journal of Membrane Biology, 140*, 69-79.

Martell, A., & Smith, R. (1976). *Critical stability constants. Volume 4: Inorganic complexes* (2nd ed.). Plenum Press.

Martins, J., Van de Ven, F., & Borremans, F. (1995). Determination of the three-dimensional solution structure of scyllatoxin by 1H nuclear magnetic resonance. *Journal of Molecular Biology, 253 (4)*, 590-603.

Martins, J., Zhang, W., Tartar, A., Lazdunski, M., & Borremans, F. (1990). Solution conformation of leiurotoxin I (scyllatoxin) by 1H nuclear magnetic resonance. Resonance assignment and secondary structure. *FEBBS Letters, 260 (2)*, 249-253.

Marty, A. (1989). The physiological role of calcium-dependent channels. *Trends in Neuroscience, 12*, 420–5.

Matsuda, S., & Koyasu, S. (2000). Mechanisms of action of cyclosporine. *Immunopharmacology, 47 (2-3)*, 119-125.

Maylie, B., Bissonnette, E., Virk, M., Adelman, J., & Maylie, J. (2002). Episodic ataxia type 1 mutations in the human Kv1.1 potassium channel alter hKv beta 1-induced N-type inactivation. *Journal of Biological Chemistry, 22 (12)*, 4786-93.

McManus, O., Helms, L., Pallanck, L., Ganetzky, B., Swanson, R., & Leonard, R. (1995). Functional role of the beta subunit of high conductance calcium-activated potassium channels. *Neuron, 14 (3)*, 645-650.

Meadows, H., & Randall, A. (2001). Functional characterization of human TASK-3, an acid-sensitive two-pore domain potassium channel. *Neuropharmacology, 40*, 551-559.

Mhatre, A., Li, J., Chen, A., Yost, C., Smith, R., Kindler, C., et al. (2004). Genomic structure, cochlear expression, and mutation screening of KCNK6, a candidate gene for DFNA4. *J Neurosci Res, 75 (1)*, 25-31.

Miller, C. (1988). Competition for block of a $Ca^{2+}$-activated $K^+$ channel by charybdotoxin and tetraethylammonium. *Neuron, 1*, 1003-6.

Miller, M., Rauer, H., Tomita, H., Rauer, H., Gargus, J., Gutman, G., et al. (2001). Nuclear localization and dominant-negative suppression by a mutant SKCa3 N-terminal channel fragment identified in a patient with schizophrenia. *Journal of Biol Chem, 276 (30)*, 27753-27756.

Minor, D., Lin, Y., Mobley, B., Avelar, A., Jan, Y., Jan, L., et al. (2000). The polar T1 interface is linked to conformational changes that open the voltage-gated potassium channel. *Cell, 102*, 657-670.

Mitsuda, H., Takii, Y., Iwami, K., & Yasumoto, K. (1975). Mechanism and regulation of thiamine pyrophosphokinase from parsely leaf. *Journal of Nutritional Science and Vitaminology (Tokyo), 21 (3)*, 189-198.

Molina, A., Castellano, A., & Lopez-Barneo, J. (1998). Pore mutations in Shaker $K^+$ channels distinguish between the sites of tetraethylammonium blockade and C-type inactivation. *Journal of Physiology, 499 (Pt 2)*, 361-367.

Monaghan, A., Benton, D., Bahia, P., Hosseini, R., Shah, Y., Haylett, D., et al. (2004). The SK3 subunit of small conductance Ca2+-activated K+ channels

interacts with both SK1 and SK2 subunits in a heterologous expression system. *Journal of Biological Chemistry, 279 (2)*, 1003-1009.

Nagayama, T., Koshika, T., Hisa, H., Kimura, T., & Satoh, S. (1997). Apamin-sensitive SK (Ca) channels modulate adrenal catecholamine release in anesthetized dogs. *European Journal of Pharmacology, 327 (2-3)*, 135-141.

Nakahira, K., Shi, G., Rhodes, K., & Trimmer, J. (1996). Selective interaction of voltage-gated $K^+$ channel beta-subunits with alpha-subunits. *Journal of Biological Chemistry, 271 (12)*, 7084-7089.

Nattie, E. (2001). Central chemosensitivity, sleep, and wakefulness. *Respir Phys, 129*, 257-268.

Navarro, B., Kennedy, M., Velimirovic, B., Bhat, D., Peterson, A., & Clapham, D. (1996). Nonselective and G beta gamma-insensitive weaver $K^+$ channels. *Science, 272 (5270)*, 1950-53.

Navon, R., Shamir, E., Dror, V., Ghanshani, S., Litmanovitch, T., Kimchi, R., et al. (1998). Strong association between schizophrenia and long CAG repeats in the hKCa3/KCNN3 gene, mapped to Iq21, among Israeli Jews. *American Journal of Human Genetics, 63 (suppl)*, A337.

Neelands, T., Herson, P., Jacobson, D., Adelman, J., & Maylie, J. (2001). Small conductance calcium-activated potassium currents in mouse hyperexcitable denervated skeletal muscle. *Journal of Physiology, 536 (Pt 2)*, 397-407.

Neely, A., & Lingle, C. (1992). Two components of calcium-activated potassium current in rat adrenal chromaffin cells. *Journal of Physiol (London), 453*, 97-131.

Nestorowicz, A., Inagaki, N., Gonoi, T., Schoor, K., Wilson, B., Glaser, B., et al. (1997). A nonsense mutation in the inward rectifier potassium channel gene, Kir6.2, is associated with familial hyperinsulinism. *Diabetes, 46 (11)*, 1743-1748.

Nestorowicz, A., Wilson, B., Schoor, K., Inoue, H., Glaser, B., Landau, H., et al. (1996). Mutations in the sulphonylurea receptor gene are associated with familial hyperinsulinism in Askenazi Jews. *Human Molecular Genetics, 5 (11)*, 1813-1822.

Nestrowicz, A., Glaser, B., Wilson, B., Shyng, S., Nichols, C., Stanley, C., et al. (1998). Genetic heterogeneity in familial hyperinsulinism. *Human Molecular Genetics, 7*, 1527.

Neyroud, N., Tesson, F., Denjoy, I., Leibovici, M., Donger, C., Barhanin, J., et al. (1997). A novel mutation in the potassium channel gene, KvLQT1 causes the Jervell and Lange-Nielsen cardioauditory syndrome. *Nature Genetics, 15 (2)*, 186-189.

Nichols, C., Ho, K., & Hebert, S. (1994). $Mg^{2+}$-dependent inward rectification of ROMK1 potassium channels expressed in *Xenopus* oocytes. *Journal of Physiology, 476*, 399-409.

Nichols, C., & Lopatin, A. (1997). Inward rectifier potassium channels. *Annu. Rev. Physiology, 59*, 171-191.

Nichols, C., Shyng, S., Nestorowicz, A., Glaser, A., & Clement, J. (1996). ADP as the intracellular regulator of insulin secretion. *Science, 272*, 1785-1787.

Noda, M., Shimizu, S., Tanabe, T., Takai, T., Kayano, T., Ikeda, T., et al. (1984).

Primary structure of the *Electrophorus electricus* sodium channel deduced from cDNA sequence. *Nature, 312*, 248-251.

Nohmi, M., & Kuba, K. (1984). Tubocurarine blocks calcium dependent $K^+$ channels of the bullfrog sympathetic ganglion cell. *Brain Research, 301*, 146-148.

North, R., & Tokimasa, T. (1983). Depression of the calcium-dependent potassium conductance of guinea-pig myenteric neurones by muscarinic antagonists. *Journal of Physiology, 342*, 253-66.

Ogden, D., Capiod, T., Walker, J., & Trentham, R. (1990). Kinetics of the conductance evoked by noradrenaline, inositol trisphosphate or $Ca^{2+}$ in guinea-pig isolated hepatocytes. *J of Physiol (Lond), 422*, 585-602.

Pacha, J., Vorlicek, J., & Teisinger, J. (1992). Identification of apamin binding sites in rat intestinal mucosa. *Life Sci, 51*, 423-9.

Pardo, L., Heinemann, H., Terlau, U., Ludewig, C., Lorra, O., Pongs, O., et al. (1992). Extracellular $K^+$ specifically modulates a rat brain $K^+$ channel. *Proc Natnl Acad Sci, USA, 89*, 2466-2470.

Park, C., & Miller, C. (1992). Mapping function to structure in a channel-blocking peptide: Electrostatic mutants of charybdotoxin. *Biochemistry, 31*, 7749-7755.

Park, C.-S., Hausdorff, S., & Miller, C. (1991). Design, synthesis and functional expression of a gene for chraybdotoxin, a peptide blocker for $K^+$ channels. *Proceedings of the Natinl Acad Sci, USA, 88*, 2046-50.

Park, Y. (1994). Ion selectivity and gating of small conductance $Ca^{2+}$-activated $K^+$ channels in cultured rat adrenal chromaffin cells. *Journal of Physiology, 481*, 555-570.

Patel, A., Honore, E., Lesage, F., Fink, M., Romey, G., & Lazdunski, M. (1999). Inhalation anesthetics activate two-pore-domain background $K^+$ channels. *Nature Neuroscience, 2*, 422-426.

Patel, A., Honore, E., Maingret, F., Lesage, F., Fink, M., Duprat, F., et al. (1998). A mammalian two pore domain mechano-gated S-like $K^+$ channel. *EMBO Journal, 17 (15)*, 4283-4290.

Patel, A., Maingret, F., Magnone, V., Fosset, M., Lazdunski, M., & Honore, E. (2000). TWIK-2, an inactivating 2P domain $K^+$ channel. *Journal of Biological Chemistry, 275*, 28722-28730.

Pedarzani, P., Kulik, A., Muller, M., Ballanyi, K., & Stocker, M. (2000). Molecular determinants of $Ca^{2+}$-dependent $K^+$ channel function in rat dorsal vagal neurones. *Journal of Physiology, 527 Pt2*, 283-290.

Pedarzani, P., Mosbacher, J., Rivard, A., Cingolani, L., Oliver, D., Stocker, M., et al. (2001). Control of electrical activity in central neurons by modulating the gating of small conductance $Ca^{2+}$-activated $K^+$ channels. *Journal of Biological Chemistry, 276 (13)*, 9762-9769.

Pennefather, P., Lancaster, B., Adams, P., & Nicoll, R. (1985). Two distinct $Ca^{2+}$-dependent $K^+$ currents in bullfrog sympathetic ganglion cells. *Proceedings of the National Acad Sci, USA, 82*, 3040-4.

Perozo, E., MacKinnon, R., Bezanilla, F., & Stefani, E. (1993). Gating currents from a nonconducting mutant reveal open-closed conformations in Shaker $K^+$ channels. *Neuron, 11*, 353-358.

Pessia, M., Tucker, S., Lee, K., Bond, C., & Adelman, J. (1996). Subunit positional

effects revealed by novel heteromeric inwardly rectifying $K^+$ channels. *EMBO Journal, 15*, 2980-2987.

Plaster, N., Tawil, R., Tristani-Firouzi, M., Canun, S., Bendahou, S., Tsunode, A., et al. (2002). Mutations in $K_{ir}2.1$ cause the developmental and episodic electrical phenotypes of Andersen's syndrome. *Cell, 105*, 511-519.

Preisig-Muller, R., Schlichthorl, G., George, T., Heinen, S., Bruggeman, A., Rajan, S., et al. (2002). Heteromerization of $K_{ir}2.x$ potassium channels contribute to the phenotype of Andersen's syndrome. *Proceedings of the National Academy of Science, USA, 99*, 7774-7779.

Pribnow, D., Johnson-Pais, T., Bond, C., Keen, J., Johnson, R., Janowsky, A., et al. (1999). Skeletal muscle and small conductance calcium-activated potassium channels. *Muscle Nerve, 22 (6)*, 742-750.

Prosser, R., Heller, H., & Miller, J. (1994). Serotonergic phase advances of the mammalian circadian clock involve protein kinase A and $K^+$ channel opening. *Brain Research, 644 (1)*, 67-73.

Rajan, S., Wischmeyer, E., Xin, L., Preisig-Muller, R., Grzeschik, K., Daut, J., et al. (2000). THIK-1 and THICK-2, a novel subfamily of tandem pore domain $K^+$ channels. *Journal of Biological Chemistry, 275*, 16650-16657.

Ramirez, B., Behrens, M., & Vergara, C. (1996). Neural control of the expression of a $Ca^{2+}$-activated $K^+$ channel involved in the induction of myotonic-like characteristics. *Cell Mol Neurobiol, 16 (1)*, 39-49.

Ranganathan, R., Lewis, J., & MacKinnon, R. (1996). Spatial localization of the $K^+$ channel selectivity filter by mutant cycle-based structure analysis. *Neuron, 16 (1)*, 131-139.

Rauer, R., Lanigan, M., Pennington, M., Aiyar, J., Ghanshani, S., Cahalan, M., et al. (2000). Structure guided transformation of charybdotoxin yields an analog that selectively targets $Ca^{2+}$-activated over voltage-gated $K^+$ channels. *J Biol Chem, 275*, 1202-8.

Reddy, P., & Housman, D. (1997). The complex pathology of trinucleotide repeats. *Current Opinion in Cell Biology, 9/3*, 364-372.

Reid, G., & Flonta, M. (2001). Cold transduction by inhibition of a background potassium conductance in rat primary sensory neurones. *Neuroscience Letters, 297*, 171-174.

Rekling, J., Funk, G., Bayliss, D., Dong, X., & Feldman, J. (2000). Synaptic control of motoneuronal excitability. *Physiol Reviews, 80*, 399-410.

Rettig, J., Sheng, Z., Kim, D., Hodson, C., Snutch, T., & Catterall, W. (1996). Isoform-specific interaction of the alpha 1A subunits of brain $Ca^{2+}$ channels with the presynaptic proteins syntaxin and SNAP-25. *Proc Natl Acad Sci USA, 93 (14)*, 7363-7368.

Ribalet, B., John, S., & Weiss, J. (2000). Regulation of cloned ATP-sensitive $K^+$ channels by phosphorylation, MgADP, and phosphatidylinositol bisphosphate ($PIP_2$): a study of channel rundown and reactivation. *Journal of General Physiology, 116 (3)*, 391-410.

Richter, T., Dvoryanchikov, G., Choudhari, N., & Roper, S. (2004). Acid-sensitive two-pore domain potassium (K2P) channels in mouse taste buds. *J Neurophysiol, 92 (3)*, 1928-36.

Roman, R., Feranchak, A., Troetsch, M., Dunkelberg, J., Kilic, G., Schlenker, T., et al. (2002). Molecular characterization of volume-sensitive $SK_{Ca}$ channels in human liver cell lines. *American Journal of Physiology. Gastrointestinal Liver Physiology, 282*, G116-G122.

Roncarati, R., Di Chio, M., Sava, A., Terstappen, G., & Fumagalli, G. (2001). Presynaptic localization of the small conductance calcium-activated potassium channel SK3 at the neuromuscular junction. *Neuroscience, 104 (1)*, 253-262.

Rosa, J., Galankis, D., Ganellin, C., Dunn, P., & Jenkinson, D. (1998). Bis-quinolinium cyclophanes: 6,10-diaza-3(1,3),8(1,4)-dibenzena-1,5(1,4)-diquinolinacyclodecaphane (UCL 1684), the first nanomolar, non-peptidic blocker of the apamin-sensitive $Ca^{2+}$-activated $K^+$ channel. *Journal of Medicinal Chemistry, 41 (1)*, 2 -5.

Roux, B., & MacKinnon, R. (1999). The cavity and pore helices in the KcsA $K^+$ channel: Electrostatic stabilization of monovalent cations. *Science, 285*, 100–102.

Sah, P. (1995). Properties of channels mediating the apamin-insensitive afterhyperpolarization in vagal motoneurones. *J Neuroscience, 74*, 1772-76.

Sah, P. (1996). $Ca^{2+}$-activated $K^+$ currents in neurones: Types, physiological roles, and modulation. *Trends in Neuroscience, 19*, 150-154.

Sah, P., & Davies, P. (2000). Calcium-acivated potassium currents in mammalian neurons. *Clinical and experimental pharmacology and physiology, 27*, 657-663.

Sah, P., & Isaacson, J. (1995). Channels underlying the slow afterhyperpolarization in hippocampal pyramidal neurones: Neurotransmitters modulate the open probablility. *Neuron, 15 (2)*, 435-441.

Sailer, C., Hu, H., Kaufmann, W., Trieb, M., Schwarzer, C., Storm, J., et al. (2002). Regional differences in distribution and functional expression of small-conductance $Ca^{2+}$-activated $K^+$ channels in rat brain. *Journal of Neuroscience, 22 (22)*, 9698-9707.

Sakura, H., Ammala, C., Smith, P., Gribble, F., & Aschcroft, F. (1995). Cloning and functional expression of the cDNA encoding a novel ATP-sensitive potassium channel subunit expressed in pancreatic beta-cells, brain, heart and skeletal muscle. *FEBS Letters, 377*, 338-44.

Sanguinetti, M., Curran, M., Zou, A., Shen, J., Spector, P., Atkinson, D., et al. (1996). Coassembly of K(V)LQT1 and minK (IsK) proteins to form the cardiac I(Ks) potassium channel. *Nature, 384 (6604)*, 80-83.

Satler, C., Vesely, M., Duggal, P., Ginsburg, G., & Beggs, A. (1998). Multiple different missense mutations in the pore region of hERG in patients with long QT syndrome. *Human Genetics, 102 (3)*, 265-272.

Savic, N., Pedarzani, P., & Sciancalepore, M. (2001). Medium afterhyperpolarization and firing pattern modulation in interneurons of stratum radiatum in the CA3 hippocampal region. *Journal of Neurophysiology, 85 (5)*, 1986-1997.

Schetz, J., & Anderson, P. (1995). Pharmacology of the high-affinity apamin receptor in rabbit heart. *Cardiovascular Research, 30 (5)*, 755-762.

Schlichter, L., Pahapill, P., & Schumacher, P. (1993). Reciprocal regulation of $K^+$ channels by $Ca^{2+}$ in intact human T lymphocytes. *Receptors Channels, 1 (3)*, 201-215.

Schmid-Antomarchi, H., Hugues, M., Norman, R., Ellory, C., Borsotto, M., & Lazdunski, M. (1984). Molecular properties of the apamin-binding component of the $Ca^{2+}$-activated $K^+$ channel. Radiation-inactivation, affinity labelling and solubilization. *European J of Biochemistry, 142*, 1-6.

Schmid-Antomarchi, H., Renaud, J., Romey, G., Hugues, M., Schmid, A., & Lazdunski, M. (1985). The all-or-none role of innervation in expression of apamin receptor and of apamin-sensitive $Ca^{2+}$-activated $K^+$ channel in mammalian skeletal muscle. *Proc Natl Acad Sci USA, 82 (7)*, 2188-2191.

Schroeder, B., Kubisch, C., Stein, V., & Jentsch, T. (1998). Moderate loss of function of cyclicAMP-modulated KNCQ2/KCNQ3 $K^+$ channels causes epilepsy. *Nature, 396 (6712)*, 687-690.

Schumacher, M., Rivard, A., Bachinger, H., & Adelman, J. (2001). Structure of the gating domain of a $Ca^{2+}$-activated $K^+$ channel complexed with $Ca^{2+}$/calmodulin. *Nature, 410*, 1120-24.

Schwalbe, R., Bianchi, L., Accili, E., & Brown, A. (1998). Functional consequences of ROMK mutants linked to Bartter's syndrome and implications for treatment. *Human Molecular Genetics, 7 (6)*, 975-980.

Schwindt, P., Spain, W., Foehring, R., Stafstrom, C., Shubb, M., & Crill, W. (1988). Multiple $K^+$ conductances and their functions in neurones from cat sensorimotor cortex *in vitro*. *Journal of Neurophysiology, 59*, 424-49.

Seagar, M., Deprez, P., Martin-Moutot, N., & Couraud, F. (1987). Detection and photoaffinity labeling of the $Ca^{2+}$-activated $K^+$ channel-associated apamin receptor in cultured astrocytes from rat brain. *Brain Research, 411 (2)*, 226-30.

Seagar, M., Labbe-Jullie, C., Granier, C., Goll, A., Glossmann, H., Van Ritschotten, J., et al. (1986). Molecular structure of rat brain apamin receptor : Differential photoaffinity labelling of putative potassium channel subunits and target size analysis. *Biochemistry, 25*, 4051-57.

Seagar, M., Labbe-Jullie, C., Granier, C., Van Rietschoten, J., & Couraud, P. (1985). Photoaffinity labelling of components of the apamin sensitive $K^+$ channel in neuronal membranes. *J Biol Chem, 260*, 3895-98.

Shah, M., & Haylett, D. (2000). The pharmacology of hSK1 $Ca^{2+}$-activated $K^+$ channels expressed in mammalian cell lines. *Br J of Pharmacology, 129*, 627-30.

Shakkottai, V., Regaya, I., Wulf, H., Fajloun, Z., Tomita, H., Fathallal, M., et al. (2001). Design and characterization of a highly selective inhibitor of the small conductance calcium-activated potassium channel. *Journal of Biol Chemistry, 276 (46)*, 43145-43151.

Shindo, M., Imai, Y., & Sohma, Y. (2000). A novel type of ATP block on a $Ca^{2+}$-activated $K^+$ channel from bullfrog erythrocytes. *Biophysical Journal, 79*, 287-97.

Simon, D., Karet, F., Rodriguez-Soriano, J., Hamdan, J., DiPietro, A., Trachtman, H., et al. (1996). Genetic heterogeneity of Bartter's syndrome revealed by mutations in the $K^+$ channel, ROMK. *Nature Gen, 14 (2)*, 152-156.

Simon, D., & Lifton, R. (1998). Ion transporter mutations in Gitelman's and Bartter's syndrome. *Curr Opin Nephrol Hypertens, 7 (1)*, 43-47.

Sirois, J., Lei, Q., Talley, E., Lynch, C., & Bayliss, D. (2000). Multiple ionic mechanisms mediate inhibition of rat motoneurones by inhalation anesthetics. *Journal of Physiology (London), 512*, 851-862.

Slesinger, P., Patil, N., Liao, Y., Jan, Y., Jan, L., & Cox, D. (1996). Functional effects of the mouse weaver mutation on G protein-gated inwardly rectifying $K^+$ channels. *Neuron, 16*, 321-31.

Smith, P., Baukrowitz, T., & Yellen, G. (1996). The inward rectification mechanism of the HERG cardiac potassium channel. *Nature, 379*, 833.

Soh, H., & Park, C. (2002). Localization of divalent cation binding site in the pore of a small conductance $Ca^{2+}$-activated $K^+$ channel and its role in determining current-voltage relationship. *Biophys J, 83 (5)*, 2528-2538.

Soh, H., & Park, C.-S. (2001). Inwardly rectifying current-voltage relationship of small conductance $Ca^{2+}$-activated $K^+$ channels rendered by intracellular divalent cation blockade. *Biophysical Journal, 80*, 2207-2215.

Spassova, M., & Lu, Z. (1998). Coupled ion movement underlies rectification in an inward-rectifier $K^+$ channel. *J Gen Physiology, 112*, 211-221.

Splawski, I., Tristani-Firouzi, M., Lehmann, M., Sanguinetti, M., & Keating, M. (1997). Mutations in the hminK gene cause long QT syndrome and suppress IKs function. *Nature Gen, 17 (3)*, 338.

Splitt, H., Meuser, D., Borovok, I., Betzler, M., & Schrempf, H. (2000). Pore mutations affecting tetrameric assembly and functioning of the potassium channel KcsA from *Streptomyces lividans. FEBS Letters, 472*, 83-7.

Spreadbury, I., Kros, C., & Meech, R. (2004). Effects of trypsin on large-conductance $Ca^{2+}$-activated $K^+$ channels of guinea-pig outer hair cells. *Hair research, 190 (1-2)*, 115-127.

Stephenson, R., & Clarke, S. (1989). Succinimide formation from aspartyl and asparaginyl peptides as a model for the spontaneous degradation of proteins. *J Biological Chem, 264 (11)*, 6164-70.

Stocker, M. (2004). $Ca^{2+}$-activated $K^+$ channels: Molecular determinants and function of the SK family. *Nature Reviews Neuroscience, 5*, 758 -770.

Stocker, M., Krause, M., & Pederzani, P. (1999). An apamin-sensitive $Ca^{2+}$-activated $K^+$ current in hippocampal pyramidal neurones. *Proc National Acad Sciences, USA, 96*, 4662-7.

Stocker, M., & Pedarzani, P. (2000). Differential distribution of three apamin-sensitive $Ca^{2+}$-activated $K^+$ channel subunits, SK1, SK2, and SK3 in the adult rat central nervous system. *J Neurosci, 15*, 476-493.

Storm, J. (1989). An after-hyperpolarization of medium duration in rat hippocampal pyramidal cells. *J of Physiol (London), 409*, 171-190.

Strobaek, D., Jorgensen, T., Christophersen, P., Ahring, P., & Olsen, S. (2000). Pharmacological characterization of small conductance $Ca^{2+}$-activated $K^+$ channels expressed in HEK 293 cells. *Br J Pharmacology, 129*, 991-999.

Stuhmer, W., Ruppersberg, J., Schroter, K., Sakmann, B., Stocker, M., Giese, K., et al. (1989). Molecular basis of functional diversity of voltage-gated potassium channels in mammalian brain. *EMBO J, 8 (11)*, 3235-3244.

Svensson, T. (2000). Dysfunctional brain dopamine systems induced by psychotomimetic NMDA–receptor antagonists and the effects of anti-psychotic

drugs. *Brain Research Rev, 31*, 320-39.

Tacconi, S., Carletti, R., Bunnemann, B., Plumpton, C., Merlo Pich, E., & Terstappen, G. (2001). Distribution of the messenger RNA for the small conductance calcium-activated potassium channel SK3 in the adult brain and correlation with immunoreactivity. *Neuroscience, 102 (1)*, 209-215.

Takanashi, H., Sawanobori, T., Kamisaka, K., Maezawa, H., & Hiraoka, M. (1992). $Ca^{2+}$-activated $K^+$ channel is present in guinea-pig but lacking in rat hepatocytes. *Jpn J of Physiology, 42 (3)*, 415-430.

Takumi, T., Ohkubo, H., & Nakanishi, S. (1988). Cloning of a membrane protein that induces a slow voltage-gated potassium current. *Science, 242 (4881)*, 1042-1045.

Talley, E., Lei, Q., Sirois, J., & Bayliss, D. (2000). TASK-1, a two-pore domain $K^+$ channel, is modulated by multiple neurotrnsmitters in motoneurones. *Neuron, 25*, 399-410.

Talley, E., Solorzano, G., Lei, Q., Kim, D., & Bayliss, D. (2001). CNS distribution of members of the two-pore-domain (KCNK) potassium channel family. *J Neurosci, 21*, 7491-7505.

Tawil, R. (1994). Andersen's syndrome: Potassium-sensitive periodic paralysis, ventricular ectopy, dysmorphic features. *Ann. Neurology, 35*, 326-330.

Teshima, K., Kim, S., & Allen, C. (2003). Characterization of an apamin-sensitive potassium current in suprachiasmatic nucleus neurones. *Neuroscience, 120 (1)*, 65-73.

Thomas, P., Cote, G., Wohlick, N., Haddad, B., Mathew, P., Rabl, W., et al. (1995). Mutations in the sulfonylurea receptor gene in familial persistent hyperinsulinemic hypoglycemia of infancy. *Science, 268*, 426-429.

Thomas, P., Ye, Y., & Lightner, E. (1996). Mutation of the pancreatic islet inward rectifier $K_{ir}6.2$ also leads to familial persistent hyperinsulinemic hypoglycemia of infancy. *Human Molecular Genetics, 5 (11)*, 1809-1812.

Thompson, J., & Begenisich, T. (2000). Electrostatic interaction between charybdotoxin and a tetrameric mutant of Shaker $K^+$ channels. *Biophysical J, 78*, 2382-91.

Timpe, L., Schwarz, T., Tempel, B., Papazian, D., Jan, Y., & Jan, L. (1988). Expression of functional potassium channels from Shaker cDNA in *Xenopus* oocytes. *Nature, 331 (6152)*, 143-145.

Tomita, H., Shakkottai, V., Gutman, G., Sun, G., Bunney, W., Cahalan, M., et al. (2003). Novel truncated isoform of SK3 potassium channel is a potent dominant-negative regulator of SK currents: Implications in schizophrenia. *Mol Psychiatry, 8 (5)*, 524-535.

Tsien, R. (1989). Measurement of cytosolic free calcium with Quinn 2. *Methods in Enzymology, 172*, 256-262.

Tu, L., & Deutsch, C. (1999). Evidence for dimerization of dimers in $K^+$ channel activity. *Biophysics Journal, 76 (4)*, 2004-2017.

Ukomadu, C., Zhou, J., Sigworth, F., & Agnew, W. (1992). Mu1 $Na^+$ channels expressed in human embyonic kidney cells: Biochemical and biophysical properties. *Neuron, 8/4*, 663-676.

Vandenberg, C. (1987). Inward rectification of a potassium channel in cardiac

ventricular cells depends on internal magnesium ions. *Proc Natl Acad Sci USA, 84 (8)*, 2560-2564.

Vasilyev, A., Indyk, E., & Rakowski, R. (2002). Properties of a sodium channel (Na(x)) activated by strong depolarization of *Xenopus* oocytes. *Journal of Membrane Biology, 185 (3)*, 237-247.

Vergara, C., Latorre, R., Marrion, N., & Adelman, J. (1998). Calcium-activated potassium channels. *Current Opinion in Neurobiology, 8*, 321-29.

Vergara, C., Ramirez, B., & Behrens, M. (1993). Colchicine alters apamin receptors, electrical activity, and skeletal muscle relaxation. *Muscle Nerve, 16 (9)*, 935-940.

Vergara, L., Rojas, E., & Stojilkovic, S. (1997). A novel calcium-activated apamin-insensitive potassium current in pituitary gonadotrophs. *Endocrinology, 138*, 2658-64.

Viana, F., De La Pena, E., & Belmonte, C. (2002). Specificity of cold thermotransduction is determined by different ionic channel expression. *Nat Neuroscience, 5*, 254-260.

Vincent, J., Schweitz, H., & Lazdunski, M. (1975). Structure-function relationships and site of action of apamin, a neurotoxic polypeptide of bee venom with an action on the central nervous system. *Biochemistry, 14 (11)*, 2521-25.

Wadsworth, J., Doorty, K., & Strong, P. (1994). Comparable 30 kDa apamin binding polypeptides may fulfill equivalent roles within putative subtypes of small conductance $Ca^{2+}$-activated $K^+$ channels. *J Biol Chem, 269*, 18053-61.

Wadsworth, J., Torelli, S., Doorty, K., & Strong, P. (1997). Structural diversity among subtypes of small-conductance $Ca^{2+}$-activated $K^+$ channels. *Arch Biochem Biophys, 346*, 151-60.

Wagner, P., & Wu, N.-D. (1990). Regulation of norepinephrine secretion in permeabilized PC12 cells by $Ca^{2+}$-stimulated phosphorylation. *The Journal of Biological Chemistry, 265/18*, 10352-10357.

Wang, Q., Curran, M., Splawski, I., Burn, T., Millholland, J., VanRaay, T., et al. (1996). Positional cloning of a novel potassium channel gene : KvLQT1 mutations cause cardiac arrhythmias. *Nature Genetics, 12 (1)*, 17-23.

Ward, S., Dalziel, H., Thornbury, K., Westfall, D., & Sanders, K. (1992). Noradrenergic, noncholinergic inhibition and rebound excitation in canine colon depend on nitric oxide. *American Journal of Physiology, 262*, G237-G243.

Washburn, C., Sirois, J., Talley, E., Guyenet, P., & Bayliss, D. (2002). Serotonergic raphe neurones express TASK chnnel transcripts and a TASK-like pH and halothane-sensitive $K^+$ conductance. *Journal of Neuroscience, 22*, 1256-1265.

Watson, M., Bywater, R., Taylor, G., & Lang, R. (1996). Effects of nitric oxide (NO) and NO donors on the membrane conductance of circular smooth muscle cells of the guinea-pig proximal colon. *British Journal of Pharmacology, 118*, 1605-1614.

Weller, M. (1979). The time course of the phosphorylation of proteins in the synaptic plasma membrane and the effect of certain cations. *Molecular Cell Biochemistry, 27 (2)*, 71-78.

Wible, B., Yang, Q., Kuryshev, Y., Accili, E., & Brown, A. (1998). Cloning and expression of a novel $K^+$ channel regulatory protein, KChaP. *Journal of*

*Biological Chemistry, 273 (19)*, 11745-51.

Wiener, K., Klaerke, D., & Jorgensen, P. (1990). Rabbit distal colon epithelium: III. $Ca^{2+}$-activated $K^+$ channels in basolateral plasma membrane vesicles of surface and crypt cells. *J Membrane Biology, 117*, 275-283.

Williams, A., West, D., & Sitsapesan, R. (2001). Light at the end of the $Ca^{2+}$ tunnel: Structures and mechanisms involved in ion translocation in ryanodine receptor channels. *Q Rev Biophys, 34 (1)*, 61-104.

Williams, T., Kelley, C., Lang, R., Kotz, D., Campbell, J., Elber, G., et al. (1999, Oct). *Gnuplot.* (Das Programm)

Wissmann, R., Bildl, W., Neumann, H., Rivard, A., Klocker, N., Weitz, D., et al. (2002). A helical region in the C-terminus of small conductance $Ca^{2+}$-activated potassium channels controls assembly with apo-calmodulin. *The Journal of Biological Chemistry, 277 (6)*, 4558-4564.

Wolfart, J., Neuhoff, H., Franz, O., & Roeper, J. (2001). Differential expression of the small conductance, calcium-activated potassium channel SK3 is critical for pacemaker control of dopaminergic midbrain neurons. *J Neurosc, 21*, 3443-3456.

Wolfart, J., & Roeper, J. (2002). Selective coupling of T-type calcium channels to SK potassium channels prevents intrinsic bursting in dopaminergic midbrain neurons. *Journal of Neuroscience, 22 (9)*, 3404-3413.

Woodhull, A. (1973). Ionic blockage of sodium channels in nerve. *Journal of General Physiology, 61*, 687-708.

Wrisch, A., & Grissmer, S. (2000). Structural differences of bacterial and mammalian $K^+$channels. *J Biological Chemistry, 275 (50)*, 39345-53.

Wu, L., Bauer, C., Zhen, X., Xie, C., & Yang, J. (2002). Dual regulation of voltage-gated calcium channels by PtdIns(4,5)P2. *Nature, 419 (6910)*, 947-952.

Xia, X.-M., Fakler, B., Rivard, A., Wayman, G., Johnson-Pais, T., Keen, J., et al. (1998). Mechanism of calcium gating in small conductance calcium-activated potassium channels. *Nature, 395*, 503-507.

Xie, L.-H., Takano, M., Kakei, M., Okamura, M., & Noma, A. (1999). Wortmannin, an inhibitor of phosphatidylinositol kinases, blocks the MgATP-dependent recovery of Kir6.2/SUR2a channels. *J of Physiology, 514*, 655-665.

Xu, J., Hao, L., Kameyama, A., & Kameyama, M. (2004). Calmodulin reverses rundown of L-type Ca(2+) channels in guinea pig ventricular myocytes. *Am J Physiol Cell Physiol., 287 (6)*, C1717-C1724.

Xu, J., & Li, M. (1998). Auxiliary subunits of Shaker-type potassium channels. *Trends in Cardiovascular Medicine, 8 (5)*, 229-234.

Yamamoto, Y., Kummer, W., Atoji, Y., & Suzuki, Y. (2002). TASK-1, TASK-2, TASK-3 and TRAAK immunoreactivities in the rat carotid body. *Brain Research, 950 (1-2)*, 304-307.

Yang, Y., Yan, Y., & Sigworth, F. (1997). How does the W434F mutation block current in *Shaker* potassium channels. *J General Physiol, 109*, 779-89.

Yellen, G., Sodickson, D., Chen, T.-Y., & Jurman, M. (1994). An engineered cysteine in the external mouth of a $K^+$ channel allows inactivation to be modulated by metal binding. *Biophys. Journal, 66*, 1068-1075.

Yokoyama, S., Imoto, K., Kawamura, T., Higashida, H., Iwabe, N., Miyata, T., et

al. (1989). Potassium channels from NG108-15 neuroblastoma-glioma hybrid cells. Primary structure and functional expression from cDNAs. *FEBS Letters, 259 (1)*, 37-42.

Yool, A., & Schwarz, T. (1991). Alteration of ionic selectivity of a $K^+$ channel by mutation of the H5 region. *Nature, 349*, 700-704.

Yu, S., & Kerchner, G. (1998). Endogenous voltage-gated potassium channels in human embryonic kidney (HEK 293) cells. *Journal of Neuroscience Research, 52 (5)*, 612-617.

Zeilhofer, H., Blank, N., Neuhuber, W., & Swandulla, D. (2000). Calcium-dependent inactivation of neuronal calcium channel currents is independent of calcineurin. *Neuroscience, 95 (1)*, 235-241.

Zeniou, M., Ding, T., Trivier, E., & Hanauer, A. (2002). Expression analysis of RSK gene family members: The RSK2 gene, mutated in Coffin-Lowry syndrome, is prominently expressed in brain structures essential for cognitive function and learning. *Human Mol Genetics, 11 (23)*, 2929-2940.

Zhou, M., & MacKinnon, R. (2004). A mutant KcsA $K^+$ channel with altered conduction properties and selectivity filter ion distribution. *Journal of Molecular Biology, 338 (4)*, 839-846.

Zhu, G., Zhang, Y., Xu, H., & Jiang, C. (1998). Identification of endogenous outward currents in human embryonic kidney (HEK 93) cell line. *Journal of Neuroscience Methods, 81*, 73-83.

Zhu, Q., Liang, S., Martin, L., Gasparini, S., Menez, A., & Vita, C. (2002). Role of disulphide bonds in folding and activity of leiurotoxin: Just two disulphides suffice. *Biochemistry, 41 (38)*, 11488-11494.

Zhuchenko, O., Bailey, J., Bonnen, P., Ashizawa, T., Stockton, D., Amos, C., et al. (1997). Autosomal dominant cerebellar ataxia (SCAG) associated with small polyglutamine expansions in the alpha (1A)-voltage-dependent calcium channel. *Nature Genetics, 15/1*, 62-69.

# Publication

**"The SK3 subunit of small conductance $Ca^{2+}$-activated $K^+$ channels interacts with both SK1 and SK2 subunits in a heterologous expression system"**

Monaghan AS, Benton DC, Bahia PK, Hosseini R, Shah YA, Haylett DG, Moss GW

Journal of Biological Chemistry (2004), vol.279 (2), p.1003-1009